Microwave Swing Adsorption for post-combustion CO_2 capture from flue gases using solid sorbents

Theodore Chronopoulos

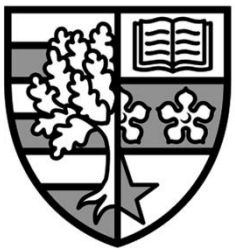

A thesis submitted for the degree of Doctor of Philosophy

Heriot-Watt University

Chemical Engineering

Institute of Mechanical, Process and Energy Engineering

School of Engineering and Physical Sciences

July 2016

Abstract

In recent years, there has been an increasing global interest in carbon dioxide capture and storage (CCS) as an important technology for climate change mitigation. However, improved technologies for the CO_2 capture process that could possibly lead CCS to be highly competitive against the renewable energy market, are necessary. The evaluation of a CO_2 capture system is often driven by energy demands and in adsorption technology this energy is particularly required for the desorption step. As a result, efficient regeneration systems ensuring multiple re-use of adsorbent materials, while minimizing energy use, are required, in an attempt to replace the conventional PSA (Pressure Swing Adsorption) and TSA (Temperature Swing Adsorption) technologies.

This study presents and analyses a relatively new approach for CO_2 sorbent regeneration, namely Microwave Swing Adsorption (MSA). The aim of this research is to intensify the CO_2 desorption process from solid materials, focusing on improving the regeneration efficiency and kinetics as well as the energy spent during this step. The hypothesis that the direct absorption of energy during microwave heating by the solid adsorbent may enable a fast process with a low purge gas flow rate low desorption temperature resulting in low energy demands, is examined. However, MSA depends on numerous parameters, divided in two main categories, namely process parameters (flue gas composition, desorption temperature, moisture presence, gas flow rate) and material parameters (adsorbent shape and size, porosity, surface modifications, dielectric properties). To this regard, an extensive investigation of the above criteria and their connection with the performance of the MSA system is studied.

In terms of the adsorption step, it was found that a switch to higher total flow rates results in an increase in the CO_2 adsorption capacity of the GAC. Moreover, moisture presence also enhances the CO_2 adsorption, as a result of an increase in the total flow rate and in the adsorption temperature. With regards to the desorption step, it was shown that MSA technology leads to enhanced performance efficiency of the sorbent by ~10%, while preserving its porous structure. Moreover, the regeneration time and the energy consumption were also considerably reduced (30% and 40%, respectively), for MSA compared to TSA.

Acknowledgements

Looking back at the past three years, I had the pleasure to meet people from all over the world and take the best from their experiences and knowledge. Undertaking this PhD has been a truly life-changing experience for me and it would not have been possible to accomplish anything without the support and guidance that I received from those people. Therefore, I want to make use of this page to thank those who effectively influenced and supported my PhD journey.

Firstly, I would like to thank my first supervisor Mercedes Maroto-Valer for her continuous guidance and encouragement. Mercedes has been very supportive, not only about technical issues, but also in times when things were going bad. It was a pleasure for me to work under her guidance and I am grateful for giving me the opportunity and the freedom to undertake this project. Without her guidance and constant feedback this PhD project would not have been achievable.

I would also like to thank my second and third supervisors, David A. Reay and Raffaella Ocone for their invaluable advice, support and availability whenever needed.

Furthermore, I would like to thank the CICCS team for their support, especially with regards to technical lab issues. I also thank Prof. Adrian Porch from Cardiff University for his technical insights and advice. Moreover, I would like to thank INCAR-CSIC and Rey Juan Carlos University for providing some of the materials used in this study.

A special *thanks* goes to my parents for always believing in me and encouraging me to follow my dreams, being supportive when things go rough and sharing my joy during my good moments. They have taught me about hard work and self-respect, about persistence and about how to be independent and this thesis is also the result of their efforts.

Finally yet importantly, I am indebted to all the people that made my journey lighter and happier with their friendship, having to cope with me and my worries. Therefore, thanks to everyone that we shared a flat, a night out, a nice dinner and a constructive discussion through all those years. Patience is the greatest virtue.

Declaration statement

ACADEMIC REGISTRY

Research Thesis Submission

Name*:*	Theodore Chronopoulos		
School/PGI:	School of Engineering and Physical Sciences		
Version: *(i.e. First, Resubmission, Final)*	First	Degree Sought (Award **and** Subject area)	**PhD** in Chemical Engineering

Declaration

In accordance with the appropriate regulations I hereby submit my thesis and I declare that:

1) the thesis embodies the results of my own work and has been composed by myself
2) where appropriate, I have made acknowledgement of the work of others and have made reference to work carried out in collaboration with other persons
3) the thesis is the correct version of the thesis for submission and is the same version as any electronic versions submitted*.
4) my thesis for the award referred to, deposited in the Heriot-Watt University Library, should be made available for loan or photocopying and be available via the Institutional Repository, subject to such conditions as the Librarian may require
5) I understand that as a student of the University I am required to abide by the Regulations of the University and to conform to its discipline.

* *Please note that it is the responsibility of the candidate to ensure that the correct version of the thesis is submitted.*

Signature of Candidate*:*		Date:	

Submission

Submitted By *(name in capitals):*	THEODORE CHRONOPOULOS
Signature of Individual Submitting:	
Date Submitted:	

For Completion in the Student Service Centre (SSC)

Received in the SSC by *(name in capitals):*			
Method of Submission *(Handed in to SSC; posted through internal/external mail):*			
E-thesis Submitted **(**mandatory for final theses)			
Signature:		Date:	

Table of Contents

List of Tables

List of Figures

Nomenclature

Abbreviations

2-amino-2-methyl-1-propanol	AMP
Air Separation Unit	ASU
Brunauer, Deming, Deming and Teller	BDDT
Brunauer, Emmett and Teller	BET
Capital costs	CAPEX
Carbon Capture and Storage	CCS
Carbon Hydrogen Nitrogen analysis	CHN
Conventional heating	CH
Cost of Electricity	COE
Density Functional Theory	DFT
Department of Energy	DOE
Diethanolamine	DEA
Diglycol-amine	DGA
Dubinin Radushkevich method	DR
Energy Information Agency	EIA
Engineering and Physical Sciences	EPS
Enhanced Oil Recovery	EOR
Environmental Non-Government Organisation	ENGO
Equilibrium zone	EZ
European Union	EU
Focused Ion Beam	FIB
Forward Looking Infrared	FLIR
Global CCS Institute	GCCSI
Granular Activated Carbon	GAC
Greenhouse Gases	GHG
Heat Recovery Steam Generator	HRSG
Infrared optical pyrometer	IRP
Infrared	IR
Instituto Nacional del Carbón	INCAR
Integrated Coal Gasification Combined Cycle	IGCC
Intergovernmental Panel of Climate Change	IPCC
International Energy Agency	IEA

Kawasaki CO_2 Capture system	KCC
Levelised COE	LCOE
Mass transfer zone	MTZ
Metal Organic Framework	MOF
Methyl-ethyl-ketone	MEK
Microwave heating	MW
Microwave Swing Adsorption	MSA
Monoethanolamine	MEA
National Energy Technology Laboratory	NETL
N-methyldiethanolamine	MDEA
Operational costs	OPEX
Organisation for Economic Co-operation and Development	OECD
Photovoltaics	PV
Powdered Activated Carbon	PAC
Pressure Swing Adsorption	PSA
Process intensification	PI
Proportional Integral Derivative	PID
Pulverized coal	PC
Quality factor	Q-factor
Scottish Carbon Capture and Storage	SCCS
Temperature Swing Adsorption	TSA
Tetraethylenepentamine	TEPA
Thermo-gravimetric analysis	TGA
Time-of-Flight Mass Spectrometer	TOF-MS
United Nations Development Programme	UNDP
United States Environmental Protection Agency	US EPA
Vacuum Pressure Swing Adsorption	VPSA
Volatile Organic Compounds	VOC

Latin characters

Ambient temperature	T_{amb}
Arrhenius pre-exponential factor	A
Average microwave absorbed power	P_{abs}
Bandwidth	f_B
Bed diameter	d_b

Bed height	h_b
Bed length to diameter ratio	L/d_b
Bed volume	V_b
BET surface area	S_{BET}
Boltzman's constant	k_B
Breakthrough time	t_b
Change in bandwidth	Δf_B
Change in resonant frequency	Δf_0
Colburn-Chilton j-Factor	j_d
Concentration of CO_2 entering the reactor	$C_{CO_2}^{in}$
Concentration of CO_2 leaving the reactor	$C_{CO_2}^{out}$
Concentration of N_2 entering the reactor	$C_{N_2}^{in}$
Concentration of N_2 leaving the reactor	$C_{N_2}^{out}$
Concentration of the adsorbed species	N
Desorption activation energy	E_A^{des}
Desorption efficiency	n_{des}
Desorption temperature	T_{des}
Diffusion coefficient of A to B	D_{AB}
Distance from front of the sensing head to the object	D
Effective cavity volume	V_{eff}
Effective particle diameter	d_p
Energy consumed for 70% desorption at 130°C	$E_{70}^{130°C}$
Energy consumed for 70% desorption at 70°C	$E_{70}^{70°C}$
Energy consumed for 70% desorption	E_{70}
Enthalpy of adsorption of the gas on the solid	H_a
Equilibrium CO_2 adsorbed amount	q_{eq}
Flight-times	t_{fl}
Fluid superficial linear velocity	u
Frequency	f
Gravitational constant	g_c
Heat produced on forming the second and higher layers	H_L
Henry's adsorption constant	K_H
Ideal gas constant	R

Inner diameter of the reactor	ID_r
Kinetic energy	E_{kin}
Length of the drift	l_{dr}
Length of the reactor	l_r
Light velocity	c
Magnitude of the internal electric field	$\|E\|$
Mass of each ion	m_i
Mass of the adsorbent	m_{ads}
Mass transfer coefficient	k
Mass	m
Monolayer volume	V_m
Outside diameter of the reactor	OD_r
Packed bed diameter	d_b
Partial pressure of the adsorbate x	P_x
Penetration depth	D_p
Pressure	P
Pressure drop	ΔP
Radius of the dipole	r
Rate constant for the desorption process	k_{des}
Rate of desorption of an adsorbate	R_{des}
Resonant frequency	f_0
Reynolds number	Re
Sample volume	V_s
Saturated pressure of adsorbing gas	P^0
Schmidt number	Sc
Spot size	S
Strength of the electric field of microwaves	$\|E\|$
Strength of the magnetic field of microwaves	$\|H\|$
Surface coverage	X
Temperature at depth z	T_z
Temperature at the starting point of the slab	T_0
Temperature difference	ΔT
Temperature	T
Theoretical radiation	B_λ

Thermal conductivity	C_p
Thermal energy	P_{th}
Time for 70% of total CO_2 desorbed	t_{70}
Time required to complete the desorption process	$t^{0.5}$
Time	t
Total bed volume	V_t
Total pore volume	V_p
Total specific amount of CO_2 desorbed	q_{des}
Total volumetric flow rate	F_{tot}^{in}
Velocity	u
Void volume	V_{void}
Volume of gas adsorbed	V

Greek characters

Angular frequency	ω
Apparent bed density	ρ_{ap}
Bed density	ρ_b
Bed void fraction	ε_B
CO_2 density	ρ_{CO_2}
Dielectric constant value	ε_i
Dynamic viscosity	μ_d
Effective dielectric constant	ε_{eff}
Electrical conductivity	σ_{el}
Fluid density	ρ
High frequency constant	ε'_∞
Location parameter	μ
Loss angle	δ
Magnetic permeability in vacuum	μ_0
Particle density	ρ_{ads}
Permittivity in vacuum	ε_0
Relative dielectric loss factor	ε''_r
Relative magnetic loss	μ''_0
Relative permittivity	ε'_r
Relaxation time	τ

Scale parameter	σ
Void fraction	ε
Wavelength	λ

List of Publications

Publications in Reviewed Journals

Chronopoulos, T.; Fernandez-Diez, Y.; Maroto-Valer, M.M.; Ocone, R.; Reay, D.A. (2014) '*CO_2 desorption via microwave heating for post-combustion carbon capture'*, Microporous and Mesoporous Materials, Vol. 197, pp. 288-290; DOI: 10.1016/j.micromeso.2014.06.032

Chronopoulos, T.; Fernandez-Diez, Y.; Maroto-Valer, M.M.; Ocone, R.; Reay, D.A. (2014) '*Utilisation of microwave energy for CO_2 desorption in post-combustion carbon capture using solid sorbents*', Energy Procedia, vol. *63*, pp. 2109–2115; DOI: 10.1016/j.egypro.2014.11.227

Chronopoulos, T., Porch, A., Ocone, R., Reay, D. and Maroto-Valer, M.M. (2016) '*Microwave Swing Adsorption of Activated Carbon under dry and wet flue gas conditions for post-combustion CO_2 capture'*, Fuel Processing Technology (paper submitted, currently under review)

Conferences

Oral presentation: Chronopoulos, T., Ocone, R., Reay, D. and Maroto-Valer, M.M. *'Making Carbon Capture feasible: Development of a circulating fluidised bed with microwave regeneration'*, Process Intensification meeting, Newcastle, 2013

Oral presentation: Chronopoulos, T., Ocone, R., Reay, D. and Maroto-Valer, M.M. *'Microwave desorption of solid adorbents for CO_2 capture'*, Process Intensification meeting, Newcastle, 2014

Awards

Best Poster award, as voted by Research Fellows/Associates and PhD students, '*Process Intensification of CO_2 Capture towards a more Sustainable CCS Technology',* 1st Year Institute of Mechanical, Process and Energy Engineering (IMPEE) conference, 2014

Chapter 1 – Introduction

1.1. Energy trilemma

The World Energy Council's definition of energy sustainability is based on three core dimensions – energy security, energy equity, and environmental sustainability (World Energy Council, 2013). In other words, creating a policy framework that could simultaneously provide secure, affordable, and environmentally sustainable energy, contributing to a continuously feasible energy system, is one of the most important challenges that societies face these days. This tri-polar challenge is also known as the *'energy trilemma'* (Figure 1.1). In philosophy, a trilemma is a choice between three unfavourable options, whereas in economics it is also known as the *'impossible trinity'* - a trade-off between three goals, in which two are pursued at the expense of the third. However, the energy trilemma appears to be different: meeting it requires achieving all three goals, while staying within the boundaries of each particular vector.

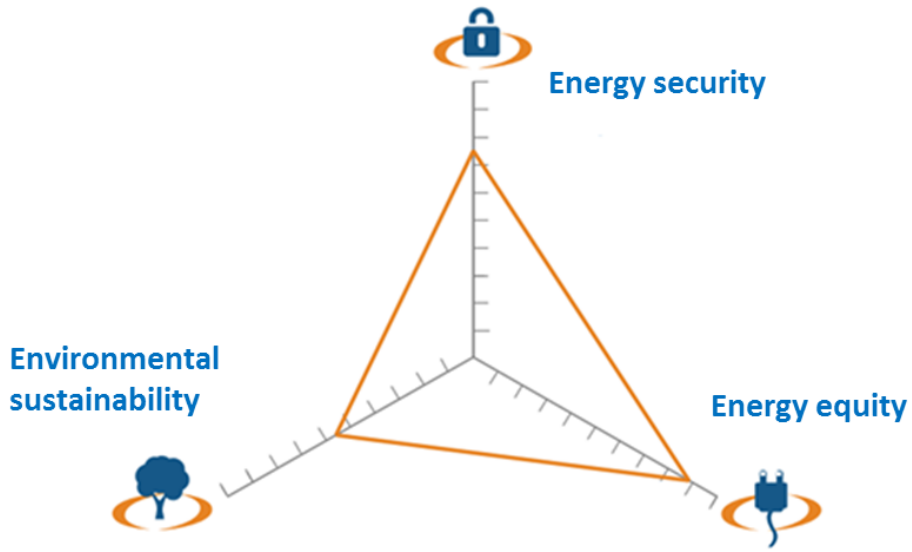

Figure 1.1: World Energy Trilemma (World Energy Council, 2013)

Each of the triangle edges of the trilemma is critical to the social and economic expansion of a country. However, perspectives on urgency of the three vectors of energy trilemma vary across countries, especially when comparing developed and developing economies. While energy security is prioritised to a great extent by many countries, as it is critical to fuelling economic growth, there is more inconsistency when

it comes to energy access and affordability – the energy equity vector – and even worse for the environmental sustainability vector.

Environmental sustainability is the word that is mostly used in today's world and is based on a very simple principle, according to the United States Environmental Protection Agency (US EPA): *'Everything that we need for our survival and well-being depends, either directly or indirectly, on our natural environment'*. Sustainability creates and maintains the conditions under which humans and nature can exist in productive harmony, that permit fulfilling the social, economic and other requirements of present and future generations. It is important to make sure that we have and will continue to have water, energy, materials, and resources to protect human health in parallel with environmental preservation.

However, energy security, economic development and environmental preservation are uncertain nowadays as evolution of economies is firmly associated with energy demand; when the future of global energy markets is discussed, two main concerns feature regularly, with the first one being climate change. The other is the question whether the world has enough energy resources to fuel continued economic growth and industrialisation, especially in the economies that are not members of the Organisation for Economic Co-operation and Development (OECD) (Rühl et al., 2012). Fossil fuels are still the prevalent energy resource by being responsible for 82% of the total energy demand and over 90% of energy-related emissions are CO_2 from fossil-fuel combustion, while energy consumption is predicted to increase rapidly by 2030 (EIA, 2015). Coal is presently the world's primary fossil fuel for generating electrical power - 40% coal, compared to 30% natural gas, 19% nuclear and 11% renewable sources - and, being more abundant and currently less expensive than oil or natural gas, is expected to continue its dominance well into the future (IEA, 2015). Moreover, coal is more carbon intensive than natural gas and oil, namely 91.50gCO_2-eq/MJ_{th} in contrast to 68.20gCO_2-eq/MJth and 73gCO_2-eq/MJth respectively (Dowlatabadi and Hanova, 2007), and consequently, coal-fired power plants are large point source emitters of CO_2. Therefore, the global economic development is responsible for various environmental issues with atmospheric pollution and climate change being the most important and urgent ones.

It is apparent that, sustainable energy technologies can contribute to address the energy trilemma, controlling climate change and protecting provision of the increased energy demand only if significant decisions are taken, as reported by Committee on Climate Change (2013). The report includes five important solutions:

- ✓ Decarbonisation of the power sector;
- ✓ Reduction of emissions from buildings;
- ✓ Forest preservation;
- ✓ Reduction of emissions from industry;
- ✓ Reduction of transport emissions.

Nowadays, developing countries, especially in Asia, are facing a major concern, regarding the above steps: they have to cope with the adverse impacts of climate change and consider whether they should take action to mitigate the risk of more extreme impacts in the future while at the same time reduce social and energy poverty. Traditionally, fast developing and emerging nations have struggled to cultivate an environmentally sensitive perspective as they focus on improving their economic growth and their populations' access to energy (World energy council, 2013). For example, statistics from the International Energy Agency (IEA 2007) and the United Nations Development Programme (UNDP 2007/2008) indicate that there are still roughly 2.5 billion people who rely heavily on traditional cooking fuels, and around 1.6 billion who have no access to electricity in developing countries (IEA 2007, UNDP 2007/2008). However, economic growth as well as improved living standards, are critically linked with the availability of state-of-the-art energy provision. Increasing energy demand can only be met by the use of fossil fuels in the developing countries, so far, leading to increasing trends of overall CO_2 emissions.

One example supporting the above statement is China, which, according to IEA (2013), has outdistanced the European Union (EU) for the first time with regards to emissions per capita in 2013. The report states that if pollution rates progress at the same pace, the limit for atmospheric CO_2 will be reached in no more than 30 years. It is remarkable that the world's most populous country and second largest economy is now producing a greater amount of CO_2 than both the EU and US, where the first and second industrial revolution took place. Figure 1.2 shows the emissions share in 2013, proving that China

(24%), USA (14%), EU (10%), and India (6%) possess the largest share with regards to CO_2 emissions, meaning that the top four polluters are responsible for 54% of the global pollution map. In addition, CO_2 emissions, excluding OECD and China, increased by approximately 290 Mt in 2014, mostly due to an increased use of coal for power generation in Southeast Asia and India (IEA, 2015). India's emissions increased by 5.1% between 2012 and 2013, while China and the US were up 4.2% and 2.9%, respectively.

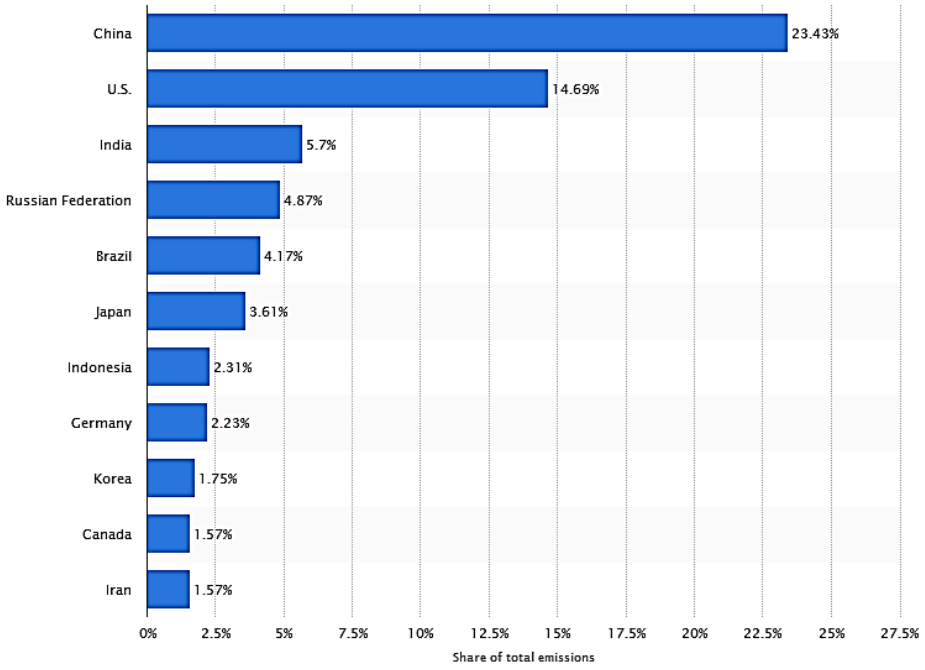

Figure 1.2: Largest producers of energy-related carbon dioxide emissions in 2014, based on their share of global energy-related CO_2 emissions

On the other hand, the 28-nation EU managed to slash emissions by 1.8% between 2010 and 2012, mostly because of the introduction of renewable energy technology. These trends suggest that India will be following China in due time, also out-polluting the EU; specifically, it is estimated that coal-fired power plants capacity is going to grow by 35% in the next 10 years, with the highest increase rate to be recorded in India - from 95,000 MW to 294,000 MW - which will result in a rise of CO_2 emissions of 955 Mtpa (million tons per annum) – and overall in Asia from 918,000 MW in 2011 to 1,464,000 MW in 2020 (Mcilvaine company, 2012). It becomes clear that, the relationship between economic growth and emissions growth remains strong across most emerging and developing countries, as these countries are in the energy-intensive process of building up their capital stock. Consequently, even if the US and Europe were to cut

CO_2 emissions by far more than the targeted 20%, the total CO_2 increase from developing countries will offset it by a wide margin.

However, according to the Global CCS Institute (GCCSI, 2015), an agreement between China and the US was reached recently with regards to limiting greenhouse gases, binding China to introduce a cap-and-trade system for its polluting industries. The program will commence in 2017 and will set annual emission limits to specific industries. According to this cap-and-trade system, industries that surpass the pre-agreed limits will need to purchase credits from firms that pollute less. As a result, China, will be expected to commit to prioritizing low-carbon and efficient electricity production technologies. This deal is predicted to put pressure on India in terms of implementing low-carbon technologies as well.

Furthermore, following COP-21 Paris climate summit agreement, representatives of both international governments and business leaders in the private sector announced commitments and partnerships to achieve a major increase in investments for research and development in low-carbon technologies and ways to speed up their diffusion in developing countries. The importance of this commitment lies behind one of the most surprising outcomes of the agreement, namely the aim of limiting warming to 1.5°C (Article 2).

To this end, it is apparent that the benefits from accelerating the commercial implementation of Carbon Capture and Storage (CCS) can potentially be very large, especially in the short-term (20-50 years). Large scale CO_2 capture is most efficient for industries that create large quantities of CO_2, both in terms of flow-rates and concentration in the exhaust stream, such as large electricity generation power plants that utilise fossil fuels or biomass. In addition, considering that >25% of the current global CO_2 emissions – which rises up to 50% in the developing countries (IPCC, 2014) – derives from large industrial sources (iron and steel, cement, aluminium, chemicals production and refineries), it is crucial to examine the potential of commencing commercialisation of CCS to those sources (SCCS, 2014). The Boundary Dam project in Canada – being in operation from October 2014 - (developed by SaskPower) can show the road forward to the development of CCS globally.

Another factor that supports advancement of CCS is the abundance of fossil fuel reserves; it is believed that the most significant effect of a successful implementation of CCS will possibly be that Greenhouse Gases (GHG) abatement targets will be met easier by fossil fuel-dependent economies, without the need of purchasing CO_2 credits, as previously mentioned. This is an extremely important parameter since it will prevent developing countries from being isolated from security of supply, while economic competition between regions will not be an issue, due to restrictions on GHG emissions. Commercialisation of CCS would result in enhanced energy security of supply since the use of coal for power generation will be continued, especially with regards to domestic lignite in countries such as China, Korea, Japan and Turkey (DOE/EIA, 2015). In contrary, failure to adopt CCS would mean that the global energy community will almost immediately start ruling out the utilisation of fossil fuels, a scenario which seems rather unlikely, taking into consideration the vast amount of coal in developing countries such as India and China (Johnsson et al., 2012).

1.2. Progress and costs of CCS

As discussed above, fossil fuels are still predominant for energy production, with the IEA predicting that they will provide ~75% of the world's primary energy in 2040. As a result, it is evident that CCS can play a very significant role in terms of climate change mitigation and it is already considered a significant component of the low-carbon technologies. It is true that CCS is able to provide a short-term solution in order to stop the resultant CO_2 getting into the atmosphere and countries that have committed to the carbon trade scheme are expected to benefit greatly from this technology. Specifically, according to the IEA (2014), CCS has the potential to provide 14-19% of the global abatement in GHG emissions required by 2050 and notably more in the following decades.

However, progress on deployment of CCS has been significantly delayed nowadays (IEA, 2014), since commercially available technologies still remain unprofitable; in simple terms, employment of CCS in the power industry increases electricity costs and prices (BGS, 2014). As a result, there is a noticeable reluctance by electricity generators to apply this technology, since it is a substantial additional capital and operational cost (CAPEX & OPEX) on their sites and reduces the flexibility of their plants (Carbon Capture Journal, 2012). The economic affordability of CCS depends

largely on the value and price put on environmental and ecosystem sustainability; however, improved technologies for CO_2 capture are also necessary to achieve lower costs and energy penalties in order for CCS to be highly competitive against the renewable energy market. Effective solutions need to be derived from the research projects that are now under investigation all over the world, with UK alone funding a 4-year (2011-2015) £125 million cross-governmental CCS research, according to the Department of Energy and Climate Change (DECC, 2013).

When applied to electricity generation, CCS has four main impacts on the cost structure for any project seeking to meet a given level of electricity demand:

- ✓ Additional capital expenditure associated with the CO_2 capture and compression plants;
- ✓ Additional fuel costs for the energy used in the capture process;
- ✓ Additional capital expenditure to build a larger power plant (to ensure net power output is unchanged) in order to compensate for the energy used in the capture process (i.e. host plant compensation); and
- ✓ Additional operations and maintenance costs associated with both the larger plant and the capture and compression requirements (Zero Emissions Platform, 2011).

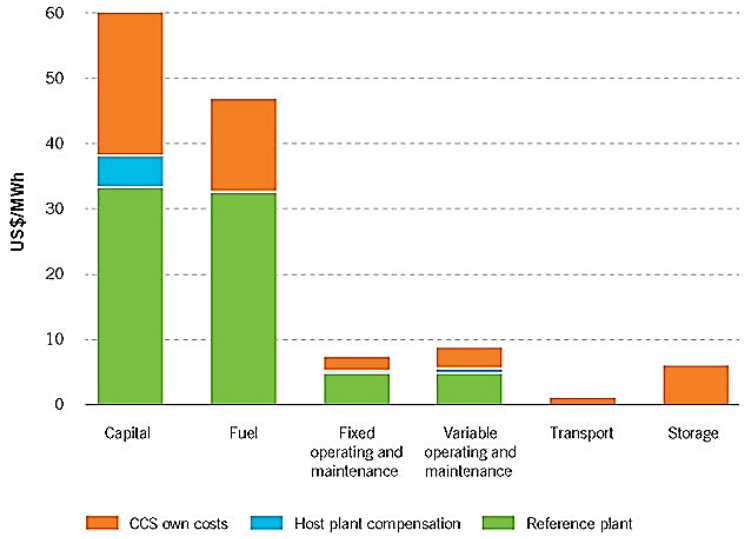

Figure 1.3: Cost impacts of adding CCS to a power station for a supercritical post-combustion plant (Global CSS Institute and WorleyParsons, 2011)

The relative share of the above cost increases varies across the different capture technologies reflecting differences in the processes. However, regardless of the process, it is the capture facilities and the additional energy requirements as part of the capture process that have the largest impact on costs (GCCSI, 2011); as seen in Figure 1.3, a reference coal power plant without the use of CCS corresponds to £55/MWh, whereas this price increases to £95/MWh when adding CCS. 70% of this increase in the price of MWh comes from capital costs and energy penalties, with another 10% coming from storage.

In 2011, the GCCSI presented a comparison of low-carbon technologies (Global CCS Institute, 2011) in the electric power sector based on a review of technology cost studies by a number of agencies including the IEA, the IPCC, the US Energy Information Agency (EIA), WorleyParsons, the US National Energy Technology Laboratory (NETL) and US National Renewable Energy Laboratory. This comparison shows that there are technologies that have zero or negative avoided costs, such as conventional geothermal and hydropower plants among others. Negative avoided costs can occur if the cost of the low-carbon technology is less than the fossil fuel technology. The finite availability of wind and hydro resources limits their role in meeting emission targets and requires higher cost options of CCS, solar and nuclear technologies. Figure 1.4 shows that CCS still remains a cost-competitive technology alongside other large-scale abatement options in the power generation sector, such as offshore wind and solar thermal or Photovoltaic (PV) processes. As a result, CCS technology is the only means of reducing CO_2 emissions in the near term and could serve as a bridging strategy to a time when non-carbon energy technologies are broadly deployed.

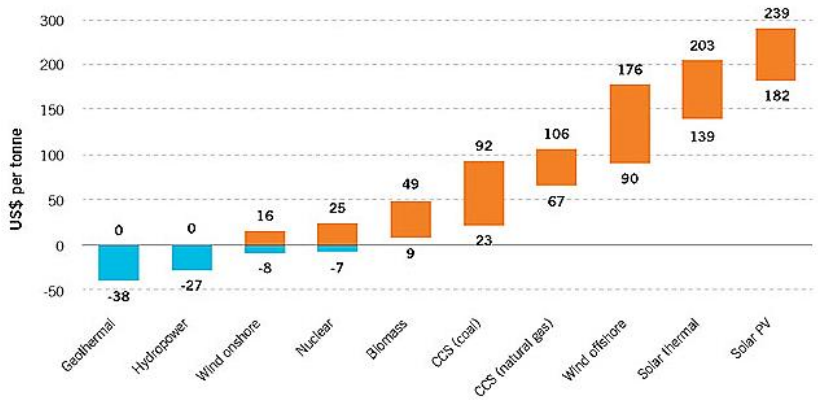

Figure 1.4: Costs of CO_2 avoided - Note: For all technologies except gas-fired CCS plants, the amount of CO_2 avoided is relative to the emissions of a supercritical pulverised coal plant. For gas-fired CCS, the reference plant is an unabated combined cycle plant (Global CCS Insitute and WorleyParsons, 2011)

1.3. Challenges in CO_2 capture

The issue of an efficient and scalable CO_2 capture process is regarded as one of most challenging processes in the energy research sector (NETL-DOE, 2012). When applied to power generation, there are three main pathways for CO_2 capture, namely post-combustion, pre-combustion and oxy-fuel combustion. This research focuses on post-combustion capture, since it is believed to be the best candidate for short term CCS application to CO_2 emission sources (NETL-DOE, 2014), as it can be retrofitted to existing plants. However, retrofitting has a significant impact on the efficiency of the power generation process, since additional energy and costs are associated with the operation of the capture plant. Post-combustion CCS requires significantly innovative advancements in the field of process engineering, as well as materials design and synthesis, in order to compete with the other carbon neutral technologies (nuclear, renewables, biomass). CO_2 capture process represents typically about 70% of the total cost of the CCS chain, and therefore, novel technologies that can offer various advantages over conventional absorption technologies using alkanolamines, such as high operating flexibility and low maintenance costs, are gaining support (IEA, 2013).

Firstly, CO_2 needs to be rapidly and selectively separated from an exhaust gas mixture that consists of various other gaseous components; a typical 550 MW coal-fired power plant produces approximately $3Mft^3/h$ of flue gas at atmospheric pressure and CO_2 concentration accounts for approximately 12–15% with the rest being nitrogen, water, oxygen as well as traces of sulphur and nitrogen oxides. Hence, production of a high purity CO_2 stream from separating and capturing it from this complex mixture requires highly efficient and cost-effective technologies. Secondly, CO_2 is a thermodynamically stable molecule and capturing it requires a distortion of the molecule away from its linear and symmetric arrangement. However, the binding of CO_2 to the capture medium cannot be too strong, since the sheer quantity of CO_2 that is present in large scale plants exhausts necessitates the need to re-use this medium for further CO_2 capture (Meisen and Shuai, 1997). As a result, the CO_2 must be released from the capture medium relatively fast, meeting the kinetics of the capture process and with the least possible energy input, in order for the process to be economically feasible (Plasynski and Chen, 1998).

The economic evaluation of a CO_2 capture system is often driven by energy demands and in adsorption technology this energy is particularly associated with the desorption step. Hence, it is evident that, CO_2 capture is the most energy demanding step in the CCS chain and as a result it directly affects the overall cost of the CCS process; CO_2 separation, capture and regeneration represent about 70% of the total CCS cost (Davison, 2007). It is this conjugation of high-speed and efficient capture as well as regeneration systems with high selectivity and minimal energy loss that makes this a truly grand challenge problem whose possible solution will drive today's world's energy policies to a new level of discussions.

Two cyclic capture procedures are typically followed in laboratory and/or industrial applications nowadays, namely Pressure Swing Adsorption (PSA) and Temperature Swing Adsorption (TSA). However, PSA and TSA are not considered to be the optimum pathways for post-combustion CO_2 adsorption technology. PSA is fully efficient for processes that take place at elevated pressures; otherwise the installation of additional compressors and/or vacuum pumps is required, which complicates the process while having a negative effect on the overall efficiency (Cherbanski et al., 2008). TSA systems, on the other hand, provide a stronger driving force for CO_2 desorption contributing to higher regeneration efficiencies, but unfortunately, they are time and energy consuming, resulting in increased energy penalties for the power plant. This is mostly associated with the large time scale involved in heating and cooling large adsorbent vessels, as well as with the massive amount of hot purge gas needed for the heating of the sorbents (Bonjour et al., 2002). In addition, this hot purge gas (e.g. steam) dilutes the recovered CO_2 and a separate downstream separation is required. Finally, successive heating cycles have a deteriorating effect on the textural characteristics of the sorbent, leading to a further decrease of its CO_2 adsorption and working capacity. Accordingly, research towards the development of innovative cyclic capture technologies that involve rapid thermal processes avoiding the aforementioned disadvantages is required.

1.4. Aim and objectives

The aim of this study is to develop and analyse the use of Microwave Swing Adsorption (MSA) to intensify the CO_2 desorption process from solid materials, focusing on improving the regeneration efficiency and kinetics as well as the energy spent during

this step. The above aim was based on the hypothesis that direct absorption of energy during microwave heating by the solid adsorbent, in contrast to the indirect supply of heat by thermal conduction, may enable a much faster process with a lower purge gas flow rate and lower process temperature. Consequently, this may result in energy savings and faster desorption kinetics, making the desorption process more efficient and cost-effective than conventional heating technologies. As a result, the first objective of this research is to compare MSA against TSA in terms of sorbent regeneration efficiency, CO_2 desorption kinetics and energy consumption. Secondly, the optimum conditions for the MSA process and the importance of the nature of the sorbent (raw material, shape, size) during microwave heating are also examined and discussed.

Utilisation of microwave energy for heating processes has been known for a long time, and the development of microwave ovens has more than 60 years of history. However, the concept of using microwave energy in CO_2 capture applications to replace the conventional TSA and/or PSA cyclic processes has not been studied yet. As a result, microwave energy was extensively studied in order to evaluate its application in the field of CO_2 capture and a comprehensive study on the main parameters that affect the dielectric heating of a sorbent material is presented. Moreover, a comparison with the existing conventional heating technology (TSA) was conducted, trying to propose alternative solutions to the critical issue of the high-cost desorption step in the CCS chain. Finally, the preservation of the textural, chemical and dielectric characteristics of the sorbent materials under consecutive adsorption/desorption cycles was investigated, since the stability of the material has an immediate effect on the operating costs of the CO_2 capture process.

1.5. Methodology

This section includes all the steps that were followed during this study, broken down into three major tasks:

Task I: Preparation and characterisation of six different kinds of solid sorbents

The first task of this three-year PhD study included the selection, preparation and characterisation of the solid sorbents under investigation. A wide selection of sorbents with regards to form, size, shape and physical, chemical and dielectric properties was

used, in order to examine the effect that microwave heating has on each one. This study would later help to understand which parameters play the most important role in microwave applications and consequently predict the heating performance of similar materials. As a result, the following solid sorbents were selected:

a. Carbon based sorbent materials:
   - ✓ Microporous granular activated carbon (GAC):
     i. Made from palm shell, obtained by NORIT, used as the reference sample – Chapter 4.
   - ✓ Activated carbon, obtained by Desotec:
     ii. Pellet form, from coconut shell, with product name Organosorb 10-CO (Org) – Chapter 5.
     iii. Powder form, obtained after grinding the original Organosorb (OrgP) – Chapter 5
   - ✓ Granular AC from almond shells (AS), obtained from Instituto Nacional del Carbón (INCAR), Spain:
     iv. Parent sample, referred to as GKAS – Chapter 5
     v. GKAS – N800, treated with ammonia, introducing basic functionalities on the parent sample's surface, resulting in better CO_2 adsorption capacities as reported at INCAR – Chapter 5.

b. Silica-based sorbent materials, obtained from Rey Juan Carlos University, Madrid, Spain
   - ✓ SBA-15-TEPA (30):
     vi. Mesoporous silica, impregnated with tetraethylenepentamine (TEPA), resulting in considerable CO_2 uptake, previously examined at Rey Juan Carlos University. However, slow desorption rates as well as a slow but steady loss of adsorption capacity were reported with continuous-cyclic use due to TEPA evaporation – Chapter 5.

Task II: Design of the microwave system

The second main task was the design of the MSA system. An initial investigation for the suitability of several commercially available microwave systems was undertaken

and after careful consideration, a multimode microwave system was purchased and modified accordingly:

a. Design of the microwave cavity and its chambers in terms of dimensions and maximum power output;
b. Design of the glass reactor for the adsorption/desorption experiments;
c. Design of the temperature control and measurement system of the microwave cavity;
d. Thermal distribution studies, in order to explore the optimum position of the reactor inside the cavity in terms of microwave absorbance.

Task III: Regeneration studies

Lastly, the main part of this PhD research was the comparison of TSA and MSA processes, using the aforementioned sorbents and microwave system. An investigation of the process parameters was completed, including the effect of temperature, CO_2 concentration, moisture presence and exhaust gas flow rate. Moreover, the preservation of the sorbents after 25 cyclic adsorption/desorption tests was also studied, in an attempt to examine the effect of microwave and conventional heating on the structure of each material. As such, the following steps were completed:

a. Microwave Swing Adsorption (MSA) studies of the aforementioned sorbent materials using a fixed bed reactor at ambient pressure and comparison with conventional heating – temperature swing Adsorption (TSA) - under various parameters:
   - ✓ Desorption temperature:
     i. 70°C;
     ii. 130°C;
   - ✓ Concentration of CO_2 in the gas mixture:
     iii. 5% (vol.), simulating the exhaust gas of a gas fired power plant;
     iv. 15% (vol.), simulating the exhaust gas of a coal fired power plant;
     v. 40% (vol.), simulating the exhaust of the cement industry;
   - ✓ Exhaust gas condition:
     vi. Anhydrous;

vii. Wet (10% H_2O);

- ✓ Total gas flow rate:
  - viii. 100ml/min;
  - ix. 150ml/min.

b. Energy consumption measurements;

c. Material preservation experiments, including material characterisation after 5, 10 and 25 cycles in terms of:
   - ✓ CO_2 adsorption capacity;
   - ✓ BET surface area;
   - ✓ Chemical composition;
   - ✓ Dielectric properties;
   - ✓ Pore volume.

1.6. Thesis structure

Chapter 1 introduces the issue of global warming and focuses on the measures that need to be taken in order to mitigate climate change. Chapter 2 is divided in two main sections, presenting a thorough literature study of CCS and MSA technologies. Thereafter, a detailed analysis of the experimental process used for this research is presented in Chapter 3.

Chapter 4 investigates the comparison between TSA and MSA for a granular activated carbon (GAC), which acts as the reference material for this study, examining the most important process parameters; total volumetric flow rate, CO_2 composition in the feed gas mixture, anhydrous/wet feed gas conditions and desorption temperature are investigated. Subsequently, the optimal process conditions for MSA lab scale CO_2 capture technology are decided. Those conditions are then be used in Chapter 5, which investigates the effect of material properties – surface chemical modifications and adsorbent shape and size - on the CO_2 desorption process via MSA and TSA. A total of five different adsorbents with diverse properties are tested and compared to the reference material. Chapter 6 summarises the conclusions of the previous chapters, followed by future work suggestions in the field of MSA technology, including an introduction to the issue of microwave processes scaling up.

References

Bonjour, J., Chalfen, J.-B., Meunier, F. (2002) *'Temperature swing adsorption process with indirect cooling and heating'*, Industrial & Engineering Chemistry Research, vol. 41 (23), pp. 5802–5811

Cherbanski, R. and Molga, E. (2009) '*Intensification of desorption process by use of microwaves-an overview of possible applications and industrial perspectives'*, Chemical Engineering and Processing, vol. 48, pp. 48-58

Climate Change (2007) '*Mitigation of Climate Change'*, Contribution of Working Group III to the Fourth Assessment Report of the Intergovernmental Panel on Climate Change, Cambridge University Press, Cambridge

Committee on Climate Change (2013) *'Meeting Carbon Budgets – 2013 Progress Report to Parliament'*, Presented to Parliament pursuant to Section 36(1) of the Climate Change Act 2008, June

Dowlatabadi, H and Hanova, J. (2007) '*Strategic GHG reduction through the use of ground source heat pump technology*', Environmental Research Letters II, 9 November, Online atstacks.iop.org/ERL/2/044001

Global CCS Institute (2012) *'CO_2 capture technologies - pre combustion capture'*, Global Carbon Capture and Storage Institute, Canberra, Australia

Global CCS Institute (2012) *'The global status of CCS: 2012',* 10 October

Herzog, H., Meldon, J. and Hatton, A. (2009) *'Advanced post-combustion CO_2 capture'*, Clean Air Task Force

IEA - International Energy Agency (2015) *'Energy and climate change, World energy outlook special report*', OECD/IEA, Paris.

IEA - International Energy Agency (2013) *'Technology roadmap: Carbon capture and storage*', OECD/IEA, Paris.

Johnsson, F., Kjarstad, J. and Odenberger, M. (2012) *'The importance of CO_2 Capture and Storage - a geopolitical discussion',* Thermal science, vol. 16 (3), pp. 655-668, DOI: 10.2298/TSCI120608135J

Karg, J. (2009) *'IGCC experience and further developments to meet CCS market needs'*, Siemens AG Energy Sector Fossil Power Generation Division

Klare, M. (2007) *'Global warming: It's all about energy'*, Foreign Policy In Focus, 15 February. Available from: http://www.fpif.org/articles (accessed 25 May 2013)

Lacis, A., Schmidt, G.,Rind, D. and Ruedy, R. (2010) *'Atmospheric CO_2: Principal control knob governing Earth's temperature'*, Science, vol. 330, pp. 356–359 doi: 10.1126/science.1190653

MacNaughton, J. (2013) *'World energy trilemma'*, World energy council, presented at: UCL Energy for sustainable resources, 20 June

Maurstad, O. (2005) *'An overview of coal based Integrated Gasification Combined Cycle (IGCC) Technology'*, Laboratory for Energy and the Environment, Publication No. LFEE 2005-002 WP

Meisen, A and Shuai, X. (1997) *'Research and Development Issues in CO_2 Capture'*, Energy Conversion Mgmt, Vo1.38, pp. S37-S42

NETL-DOE (2012) *'Basic Research Needs for Carbon Capture: Beyond 2020'*, DOE Basic Energy Sciences Workshop, available at http://www.sc.doe.gov/bes/reports/files/CCB2020_rpt.pdf

Petit, J., Jouzel, J., Raynaud, D., Barkov, N., Barnola, J., Basile, I., Bender, M., Chappellaz, J., Davis, M., Delaygue, G., Delmotte, M., Kotlyakov, V., Legrand, M.,

Lipenkov, M., Lorius, C., Pépin, L., Ritz, C., Saltzman, E. and Stievenard, M. (1999) *'Climate and atmospheric history of the past 420,000 years from the Vostok ice core, Antarctica'*, Nature, vol. 399, pp. 429–436, June 3, doi:10.1038/20859.

Plasynski, S. and Chen, Z. (1998) *'Review of CO_2 capture technologies and some improvement opportunities'*, US DOE National Energy Technology Laboratory and Science Applications International Corporation

Rühl, C., Appleby, P., Fennema, J., Naumov, A. and Schaffer, M. (2012) *'Economic development and the demand for energy: a historical perspective on the next 20 years'*, BP plc. London, Heriot-Watt University, Edinburgh

Ruthven, D.M. (1984) *'Principles of Adsorption and Adsorption Processes'*, J. Wiley, NY

Ruthven, D.M. (1997) *'Encyclopedia of Separation Technology'*, J. Willey & Sons, vols. 1 & 2, NY

SCCS (2015) *'A CCS future for Europe: catalysing North Sea action',* Recommendations and Conference 2014 Report, University of Edinburgh, January

Sjostrom, S., Krutka, H., Starns, T. and Campbell, T. (2010) *'Pilot test results of post-combustion CO_2 capture using solid sorbents'*, [Presentation], Ninth Annual Conference on Carbon Capture & Sequestration, Pittsburgh, Pennsylvania, 10-13 May

Suzuki, M. (1990) *'Adsorption Engineering'*, Elsevier, Amsterdam

Chapter 2 – Literature review

2.1. Carbon Capture and Storage (CCS)

In December 2015, the GCCSI together with the Environmental Non-Government Organisation (ENGO) published a report, highlighting the importance of keeping CCS on the international agenda, stating that the technology can make a significant contribution toward reducing carbon emissions from the widespread use of fossil fuels nowadays. The report also states that CCS can play a significant role in achieving the international goal of avoiding global warming of two degrees Celsius above pre-industrial temperatures, however, progress has been too slow (ENGO Network on CCS, 2015). The report mentions that CCS projects, if implemented, will be able to achieve 70% of the IEA's target mitigation activities for CCS by 2020. However, a substantial increase in new projects will be required to meet the challenges of 2050 target. This target, according to the OECD, will be accomplished if GHG emissions would be reduced by almost 40% compared to 2000 levels, and if new technologies could move emissions onto a pathway that would stabilise atmospheric concentrations at low levels and significantly limit the risk of climate change impacts in the long-term. CCS is seen as a technology that is able to contribute to IEA's 2050 targets by as much as 20%, however, immediate steps need to be taken in order to persuade governmental bodies and industries to invest on this technology.

During 2014-2015, there have been a number of promising steps regarding CCS development, with the most important being the beginning of operation of the Boundary Dam Integrated Carbon Capture and Sequestration Demonstration Project, the world's first CCS project in the power sector at large scale. The successful operation of the Boundary Dam power plant will work as a benchmark activity for future CCS projects and until now, the results look encouraging; according to its operator, SaskPower, Boundary Dam extracts 90% of the CO_2 from its exhaust gas, which then is used for Enhanced Oil Recovery (EOR) activities into nearby oil wells. So far, it has captured 0.4 Mt of CO_2, while when operating at full throttle by the end of this year, that number will go up to 1Mt CO_2/year, equivalent to taking more than 200,000 cars off the road.

Moreover, two projects, including the Petra Nova CO_2 Capture Project in Texas (formerly the NRG Energy Parish CCS Project), the third large-scale power sector CCS

project to have taken a positive financial investment decision, and the Abu Dhabi CCS Project, the first large-scale CCS project in the iron and steel sector, moved to the construction stage. Meanwhile two projects moved to the define stage, one in the US (Sargas Texas Point Comfort Project) and one in China (Yanchang Integrated Carbon Capture and Storage Demonstration Project). Furthermore, a new project in the power sector utilising post-combustion capture was identified in China, currently examining offshore geologic storage (China Haifeng Resources Power Integrated Carbon Capture and Sequestration Demonstration Project with a CO_2 capture capacity of 1 Mtpa).

On the other hand, fourteen projects were unfortunately cancelled or put on hold during the same period. Most of those (seven) were projects located in Europe - two of them in the UK (White Rose and Peterhead CCS Project) - while two were in the US and one in Australia, China and the UAE, respectively. Eight of those were in the early development stage, with the rest being in the define stage (including the Porto Tolle Project in Italy, the OXY-CFB 300 Compostilla Project in Spain, the Low-Impact Steel Project in France and the Lake Charles CCS Project in the US). The majority of the abandoned projects were related to power generation, with post-combustion capture suffering the largest decline. In addition, Drax Group is reported to withdraw as a partner of Capture Power Ltd, the developer of the White Rose CCS project, stating that even if they would continue to be involved with the pre-construction feasibility study, they will not invest any more money into the project, mostly because of governmental changes to the subsidy regime for renewable energy (Tunnicliffe, 2015). Lastly, the shut-down of the SSI Redcar steel plant in Teeside, UK, will affect the so called "Teeside-collective", a cluster initiated by industries with a shared vision: to establish Teesside as the go-to location for future clean industrial development by creating Europe's first CCS equipped industrial zone (BBC, 2015).

However, it is generally believed that there is still future for CCS in the UK; the Secretary of State specified that in the next decade emphasis will be given in gas-fired power stations. Combined with nuclear, renewables and demand-reduction, the replacement of coal with gas will play an important role in reducing UK emissions. Nevertheless, a push for gas cannot get the UK to its 2050 targets without utilisation of CCS. The Prime Minister, David Cameron, acknowledged this when he stated that he would *'not commit to the decarbonisation targets that people sometimes want [him] to*

until we know about carbon capture and storage' (Energy and Climate Change Committee, 2016).

In addition to the above, it is also true that the demonstration stage of the on-going large-scale CCS projects has progressed far more slowly than it is required towards climate change mitigation, as seen in Figure 2.1. With growth of only 6% per year over the last five years and a forecast 50MtCO_2/year in operation by 2017, the IEA's recommended pathway to achieve decarbonisation appears out of reach (37% annual growth required and 255MtCO_2/year stored by 2020, respectively). Even though financial support for large demonstration projects (below $3 billion a year, with no sign of an increase) remains considerably below that of renewable energy sources such as wind and solar ($131 billion and $75 billion in 2011, respectively), it remains too large for the governments and as a result they rarely have the political will to subsidize CCS to the extent required.

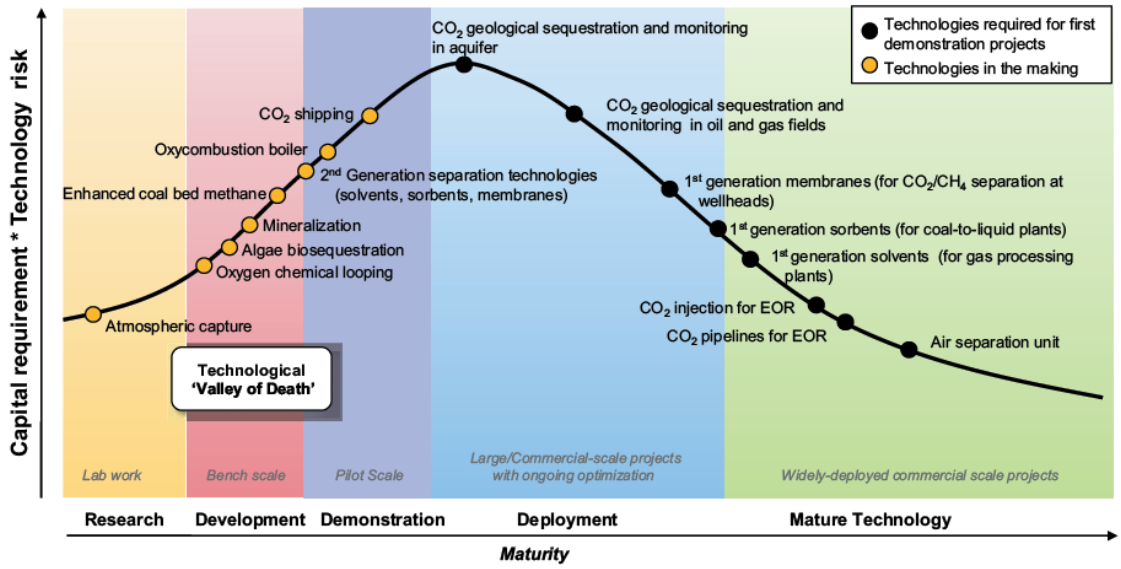

Figure 2.1: Investment risk curve of individual CCS technologies (©SBC Energy Institute)

CCS is seen as a costly technology because of its high up-front costs and uncertain long-term benefits (CCJ, 2013). Each commercial scale CCS project can cost up to a billion dollars in capture costs alone, although they are capable of abating over a million tonnes of CO_2 per year for several decades. The OECD governments have committed £15-20 billion to help CCS demonstration projects, but grants allocated so far have represented an average of just €15/tCO_2 avoided over the lifetime of each project. In

addition, there is no carbon-price mechanism to enable the recovery of CCS costs: globally, the market price of CO_2 averaged £5.5/tCO_2 in 2015, while most carbon taxes are set below £18/tCO_2.

However, there is still much space for improvement in CCS, which will subsequently attract governments to turn to and invest in this clean energy production technology. Figure 2.2 shows the prediction of CCS large scale projects deployment until 2017, depicting an optimistic point of view about this technology. Moreover, looking beyond 2020, there are circumstantial reasons that support that CCS may accelerate, since more stringent carbon policies will be required to develop CCS beyond upstream oil and gas and at the scale needed to tackle climate change. Growing demand for the beneficial reuse of CO_2 for EOR should drive CCS forwards during this decade and help to demonstrate the technology, in conjunction with large government grants. Oil prices above $100/bbl have tended to boost CO_2 contract prices above $30/t$CO_2$, greatly improving CCS-EOR economics. China is also rapidly driving down the cost of capture, having openly expressed the ambition to build capture-only coal power plants for its own needs and to export low cost capture technologies.

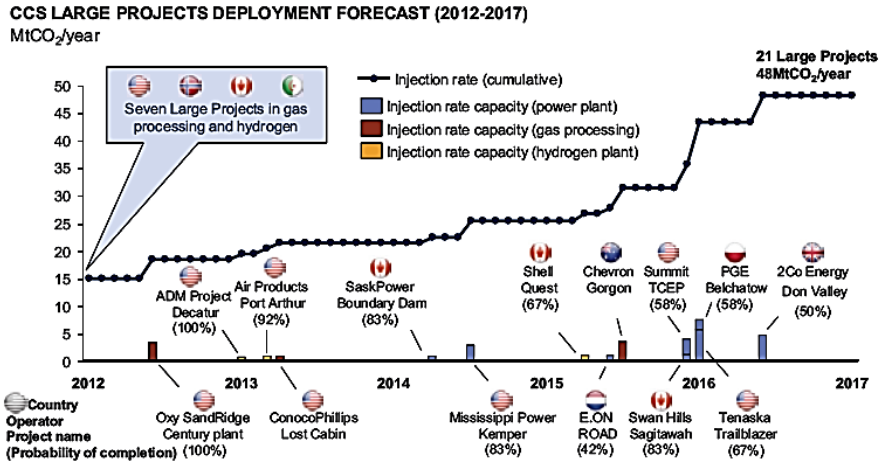

Figure 2.2: CCS large projects deploymeny forecast, 2012-2017 (©SBC Energy Institute analysis, based on Bloomberg New Energy Finance database, March 2012)

2.1.1. CO_2 capture technologies

Carbon dioxide Capture and Storage (CCS) is a process consisting of the separation of CO_2 from energy-related and industrial sources, transport to a storage location and long-

term isolation from the atmosphere (IPCC, 2005). CCS encompasses a range of technologies that may cut CO_2 emissions by up to 90%. It is well known that CO_2 capture can be achieved mainly by three different technologies, presented in Figure 2.3 (Leung et al., 2014):

i. Post-combustion, where CO_2 is separated from exhaust gases after combustion:

Post combustion carbon capture removes CO_2 from the exhaust flue gas after combustion of the fuel. The flue gas is directed through adequate equipment which separates CO_2 from other gases while capturing it, reaching capture efficiencies of over 90% (Herzog et al., 2009). It is the most established technology for CCS nowadays, also used on a commercial scale in SaskPower Boundary Dam power plant in Canada.

ii. Pre-combustion, where CO_2 is removed before combustion (Davidson, 2011):

As the name implies, pre-combustions carbon capture is a process in which CO_2 is captured prior to the fuel combustion. This process is not feasible for pulverized coal (PC) power plants, which is the dominant type of power generation plants across the globe, however it is a competent process for an Integrated Coal Gasification Combined Cycle (IGCC) plant. In this type of plants, coal is initially gasified forming synthesis gas (syngas, a mixture containing mostly CO and H_2). Then, the syngas undergoes the water-gas shift reaction, during which CO reacts with steam to form CO_2 and supplementary H_2. At this point, the CO_2 is separated and captured, whereas the H_2 is diluted with N_2 and directed into a typical gas turbine combined cycle. This process is expected to provide a cost-effective solution compared to post-combustion, however, there are only a few IGCC plants in the current coal to energy process, mainly because IGCC plants themselves are more expensive than PC plants.

iii. Oxy-fuel combustion, where the fuel is burned under oxygen conditions to produce an almost pure CO_2 exhaust (Perrin et al., 2013):

The rationale behind oxy-fuel combustion is simply that if there was no nitrogen, CO_2 capture from flue gas would be considerably simplified. As a result, instead of air, the power plant uses a high purity ($\geq$95%) oxygen stream for coal combustion. The flue gas

that is created from combustion in an O_2-rich environment comprises of CO_2, water, particulates and SO_2. Particulates and SO_2 can be removed by conventional electro-static precipitator and flue gas desulphurization methods, respectively. The remaining gases, containing high concentration of CO_2 (80–98% depending on fuel used), can be compressed, transported and stored. The oxygen for combustion is produced on-site in an air separation unit (ASU), a feasible but expensive process, representing the largest cost component during CO_2 capture.

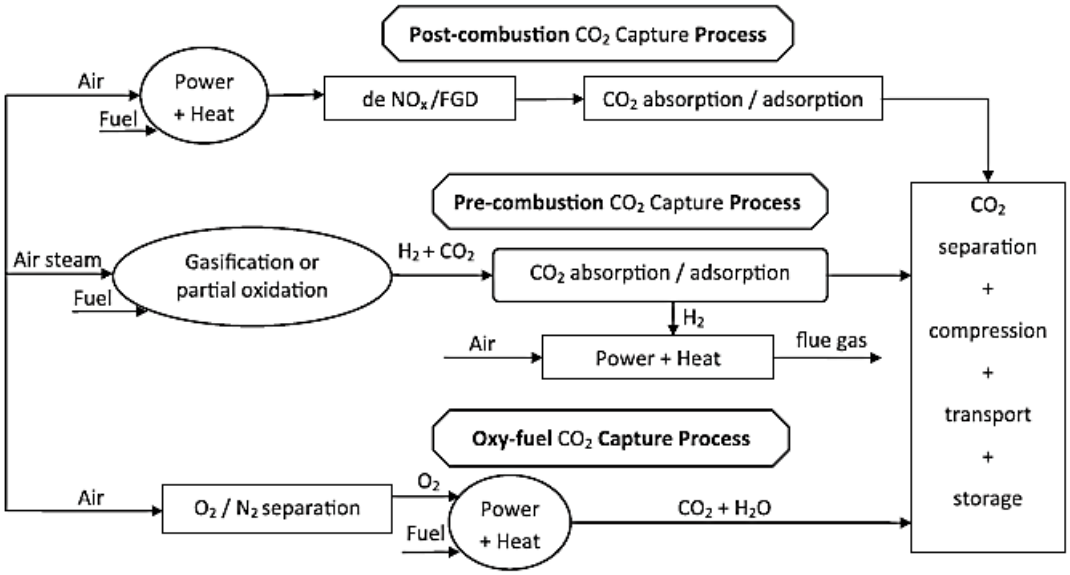

Figure 2.3: CO_2 capture technologies (Leung et al., 2014)

It has not been clear yet, which of these technologies is the most suitable to follow; as previously mentioned, it is true that post combustion CO_2 capture is the most mature technology right now, followed by a vast amount of research. Most of the studies, though, are showing that there is no clear winner at present, given the current technology maturity of power generation, according to Martin Oettinger, Principal Manager for the GCCSI (2011). Table 2.1 summarises the advantages and drawbacks of the three CO_2 capture technologies described above. Post-combustion capture technology offers various advantages, the most important being that it can be retrofitted to existing plants. However, retrofitting results in a reduction of the efficiency of the power generation process, as will be discussed later. Moreover, another important advantage of post-combustion CO_2 capture is that it presents great flexibility; considering that the capture plant shuts down, the power plant process is not affected and can still continue operating. The other two capture options are highly integrated

within the power plant, resulting in complete closure of the plant in case of a failure in the capture system. Pre-combustion, the process with the most significant disadvantages, is mostly suitable for coal-gasification plants, whereas post- and oxy-fuel combustion can be successfully applied to both coal and gas fired power plants.

Table 2.1: Advantages and disadvantages of the different CO_2 capture technologies

Capture process	Application area	Advantages	Disadvantages
Post-combustion	Coal-fired and gas-fired plants	a) Technology more mature than other alternatives b) Can easily be retrofitted into existing plants	a) Low CO_2 concentration affects the capture efficiency b) High parasitic loss, leading to high energy penalties
Pre-combustion	Coal-gasification plants	a) High CO_2 concentration enhances sorption efficiency b) Fully developed technology, commercially deployed at the required scale in some industrial sectors c) Smaller energy penalty (~20%) than current PCC technology (~30%) at 90% CO_2 capture d) Opportunity for retrofit to existing plant	a) Temperature associated heat transfer problem and efficiency decay issues associated with the use of H_2-rich gas turbine fuel b) High parasitic power requirement for sorbent regeneration c) High capital and operating costs for current sorption systems
Oxyfuel combustion	Coal-fired and gas-fired plants	a) No CO_2 separation required b) Mature air separation technologies available c) Reduced volume of gas to be treated (hence required smaller boiler and other equipment)	a) High efficiency drop and energy penalty b) Cryogenic O_2 production is costly c) Corrosion problem may arise

Until very recently, it had been widely expected that IGCC power plants with pre-combustion capture would offer the most cost-effective path forward for CCS. In early 2007, for example, there were more than a dozen IGCC project proposals in the US alone, however there has been very slow progress in the commercialization of these plants for power generation applications (Siefert and Litster, 2013). Due in part to dramatic capital cost increases for this technology - total project costs far higher than expected (> €3 billion) - few IGCC proposals survive today (Wolf, 2013). In addition, much of the energy production in the developing world continues to be based on coal combustion technology. As a result, these facts have stimulated a re-examination of the role of post-combustion capture and its proposed technologies, suggesting that it is the only viable way for short-term CCS implementation into power plants.

However, one important drawback for the process of post-combustion is its large parasitic load. Parasitic load is defined as the energy spent used to run the CO_2 capture system, i.e. regeneration of solvents/sorbents, compression of captured CO_2 for

transport and injection, etc. The concentration in the exhaust flue gas of a combustion process is normally relatively low (specifically 12-15% for a coal-fired and 4-5% for a gas-fired power plant), resulting in increased energy penalties and associated costs for the capture unit to reach the required CO_2 concentration (above 95.5%) for transport and storage (de Visser et al., 2008 and Olajire, 2010). The U.S. National Energy Technology Laboratory (NETL) concluded that implementation of a CO_2 post-combustion capture unit would increase the electricity production cost by 70% (Elwell and Grand, 2006). Recent studies estimated that the cost of electricity would increase by 65% and 32% for post-combustion CO_2 capture in coal and gas-fired plants, respectively (Kanniche et al., 2010).

Table 2.2 presents a cost comparison of the three capture processes for both gas and coal-fired plants, according to Gibbins and Chalmers (2008). They stated that the lowest cost per tonne of CO_2 avoided was reported for coal-fired plants using pre-combustion technology, while post-combustion and oxy-fuel processes presented comparable costs. However, it is remarkable that the same report stated that, the cost per tonne of CO_2 avoided for gas-fired plants using post-combustion capture technology was approximately 50% lower than pre- and oxy-fuel combustion technologies. Furthermore, the pre-combustion CO_2 capture is reported to be the least efficient option, with a thermal efficiency penalty of about 13% and 16% for the coal-fired and gas-fired plants, respectively, according to Leung et al. (2014).

Table 2.2: Cost comparison for different capture processes (IEA, 2006). Costs include CO_2 compression to 110 bar but excluding storage and transportation costs

Fuel type	Parameter	Power plant			
		No capture	Post-combustion	Pre-combustion	Oxy-fuel
Coal-fired	Thermal efficiency (% LHV)	44	34.8	31.5	35.4
	Capital cost ($/kW)	1410	1980	1820	2210
	Electricity cost (c/kWh)	5.4	7.5	6.9	7.8
	Cost of CO_2 avoided ($/t CO_2)	-	34	23	36
Gas-fired	Thermal efficiency (% LHV)	55.6	47.4	41.5	44.7
	Capital cost ($/kW)	500	870	1180	1530
	Electricity cost (c/kWh)	6.2	8	9.7	10
	Cost of CO_2 avoided ($/t CO_2)	-	58	112	102

2.1.2. Post-combustion CO_2 Capture retrofit options

In order to understand the technical - and the associated economical - considerations with regards to retrofitting a CO_2 capture unit to existing power plants, it is critical to examine the differences between the two most important power generation technologies that post-combustion can be applied, namely PC and Natural Gas Combined Cycle (NGCC) power plants. This section provides a fundamental technical description of those two technologies without including a CO_2 capture unit. An overview of the variations between these configurations, mainly focusing on the differences in their exhaust gas composition, temperature and pressure are presented.

2.1.2.1. Pulverized Coal (PC) power plants

The most common power generation technology is the PC power plant. In this technology, coal is combusted with air in a boiler producing high pressure steam (20-25MPa). The steam then drives a steam turbine, which is coupled to a generator producing electricity, as seen in Figure 2.4. The low pressure steam (6-7MPa) exiting the steam turbine is condensed and pumped back to the boiler for the cyclic operation to start over. This thermodynamic cycle converting the thermal energy of the fuel to electric energy is called the Rankine cycle. The flue gas from the boiler is driven to a gas clean-up process that removes particulates and acid gases. The remaining exhaust gas emitted through the stack to the atmosphere contains typically 70% N_2, 13-15% CO_2, 5-10% H_2O, ~800ppm SO_x and ~500ppm NO_x (vol.), cooled at temperatures between 40 and 60°C (Feron, 2016) and at an atmospheric pressure (Herzog, 2001).

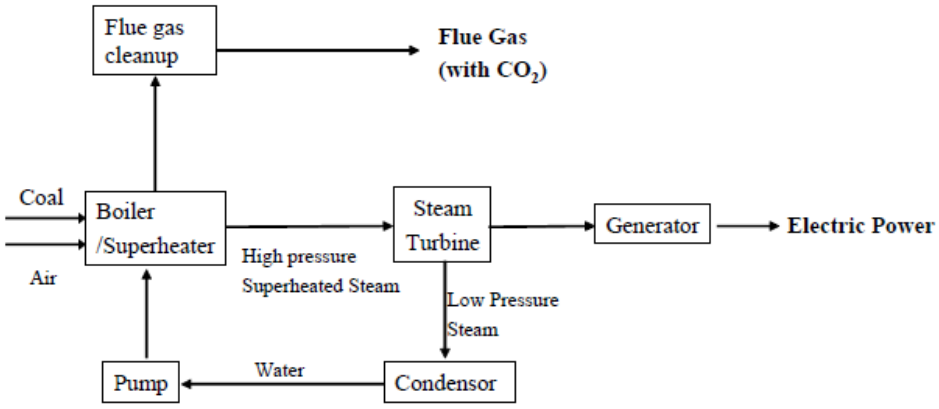

Figure 2.4: Electricity generation in a PC power plant (The national academy press, 2007)

2.1.2.2. Natural Gas Combined Cycle (NGCC) power plants

NGCC power plants use natural gas as a fuel instead of coal and generate electricity utilising a steam as well as a gas turbine, reaching efficiencies up to 50% of the total thermal energy input, significantly higher compared to PC power plants, which typically present an efficiency of 38-45%. These power plants do not require any of the flue gas clean-up units mentioned for the PC plants, since the natural gas is primarily a clean mixture of hydrocarbons, mostly methane, which contains no sulphur and does not produce any particulates when burning (Berstad, 2012).

Figure 2.5 shows the layout of a typical NGCC plant without post-combustion CO_2 capture. The flue gas composition differs significantly from that of the coal-fired power plants; CO_2 is typically 4-5% (vol.), meaning that CO_2 is more diluted than in the case of PC's flue gas, thus creating a lower CO_2 partial pressure, resulting in a smaller driving force for successful initiation and completion of the separation process (IEA, 2012). In terms of flue gas conditions, the waste exhaust gas temperature from the gas turbine decreases as it flows into the heat recovery steam generator (HRSG), which consists of a superheater, an evaporator and an economizer, cooling down the temperature to 30°C for typical NGCC exhaust gas conditions (Mohanty, 2014), while the pressure is atmospheric, similar to a PC power plant.

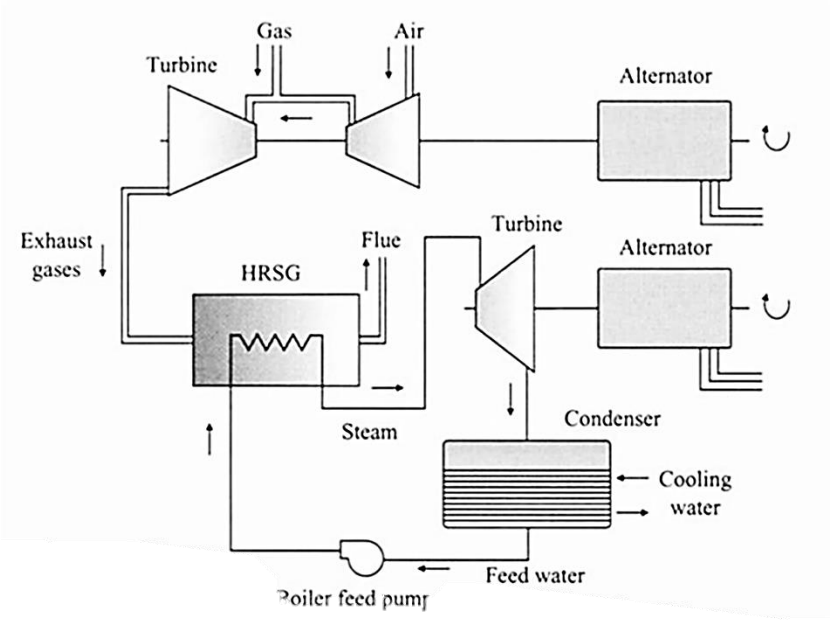

Figure 2.5: Electricity generation in a NGCC power plant (Ramireddy, 2012)

2.1.3. Post-combustion separation technologies

Fossil-fuelled power plants generate the largest amounts of CO_2 emissions among all the industries emitting CO_2 nowadays, responsible for about 33–40% of the total CO_2 emitted in the atmosphere (Carapellucci and Milazzo, 2003; Stewart and Hessami, 2005). CO_2 needs to be separated and captured from the flue gases of these sources before transport and storage. Post-combustion capture can be achieved via various separation technologies, including physical and chemical absorption, cryogenics separation, membranes and adsorption, as seen in Figure 2.6 (Wang et al., 2011). Table 2.3 summarises the advantages and disadvantages of each separation technology.

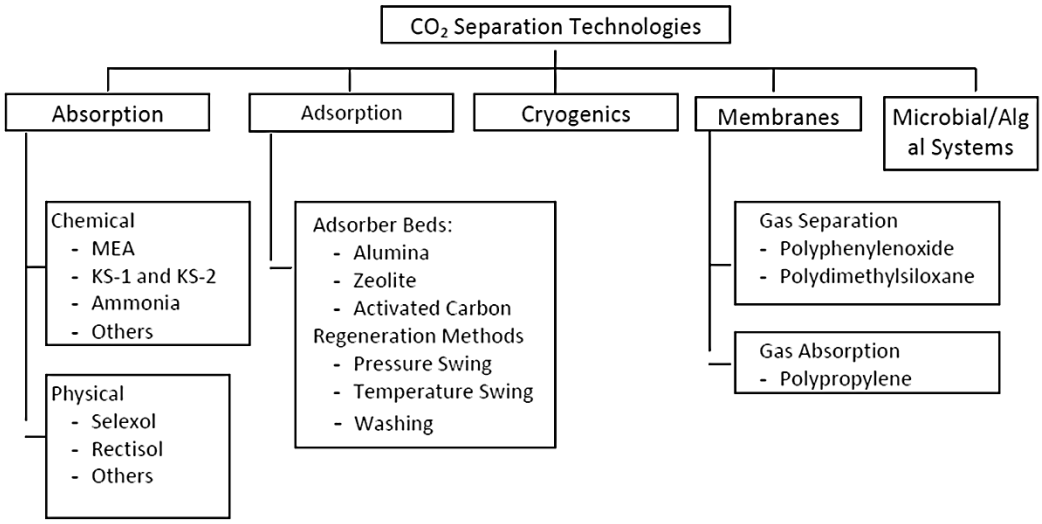

Figure 2.6: Options for post-combustion separation technologies (Wang et al., 2011)

i. Absorption

CO_2 is physically absorbed into a solvent according to Henry's law, while solvent regeneration occurs by applying heat or reducing the pressure or both. Absorption takes place at high CO_2 partial pressures, hence the main energy requirements originate from the flue gas pressurization. As a result, physical absorption is not economically feasible for gas streams with CO_2 partial pressures lower than 15% vol. (Chakravati et al, 2001, IEA, 2004). Typical solvents are Selexol (dimethyl ethers of polyethylene glycol) and Rectisol (methanol).

Apart from physical absorption, chemical absorption has also drawn attention recently. During chemical absorption, CO_2 reacts with a chemical solvent and forms a weakly

bonded intermediate compound. This compound can be regenerated via TSA producing the original solvent and a CO_2 stream (IPCC, 2005). The advantages of this method are that selectivity is comparatively high, producing a relatively pure CO_2 stream. A CO_2/N_2 selectivity of 276 was reported by Trachtenberg and Bao (2005), when using diethanolamine (DEA) 20% (wt.) solution. As a result, chemical absorption is a well suited application for CO_2 separation and capture from industrial flue gases.

Amine-based regenerative chemical absorption processes using aqueous solutions of amine, such as monoethanolamine (MEA), diethanolamine (DEA), diglycol-amine (DGA), N-methyldiethanolamine (MDEA), and 2-amino-2-methyl-1-propanol (AMP) have been widely used for several years for CO_2 capture from gas streams in natural gas, refinery off-gases and synthesis gas processing (Astarita et. al, 1983, Kohl et. al., 1997, Maddox et al, 1998). However, the main problem associated with chemical absorption using amines is degradation through irreversible side reactions, mainly with CO_2 and O_2 but also with NOx and SOx. These reactions can lead to different problems within the process, such as solvent loss, formation of volatile compounds potentially dangerous for the environment, foaming, fouling and corrosion (Gouedard et al., 2012). As a result, a flue gas desulphurisation unit is also needed in the cases where SO_x concentration is higher than 10ppm in the exhaust flue gas, leading to an increased cost of the total plant configuration. Another important drawback of chemical absorption is the large parasitic loss that leads to increased energy penalties, resulting in high Cost of Electricity (COE). Specifically, NETL-DOE (2013) baseline case (referred to as case 10) clearly states that CO_2 capture in a subcritical bituminous coal power plant using MEA as the solvent, results in an 89% increase of Levelised COE (LCOE).

ii. Adsorption

Adsorption is typically classified in two main categories, namely physical and chemical adsorption, also known as *physisorption* and *chemisorption* respectively, depending on the bonding between adsorbate and adsorbent. According to Perry's Chemical Engineers' Handbook *physisorption* (or *physical adsorption*) is adsorption in which the forces involved are intermolecular (van der Waals forces) of the same kind, whereas *chemisorption* (or *chemical adsorption*) involves chemical bonding.

Current adsorption systems have not become suitable for application in large-scale power plant flue gas treatment yet, due to various reasons. Firstly, most commercially available materials present a low CO_2 adsorption capacity (less than 10% w/w of sorbent), which may lead in significant challenges at such scale. Moreover, they also present a generally low selectivity (less than 100 for CO_2 over N_2), being able to treat only the flue gas streams with high CO_2 concentrations, >15% (vol.) (IEA 2004, IEA 2007). However, one of the most important disadvantages of adsorption technology is the regeneration energy needed during the desorption step and as a result, this research focuses on technologies that may enable a less energy intensive process.

Nevertheless, utilisation of sorbent materials for CO_2 adsorption processes is seen as a very promising alternative separation technique, an emerging possible pathway that seeks to reduce the costs attributed to the capture step. The success of such an approach also lies in the potential development of novel materials with high adsorption capacity, high CO_2 selectivity over N_2 or H_2O, durability, relatively fast kinetics of adsorption/desorption and low regeneration energy. This technology is extensively covered in sections 4.2, 5.2.1 and 5.3.1, since it is the focus of this research.

iii. Membrane separation

Membrane separation technology can be used to selectively allow CO_2 to pass through, while blocking other flue gas components, while selectivity depends on the membranes themselves. This technology usually consists of thin polymeric films that separate mixtures based on the relative rates at which composing elements permeate. Permeability differs according to the diffusion coefficients in the membrane material or the relative sizes of the molecules. The difference in partial pressure of the components at both sides of the membrane is the driving force for this permeation. As a result, CO_2 partial pressure is the key factor that is responsible for their separation efficiency. One important advantage of this technology over absorption/adsorption is that membranes are more compact and are not prone to flooding, entrainment, channelling or foaming.

On the other hand, the selectivity of this separation technique is lower compared to other methods, and thus, only a fraction of CO_2 can be efficiently captured, which also leads to a low captured CO_2 purity. Multistage separation can be selected to capture a higher proportion of CO_2 resulting in additional operating and capital cost, according to

Chakravati et al. (2001). However, recent advances in the development of high-efficient membrane technology showed that a CO_2 separation efficiency from 82% to 88% is possible, according to Audus (2000) and Gielen (2003). Moreover, ceramic, metallic membranes (Aaron et al., 2005), as well as polymeric membranes (Yave et al., 2009) could produce membranes significantly more efficient for CO_2 separation than liquid absorption processes, however they are still on the development stage. Consequently, they are suitable for high CO_2 concentration applications (well above 20 vol.%) such as flue gas streams from oxy-fuel and IGCC processes and as a result they are not going to be considered in this research (Favre 2007, IPCC, 2005).

iv. Cryogenic separation

Cryogenic separation is a process that uses distillation principles at very low temperature and high pressure, similar to other conventional distillation processes, except that it is used to separate components of gaseous mixture (due to their different boiling points) instead of liquid. It involves the compression and cooling of gas mixtures in multiple stages to induce phase changes in CO_2 and other gases which allow them to be separated. As a result, the determining step of CO_2 separation from the flue gas stream is condensation. At atmospheric pressure, CO_2 condenses at -56.6°C. This physical technique is sufficient for the treatment of flue gas streams that contain high CO_2 concentrations (typically >90%), since the main disadvantage of this technology is the amount of energy required to complete the necessary CO_2 refrigeration for the process, particularly for dilute gas streams (Consonni et al., 2007). This statement makes cryogenic CO_2 separation an excellent candidate for oxy-fuel combustion CO_2 capture process. As a result cryogenic technology is not considered in this research.

Table 2.3: Advantages and disadvantages of different gas separation technologies

Technology	Advantage	Disadvantage
Absorption	a) High absorption efficiency (90%) b) Sorbents can be regenerated by heating and/or depressurization c) Most mature process for CO_2 separation	a) Absorption efficiency depends on CO_2 concentration b) Significant amounts of heat for absorbent regeneration are required c) Environmental impacts related to sorbent degradation d) Low resistance to impurities
Adsorption	a) Process is reversible and the solid sorbent can be recycled b) High adsorption efficiency achievable (>85%)	a) Require temperature resistant solid sorbents b) High energy required for CO_2 desorption process c) Further research with regard to solid sorbents is needed
Membrane separation	a) No need to add chemicals or regenerate a solvent with membranes b) Low capital costs c) Compact design d) High separation efficiency achievable (>80%)	a) Low driving force for separation in the membrane b) High CO_2 selectivity membranes is required c) Operational issues including low fluxes and fouling d)Limitation on the suitable operating temperature
Cryogenic separation	a) Mature technology b) The amount of CO_2 recovered can reach 90–95% of the flue gas. c) Adopted for many years in industry for CO_2 recovery	a) Only viable for very high CO_2 concentrations (>90% v/v) b) Should be conducted at very low temperatures c) Energy intensive process

2.1.4. Solid sorbents and selection criteria

Several reviews on adsorbents for CO_2 capture and their potential applications can be found in the literature (Choi et al., 2009 and 2010, Sayari et al., 2011). Wang et al. (2011) pointed out that solid sorbents can be classified according to the temperature range where adsorption is performed:

- Low-temperature solid adsorbents (<200°C), which include carbon-based, zeolite-based, metal organic framework-based (MOFs), several alkali metal-carbonate-based, and amine based solid adsorbents;
- Intermediate-temperature (200–400°C) solid adsorbents, including hydrotalcite-like compounds or anionic clays;
- High-temperature (> 400°C) solid adsorbents, such as calcium-based adsorbents and several alkali ceramic-based adsorbents.

The selection of the right sorbent for CO_2 separation is complex (Samanta et al, 2011), due to the fact that they must satisfy some significant criteria in order to be both economical and operational for CO_2 capture from flue gases. These criteria are listed in this section, as described by Yong et al, Zheng et al and Sayari et al. (2002, 2007 and 2011, respectively):

i. *CO_2 adsorption capacity:* One of the most important factors in choosing a sorbent material is its equilibrium adsorption capacity which is depicted by its equilibrium adsorption isotherm. The adsorption capacity of the sorbent determines to a great extend the capital cost of the capture system, because it prescribes the amount of adsorbent required, which also dictates the volume of the adsorber vessels. Consequently, high CO_2 adsorption capacity (>10%w/w of sorbent) leads to reduction in both sorbent quantity and process equipment size.

ii. *CO_2 selectivity:* The selectivity, which is defined as the ratio of CO_2 capacity over capacity of another component - for example N_2 or other contaminants from flue gas streams - at a given flue gas composition, is proportional to the purity of the captured CO_2. CO_2 purity can affect transportation and storage; hence it can have an important impact on CO_2 storage economics.

iii. *Adsorption/desorption kinetics:* One crucial characteristic is its ability to adsorb and desorb fast under the operating conditions. Adsorption/desorption kinetics indicate the cycle time in a fixed-bed adsorption system, which consequently has an impact on the amount of sorbent required. CO_2 adsorption kinetics on a functionalized solid sorbent are influenced by the intrinsic reaction kinetics of CO_2 with the functional group present, as well as the mass transfer or diffusional resistance of the gas phase through the sorbent structures (Serna-Guerrero and Sayari, 2010).

iv. *Sorbents regeneration:* The heat of adsorption, which is a measure of the energy required for regeneration, should be substantially low. In physisorption, adsorption heat ranges between 25 and 50 kJ mol^{-1}, whereas in chemisorption the amount is higher, namely 60 to 90 $kJmol^{-1}$. The ease of regeneration as well as the preservation of the sorbent material will also help to reduce the cost of capture. One part of this research focuses on an innovative pathway for sorbent regeneration via microwave heating and is discussed later.

v. *Mechanical strength of sorbent particles:* The sorbent must demonstrate microstructure and morphological stability and retain the CO_2 capture capacity

after multi-cycling between adsorption and regeneration steps. Microstructure and morphological stability of tailored regenerable sorbents in multi-cycle operation is critical to maintain high kinetics.

vi. *Chemical stability/tolerance to impurities:* Solid CO_2 capture sorbents - in particular, amine-impregnated sorbents - have to be durable in an oxidizing environment of flue gas and be resistant to any flue gas contaminants. It is likely that contaminants such as SO_x, NO_x and heavy metals may also require separation from flue gas, because they negatively affect the CO_2 adsorption capacity of the sorbent materials, according to Adams (2010).

vii. *Sorbent costs*: Tarka et al. (2006) have used a baseline of approximately £7/kg for sorbents in their sensitivity analysis for economic performance. According to their research, the best scenario involves sorbents that cost approximately $5/kg, whereas a non-economical sorbent is priced $15/kg sorbent.

viii. *Availability*: Another important factor for the sorbent selection is its availability in terms of quantity. Abundant raw materials for sorbent production can lead to a positive effect in the adsorption process economics (Olivares-Marin, et al., 2010). For instance, the Kawasaki CO_2 Capture system (KCC) bench plant employs a fixed bed column, loaded with one ton of the adsorption material, with a capacity of 10 t_{CO2}/day (Okumura et al., 2013).

2.1.5. Cyclic adsorption processes

CO_2 adsorption separation technology, similar to absorption, is a cyclic process, meaning that after saturation of the adsorbent with CO_2 has been achieved, a desorption step, or regeneration, is required. As a result, this step, which is fundamental for the re-use of the solid sorbent and for the recovery CO_2 for storage, is usually a crucial part of the capture chain, being significantly responsible for the efficiency of the entire process. There are two main technologies used to regenerate the adsorbents at a commercial scale nowadays, namely Pressure Swing Adsorption (PSA) and Temperature Swing Adsorption (TSA) and they are discussed in this section.

i. Pressure Swing Adsorption (PSA)

PSA is the most widely used technology applied for gas separation processes, being in practice for more than 60 years (Voss, 2005). It was firstly invented and used by

Skarstrom in 1959, for the separation of N_2 and O_2 from air applying a four step cycle (Skarstrom, 1960). The fundamental theory of the PSA process is simply based on the variations in working capacity presented by an adsorbent-adsorbate system when periodic alterations of the operating pressure are applied. However, the configuration of each PSA application depends on the required process, as a result different steps will be applied for a process aiming at purifying the less adsorbed component, or for a process that intends to concentrate the most adsorbed one. In the first case, the more adsorbed compound is released to the atmosphere, regardless its purity, using rapid PSA or piston-driven PSA systems (Ruthven et al., 1993) that result in cycles that last much shorter (less than 20 sec.) than the conventional systems (120-1200 sec.).

As a rule of thumb, PSA is fully efficient when the concentration of the components to be removed is relatively significant (>10-15% vol.). In this case, saturation of the column with the heavy compound/adsorbate is achieved relatively fast and since the pressure of the system can be changed rapidly, the time between adsorption and desorption is balanced (Grande, 2012). Moreover, the PSA process is preferred to other technologies when the process is carried out at elevated pressures (>20bara). Otherwise, when the concentration of the adsorbate is low (0-15% vol.), or when the process is at low pressure (for example atmospheric), other options like temperature swing adsorption (TSA) may need to be considered. For a low concentration adsorbate, the PSA technology may result in a much longer desorption step, whereas for low pressure processes the installation should also include additional vacuum pumps and compressors, both resulting in a more complicated process, increased capital cost and reduced efficiency (Cherbanski et al., 2009). A solution to the above issues would be to apply Vacuum PSA, known as VPSA; however, this technology is not applicable to post-combustion unless it is combined with a TSA step (Mejdell, 2010). As a result, PSA was not considered in this research, since the exhaust flue gas of PC and NGCC power plants is at atmospheric pressure and the CO_2 concentration is 12-15% and ~5% (vol.) respectively.

ii. Temperature Swing Adsorption (TSA)

Apart from PSA, an alternative technology to achieve efficient desorption of the adsorbent from a solid material is Temperature Swing Adsorption (TSA), where the increase in bed temperature operates as the driving force for the regeneration to take

place. Figure 2.7 shows the differences between TSA and PSA cyclic processes for a given adsorption isotherm. A TSA process consists mainly of three fundamental steps:

- ✓ Adsorption or production step at low temperature.
- ✓ Application of heat, breaking the physical or chemical bonds between adsorbent and adsorbate, initiating regeneration. Direct means, such as utilisation of hot steam or indirect means – external heating - including heating jackets, coils or microwave applications can be employed.
- ✓ Bed cooling back to the adsorption conditions, once desorption process is completed, often by using purge/inert gas.

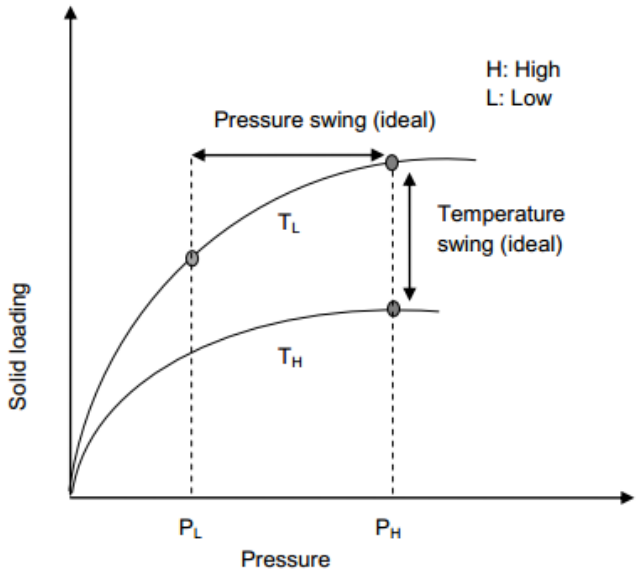

Figure 2.7: Comparison of TSA and PSA for the regeneration of solid adsorbents (Rackley, 2009)

TSA is particularly used when the adsorption step is carried out at a low temperature (Cherbanski et al., 2009), meaning that the desorption process will take place at a higher temperature, as reported in Figure 2.7. This temperature difference between the two steps is the driving force that enables the regeneration to initiate, effectively breaking the bonds between adsorbate and adsorbent. Consequently, the main advantage of TSA over PSA is its ability to separate efficiently strong-bonded adsorbates onto adsorbents (i.e. chemisorption), since a small change in temperature can result in a significant change in the loading amount. Moreover, another advantage is that the pressure of the process does not play a significant role, as in PSA, meaning that TSA can be applied to processes operating at low as well as high pressures. As a result, taking into

consideration the above statements, TSA is usually preferred for absorption/adsorption processes at low temperature (20-60°C) and atmospheric pressure, such as post-combustion CO_2 capture, where the exhaust flue gas temperature is usually between 40 and 50°C and pressure of 1atm (Cherbanski et al., 2009).

However, a major drawback of the TSA process is the high energy intensity and the relatively long duration of the aforementioned steps, compared to PSA; the significant thermal inertia of the solid sorbent bed as well as the considerably low heat capacity of the gases that are used during regeneration are the most important reasons for the long-lasting desorption step during TSA. As a result, larger sorbent beds are required for TSA for a given throughput, compared to PSA which is a faster process utilising smaller beds, since pressurisation and depressurisation can be achieved more rapidly (Rackley, 2009). It should be mentioned that pressure transients can be rapidly achieved in a fixed bed reactor by switching the valve settings, whereas TSA's temperature alterations require heating the metallic wall of the reactor at first and then conductively the total adsorbent bulk mass resulting in a long process requiring hours or even days (Bonjour et al., 2002) to complete one cycle, and hence, affecting the cycle productivity. Another disadvantage of the TSA process is that the desorbed compound, in this case CO_2, is considerably diluted with the heating gas stream, resulting in a low purity recovery gas stream (Cherbanski et al., 2009).

2.1.6. Challenges in post-combustion CO_2 capture

Post-combustion CO_2 capture technologies are believed to be the best candidates for short term implementation at fossil fuel fired power plants, since they can be retrofit to existing facilities with the least difficulty, however at the current state of development, they are presented as a costly solution for CCS. Currently, the most mature and commercially available separation technology to be used in post-combustion is chemical absorption with amine scrubbing. However, every post-combustion capture approach still suffers from the same challenge, namely the substantially large parasitic load that is imposed on the power plant, reducing its efficiency while increasing its CAPEX and OPEX. Large volumes of flue gas to be treated mean that large quantities of liquid (or solids for adsorption) are needed for CO_2 separation and capture along with large equipment. Consequently, the energy needed to regenerate the solvent/sorbent poses as the most significant challenge in the CCS chain.

As a result, intensification of the cyclic regeneration processes, such as PSA and TSA, is crucial and is the focus of this research. This can initially be achieved by reducing the cycle time, resulting in more CO_2 captured for a given quantity of sorbent. However, time reduction of a cyclic process could result in a decreased working capacity (the amount of CO_2 that is expected to be captured by a specified amount of adsorbent during one adsorption–desorption cycle) per cycle of the adsorbent. This would mean that CO_2 will be retained in its pores, decreasing CO_2 recovery and sorbent's CO_2 adsorption capacity in the next cycle, while increasing pressure drop (Rezaey et al., 2010). The second parameter that needs to be investigated is the energy consumption during the cyclic process; energy efficient steps, including waste heat utilisation, reactor optimisation and the use of innovative processes, such as microwave heating need to be considered (Song et al., 2016). Microwave Swing Adsorption (MSA) has not been a field of research for CO_2 capture, although this technology has shown great results for other processes, including removal of water vapor, methyl-ethyl-ketone (MEK) and tetrachloroethylene from contaminated air streams (Vallee, 2006 and Hashisho et al., 2005), as well as NO_x reduction (Roberts et al., 2005) and wastewater purification (Ohgushi et al., 2001). MSA technology may result in time and energy savings, mainly due to the significantly different heating method applied, compared to TSA as described in the next sections (Section 2.2).

2.2. Microwave Swing Adsorption (MSA)

2.2.1. Process intensification and microwave technology

Process intensification (PI) is widely considered as one of the most promising strategies for the power industries nowadays and one of the most important areas of research for modern chemical engineering. It includes the development of novel apparatuses and techniques that, compared to those commonly used today, are expected to bring dramatic improvements in manufacturing and processing, substantially decreasing equipment-size/production-capacity ratio, energy consumption, or waste production, and ultimately resulting in lower cost, sustainable technologies (Ramshaw, 1995). Moreover, the three most widely cited books about PI (Stankiewicz and Moulijn 2003, Keil 2007, Reay et al. 2013) describe it as a bundle of diverse technologies, while Van Gerven and Stankiewicz (2009) defined four basic principles regarding process research and development (r&d), namely spatial, thermodynamic, functional, and temporal,

which need to be addressed in order to intensify a chemical process. From a pure process engineering perspective, a PI approach is a strategy to enhance mass and energy transfer phenomena across all the plant operations, focusing mostly on the thermodynamic domain of the aforementioned principles.

As a result, the main area of study focuses on how energy can be transferred from the source to the recipient in the required form and amount, at a specific moment and position. The conventional input of energy in chemical processing systems occurs via conductive heating with a steam boiler as a typical heat source. Nonetheless, there is a large variety of other forms of energy that can be applied for PI, including ultrasound (for reactions or crystal nucleation), light (in photocatalysis) and microwaves. Utilisation of microwave energy for heating processes has been known for a long time, and the development of microwave ovens has more than 60 years of history (Clark, 1996).

During recent years, microwaves have been extensively used for carrying out chemical reactions and have become a useful non-conventional energy source for performing chemical-organic synthesis (Agazzi and Pirola, 2000), offering great advantages compared to conventional heating. In particular, lower energy consumption, reduced heating time, volumetric heating, selective and enhanced desorption and separation, are some of the advantages that heating with electromagnetic waves offers (Yuen and Hameed, 2009). In general, microwaves are considered to be an intensified solution to the problem of energy consumption using conventional heating. Microwave assisted operations are recognised as a very promising pathway for intensification of chemical processes with the potential for lowering the cost of the reaction and the efficiency penalty that is imposed on the process (Cherbanski et al., 2009).

Nowadays, microwave heating applications can be found in several sectors of chemical/process industries, such as:

- Food industry (drying, cooking, tempering, pasteurization, sterilization, thawing)
- Rubber and plastic industry (preheating of resins and rubbers, vulcanization, bonding, curing, welding, shrinking)

- Ceramics (drying, joining, sintering)
- Pharmaceutical industry (vacuum drying)
- Textile (drying, dye fixation, control of moisture content)
- Paper and wood (drying, gluing)

The most common microwave applications can be found in food industries for food processing, sterilization, pasteurization, drying, etc. Furthermore, microwaves are utilized for other processes as well, namely soil remediation, pyrolysis of biomass and organic waste and heterogeneous catalytic reactions (Menendez et al., 2010). Regeneration of various types of adsorbents via microwave heating has also gained attraction recently, including silica gel (Reuss et al, 2002), zeolites with different silica to alumina ratio (Price et al., 1997 and 1998), activated carbon (Ania et al., 2004, 2005 and 2007, Coss et al., 2000) and polymeric adsorbents (Price et al, 1997 and 1998). **However, the concept of using microwave energy in CO_2 capture applications to replace conventional cyclic TSA and/or PSA processes is quite novel. Accordingly, this research focuses on the optimisation of the desorption process by utilising electromagnetic waves for more efficient heating of the adsorbents and the parameters that affect the regeneration process via MSA and TSA are thoroughly discussed in the next chapters.**

2.2.2. Microwave heating process

Microwaves are electromagnetic waves with frequencies between 0.3 and 300 GHz (Meredith, 1998; Pozar 1998) placed in the high frequency range of radio waves (Ultra High Frequency (UHF), Super High Frequency (SHF), Extremely High Frequency (EHF)), with a corresponding wavelength (λ) between 1m and 1mm (Figure 2.8). In order to avoid interference with telecommunication devices, there are only some specific frequencies that have been allocated for industrial and domestic microwave processes. The most commonly used frequency is 2450±50MHz, typically in domestic ovens, while 915±13 MHz is used by industrial microwave systems (Meredith, 1998)), which according to the equation

$$\lambda = {}^{c}/_{f} \qquad (2.1)$$

where c is the light velocity (m/s) and f is the frequency (Hz), result in the following wavelengths (λ) of 12.24 and 32.75 cm, respectively.

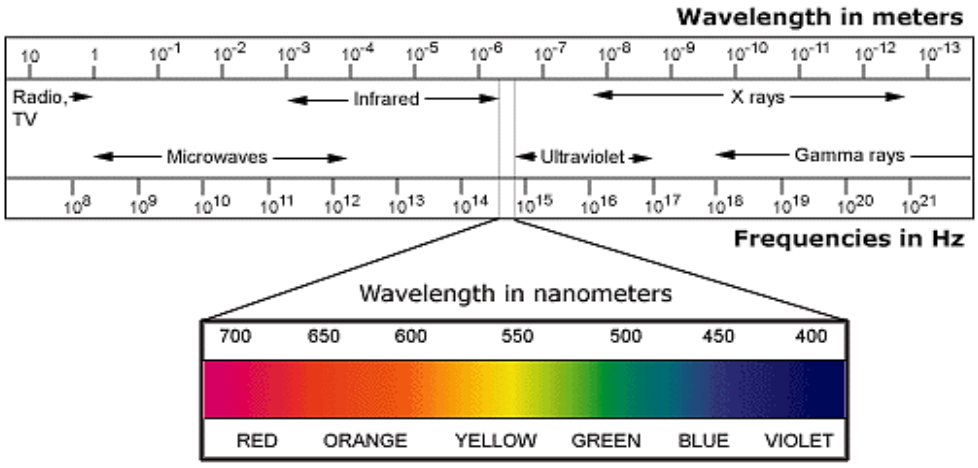

Figure 2.8: The electromagnetic spectrum and corresponding wavelengths (Jewett, 1994)

Generally, materials can be classified into three groups depending on their ability to be heated by microwaves, as seen in Figure 2.9 (Stefanidis et al., 2014):

- conductors, such as metals or graphite, that reflect microwaves from their surface;
- insulators, such as polypropylene or quartz glass, that absorb small amounts of microwave energy, as microwaves penetrate the material; and
- absorbers, or the so-called “dielectric” materials, such as silicon carbide, which absorb the microwaves, resulting in heat generation.

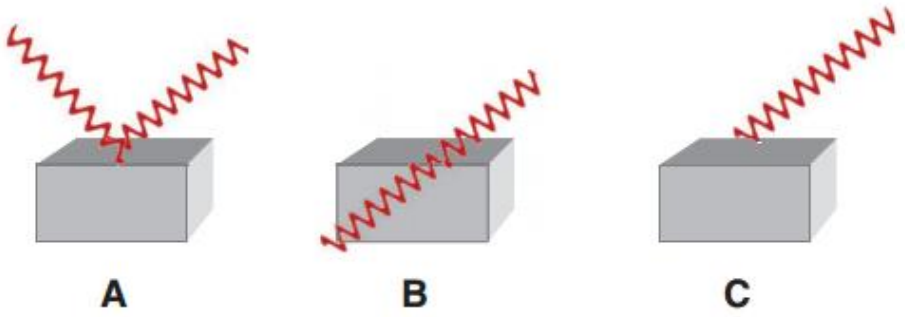

Figure 2.9: Microwave interactions with different types of materials: (A) conductive material, (B) insulating material, and (C) absorbing material (Durka et al., 2009).

However, the amount of microwave energy absorbed by the dielectric materials differs depending on the material properties, particularly the relative permittivity (ε_r') and the relative dielectric loss factor (ε_r'') of the material, as discussed below.

2.2.3. Microwave heating mechanisms

There are three types of heating phenomena caused by the application of electromagnetic waves, namely:

- Conduction loss heating
- Dielectric heating and
- Magnetic loss heating.

Combining those three mechanisms, the thermal energy (P_{th}) produced per unit volume due to microwave irradiation can be expressed by equation 2.2:

$$P_{th} = \frac{1}{2}\sigma_{el} \mid E \mid^2 + \pi f \varepsilon_0 \varepsilon_r'' \mid E \mid^2 + \pi f \mu_0 \mu_0'' \mid H \mid^2 \qquad (2.2)$$

Where σ_{el} is the electrical conductivity, |E| and |H| represent the strength of the electric and magnetic field of microwaves respectively, ε_0 is the permittivity in vacuum, μ_0 is the magnetic permeability in vacuum and μ_0'' is the relative magnetic loss. The first term of the above equation (2.2) describes heating due to conduction losses, while the second and the third terms denote the dielectric and the magnetic loss heating respectively. As a result, microwave heating depends on the electric, dielectric and magnetic properties of the substance to be heated.

2.2.4. Dielectric heating

The inability of partially bound charges to follow the rapid changes in a high frequency electric field gives rise to one mechanism of microwave heating, namely dielectric polarisation (Whittaker et al., 1994). The phenomenon of polarisation appears when a dielectric material is exposed to an electric field. In simple terms, polarisation is defined as the dipole moment per unit volume of the dielectric material. This dipole moment is equal to the product of the charge of the dipole and the distance between the

two charged partners. As seen in Figure 2.10 (von Hippel, 1954; Smyth, 1955; Metaxas and Meredith, 1983), there are several polarisation mechanisms, depending on the frequency of the applied field and the electrical characteristics of the material. For example, in the case of industrial microwave heating applications, the orientation polarization mechanism lies at frequencies above 1 GHz (Metaxas and Meredith, 1983).

Firstly, electronic polarization can be found in the ultraviolet light frequency regime and is a rapid process, requiring 10^{-15}s. It is the result of the displacement of the negative electrons with respect to the positive atomic nuclei in response to the applied electric field. Hence, an induced dipole moment is formed.

Secondly, atomic polarization stems from the unequal electron distribution between the molecule atoms which results in the displacement of the atomic nuclei, as the electron clouds are forced towards the stronger binding atom (Hashisho, 2007). In the absence of an electric field, the polar material denotes a permanent dipole moment. However, when the electric field is present, the equilibrium area of the atoms changes and an induced dipole moment is created, combined with the permanent one. This process requires about 10^{-14} s, placed within the infrared light frequencies.

Thirdly, in the case of dipole (or orientation) polarization, the electric field component of the microwaves results in induced dipoles to rotate with the alternating field. This molecular movement produces friction among the rotating molecules, and the energy is subsequently dispersed as heat. Non-polar molecules with symmetric charge distributions, such as CO_2, have a very small loss factor (ε") and dipole moment and consequently exhibit limited microwave energy absorption. On the other hand, H_2O and a wide range of organic compounds such as MEK comprise of polar molecules as they have charge asymmetry that creates large dipole moments. The time required for the dipole polarization depends on the frictional resistance of the medium to the change of molecular orientation. For gases, the process takes about 10^{-12} s, relating it with infrared light frequencies region. Low-viscocity liquids with small molecules, dipolar polarisation needs about 10^{-11}s to take place, corresponding to the microwave frequencies region, while for viscous liquids or large molecules about 10^{-6} s are needed (radio frequencies region).

Lastly, space charge (interfacial or Maxwell-Wagner) polarization occurs at the boundary of heterogeneous materials with varying dielectric properties, or in dielectric solid materials with charged particles which are free to move in a delimited zone of the material, such as π-electrons in carbon materials, as Zlotorzynski (1995) pointed out. Since the electrons cannot couple with the changes of phase of the electric field, the energy is dispersed in the form of heat, known as the Maxwell-Wagner effect. This accumulation of charge requires flow of current through the components of the material, which may require seconds or minutes, so that it may be witnessed only at very low frequencies. **As a result, the main heating mechanism used for the completion of this research was the Maxwell-Wagner effect, as most of the materials used for the experimental work were carbon based. However, the effect of moisture is also discussed and explained, trying to take advantage of a binary mechanism combining dipolar polarisation and Maxwell-Wagner effects for a more efficient microwave heating.**

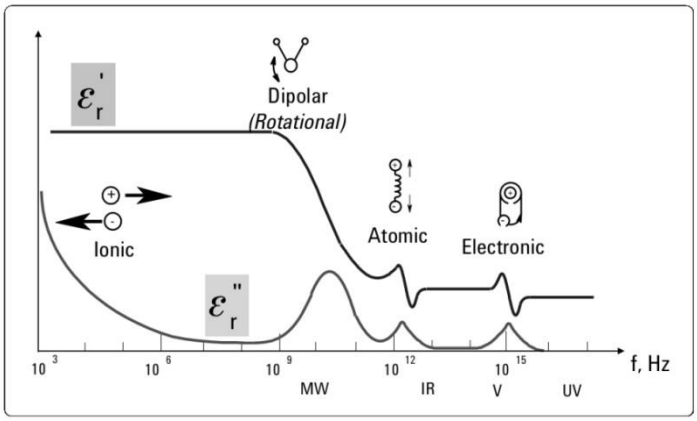

Figure 2.10: Polarization mechanisms at various frequencies (von Hippel, 1954)

2.2.5. Dielectric constant, loss factor

The ability of a material to convert microwave energy into thermal energy can be expressed by the loss tangent, also called the dissipation factor (Weissberger and Rossister, 1972), described in equation 2.3:

$$\tan \delta = {\varepsilon_r''}/{\varepsilon_r'} \qquad (2.3)$$

where, the relative permittivity (ε_r') provides the polarizing level of a molecule in an electromagnetic field. Moreover, the relative dielectric loss factor ε_r'' shows the measure of a material's ability to convert energy to heat, whereas the loss angle (δ) depends on the phase orientation of the molecules and change in the electric field.

The frequency dependencies of ε_r' and ε_r'' are presented in equations 2.4 and 2.5:

$$\varepsilon_r' = \varepsilon_\infty' + \frac{(\varepsilon_0' - \varepsilon_\infty')}{(1+\omega^2\tau^2)} \tag{2.4}$$

$$\varepsilon_r'' = \frac{(\varepsilon_0' - \varepsilon_\infty')\omega\tau}{(1+\omega^2\tau^2)} \tag{2.5}$$

where ε_∞' is the high frequency constant, ω the angular frequency ($\omega = 2\pi f$) and τ is the relaxation time which is the exponential decrease with time of the polarization in a dielectric when the externally applied electric field is removed:

$$\tau = \frac{4\pi r^3 \mu_d}{k_B T} \tag{2.6}$$

where r is the radius of the dipole, μ_d the dynamic viscosity, k_B the Boltzman's constant and T the temperature. It can also be defined as the time at which the polarization reaches 1/e (e being the Napier's constant) of its initial value (Smyth, 1955). It can be derived from equations 2.4-2.6 that the efficiency of the energy conversion depends on the dielectric properties of material as well as on the frequency of the applied electric field and the temperature (Cherbanski et al., 2009).

It is notable that the loss factor of a material depends on its physical state; for example, water in its solid form has a low loss factor, however in its liquid form has a high loss factor, as presented in Table 2.4. Moreover, this table also shows that another parameter that affects the ability of a material to absorb microwave energy and convert it into heat is its form; it is evident that coal has the lowest loss tangent value (0.02-0.08), while activated carbons' values range between 0.22 and 2.95, depending on the temperature of the sample. It is interesting to mention that the loss tangents of most of the carbons, except for coal, are higher than the loss tangent of distilled water, which is

an excellent microwave absorber due to its polar nature ($tan\delta$ of distilled water= 0.17 at 2.45 GHz and 298 K).

Table 2.4: Dielectric properties of selected materials, in various states, at 2.45GHz (Hashisho, 2007 and Menéndez et al., 2010)

Material	T (°C)	tan δ
Water, ice	-12	0.001
Water, distilled liquid	25	0.169
Water, distilled liquid	85	0.05
Coal	25	0.02-0.08
Carbon foam	25	0.05-0.2
Charcoal	25	0.11-0.29
Carbon black	25	0.35-0.83
Activated carbon	25	0.57-0.8
Activated carbon	125	0.22-2.95
Carbon nanotube	25	0.25-1.14

2.2.6. Penetration depth and heating uniformity

The penetration depth is a characteristic length that describes the gradual absorption of microwave power. This depth can be defined as when incident microwaves lose their power to about 37% of their initial value at the surface. The penetration depth (D_p) can be expressed by equation 2.7, as expressed by Bathen (2003) and Cherbanski et al. (2009):

$$D_p = -\frac{1}{Im(\beta)} \tag{2.7}$$

With

$$\beta = \frac{2\pi f}{c}\sqrt{\varepsilon_r' - j\varepsilon_r''} = \frac{2\pi f\sqrt{\varepsilon_r'}}{c}\sqrt{1 - jtan\delta} \tag{2.8}$$

Hence, for materials with low-to-moderate loss tangents (tan δ< 1) one may write the approximate relation

$$\tan\delta \sim \frac{1}{D_p} \tag{2.9}$$

meaning that a material's ability to convert (microwave) electrical energy into heat is approximately inversely proportional to its penetration depth. Consequently, D_p can be

calculated provided that ε_r' and ε_r'' are known. The thickness of the absorbing material should be less than the penetration depth. Otherwise, more than 37% of the microwave power will be lost and may contribute to overheating (Cherbanski et al., 2009).

The penetration depth could also describe how heat is distributed in the workload, i.e. the target object to be heated. A small D_p value - relatively to the workload dimensions – would suggest that most of the energy is dissipated within the proximity of the object surface and hence non-uniform heating and serious temperature gradient may be expected. This effect can be overcome if the volume of the workload is a very small proportion compared to the microwave cavity (for instance <10%). Depending on the size of the cavity relative to the workload and the location of the microwave source (magnetron), the exponential may extend from more than one face of the workload. For discrete workloads of simple rectangular shape, the sum of exponentials from each face results in addition at the edges, resulting in a high temperature increase at the corners (Meredith, 1998).

For a semi-infinite ideal slab (i.e. with homogeneous $\varepsilon_r' \; and \; \varepsilon_r''$) targeted by normal waves, the temperature rise at depth z is given by the following equation (Meredith, 1998, Datta and Anantheswaran 2001):

$$T_z = T_0 \exp(^{-z}/_{D_p}) \tag{2.10}$$

Where T_z and T_0 are the temperatures at depth z and at the starting point respectively. Particulate workloads packed in beds may also suffer from non-uniform heating due to concentration or displacement current around the contact points between single particles. One of the major drawbacks of the non-uniform heating is the creation of 'hotspots'. This phenomenon occurs due to the nonlinear relationship between the temperature and the electromagnetic and thermal properties of the material. An uncontrolled microwave heating may produce very high temperatures at various locations within the material - hotspots (Reimbert et al, 1996) - which may lead to the sintering of the adsorbent, which will inevitably reduce its adsorption capacity. The magnitude of this effect, however, depends on the thermal properties of the bed's material, which significantly influence the way heat is conducted away from the hot spot into the main thermal mass of the particle bed. When this heat flow equals the rate

of heat dissipation at the hotspot, then equilibrium is reached. Local geometry of the bed and thermal diffusivity of the particles are crucial parameters that affect the temperature uniformity of the bulk (Hossan et al., 2010).

In the literature, there has been an extensive effort to understand, model and determine the formation of hot and cold areas during microwave heating. Sakai and Wang (2005) confirmed the influence of dielectric properties of a material on the temperature distribution. Moreover, Gunasekaran and Yang (2004 & 2007) stated that parameters such as size, geometry, pulsating ratio, and microwave processing time are also factors that influence the sample temperature distribution and concluded that the pulsed microwave heating provides a higher level of uniformity compared to continuous microwave heating. Another interesting research by Funawatashi and Suzuki (2003) classified the reasons for non-uniform heating into two categories based on the size of the workload; in smaller objects (smaller than the penetration depth) heating applications, standing wave is dominant as interaction between transmission and reflection waves takes place within the object. On the other hand, for larger size workloads, the rapid decay of incident wave is the primary cause for the non-uniform heating.

Modelling of the hotspot formation has also been a wide field of research; Smyth (1992) developed a model to show the influence of material conductivity and thermal diffusivity on hotspot formation. Moreover, Kriegsmann (1997) developed a model to describe the physical mechanism and mathematical structure of hotspot formation and presented a numerical solution to the problem. The equations of this model describe both the physical mechanism as well as the mathematical structure for the hot-spot formation. Furthermore, Zhang et al. (1999) investigated hotspot formation during H_2S decomposition in a metal catalysed bed. This research estimated that hotspots in a metal catalysed bed have a dimension of 90-1000μm and occur at a temperature 100-200°C higher than that of the bulk.

In the case of carbon materials, where delocalized π-electrons are allowed to relocate between relatively broad regions, an additional and very significant phenomenon was observed during microwave heating reported by Menéndez et al. (2010), where the kinetic energy of some electrons increased allowing them to violently abandon the

material, which resulted in the ionization of the surrounding atmosphere. Macroscopically, this abnormality is noticed as sparks or electric arcs formation, however, microscopically, this hot-spot formation can be regarded as formation of plasma. More specifically, these are actually micro-plasmas, since they are restricted to a tiny area inside the sorbent bed and last for just a fraction of a second, depending on the power used for the heating process and the void space inside the packed bed that stems from the materials' shape. An extensive micro-plasmas' formation may result in more destructive implications of the workload and/or microwave system, especially if a scaled-up is considered.

2.2.7. Factors Affecting Dielectric Properties

One of the most important parameters about electromagnetic energy is the dielectric properties of the heated material, since microwave heating is controlled by the dielectric loss factor. As a result, characterization of the material's dielectric properties is essential for the proper design of microwave applicators and for the prediction of the penetration depth. However, dielectric properties are affected by various factors, depending on application:

- Temperature
- Moisture
- Frequency

A research carried out by Liu et al. (2013) proved that moisture content is the major influence factor contributing to the variation of dielectric properties. Dielectric constant, loss factor and loss tangent all increased linearly with increase in moisture content, because water content increased the microwave absorption potential of the medium. The same research showed that the penetration depth was found to decrease with an increase in the moisture content, since the penetration depth is inversely proportional to the dielectric constant. They stated that temperatures between 20 to 100^{o}C were found to have a positive effect on dielectric constant and loss factor.

The frequency of the electromagnetic waves has a significant effect on the dielectric constant and loss factor of most materials. However, this dependence has little

importance from a practical point of view; as explained previously, industrial applications of microwaves are set to two specific frequencies – 915 and 2450 MHz – selected carefully to avoid interferences with other frequencies used for telecommunications and defence applications. Moreover, frequency is not a parameter in this research, as all the experiments are conducted at a fixed value of 2.45GHz.

2.2.7.1 Effect of temperature

The dielectric properties of a material are temperature dependant; nonetheless, this dependence is a function of the dominant relaxation mechanism for each operating frequency (Metaxas and Meredith, 1983). An increase in temperature results in a decrease of the relaxation time and a shift of the peak of the loss factor at higher frequencies.

In the relaxation regime, the dielectric constant increases proportionally with increasing temperature; however, the loss factor may increase or decrease depending on whether the operating frequency is higher or lower than the relaxation frequency. Outside the relaxation regime, the dielectric constant decreases when the temperature increases. However, in the case of an increasing loss factor with temperature, the 'runaway effect' may appear. This effect is responsible for the uncontrolled increase of the workload temperature derived from the positive slope of the loss factor versus temperature response (Metaxas and Meredith, 1983, Datta and Anantheswaran, 2001).

2.2.7.2 Effect of moisture

Water is considered a great microwave absorber due to its strong polarity. It can effectively absorb microwaves either as a bulk liquid or when it is coupled with a solid material. In wet materials, water can be 'free' (residing in capillaries and cavities), 'bound' (chemically combined to other molecules) or 'adsorbed' (physically adsorbed to the surface of a solid material). As a result, the presence of water as moisture can generally increase the effective loss factor of a material and thus promotes efficient microwave heating. However, the amount that the dielectric properties are affected from moisture depends on the state of the water; 'Bound' water molecules in the first uni-molecular layer along the surface of a material are less rotationally free than 'free' water in capillaries or cavities (Hashisho, 2007). As a result, the loss factor for 'free'

water is higher than in the case of ‘bound’ water molecules (Metaxas and Meredith, 1983). For the same amount of water, the loss factor in the ‘free’ bulk state is usually > 10% compared to the value in the ‘bound’ or ‘adsorbed’ state (Meredith, 1998). Practically, for a given frequency, the change of the loss factor against the moisture content in a wet solid creates two regions related to ‘bound’ and ‘free’ water (Figure 2.11). For a low moisture content (<20%), water found in the “bound” state undergoes a slow increase of the loss factor with increasing moisture content until it reaches the critical moisture content. Then, for high moisture content (>40%), ‘free’ water is predominant and shows a faster increase in the loss factor with increasing moisture content.

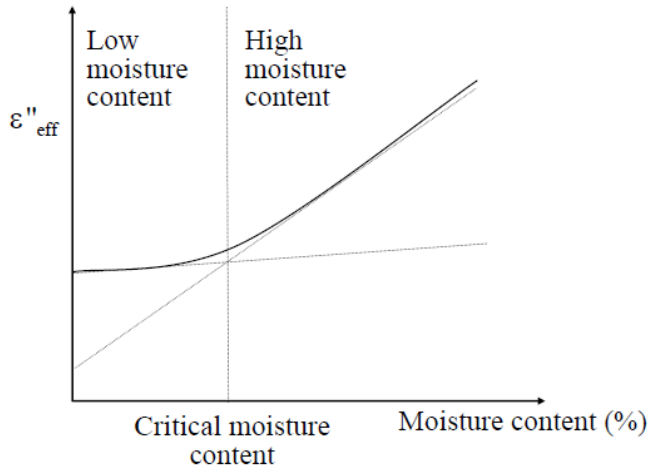

Figure 2.11: Variation of effective loss factor with moisture content (Metaxas and Meredith, 1983)

2.2.8. Basic microwave equipment

The microwave equipment - also frequently called ‘applicators’ - used in heating processing can be divided into two main categories: the multimode, being the most widespread ones, known for its flexibility to be used in various applications from domestic use to large scale industrial reactors, and the mono (or single)-mode applicators. A multimode applicator consists of a rectangular-shaped closed metal box, referred to as ‘cavity’ (Figure 2.12), with at least two dimensions of the box relatively longer than half of the free space wavelength of the radiation, 122 mm at 2450 MHz (Bradshaw et al., 1998). A waveguide, or a transmission line, carries the microwave energy into the cavity which consequently is absorbed from a high-loss material, placed within (Mehdizadeh, 2009).

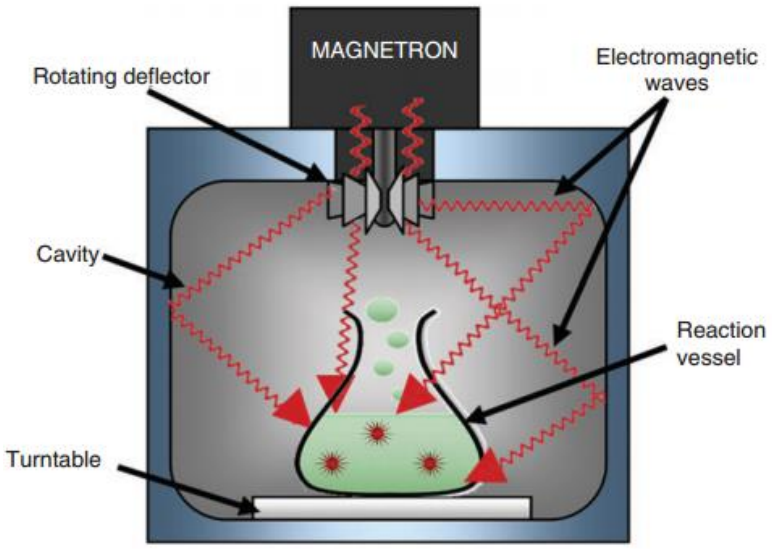

Figure 2.12: Multimode microwave applicator (Stefanidis et al., 2014)

Inside the cavity, the microwaves get reflected from the cavity metal walls, which, even though it reduces the energy losses since the waves do not escape the box, results in wave interference. Consequently the main drawback of multimode cavities is that the microwave field that heats the workload, is highly non-uniform even if a mode stirrer or a rotating disk is used. On the other hand, the most important advantage of these applicators is that they can be constructed in any size to accommodate various volumes of materials for processing. Nowadays, multimode applicators are mainly used for power applications for material heating and plasma activation. However, multimode cavities seem to gain attraction recently regarding alternative applications, such as microwave-enhanced chemistry (Singh, 2014), where microwave energy is utilized for enhancing chemical reactions, or materials' sintering, particularly ceramics (Katz, 1992).

Contrary to the multimode systems, the single (mono)-mode applicator, generates a relatively more stable single-standing wave inside the cavity. The target material is directly positioned at one of the maxima of the electromagnetic field, as seen in Figure 2.13 (Stefanidis et al., 2014). This distinguishing feature of the mono-mode cavity results in higher heating rates compared to the multimode cavity since higher electromagnetic field densities can be created inside the cavity (Ondruschka et al. 2012). However, it also dictates that their volume and the material workload are strictly limited

in terms of size. Therefore, their main limitation is the process volume of the workload that cannot exceed 200 ml and as a result it is not applied for large-scale material heating processes.

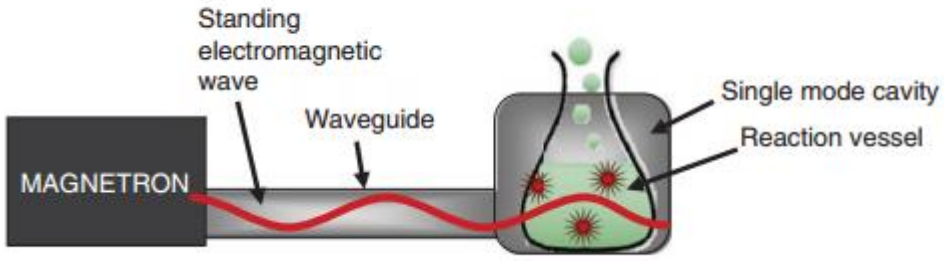

Figure 2.13: Monomode microwave applicator (Stefanidis et al., 2014)

For the purposes of this study, a multimode cavity has been utilised, mainly due to the flexibility it offers with regards to accommodating different reactors in various sizes and shapes. An extensive description of the cavity can be found in Section 3.2.2.

2.2.9. Microwave swing Adsorption (MSA)

Conventional CO_2 capture processes are expensive and would result in an 80-85% increase in the COE, as mentioned in Section 2.1.3. The major contributor to the cost, accounting about 60%, comes from the intensive energy use during desorption that results in a parasitic power loss by about 30% in the power plant (Lu et al., 2010). As a result, reducing the energy consumption in the desorption process is the key to lowering the CO_2 capture cost. Two desorption methods are typically applied in laboratory and/or industrial applications nowadays, namely PSA and TSA, as explained in Section 2.1.5. In particular, PSA is the most common technique, very well established, developed and described in the literature (Ruthven, 1984, 1997 and Suzuki, 1990). However, PSA approach is fully effective only for processes carried out at pressures higher that atmospheric pressure. Otherwise, the installation should be additionally equipped with compressors and/or vacuum pumps, which complicates the process and reduces its efficiency. Application of PSA process is also restricted to fixed-bed reactors (Cherbanski et al., 2009). Furthermore, TSA cycles have the disadvantage of the time restriction and of the massive amount of hot steam needed for the heating of the sorbents, which can be up to 400kg/hr, resulting in a heat duty of 900MJ/hr

(Yokoyama, 2012); the time needed to swing adsorbent beds over a temperature range can be relatively long, as the vessel and the adsorbent bed need to be heated. Moreover, this excess of hot purge gas used implies an increased energy penalty for the power plant (Ania et al. 2005).

Since the microwave process is not limited by the thermal conductivity of the reactor column, the result is an instantaneous localized superheating of any substance. Specifically for CO_2 desorption, the direct absorption of energy, in contrast to the indirect supply of heat by thermal conduction, by the adsorbent may enable a much faster process with a lower purge gas flow rate and lower process temperature. Consequently this may result in energy savings and faster desorption kinetics, making the desorption process more efficient and cost-effective. Microwave regeneration of a saturated adsorbent can happen by one, or a combination, of the three following mechanisms:

- only the adsorbent couples with the microwaves or
- both adsorbent and sorbate couple or
- only the sorbate couples.

From the perspective of energy efficiency, as Atwater et al. (1997) pointed out, the last mechanism offers the greatest potential savings compared to conventional heating since the energy required for regeneration is transferred directly to the sorption site. A good example of the third mechanism is H_2O bound on silica gel. A fourth mechanism for MSA can be possible by mixing the sorbent material with a microwave susceptible material such as silicon carbide (SiC). This mechanism may apply to sorbents based on lithium (Li_4SiO_4) or silver oxide (Ag_2O) in which the adsorbate, in this case CO_2, is chemisorbed, producing lithium carbonate (Li_2CO_3) and silver carbonate (Ag_2CO_3) respectively (Atwater et al., 1997). Sorbent materials that chemisorb CO_2 will generally need higher temperature and/or longer regeneration times, compared to physisorbents. Nevertheless, microwave heating provides the possibility of reaching high temperatures much faster than conventional heating and this can be a particular advantage when electromagnetic energy is applied to composite mixtures of these sorbents, making the regeneration possible, which otherwise would not be practical.

Price and Schmidt (1998) focused on Volatile Organic Compounts (VOC) abatement and recovery of the condensed organic solvents, conducting various experiments using several process configurations applicable to fixed-bed microwave regeneration systems. They clearly stated that microwave desorption performance depends on various parameters, such as adsorbent selection, column flow configuration, purge method and system pressure. A computer model was developed in order to investigate all the studied configurations. The result of this research suggested that low dielectric loss factor polymeric adsorbents, operating under low-pressure conditions (about 5 mmHg) in horizontal fixed bed columns, and adsorbent regeneration to near-zero coverage is the most favourable with regards to process and cost efficiency. Furthermore, studies in the possibility of enhancing the adsorption capacity of the sorbent via microwave regeneration have been shown very promising. Specifically, Liu et al. (2004) proved that the adsorption capacity of the GAC was higher after microwave regeneration. This can be explained after investigation of the surface area and the total pore volume, which showed an increase of 10% and 5%, respectively, compared to the initial GAC characteristics. Similarly, Cha et al. (1995) published a report proving a rise in NO_x adsorption capacity after 9 cycles from 10 to 30 g NO_x per 100 g of char.

Ania et al. (2005) observed changes in the porous structure of the TSA regenerated samples that were due to a two-fold effect; firstly, thermal heating resulted in partial collapse of porosity, and secondly, the decomposition of any molecules that did not leave the sorbent formed coke deposits within the pore network of the material. On the other hand, when MSA was performed, a temperature gradient was observed in the sorbents, which decreased from the inside towards the material's surface. As a result, all the desorbed molecules migrated expeditiously to the surface of the sorbent, the latter showing lower temperature than the core of the sample. Consequently, the formation of coke deposits inside the porous structure of the sorbents is prevented, resulting in a better preservation of the textural characteristics of the sorbent. Whereas in conventional heating, the desorbed molecules near the core decomposed inside the porous network of the material, before they could completely leave the sorbent surface. Hence, coke residues may block the pore structure of the sorbent, resulting in a greater decrease of the apparent BET surface areas and micropore volumes. Consequently, adsorptive capacities after material regeneration were found to be much higher when regeneration was carried out with the MSA technique compared to the TSA, even after various cycles of regeneration (Ania et al., 2005). Specifically, this study suggested that

the cyclic microwave process can preserve the sorbent's phenol adsorption capacity, however after the fourth cycle a decrease was reported. After 6 cycles, the decrease in phenol adsorption capacity, compared to the capacity of the original sample, was 70% when using microwaves for the regeneration process, versus an 82% decrease for conventional heating desorption. As a result, the study concluded that utilisation of microwave energy in the sorbent's regeneration process can contribute to the preservation of the sample – increasing its lifespan - and to an increase in the efficiency of its regeneration. Chang et al. (2012) concluded that the surface of the sorbent – in that case activated carbon with NO_x as sorbate - was uneven and displayed microporosity without any cracks and breaks after regeneration.

The effects of microwave regeneration of sorbent materials can vary depending on various process parameters, such as applied power, mass of saturated adsorbent, purge gas flow rate, and irradiation. Chen et al. (2009) performed microwave regeneration of activated carbon loaded with toluene, focusing on the different results that were obtained after various parameters' combinations. It was stated that the optimal conditions for the maximum regeneration ratio (77.2%) were 500 W microwave power, 60 ml/min carrier gas flow rate, and 180 s irradiation time for saturated activated carbon mass of 5.01 g. Their conclusion was that the amount of activated carbon and the packing density affect the heat transfer and temperature distribution in the vessel. It was also clear that high purge gas flow rates decrease the adsorbent bed temperature, whereas no purge gas leads to self-burning of the carbon.

Han et al. (2009) studied the effect of microwave irradiation on desorption of malachite green from natural zeolite aiming at proving a connection between applied microwave power and regeneration yield. Their results showed that the usage of different power levels, ranging from 160 to 800 W, had an effect on the thermal conditions in the loaded bed, considerably influencing the regeneration yield of zeolite. More specifically, after 10 mins of microwave heating the yield reached 85.8%, whereas in the case of conventional thermal treatment, the yield reached 78.6, 78.2, and 81.7% after 30 mins of heating at temperatures of 300, 500, and 700 C, respectively. Furthermore, they stated that the particle and the pore size of the zeolite had an effect on the regeneration yield as well; after three successive regeneration cycles, the yield decreased from 85.8 to ~80% due to the reduced microporosity of the zeolite.

Polaert et al. (2010) published an experimental study on microwave desorption, where several types of adsorbents with different dielectric properties and porosity were tested, such as activated alumina, silica, NaX, and NaY zeolites. This study reached to the conclusion that desorption is dictated by the absorbed power over the duration of the process. Moreover, it was stated that the dielectric properties of both adsorbent and adsorbate, as well as the temperature variations are more important than the porous structure of the solid adsorbent and the molecular structure of the adsorbate. They concluded that the polarity of the adsorbate is also a factor of huge importance, as it works as the initial reference of the level of electromagnetic conversion. On the other hand, Hashisho et al. (2005) claimed that the adsorbate polarity does not affect the desorption potential and it is only the heating ability of the sorbent that is important, a theory on which the present study is based on. They also suggested that microwave regeneration can be effective for both polar and nonpolar adsorbates. It was concluded that in case of low adsorbate loading, microwave heating is governed by the loss factor of the activated carbon fibre cloth.

Another interesting research on MSA technology was reported by Wang et al. (2010), focusing on desorption of dye reactive red 3BS from carbon nanotubes under microwave irradiation, heating for 15 mins by applying 500 W in a domestic multimode oven. They observed a significant decrease in the adsorption capacity to 92.8% of the original value after 4 microwave regeneration cycles, which may be due to coke formation from the decomposition of organic residues and changes in the pore structure; the surface area and pore volume of the solid sorbent were also reduced by 74% and 72%, respectively.

Liu et al. (2012) studied the application of microwave irradiation on the regeneration of activated carbon for the treatment of industrial waste-water from a chemical plant. Specifically, the regeneration of the exhausted GAC under microwave heating was investigated, reporting that a microwave power of 400 W under a radiation time of 3 min for 10g of GAC are the optimal conditions for this process. Under these conditions the regenerated GAC recovered 97.6% of its original adsorption capacity, whereas multi-cycle regeneration tests showed that it was possible to maintain a stable performance during the first cycles. However, a performance decrease was observed

after further repetitions, resulting in a GAC weight loss of about 10% after the sixth cycle, while a decrease in the surface area was also apparent.

Ondon et al. (2013) explored the microwave regeneration of modified activated carbons, previously saturated with phenol, under nitrogen conditions. In contrast to Liu et al. (2012), they reported that the optimum conditions for the regeneration were at 700W for a 3 minutes irradiation. Under these conditions, the regeneration efficiency of the modified activated carbons reached 98% even after 10 regenerations cycles. They also concluded that the time and the power of microwave irradiation plays a significant role on increasing the regenerations efficiency. Another study by Caliskan et al. (2012) studied the regeneration of activated carbons previously loaded with promethazine comparing microwave and conventional heating. In contrast with the above studies, the authors concluded that the adsorption capacity of the activated carbon decreased after successive adsorption-desorption cycles. This was due to the thermal cracking of the adsorbate, which was more affected under MSA compared to TSA (Caliskan et al. 2012). The above prove that not only the adsorbent, but also the adsorbate plays an important role to the optimum conditions of the microwave regeneration process, as well as the operating conditions (Stefanidis et al., 2014).

Recently, Webley et al. (2014) examined the use of microwave assisted vacuum in the CO_2 capture process as a way to direct thermal energy straight to the adsorbent surface in order to release water and CO_2, under both wet and dry gas conditions. The addition of microwave radiation to the existing vacuum swing regeneration system improved the rapid desorption of CO_2 and water. Under dry gas conditions, the enhancement was due to microwave heating of the 13X zeolite adsorbent, facilitated by the high cation density in the faujasite structure. On the other hand, under wet gas conditions, the temperature rise of the adsorbent upon microwave heating was much lower than that predicted by simple heating suggesting that the microwave radiation is absorbed primarily by the adsorbed water.

In terms of industrial MSA processes, according to Cherbanski et al. (2009) only five industrial-scale processes have been commissioned. The first pilot plant was built by Canada Ontario Hydro Technologies for the regeneration of activated carbon from fluidized washing applications in gold ore. Then, Arrow Pneumatics in the US,

developed a small scale adsorber for the drying/cleaning of air and simutaneously Plinke GmbH & Co created a fluidized bed adsorption coupled with a moving bed desorption for VOC recovery. Another industrial scale MSA was developed, being ready for commercial presentation in 2000, in the process of purification of contaminated air from VOCs by adsorption on GAC and subsequent regeneration of the spent carbon by microwave irradiation, presented by Cha (2000). Moreover, Opperman and Brown (1999) presented a system for continuous capturing of a broad range of VOCs on polymeric adsorbent together with a very efficient low-temperature microwave desorption under vacuum and recovery of the vapors as condensed liquids.

2.3. Summary

In recent years, there has been an increasing global interest in CCS as an important technology for climate change mitigation. However, improved technologies for the CO_2 capture process, that could possibly lead CCS to be highly competitive against the renewable energy market, are necessary. The economic evaluation of a CO_2 capture system is often driven by the energy penalties imposed in the process where CCS is applied and, in adsorption technology this energy is particularly required for the desorption step. Two desorption methods are typically applied in industrial applications nowadays, namely PSA and TSA. However, they are not considered to be the optimum pathways for CO_2 adsorption technology. As a result, efficient regeneration systems, ensuring multiple re-use of adsorbent materials, while consuming the least possible energy, are required.

The aim of this research is to intensify the CO_2 desorption using solid sorbents, trying to replace the conventional TSA with a technology that could result in an optimised regeneration process in terms of efficiency, kinetics and energy consumption. One technology that can possibly offer the above results is microwave heating, which nowadays is seen as a promising and efficient technique to intensify various types of applications. The growing interest in microwave heating regeneration processes is related to its unique features, offering reduction in heating time due to volumetric and rapid heating, high energy efficiency and better recovery of volatile elements and compounds.

As a result, the effectiveness of applying microwave heating technology to regenerate various solid sorbents previously saturated with CO_2 is the main focus of this research. The main difference between MSA and TSA heating applications lies in the way heat is generated. In TSA, thermal regeneration usually takes place in rotary kilns or vertical furnaces, the heat source is located outside the sorbent bed, and the bed is heated by conduction and/or convection. This heating process results in a significant temperature gradient inside the sorbent bed until conditions of steady state are reached. On the other hand, microwave irradiation enables a direct energy supply to the sorbent bed, since energy transfer does not happen by conduction or convection as in TSA, but is rapidly transformed into heat inside the particles by dielectric polarisation. As a result, microwave regeneration offers possible advantages over TSA, including the rapid and precise control of the sorbent bed temperature, shorter regeneration time and energy savings. Previous studies have also stated that MSA may also result in a better performance of the solid sorbent in terms of total adsorption capacity of a compound and rate of adsorption compared to conventional heating.

However, there are significant drawbacks in microwave heating applications as well. The performance of the desorption via MSA depends on the adsorbent and the adsorbate used for each process, as well as on the process parameters, i.e. power, temperature, dry/wet gas streams, flow rates etc. Moreover, the lack of uniformity in material heating, which is also dictated by the adsorbent's and adsorbate's characteristics (dielectric properties) is another disadvantage in the field of MSA applications. In addition, the high investment costs and the lack of fundamental knowledge regarding the dielectric properties or equipment design are also reasons for the delay in radical progress in the field of large scale industrial MSA processes. **Consequently, much more dedicated work and further exploration are needed to improve the performance of MSA before trying to scale-up microwave technology in the area of CCS. In other words, the parameters that significantly affect microwave heating in the field of CO_2 capture need to be addressed and extensively studied. As a result, this research focuses on studying the effects of process parameters (Chapter 4) and material structure (Chapter 5) on the performance of microwave heating, aiming at intensifying the desorption process.**

References

Aaron, D., and Tsouris, C. (2005) *'Separation of CO_2 from flue gas: a review'*, Separation Science & Technology vol. 40, pp. 321–348

Adams, D. (2010) *'Flue gas treatment for CO_2 capture'*, IEA Clean Coal Centre: London.

Anderl, H. and Zotter, T. (2001) '*Gasification in a CFB-reactor - a simple and economic way of co-firing renewable fuels in existing power plants',* Thermal science, Vol. 5, No. 2, pp. 59–67

Ania, C. O., Menendez, J. A., Parra, J. B. and Pis, J. J. (2004) *'Microwave induced regeneration of activated carbons polluted with phenol. A Comparison with conventional thermal regeneration'*, Carbon, vol. 42, p. 1377

Ania, C. O., Menendez, J. A., Parra, J. B. and Pis, J. J. (2005) *'Effect of microwave and conventional regeneration on the microporous and mesoporous network and on the adsorptive capacity of activated carbons'*, Microporous and Mesoporous Materials, vol. 85, 27 July, pp. 7-15, doi:10.1016/j.micromeso.2005.06.013

Ania, C. O., Menendez, J. A., Parra, J. B. and Pis, J. J. (2007) *'Microwave assisted regeneration of activated carbons loaded with pharmaceuticals'* Water Res. Vol. 41, p. 3299

Astarita, G., Savage, D. W. and Bisio, A. (1983) *'Gas treating with chemical solvents'*, John Wiley and Sons: New York

Atwater, J., Holtsnider, J., Wheeler, R. and Luna, B. (1997) *'Microwave-powered thermal regeneration of sorbents for CO_2, water vapor and trace organic contaminants'*, SAE technical paper series, 972430, 27th International Conference on Environmental Systems Lake Tahoe, Nevada, 14-17 July

Bathen, D. (2003) *'Physical waves in adsorption technology-an overview'* Separation and Purification Technology, vol. 33, pp. 163-177

BBC News (2015) *'SSI Redcar steelworks to be shut'*, [online]. Available at: http://www.bbc.co.uk/news/uk-england-34509329 [Accessed on 19/10/2015].

Berstad, D. (2012) *'Post-combustion CO_2 capture from a natural gas combined cycle by $CaO/CaCO_3$ looping'*, International Journal of Greenhouse Gas Control, vol. 11, pp. 25–33

Foo, K.Y. (2012) *'Microwave-assisted regeneration of activated carbon'*, Bioresource Technology, vol. 119, pp. 234-240. DOI: 10.1016/j.biortech.2012.05.061

Bonjour, J., Chalfen, J.-B., Meunier, F. (2002) *'Temperature swing adsorption process with indirect cooling and heating'*, Industrial & Engineering Chemistry Research, vol. 41 (23), pp. 5802–5811

Bradshaw, S.M., van Wyk, E.J. and de Swardt, J.B. (1998) *'Microwave heating principles and the application to the regeneration of granular activated carbon',* the Journal of The South African Institute of Mining and Metallurgy, pp. 201-212

Caliskan, E., Bermudez, J.M., Parra, J.B., Menendez, J.A., Mahramanlioglu, M., Ania, C.O. (2012) *'Low temperature regeneration of activated carbons using microwaves: revising conventional wisdom'*, Journal of Environmental Management, vol. 102, pp. 134 – 140

Carapellucci, R. and Milazzo, A. (2003) *'Membrane systems for CO_2 capture and their integration with gas turbine plants'*, Proceedings of the Institution of Mechanical Engineers Part A: Journal of Power and Energy, vol. 217, pp. 505–517

Cha, C. Y. and Kong, Y. (1995) *'Enhancement of NOx adsorption capacity and rate of char by microwaves'*, Carbon, vol. 33, p. 1141

Cha, C.Y. and Carlisle, C.T. (2001) *'Microwave process for volatile organic compound abatement'*, Journal of Air Waste Management , vol. 51, pp: 1628–1641

Chakravati, S., Gupta, A. and Hunek, B. (2001) *'Advanced technology for the capture of carbon dioxide from flue gases'*, 1st National Conference on Carbon Sequestration, Washington DC

Chen, M., Huang, J., Wang, J., Ning, P., Jiang, Y. and Xu, Y. (2009) *'Thermal behaviors and regeneration of activated carbon saturated with toluene induced by microwave irradiation'*, Journal of Chemical Engineering Japan, vol. 42, p. 325

Cherbanski, R. and Molga, E. (2009) '*Intensification of desorption process by use of microwaves-an overview of possible applications and industrial perspectives'*, Chemical Engineering and Processing, vol. 48, pp. 48-58

Choi, S., Drese, J.H. and Jones, C.W. (2009) *'Adsorbent materials for carbon dioxide capture from large anthropogenic point sources'*, Chem. Sus. Chem., vol 2, pp. 796-854

Clark, D.E. (1996) *'Microwave processing of materials'*, Annual Review of Materials Science, 26 (1996), pp. 299–331

Consonni, S., Vigano, F., Kreutz, T. and Lorenzo, L. (2007) *'CO_2 capture in IGCC plants via cryogenic separation'*, presented at the sixth annual conference on carbon capture & sequestration, May 7-10

Coss, P.M. and Cha, C.Y. (2000) '*Microwave regeneration of activated carbon used for removal of solvents from vented air*', Journal of Air Waste Management, vol. 50, pp. 529–535

Davidson, R. (2011) 'Pre-combustion capture of CO_2 in IGCC plants', IEA Clean Coal Centre, London, UK (2011) p. 98

De Visser, E., Hendricks, C., Barrio, M., Molnvik, M.J., De Koeijer, G. and Liljemark, S. (2008) *'Dynamics CO_2 quality recommendations'*, International Journal of Greenhouse Gases Control vol. 2, pp.478–484

Durka T, Van Gerven T, Stankiewicz A. (2009) *'Microwaves in heterogeneous gas-phase catalysis: experimental and numerical approaches'*, Chem. Eng. Technol., vol. 32, pp. 1301 – 1312

Elwell, L.C. and Grant, W.S. (2006) *'Technology options for capturing CO_2 – special reports'*, Power, vol. 150, pp. 60–65

Energy and Climate Change Committee (2016) '*Future of carbon capture and storage in the UK'*, Second Report of Session 2015–16, House of Commons London: The Stationery Office Limited

Favre., E. (2007) *'Carbon dioxide recovery from post-combustion processes: Can gas permeation membranes compete with absorption?'* Journal of Membrane Science, vol. 294, pp.50-59

Feron, P. (2016) '*Absorption-Based Post-Combustion Capture of Carbon Dioxide'*, Woodhead Publishing, 27 May

Foo, K.Y. and Hameed, B.H. (2012) '*Microwave-assisted regeneration of activated carbon'*, Bioresource technology, vol. 119, pp. 234-240, DOI: 10.1016/j.biortech.2012.05.061

Funawatashi, Y. and Suzuki, T. (2003) 'Numerical analysis of microwave heating of a dielectric', Heat Transfer – Asian Res., vol. 32, ed. 3, pp. 227–236

Gasparini, F., Papa, I., Wheeler, F., Criner, K. and Mary, S. (2012) *'Coal oxy-combustion in a CHP plant using the Circulating Fluidized Bed (CFB) boiler technology'*, Veolia Environnement Recherche et Innovation – France, 12-14 June

Gibbins, J. and Chalmers, H. (2008) *'Carbon capture and storage'*, Energy Policy, vol. 36, pp. 4317–4322

Gopalakrishnan, S., Munch, J., Herrmann, R. and Schwieger, W. (2006) '*Effects of microwave radiation on one-step oxidation of benzene to phenol with nitrous oxide over Fe-ZSM-5 catalyst'*, Chem. Eng. J., vol: 120, pp. 99–105

Grande, C.A. (2012) *'Advances in Pressure Swing Adsorption for Gas Separation'*, ISRN Chemical Engineering, vol. 2012, pp. 1-13, DOI: http://dx.doi.org/10.5402/2012/982934

Gunasekaran, S. & Yang, H. W. (2007) *'Effect of experimental parameters on temperature distribution during continuous and pulsed microwave heating'*, Journal of Food Engineering, vol. 78, ed. 7, pp. 1452–1456

Han, R., Wang, Y., Sung, Q., Wang, L., Song, J., He, X. and Du, C. (2009) *'Malachite green adsorption onto natural zeolite and reuse by microwave irradiation',* Journal of hazardous materials, vol. 175, pp. 1056-61

Hashisho, Z. (2007) '*Microwave-swing adsorption for the capture and recovery, or destruction for a more sustainable use of organic vapors'*, PhD thesis, University of Illinois at Urbana-Champaign

Hashisho, Z., Rood, M. and Botich, L. (2005) *'Microwave-swing adsorption to capture and recover vapors from air streams with activated carbon fiber cloth'*, Environmental Science & Technology, vol. 39, pp. 6851–6859, **doi:** 10.1021/es050338z

Hayes, B. L. (2004) *'Recent advances in microwave-assisted synthesis'*, Aldrichimica ACTA, vol. 37, pp. 66-76

Hossan, M.R., Byun, D. and Dutta, P. (2010) '*Analysis of microwave heating for cylindrical shaped objects',* International Journal of Heat and Mass Transfer, vol. 53, pp. 5129–5138

Hua-Shan, T. and Chih-Ju, G.J. (1999) *'Application of granular activated carbon packed-bed reactor in microwave radiation field to treat phenol'*, Chemosphere, vol. 38, pp. 2667–2680

IEA (2004) *'Prospects for CO_2 capture and storage'*, Paris, France: OECD/IEA

International Energy Agency Report (2006) *'CO_2 capture as a factor in power station investment decisions',* Report No.2006/8, May

IPCC (2005) *'Intergovernmental Panel on Climate Change (IPCC) special report on carbon dioxide capture and storage'*, Cambridge University press, Cambridge, UK

J.D. Katz, J.D. (1992) 'Microwave Sintering of Ceramics', Material Science, vol. 22, pp. 153–170

Kanniche, M., Gros-Bonnivard, R,, Jaud, P., Valle-Marcos, J., Amann, J.M. and Bouallou, C. (2010) 'Pre-combustion, post-combustion and oxy-combustion in thermal power plant for CO2 capture', Applied Thermal Engineering, vol. 30, pp. 53–62

Kim, S.I., Aida, T. and Niiyama, H. (2005) *'Binary adsorption of very low concentration ethylene and water vapor on mordenites and desorption by microwave heating*', Separation Purification Technology, vol. 45, pp. 174–182.

Kim, S.I., Watabe, Y., Aida, T. and Niiyama, H. (2005) *'Complete oxidation of ethylene y Co-modified mordenites under microwave irradiation*', Journal of Chemical Engineering, Japan, vol. 38, pp. 828–834

Kohl, A. L. and Nielsen, R. B. (1997) *'Gas purification'*, 5th ed., Gulf Publishing Company: Houston, TX

Kong, Y. and Cha, C.Y. (1996) '*Reduction of NOx adsorbed on char with microwave energy'*, Carbon, vol. 34, pp. 1035–1040

Kriegsmann, G. (1997) *'Hot spot formation in microwave heated ceramic fibres'*, IMA Journal of Applied Mathematics, vol. 59, pp. 123-124

Leung, D., Caramanna, G. and Maroto-Valer, M.M. (2014) *'An overview of current status of carbon dioxide capture and storage technologies'*, Renewable and Sustainable Energy Reviews, vol. 39, pp. 426–443

Li, J.R., Ma, Y., McCarthy, M., Sculley, J., Yu, J., Jeong, H., Balbuena, P. and Zhou, H. (2011) *'Carbon dioxide capture-related gas adsorption and separation in metal-organic frameworks'*, Coordination Chemistry Reviews, vol. 255, pp. 1791–1823

Liu, C., Zhang, L., Peng, J., Srinivasakannan, C., Liu, B., Xia, H., Zhou, J. and Xu, L. (2013) '*Temperature and Moisture Dependence of the Dielectric Properties of Silica Sand'*, Journal of Microwave Power and Electromagnetic Energy, vol. 47 (3), pp. 199-209

Liu, Q.S., Wang, P., Zhao, S. and Zhang, W. (2012) *'Treatment of an industrial chemical waste-water using a granular activated carbon adsorption-microwave regeneration process'*, Journal of Chemical Technology and Biotechnology, Vol. 87, Issue 7, Pp. 1004–1009, DOI: 10.1002/jctb.3720

Liu, X., Quan, X., Bo, L., Chen, S. and Zhao, Y. (2004) *'Simultaneous pentachlorophenol decomposition and granular activated carbon regeneration assisted by microwave irradiation'*, Carbon, vol. 42, p. 415

Lu, Y., Ye, X., Zhang, S., Rostam-Abadi, M., Hirschi, J. and Jones, A. (2013) *'An Integrated Vacuum Carbonate Absorption Process Enabled with an Enzyme Biocatalyst for CO_2 Absorption'* U.S. Department of Energy, National Energy Technology Laboratory

Maddox, R. N. and Morgan, D. J. (1998) *'Gas conditioning and processing'*, Gas Treating and Liquid Sweetening, 4th Ed., vol. 4, Campbell Petroleum Series: Norman, OK

Mehdizadeh, M. (2009) '*Microwave/RF Applicators and Probes for Material Heating, Sensing, and Plasma Generation: a Design Guide'*, William Andrew, Norwich, N.Y

Menendez, J., Arenillas, A., Fidalgo, B., Fernandez, Y., Zubizarreta, L., Calvo, E. and Bermudez, J.M. (2010) *'Microwave heating processes involving carbon materials'*, Fuel Processing Technology, vol. 91, pp. 1-8

Meredith, R.J. (1998) *'Engineers' handbook of industrial microwave heating'*, the Institution of Electrical Engineers, 0852969163, London, UK

Metaxas, A. and Meredith, R. (1983) '*Industrial Microwave Heating'*, Power Engineering Series 4, Peter Peregrinus Ltd. (on behalf of the IEE)

Michael, D., Mingos, P. and Baghurst, D.R. (1991) *'Applications of microwave dielectric heating effects to synthetic problems in chemistry'*, Chemical Society Review, vol. 20, pp. 1-47

Mohanty, D., Venkatesh, V. (2014) *'Performance analysis of a combined cycle gas turbine under varying operating conditions'*, Mechanical Engineering: An International Journal (MEIJ), Vol. 1, No. 2, August

Munch, J., Herrmann, R. and Schwieger, W. (2005) *'A new reactor for combined conventional and microwave heating'*, Chem. Eng. Technol., vol: 28, pp. 672–676

Ohgushi, T., Komarneni, S. and Bhalla, A.S. (2001) *'Mechanism of microwave heating of zeolite A'*, Porous Materials, vol. 8, pp. 23–35

Okumura, T., Ogino, T., Nishibe, S., Nonaka, Y., Shoji, T. and Watanabe, T. (2013) *'Study on Solid Adsorbent for CO_2-Capture from Post Combustion Gases Utilizing Low-Temperature Thermal Energy'*, 2nd Post Combustion Capture Conference (PCCC2), IEAGHG, Bergen, 17th-20th September

Olajire, A.A. (2010) *'CO_2 capture and separation technologies for end-of-pipe application – a review'*, Energy, vol. 35, pp. 2610–2628

Olivares-Marin, M. and Maroto-Valer, M. (2010) *'Preparation of a highly microporous carbon from a carpet material and its application as CO_2 sorbent'*, Elsevier, Fuel Processing Technology, vol 92, 14 September, pp. 322-329, doi:10.1016/j.fuproc.2010.09.022

Ondon, B., Bing, S., Yan, Z., Zhu, X. and Liu, H. (2013) *'Investigation of the Optimal Condition for Microwave Regeneration of Modified Activated Carbons Saturated with Phenol*', International Proceedings of Chemical, Biological & Environmental, Vol. 54, p. 31

Ondruschka B, Bonrath W, Stuerga D., de la Hoz, A. and Loupy A, (2013) *'Development and design of reactors in microwave-assisted chemistry'*, Microwaves in organic synthesis, vol. 1 (3). DOI: 10.1002/9783527651313.ch2

Perrin, N., Dubettiera, R., Lockwooda, F., Courta, P., Tranierb, J., Bourhy-Weberb, C. and Devauxb, M. (2013) *'Oxy-combustion for carbon capture on coal power plants and industrial processes: advantages, innovative solutions and key projects'*, Energy Procedia, vol. 37, pp. 1389–1404

Polaert, I., Estel, L., Huyghe, R. and Thomas, M. (2010) *'Adsorbents regeneration under microwave irradiation for dehydration and volatile organic compounds gas treatment*' Chem. Eng. J., vol. 162, p. 941

Price, D. W. and Schmidt, P. S. (1997) *'Microwave regeneration of adsorbents at low pressure: experimental kinetics studies'*, J. Microwave Power Electromagnetic Energy, vol. 32, p. 145.

Price, D.W. and Schmidt, P.S. (1998) *'VOC recovery through microwave regeneration of adsorbents: process design studies'*, Air Waste Management, vol. 48, pp. 1135–1145

Price, D.W. and Schmidt, P.S. (1998) *'VOC recovery through microwave regeneration of adsorbents: comparative economic feasibility studies'*, Air Waste Management, vol. 48, pp. 1146–1155

Rackley, S.A. (2010) 'Carbon Capture and Storage', Elsevier, Oxford

Ramireddy, V. (2012) *'An Overview of Combined Cycle Power Plant'*, available online at: http://electrical-engineering-portal.com/an-overview-of-combined-cycle-power-plant

Ramshaw, C. (1995) *'The Incentive for Process Intensification*' Proceedings, 1st International Conference on Process Intensification for Chemical Industries, 18, BHR Group, London, p. 1

Reimbert, C.G, Minzoni, A.A. and Smyth, N.F. (1996) *'Effect of radiation losses on hotspot formation and propagation in microwave heating'*, IMA Journal of Applied Mathematics, vol. 57, pp. 165-179

Rezaei, F. and Webley, P. (2010) *'Structured adsorbents in gas separation processes'*, Separation and Purification Technology, vol. 70, pp. 243–256

Ruthven, D., Farooq, S. and Knaebel, K. (1993) '*Pressure Swing Adsorption'*. John Wiley and Sons Inc.

Samanta, A., Zhao, A., Shimizu G., Sarkar, P. and Gupta, R. (2011) *'Post-combustion CO_2 capture using solid sorbents: A review'*, Ind. Eng. Chem. Res., vol. 51, pp. 1438–1463

Sayari, A., Belmabkhout, Y. and Serna-Guerrero, R. (2011) *'Flue gas treatment via CO_2 adsorption'*, Chemical Engineering Journal, vol. 171, pp. 760–774.

Serna-Guerrero, R. and Sayari, A. (2010) *'Modeling adsorption of CO_2 on amine functionalized mesoporous silica. 2: Kinetics and breakthrough curves'*, Chemical Engineering Journal, vol. 161, pp. 182–190

SGR Newsletter (2011) *'Shale gas: will it undermine progress on tackling climate change?'*, Issue 40, Autumn

Siefert, N. and Litster, S. (2013) *'Exergy and economic analyses of advanced IGCC–CCS and IGFC–CCS power plants'*, Applied Energy, 2013, vol. 107, issue C, pp. 315-328

Singh, S., Gupta, D., Jain, V., & Sharma, A. (2014) *'Microwave processing of materials and applications in manufacturing industries: A Review'*, Materials and Manufacturing Processes, vol. 30 (1), pp. 1-29, DOI: 10.1080/10426914.2014.952028

Skarstrom, C. W., (1959) *'Use of adsorption phenomena in automatic plant-type gas analyzers'*, Ann. N.Y. Acad. Sci. vol. 72, pp. 751-760

Smyth, N.F. (1992) *'The effect of conductivity on hotspots'*, Journal of Australian Mathematical Society, Series B, vol. 33, pp. 403-413

Song, C., Kansha, Y., Fu, Q., Ishizuka, M. and Tsutsumi, A. (2016) *'Reducing energy consumption of advanced PTSA CO_2 capture process–Experimental and numerical study'*, Journal of the Taiwan Institute of Chemical Engineers, DOI:10.1016/j.jtice.2015.12.006

Stefanidis, G., Muñoz, A. N., Sturm, G. and Stankiewicz, A. (2014) '*A helicopter view of microwave application to chemical processes: reactions, separations, and equipment concepts*', Rev Chem Eng, DOI 10.1515/revce-2013-0033

Stewart, C. and Hessami, M. (2005) *'A study of methods of carbon dioxide capture and sequestration - the sustainability of a photosynthetic bioreactor approach'*, Energy Conversion and Management, vol. 46, pp. 403–420

Tarka, T. J., Ciferno, J. P., Gray, M. L. and Fauth, D. (2006) *'CO_2 capture systems using amine enhanced solid sorbents'*, Presented at the Fifth Annual Conference on Carbon Capture & Sequestration, Alexandria, VA, USA, May 8-11, Paper No. 152

The National Academies Press (2007) *'Coal: Research and Development to Support National Energy Policy'*, Committee on Coal Research, Technology, and Resource Assessments to Inform Energy Policy, DOI: 10.17226/11977

Trachtenberg, M. and Bao, L. (2005) *'CO_2 capture: Enzyme vs. amine'*, presented at the fourth annual conference on carbon capture and sequestration, May 2-5

Tunnicliffe, H. (2015) *'Drax pulls out of White Rose CCS project'*, The Chemical Engineer Today [online]. Available at: http://www.tcetoday.com/latest%20news/2015/september/drax%20pulls%20out%20of%20white%20rose%20ccs%20project.aspx#.ViTwxE2FPIV [Accessed on 19/10/2015].

Vallee, S.J. and Conner, W.C. (2006) *'Microwaves and sorption on oxides: a surface temperature investigation'*, J. Phys. Chem. B vol. 110, pp. 15459–15470

Voss, C., (2005) *'Applications of Pressure Swing Adsorption Technology'*, Adsorption vol. 11, pp. 527-529

Wang, J., Peng, X., Luan, Z. and Zhao, Z. (2010) *'Regeneration of carbon nanotubes exhausted with dye reactive red 3BS using microwave irradiation',* Journal of hazardous materials, vol. 178, pp. 1125-1127

Wang, Q., Luo, J., Zhong, Z. and Borgna, A. (2011) *'CO_2 capture by solid adsorbents and their applications: Current status and new trends'*, Energy Environ. Sci. vol. 4, 30 July, pp. 42–55**, doi:** 10.1039/C0EE00064G

Wang M., Lawala, A., Stephensonb, P., Siddersb, J., Ramshawa, C. and Yeung, H. (2011) *'Post-combustion CO_2 capture with chemical absorption: A State-of-the-art review'*, Chemical Engineering Research and Design, Volume 89, Issue 9, September, pp. 1609-1624

Webley, P.A. and Zhang, J. (2014) *'Microwave assisted vacuum regeneration for CO_2 capture from wet flue gas'*, Adsorption, Vol. 20, Issue 1, pp. 201-210

Whittaker, G. and Mingos, M. (1994) '*The application of microwave heating to chemical synthesis'*, Journal of microwave power and electromagnetic energy, Vol. 29 (4), pp. 195-219

Wolf, K.J. (2013) *'CCS at RWE: Struggling for solutions, acknowledging the obstacles'*, RWE Power, 31 January

Yang, H. W. & Gunasekaran, S. (2004) *'Comparison of temperature distribution in model food cylinders based on Maxwell's equations and Lambert's law during pulsed microwave heating*', Journal of Food Engineering, vol. 64, ed. 4, pp. 445-453

Yang, H., Xu, Z., Fan M., Gupta, R., Slimane, R., Bland, A. and Wright, I. (2008) *'Progress in carbon dioxide separation and capture: A review'*, Journal of Environmental Sciences, vol. 20, pp. 14–27

Yang, R. T. (2003) *'Adsorbents: fundamentals and applications',* Wiley Interscience: Hoboken, NJ

Yokoyama, T. (2012) *'Analysis of reboiler heat duty in MEA process for CO_2 capture using equilibrium-staged model'*, Separation and Purification Technology, Vol. 94, pp. 97–103

Yong, Z., Mata, V. and Rodrigues, A. E. (2002) *'Adsorption of carbon dioxide at high temperature - A review'*, Separation Purification Technologies, vol. 26, pp. 195–205

Yuen, F. and Hameed, B. (2009) *'Recent developments in the preparation and regeneration of activated carbons by microwaves'*, Advances in Colloid and Interface Science, vol. 149, pp. 19-27

Zhang, X., Hayward, D.O., Mingos, D. and Michael, P. (1999) *'Apparent equilibrium shifts and hot-spot formation for catalytic reactions induced by microwave dielectric heating'*, Chemical Communications, vol. 11, pp. 975-976

Zhao Z, Cui X, Ma J and Li R. (2007) *'Adsorption of carbon dioxide on alkali-modified zeolite 13X adsorbents'*, International Journal of Greenhouse Gas Control, vol. 1, pp. 355-359

Zheng, F., Addleman, R. S., Aardahl, C. L., Fryxell, G. E., Brown, D. R. and Zemanian, T. S. (2007) *'Amine functionalized nanoporous materials for carbon dioxide (CO_2) capture'*, Environmental Applications of Nanomaterials: Synthesis, Sorbents and Sensors; Fryxell, G. E., Cao, G., Eds.; Imperial College Press: Singapore, pp 285_311

Zlotorzynski, A. (1995) *'The application of microwave radiation to analytical and environmental chemistry'*, Critical Reviews in Analytical Chemistry, Vol. 25, No. 1, January, pp. 43-76

Chapter 3: Experimental methodology

This chapter describes the guiding principles for designing an integrated MSA system as well as the experimental procedure followed for the completion of this research. Initially, the adsorption step was taken into consideration and as a result the principles that influence an adsorption system are discussed first (Section 3.1.1). Next, the basic criteria for designing the desorption process and selecting the MSA components are presented (Section 3.1.2), followed by a detailed description of the experimental setup (Section 3.2). Furthermore, the materials' characterisation techniques and experimental parameters that were examined throughout this research are introduced (Sections 3.3 to 3.5), followed by a description of the experimental procedure (Section 3.6).

3.1. Key principles for designing the MSA system

The primary principles that influence the successful operation of an MSA/TSA system in a continuous CO_2 capture process are mainly related with the adsorption and regeneration steps. Therefore, the most important principles that control these two processes are discussed in this section.

3.1.1. Adsorption step principles

Adsorption properties that need to be taken into consideration for adsorber design processes, include isotherms, kinetics, and fixed bed dynamics. Moreover, textural properties, such as shape, porosity, density and void fractions of the solid material, need to be addressed as well. In addition, though not strictly a property, cost is involved in every design decision.

Adsorption isotherms: Adsorption equilibrium data are usually obtained at a fixed temperature and are plotted as capacity or loading versus the sorbate concentration (or partial pressure for gases and vapors) in order to generate the so-called adsorption isotherms (Knaebel, 1990). As discussed in the previous chapter (Section 2.1.4), the adsorption capacity of the sorbent significantly affects the capital cost of the whole process, since it helps to estimate the amount of sorbent needed, which in turn fixes the volume of the adsorption columns/vessels. This adsorption capacity depends on (i) the

concentration of the solute in the feed (Section 4.2.1), (ii) the temperature of the gas stream, (iii) the total flow rate of the feed (Section 4.2.2), (iv) the impurities found inside the feed, including moisture content (Section 4.2.3), (v) the sorbent material and (vi) the interactions between sorbent and sorbate (Jana et al., 2015, Kazachkin et al., 2009).

Adsorption kinetics: Adsorption kinetics are directly associated with intraparticle mass transfer resistance and can dictate the overall time of a cyclic fixed bed adsorption process (Balsamo et al., 2014). As expected, fast kinetics could lead to sharp breakthrough curves with high throughput ratio, resulting in a more effective use of the sorbent, whereas slow kinetics leads to a broader breakthrough curve. The throughput ratio is defined as the ratio of elapsed run time to stoichiometric time, or the ratio of actual effluent volume to the feed volume that ideally could saturate the column. Thus, the throughput ratio (or throughput parameter) measures the stoichiometry of a system (McKetta et al., 1978). One solution to the issue of slow kinetics is to increase either the amount of adsorbent used, or the time of the cycle, which would result in an increase of the throughput per unit of adsorbent. Unfortunately, both of these solutions would lead to an increase in the amount of adsorbent needed. Another way to overcome a slow diffusion is to use small adsorption particles; however, this would in turn lead to an increased pressure drop (Ling et al., 2014).

Pressure drop: This is a very important parameter for the dynamics of the bed during adsorption, since a high pressure drop inside the bed could result in the need of installing large pumps which consequently would lead to increased power consumption. As a result, this can significantly affect the operating and overall cost of the adsorption system (Richardson et al., 2002). Most adsorption columns are designed to work at a relatively low pressure drop (ΔP), because the velocity is typically low to enhance equilibration of the fluid with the adsorbent and also because large particles are commonly used (granules or pellets). Moreover, a small bed length to diameter ratio (L/d_b) results in low pressure drop, while a large L/d_b ratio could result in a good flow distribution and low dead volume in the adsorption column. The most applicable equation that describes the pressure drop in a fixed bed reactor is the Ergun equation:

$$\frac{\Delta P}{L} = \left(150\,\frac{1-\varepsilon_B}{Re} + 1.75\right)\left(\frac{\rho\, u_s^2}{g_c d_p}\frac{1-\varepsilon_B}{\varepsilon_B^3}\right) \tag{3.1}$$

Where ε_B is the bed void fraction and g_c the gravitational constant. Re represents the Reynolds number, a dimensionless parameter that determines the behaviour of viscous flow patterns and is determined by the following equation:

$$Re = \frac{\rho u_{sd_p}}{\mu_d} \quad (3.2)$$

where ρ and v_s are the density and the superficial linear velocity of the fluid, respectively, whereas d_p is the effective particle diameter. In general, the pressure drop in the adsorbent bed is also equivalent to the flow restrictions that are also evident in the pipes, valves, and fittings.

Adsorbent purity: The purity of the adsorbent could affect the safety and the efficiency of the adsorption and regeneration cycles. For instance, impurities such as metallic micro-particles could lead to arcs and sparks during the regeneration with microwaves, seriously affecting the MSA system and the desorption process.

3.1.2. Regeneration step principles

There are various parameters that need to be taken into consideration when designing a desorption system, such as adsorbent properties, shape and desorption kinetics and are described in this section.

Thermal and dielectric properties of the adsorbent: The thermal conductivity and diffusivity of the adsorbent dictate the uniformity of the heating in the adsorption column as well as the pace at which the energy flows through the adsorbent. Moreover, in the case of MSA, the dielectric constant of the sorbent is closely related to its ability to convert the electromagnetic energy to heat. For example, a sorbent's low thermal conductivity – such as aluminium oxide with a thermal conductivity of 30 $^{W}/_{mK}$ - could result in temperature gradients through the bed, whereas non-favourable dielectric properties could lead to high energy consumption and possible damage of the MSA system due to overheating of the magnetron (Gaal et al., 1999).

Adsorbent shape: The shape of the adsorbent particles affects directly the packing of the bed, as it determines the void space between the adsorbent particles (Rousseau, 1987). This parameter also affects the heating uniformity of the bed as it will be shown later

(Section 5.3). In the case of microwave heating, the shape of the adsorbent has an impact on the formation of micro-plasmas as well (Menendez et al., 2010). In general, the bigger the void space between the particles, the bigger the sparks inside the bed.

Desorption kinetics: The kinetics of desorption affect the rate at which the adsorbent releases the adsorbate under the effect of the desorption driving force, which in this case is the temperature difference (Cherbanski et al., 2009). As a result, fast desorption kinetics correspond to a shorter desorption step, resulting in a time- and energy-effective process.

3.1.3. MSA design principles and equipment

In addition to the general design principles of a continuous adsorption/desorption system, specific guidelines for designing an MSA system need to be addressed as well. Five important parameters should be taken into account when designing a microwave regeneration process, including the nature of the propagation of the electromagnetic waves in the adsorbent/adsorbate system, the microwave cavity selection and design, the reactor design, the temperature monitoring and the heat distribution inside the cavity and the bed. Moreover, equipment for data analysis, is also discussed here. The safe performance and the efficiency of the MSA system is influenced by all the aforementioned parameters and reciprocal sacrifices may be needed in order to ensure an effective regeneration process.

Process principles of the MSA system: The relation between the sorbate and the adsorbent with regards to the electromagnetic energy is a very important parameter for the working principles of an MSA system, since it affects the efficiency of the heating process (Hashisho, 2007). As briefly described in Chapter 2 (Section 2.2.9), four different scenarios can be distinguished:

- *Microwave transparent adsorbent-microwave absorbing adsorbate:* This is the ideal case for operating the MSA system from an energy point of view, as the microwaves heat selectively only the sorbate, which is immediately desorbed. One example of this case is the regeneration of polar adsorbates (for example water) from microwave transparent adsorbents. In this case,

the polar adsorbate would absorb the microwave energy and directly convert it to heat, while the adsorbent would be indirectly heated through conductive transfer of heat from the adsorbate.

- *Microwave absorbing adsorbent-microwave absorbing adsorbate:* This scenario provides excellent and fast heating of the bed; however, selective heating of either the adsorbate or adsorbent is not feasible.
- *Microwave absorbing adsorbent-microwave transparent adsorbate:* Here, the adsorbent is directly heated by the electromagnetic waves, while the adsorbate is indirectly heated through thermal conduction.
- *Microwave transparent adsorbent-microwave transparent adsorbate:* In this case, neither the adsorbate nor the adsorbent are able to absorb microwave energy, and as a result direct microwave heating is not possible. However, solutions that involve mixing the adsorbent with a highly dielectric material, such as SiC, could help to overcome this hurdle, as it is investigated in Chapter 5 (Section 5.4) for silica based materials.

The case that is examined in this research is microwave absorbing adsorbent-microwave transparent adsorbate, as CO_2, is a non-polar molecule and as such it cannot be directly heated by microwaves. However, most of the sorbents selected for this work are excellent microwave absorbents, resulting in fast and efficient heating of the bed and their dielectric properties are discussed in the next chapters (Sections 4.1 and 5.1).

3.2. MSA equipment

When a microwave system is utilised for chemical processes, it usually comprises of a microwave source – known as magnetron or, more recently, solid state generators – connected to a power supply and a control system that transmits the electromagnetic waves into a metallic cavity, where the actual process takes place (Stefanidis et al., 2014). Hence, the first part to be examined is the reactor that is placed inside the microwave cavity. Moreover, other important factors include the microwave cavity and the temperature monitoring system. Furthermore, a proper gas detection system is important to be added after the microwave reactor, in order to monitor the gases that

come out of the system continuously. The following sections describe the main components of the lab-scale MSA system developed for this research.

3.2.1. Reactor design

The selection of the material of the reactor column is crucial, as it needs to be a microwave transparent material in order to allow the transfer of electromagnetic energy. Moreover, it should possess high chemical, heat and pressure resistance. Common materials for such applications include borosilicate or quartz glass, depending on the application and the temperatures that need to be reached. For low temperature applications (less than 250°C), glass borosilicate (Pyrex) is preferred, since it is cheaper than other types of glass. However, when temperatures exceed 250°C, for example in pyrolysis applications where temperatures may reach ~800°C, reactors made from quartz are generally preferred (Wharton, 2012). In other cases, the reactor can be made from a microwave-absorptive material (such as SiC), in order to supply additional heat contribution to the load, via thermal conduction. These materials are commonly known also as susceptors (Leonelli and Veronesi, 2015).

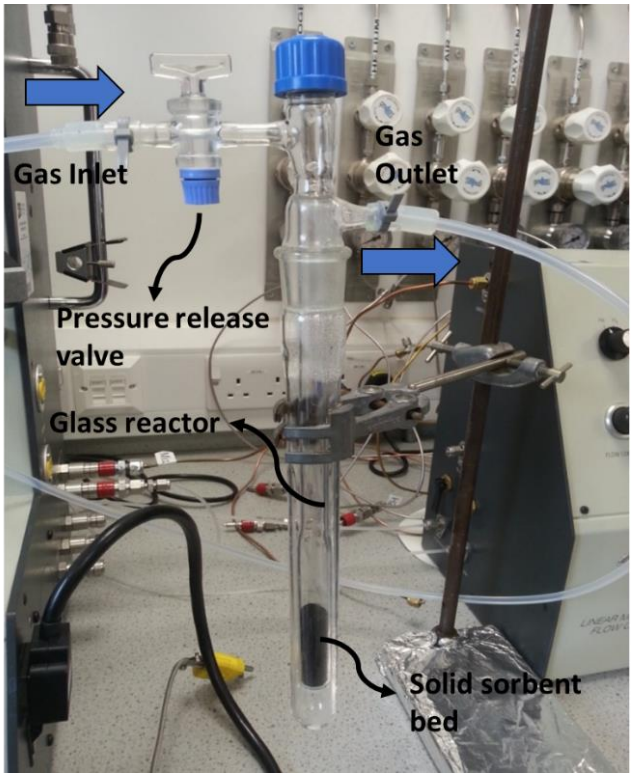

Figure 3.1: Photo of the glass reactor used for the experimental work during MSA and TSA processes

For the purposes of this research, glass borosilicate (Pyrex) was used as a raw material for the construction of the reactor, as seen in Figure 3.1. Figure 3.2 illustrates how the fluid moves inside the reactor, as well as where the feed and the exit are positioned and also depicts the place that the material is placed in order to be heated. This material is held inside the reactor by a grade 1 (90–150 μm) porous disk.

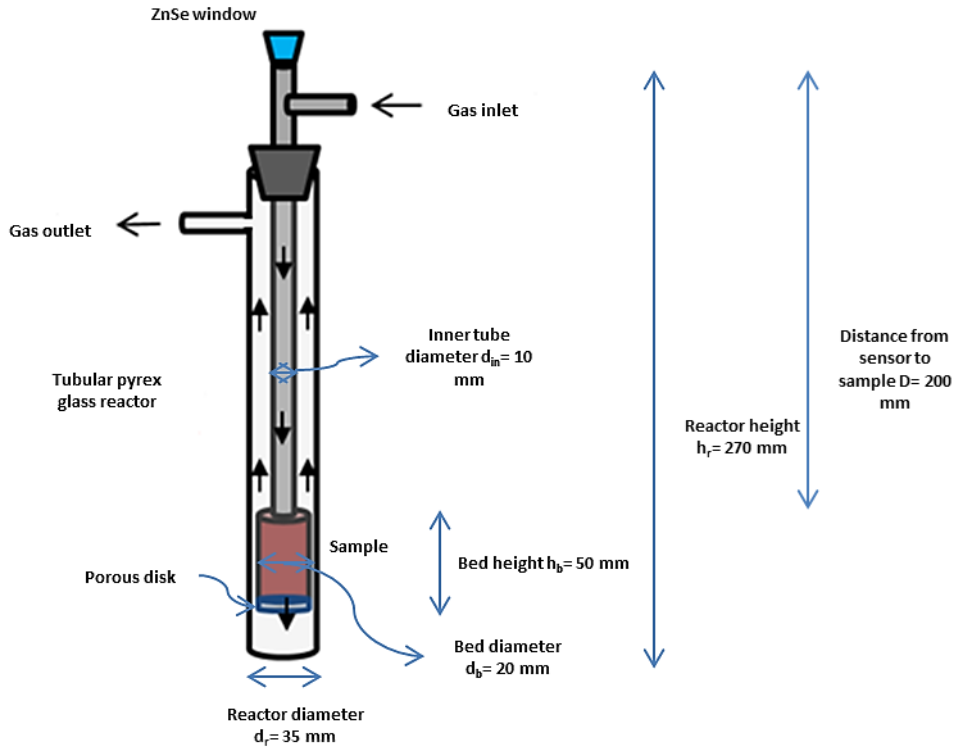

Figure 3.2: Schematic representation of the glass reactor, depicting the inlet/outlet, the fluid flow (arrows) and the position of the sample

3.2.2. Microwave cavity

An initial investigation for the suitability of several available microwave systems was undertaken, mostly exploring the differences between a single and a multimode cavity system. As explained in Chapter 2 (Section 2.2.8), the biggest advantage of a mono-mode application is that higher electromagnetic field densities can be created inside the cavity resulting in higher heating rates, which in turn contributes to the issue of non-uniform heating across the heated object. However, the main limitation of a single mode cavity is the process volume (<200ml) of the workload, which would critically limit the flexibility of the amount of sorbent used during the MSA process.

Considering the above limitations, a multimode microwave system, purchased from Sharp (R28STM) and modified by Tan-Delta as explained below, was used. This system was also equipped with an external Proportional Integral Derivative (PID) controller provided from Eurotherm (3405) that was needed in order to regulate the output temperature or power, as seen in Figure 3.3. This system was selected for the following characteristics: the cavity itself was a robust, stainless steel box of a relatively large size able to accommodate different reactors in various sizes and shapes. Moreover it was equipped with an 800-W magnetron, sufficient for the scope of this research, since the temperature of the desorption experiments did not exceed 150°C, while it also included overheat protection via an effective cooling system of the magnetron.

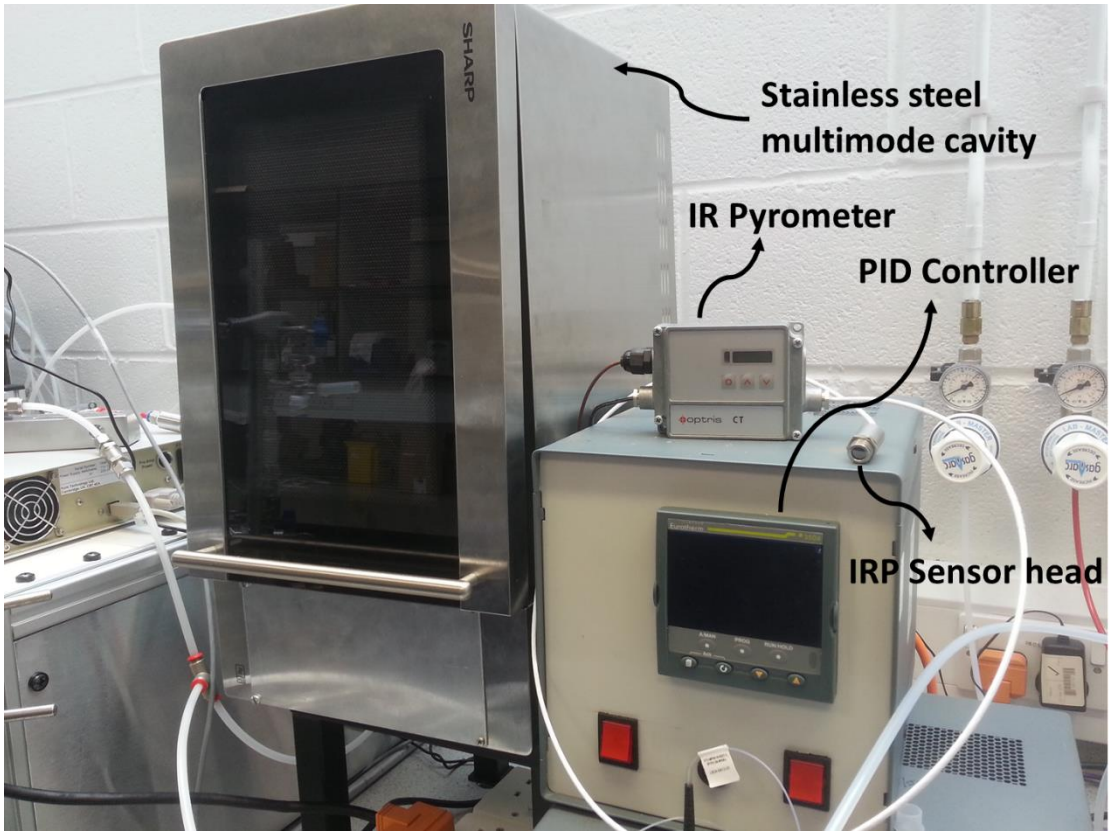

Figure 3.3: The multimode microwave system; the stainless steel cavity on the left and the Eurotherm 3504 controller on the right

Regarding the Eurotherm PID controller, its easy programming of various heating steps (time vs temperature/power rates) and the exceptional power control - allowing power levels to be adjusted in 1% increments, while temperature levels could be adjusted in 0.1°C increments - were the main advantages that could give enough flexibility for the purposes of this research. Another interesting fact about this PID controller is that it provides the flexibility to choose from two different modes: either use a fixed

temperature value as an output, making the magnetron to operate in pulses until the object reaches the required temperature, or use a desired power percentage output signal resulting in a continuous operation at that specific power. However, for the purposes of this work, the pulse mode with a fixed output-target temperature was used, since the fixed parameter in this research was the desorption temperature.

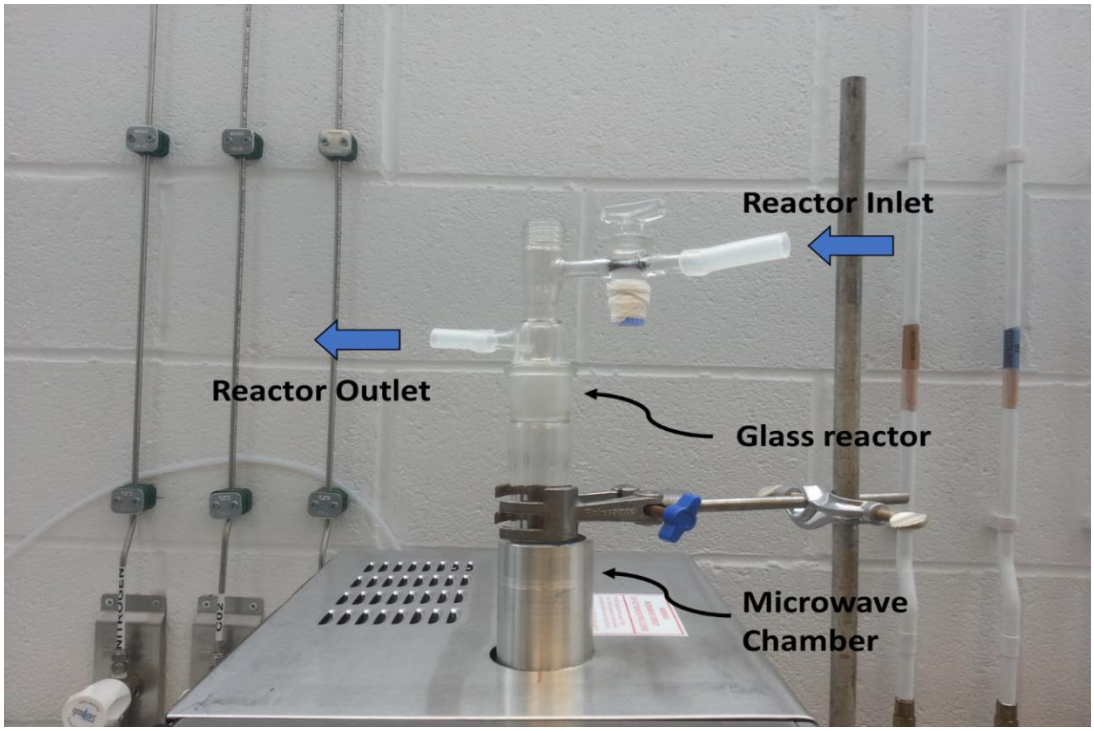

Figure 3.4: Photo of the microwave chamber/port that allows the reactor to penetrate into the cavity

The microwave cavity was modified in order for the reactor to pass through the cavity walls; two stainless-steel chambers (41.3 mm i.d., 130 mm long) were fitted to the cavity by bolting double flanges on its left and right sides and then the cavity was turned vertically on its side (visible in Figure 3.4). The modifications were performed from Tan-Delta Microwaves Limited; the dimensions of the chambers were estimated from the diameter and the length of the reactor as well as from the wavelength of the microwave radiation in terms of safety, in order to prevent any microwave leakages. In general, ports of ~40mm of diameter are completely safe providing that less than the equivalent of 1.5 cm diameter of dielectric material with a relative permittivity of 2 is inserted through them. The glass reactor, which is a microwave insulator leaving the microwaves to penetrate through material (Section 2.2.2), used in this research has the equivalent diameter of ~4mm, which according to the above, makes the process safe. As mentioned in Section 2.2.2, the wavelength (λ) can be calculated by equation 2.1 and

as a result, it can be calculated that the wavelength in standard frequency microwave applications is almost equal to $\lambda \approx 12$cm, which is very large, compared to the size of the ports.

Another important factor is the position of the reactor inside the cavity; since there was no flexibility in terms of the position of the metallic chambers/ports, the height in which the best microwave performance can occur, was investigated. This would also affect the length of the reactor.

In order to investigate which height is the optimum position inside the cavity, tests with water were conducted as follows: A 500ml beaker filled with water was placed in 7 different positions, with an increment of 5cm, with the h = 0cm being the position where the door opens (Figure 3.3). The water was then heated using the temperature mode of the PID controller, meaning that an output temperature of 100°C was set and the magnetron was operating in pulse mode, providing different percentages of power whenever needed. The time needed for the water to reach 100°C was monitored and the results can be seen in Figure 3.5. It is quite evident that, the optimum positions inside the microwave cavity are on the top (30cm), bottom (0cm) and in the centre (15cm), with the result being in agreement with previous studies (Requena-Pérez et al., 2005). More interestingly, it should be noted that, when the water was placed in the centre, the performance of the magnetron was the highest, being able to heat to 100°C in less than 20 seconds. As a result, in this research, it was decided that the material bed should be placed in the centre of the cavity (15cm).

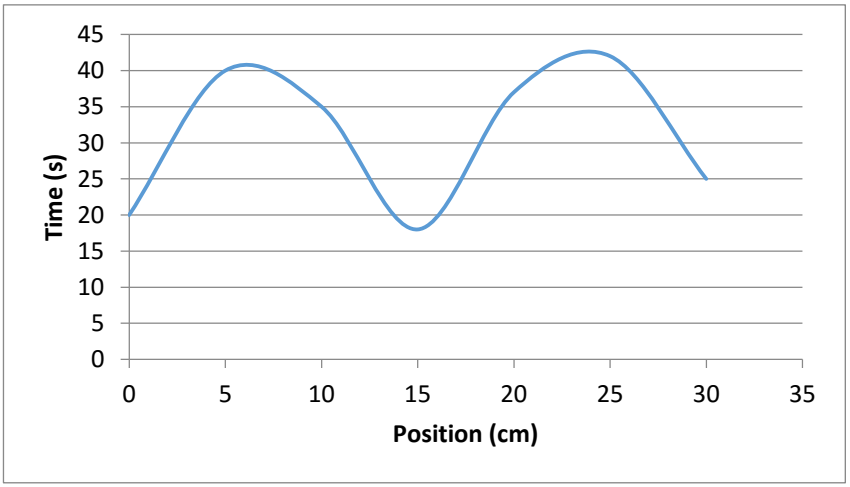

Figure 3.5: Time needed to heat a 500ml beaker filled with water at different positions inside the microwave cavity

3.2.3. Temperature monitoring

A reliable system of measuring and/or controlling the temperature of an object while heated in an electromagnetic field is of great importance for the efficient application of the process. Apart from the temperature control, power feedback control systems that are operated in parallel in most microwave reactors, could also be of help, enable a heating process to be carried out without knowing the exact dielectric properties and/or conductive properties of the material heated. However, temperature control is by far the most common technology followed for microwave assisted applications, but does not come without its own disadvantages. For example, inaccuracies in temperature measurements could result in erroneous indications and misleading interpretations of the final outcome. Moreover, a possible thermal runaway could lead to severe damage of the microwave system and/or reactor. In general, temperature in a microwave cavity can be measured by one of the following instruments:

- Shielded thermocouple
- Fiber-optic thermocouple
- Infrared optical pyrometer (IRP)

Application of conventional metallic thermocouples may not provide an accurate measurement, mostly due to the metallic nature of the instrument; electromagnetic interference is possible to occur, which could lead to arcing between the thermocouple shield and the cavity walls, resulting in failure of thermocouple and system performance. Moreover, a metallic thermocouple inserted into the aforementioned ports while the microwave is in operation would form a coaxial line and the microwaves would transmit very efficiently through the port, leading to significant microwave leakage (Menendez et al., 1999).

On the other hand, optical fibre sensors, known for their glass-based nature, are not affected by electromagnetic fields and can maintain a high level of accuracy in temperature measurement (Ong and Akbarnezhad, 2014). However, fibre-optic thermocouples can only be applied up to 300°C and are too fragile for real industrial-scale applications. Last but not least, the most important disadvantage of both conventional and optical fibre thermocouples is that they require contact with the

material, which would mean that further modifications in the reactor or in the microwave chamber should take place.

A third way of measuring the temperature of an object inside the microwave cavity is by inserting a metallic thermocouple into the hot material immediately after switching off microwave power, in order to avoid the aforementioned disadvantages. This rather simplistic approach may sometimes help in the cases that temperature control is not required and large and bulky items are to be measured while no modifications in the cavity are possible. However, it should be pointed out that the temperature of some materials can drop instantaneously as soon as microwave power is turned off, resulting in a substantial error (>20% temperature decrease after 5 seconds) in the measurement (Bogdal, 2005).

Consequenlty, in this work an infrared pyrometer was used as it provides contactless and fast (response time: 6 ms) temperature measurements with a high level of precision (accuracy of thermocouple output: ±1%). Infrared thermometers are easy to use, by simply pointing the instrument at the object to be measured and the temperature is digitally shown on the PC. Temperature monitoring was performed by an IRP, purchased from Optris (Optris CTfast CT LT 25F), which was assembled to the PID controller (Figure 3.6), and its operating principles are described in the next section. Unfortunately, infrared pyrometers measure only the temperature of the surface of the sample, which in some cases could be substantially lower than the bulk temperature during desorption processes due to non-uniform heating, as shown in the next chapters. As a result, the geometry of the adsorbent bed, which depends on the shape and density of the adsorbent particles, affects the temperature distribution and consequently the precision in temperature measurement. Hence, detailed heat maps investigating the differences between surface and bulk temperature are presented for each different geometry in the following chapters (Sections 4.5 and 5.3.2.5).

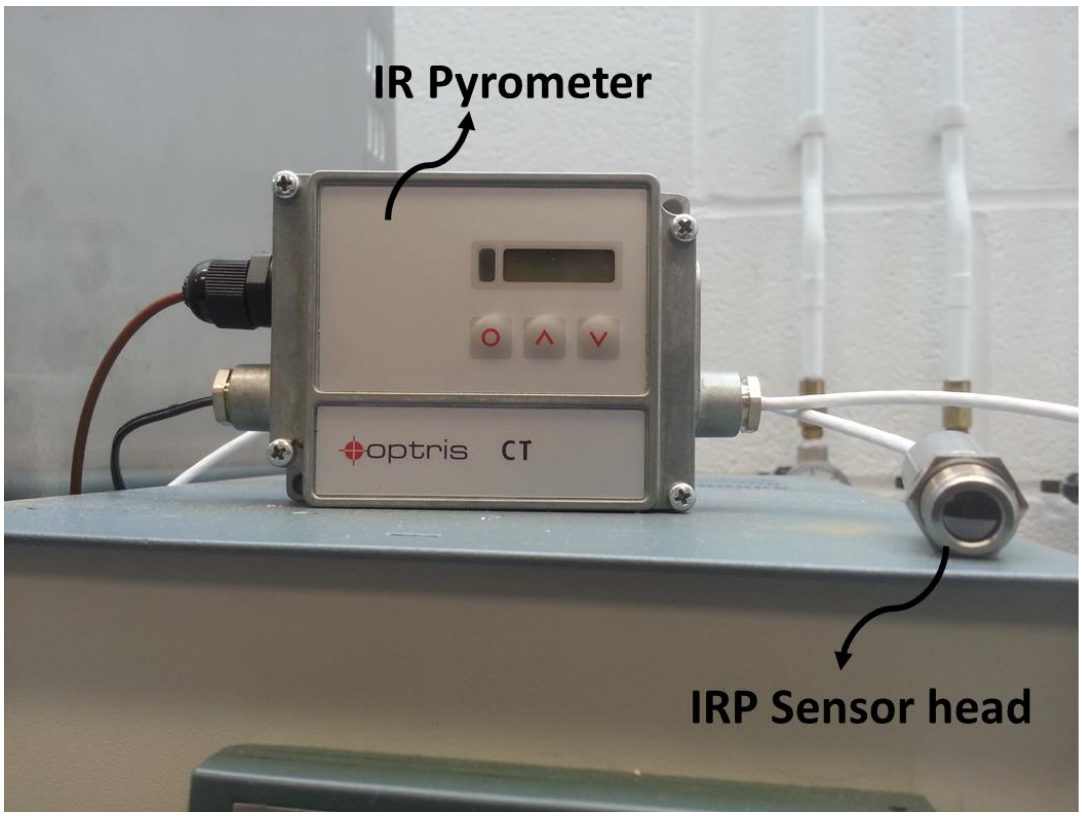

Figure 3.6: Photo of the IRP, assembled to the PID controller. The sensor head can be seen on the right

3.2.3.1. Infrared radiation

Every object that has a temperature above absolute zero (0K or -273.15°C) emits a specific infrared radiation. This radiation is part of the electro-magnetic spectrum, with the primary source being heat or thermal radiation. It is produced by the motion of atoms and molecules of the object in such a way that the higher the temperature, the more the atoms and molecules move and consequently the more infrared radiation they produce. When the object is not hot enough to produce detectable light, it will emit most of its energy in the form of infrared. Hot charcoal, for instance, may not produce light, however it still emits infrared radiation which from a human perspective can be understood as heat (Nutter, 1988).

In principle, the wavelength of infrared radiation lies between a fraction of a micron up to several hundred microns. As such, infrared pyrometers use a wavelength of between 4 and 14 microns for accurate temperature measurement. However, since the infrared radiation of an object is emitted from its surface, the IRP is not able to measure its internal (bulk) temperature. Another disadvantage when using the IRP is that it cannot accurately measure the temperature of an object through any covering material; this

means that since the reactor is made from glass, an optical window – transparent to infrared radiation is needed in order for the IRP to be able to 'meet' the object's surface. As a result, in this research an optical polished window made from a chemically deposited material, zinc selenide (ZnSe), was used, with thickness of 1mm and diameter of 22mm, purchased from Crystan, which can be seen in Figure 3.7. Moreover, air temperature cannot be measured by an IRP, so the void space between the window and the material plays no important role on the IRP temperature measurement.

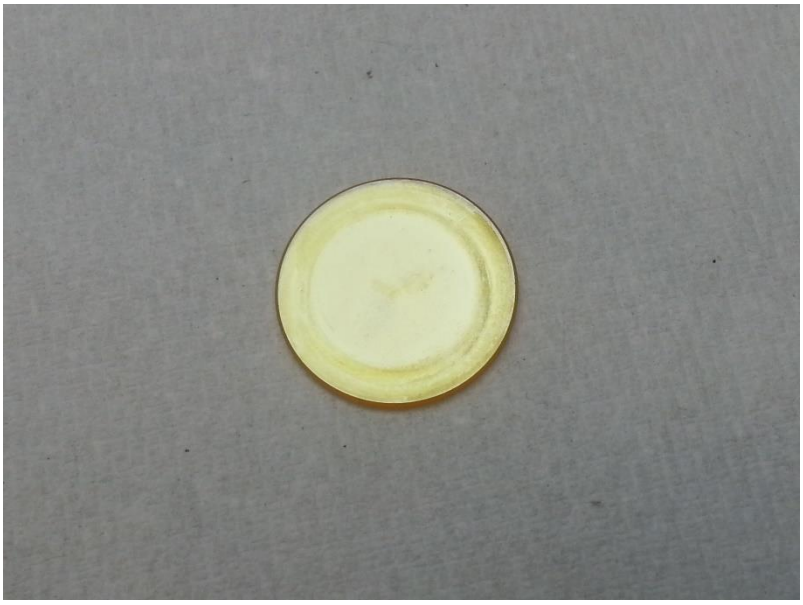

Figure 3.7: Photo of the zinc selenide window (ZnSe)

ZnSe windows are an excellent choice for a broad range of infrared applications including thermal imaging, Forward Looking infrared (FLIR) cameras, medical systems, as well as high power CO_2 laser systems because of their low absorption coefficient and high resistance to thermal shock. ZnSe is a relatively soft material that scratches easily and it is not recommended in harsh environments, since its Knoop Hardness is only 120. It can be found in various diameters and thicknesses, which affects the % of signal transmittance through the window. However, as mentioned above, for the temperature measurement application, the IRP works at a wavelength between 8 and 14μm, for which the signal transmittance is ~72% for every thickness, as seen in Figure 3.8.

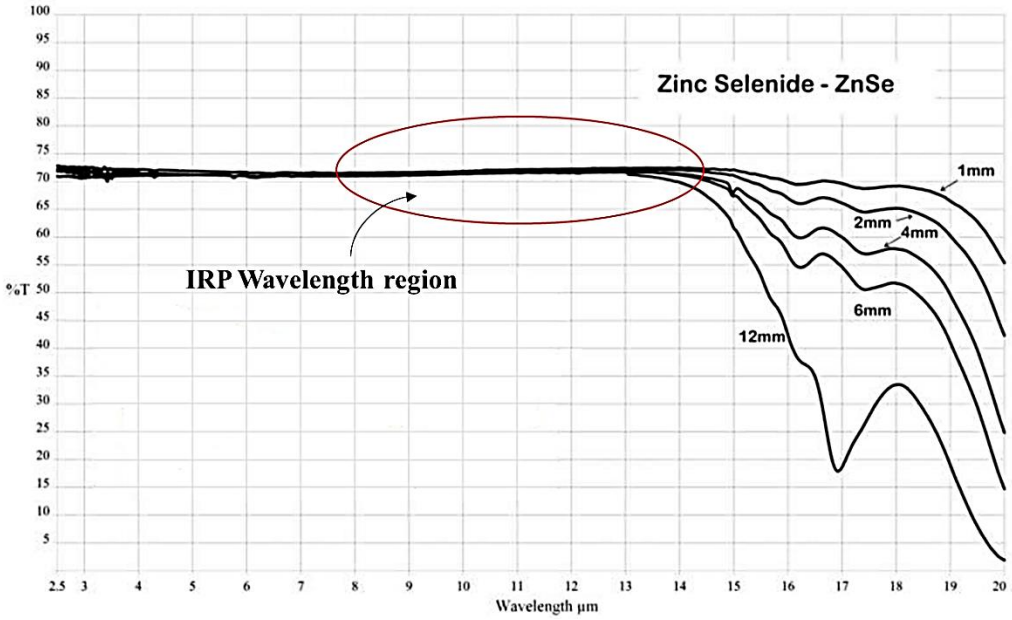

Figure 3.8: ZnSe Transmittance % versus wavelength for 5 different thicknesses

3.2.3.2. Emissivity factor

Another important parameter for the proper handling of infrared measurements, including measurements with an IRP, is the emissivity of the object investigated. Emissivity is defined as the ratio of radiation emitted by a surface or blackbody and its theoretical radiation predicted from Planck's law:

$$B_\lambda(T) = \frac{c_1}{\lambda^5(e^{c_2/\lambda T}-1)} \tag{3.3}$$

where $c_1 = 1.19 * 10^8 W m^{-2} \mu m^4$, $c_2 = 1.44 * 10^4 \mu m K$ and T is the object's temperature. Emissivity, in other words, is a measure of the efficiency in which a surface emits thermal energy (He et al., 2009). The emissivity value of the black body is 1, since it is a perfect emitter of heat energy, as such the emissivity value of most objects lies between 0 and 1. Emissivity value of 0 would indicate that the material is a perfect thermal mirror. However, in reality there are no perfect "black bodies" and very few perfect infrared mirrors (The pyrometer handbook, 2004).

Table 3.1 presents the emissivity values of the materials used in this research. A material's surface emissivity is measured by the amount of energy emitted when the surface is directly observed. However, the accuracy of those numbers can be

questioned, since the emissivity factor strongly depends on the surface texture and colour as well as on wavelength of interest and the material's temperature at the time of measurement. Taking that into consideration, each material was specifically calibrated for the temperature ranges needed, using a conventional thermocouple and adjusting the IRP's emissivity factor until the reading of the IRP matched the temperature measured by the thermocouple.

Table 3.1: Emissivity factor of some specific materials at 25°C and 1 bar (Scigiene Corp., 'Infrared Thermometer Emissivity tables')

Material	Emissivity
Activated carbon (<100μm)	0.95
Activated carbon (100-300μm)	0.9
Activated carbon (1-3mm)	0.75
Activated carbon (300-700μm)	0.8
Carbon (graphite)	0.98
Glass	0.92
Quartz	0.93
Silicon Dioxide (SiO_2)	0.55
Water	0.95

3.2.3.3. Infrared pyrometer sensing head

Figure 3.9 presents how the diameter of the measuring spot changes with regards to the distance between measuring object and sensing head and is described as D:S ratio, where D is the distance from front of the sensing head to the object and S corresponds to spot size. The distance is measured from the front edge of the sensing head, whereas the spot size refers to 90% of the radiation energy emitted. As a result, the size and the diameter of the measuring object, as well as the optical resolution of the IRP regulate the maximum distance between heated object and sensing head. In order to avoid significant measuring errors, it is usually preferred the object to fill out the optics' field of view completely. Hence, the spot should at all times have the same (or smaller) size as the target object.

In this research, the diameter of the inner tube of the reactor is 10mm, as explained above (Figure 3.2). Moreover, the distance from the sensing head to the sample's surface is 200mm (Figure 3.2), which results in a ratio of 200:10, i.e. 20:1. As a result,

the IRP sensor head that was selected was the one with a D:S ratio of 25:1, which means that at 200mm distance from the head, the measuring spot would be 8mm, as seen in Figure 3.9. Hence, it is clear that, this is well inside the limits and restrictions posed from the IRP measurements.

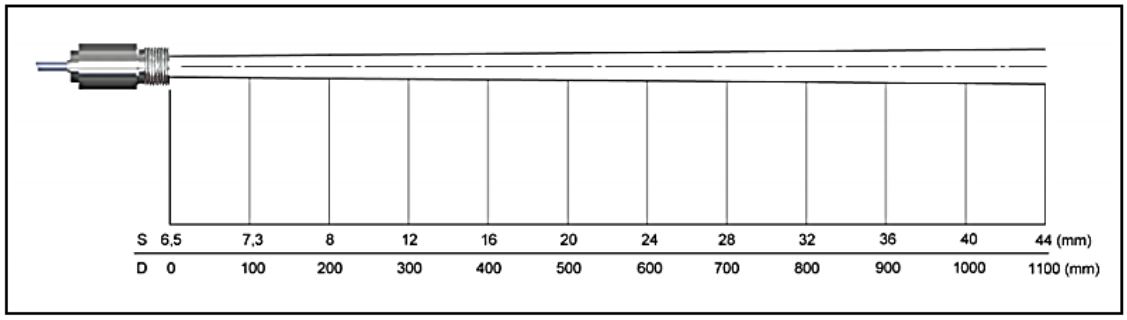

Figure 3.9: D:S ratio for the selected IRP for this research

3.2.4. Time-of-Flight Mass Spectrometer (TOF-MS)

A TOF-MS was used for the detection of the gases exiting the reactor during the MSA and TSA experiments. In general, a mass spectrometer – or analyser - takes advantage of the difference in mass-to-charge ratio (m/z) of ionized atoms or molecules in order to separate them. Hence, mass spectroscopy is used for atom (or molecule) quantification while providing important structural information by the identification of distinctive fragmentation patterns.

In theory, mass analysers can separate ions of different masses in various, well developed, ways. There are systems that work in an electric or magnetic field and use the mass dependent deflection of a beam of analyte ions, to ensure that only ions of a finite range pass through a slit and are identified. Another common technology of mass spectroscopy is the production of static and radio frequency electric fields so that only a small amount of ion masses have constant trajectories and are able reach a detector. As the name implies, a time-of-flight mass spectrometer measures masses by recording the ion flight time.

Figure 3.10 shows in a simplistic way the governing principle of the TOF-MS. The two ions, in red and green colours, in the above schematic have slightly different masses and they start simultaneously from the extraction region, which initially is field free,

possessing little velocity at that time. The extraction operates under a more positive potential than the rest of the spectrometer regions. Suddenly, an extraction field is applied and the ions are abruptly accelerated out of the extraction region, through the acceleration region, falling into the field-free drift tube operating at the lower potential. In principle, both ions obtain roughly the same kinetic energy (E_{kin}) during this 'flight' which can be determined by the potential difference between the extraction and drift regions. However, the ions do not reach the detector at the same time, indicating that their velocities are different. As expected, the lighter ion 'flies' faster and reaches the detector quicker than the heavier ion. Two pulses are recorded at the detector, one for each ion at the moment of arrival.

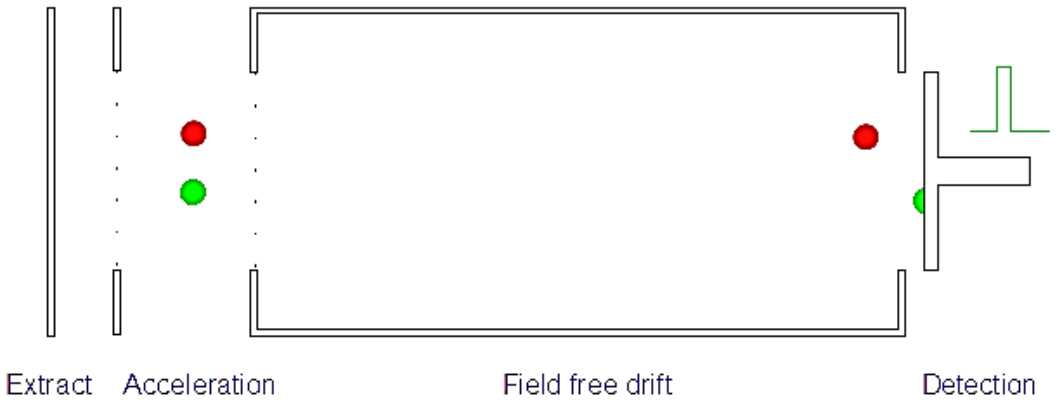

Figure 3.10: TOF-MS ions analysis: the red and green ions start simultaneously from the accelerator, but reach the detector in different times

The velocity (u) of the ions is simply calculated by the following equation:

$$u = \sqrt{\frac{2*E_{kin}}{m_i}} \tag{3.4}$$

Where m_i is the mass of each ion.

Flight-times (t_{fl}) are measured with respect to the start of the extraction pulse. It is fairly easy to conclude that t_{fl} is proportional to the square-root of the mass in the drift region:

$$t_{fl} = \frac{l_{dr}}{v} = l_{dr} * \sqrt{\frac{m}{2* E_{kin}}} \tag{3.5}$$

Where l_{dr} is the length of the drift.

There are various advantages that come with the use of TOS-MS, including excellent sensitivity, high ion transmission and high mass range as well as high-speed analysis (Hart-Smith and Stephen J. Blanksby, 2012). This made TOF-MS an excellent instrument for the purposes of the continuous monitoring of CO_2 separation from a mixture of CO_2 and N_2, even at low concentrations, being also able to detect possible impurities along with the simulated gas mixture. Figure 3.12 shows the TOF-MS used during this research. It was supplied by KORE Technology along with two software packages, one for spectra analysis and one functioning as a gas chromatographer, enabling a continuous monitoring of the signal, which would result in breakthrough curves and desorption profiles, as described in Chapter 4.

3.2.5. Flow controllers

Two flow-controllers were used for the completion of the MSA and TSA experiments. The first was purchased from Omega (FL-6GP-45ST-41SA-41C) and was a simple analogue bubble flow controller, used to regulate the inlet flow of the gas mixture. The second one was purchased from Bronkhorst (Coriflow TM-13) and was only used as a flow-meter, in order to obtain an accurate value of the flow at the exit of the reactor, prior reaching the TOF-MS. The Coriflow TM-13 is a precise and compact mass flow controller, based on the Coriolis measuring principle. The so called "Coriolis effect" started to find application in 1970's, named after the French scientist Gaspard-Gustave Coriolis, who in 1835 examined the effect that moving objects deflect from a straight path when they are viewed from a rotating frame of reference. With regards to the Coriolis flow controller, the above statement can be related to the change in frequency, phase shift or amplitude, caused by the flow of a fluid through a vibrating tube and is proportional to the mass flow through the tube, giving the density of the fluid as secondary output.

The Coriflow TM-13 consists of single loop sensor tube, creating part of an oscillating system. As seen in Figure 3.11, when the fluid – in this case the gas mixture - flows through this tube, the Coriolis effect takes place causing a variable phase shift, which is detected by the flow-controller's sensors and is transmitted into the pc-board. The

resulting digital output signal is proportional to the real mass flow rate of the fluid, while as secondary output there is the option to choose from fluid density or temperature.

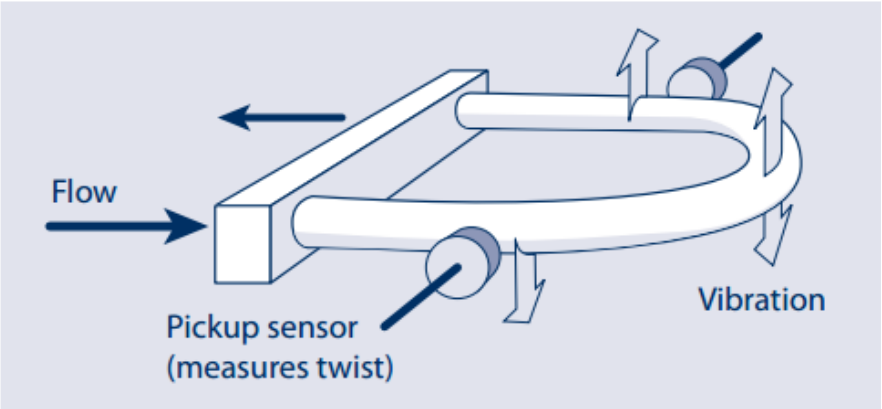

Figure 3.11: Schematic of a Coriolis flow sensor

The use of the Coriolis measuring principle has many advantages over conventional thermal mass flow devices, especially when applied on gases, including:

- no conversion factors are needed (if scaled in units of weight);
- it is possible to measure unknown fluids or variable mixtures;
- (super-) critical gases can also be measured;
- superior accuracy and response time are provided.

Figure 3.12 shows the setup of the Coriflow TM-13 (accuracy <±0,5%), connected to the TOF-MS.

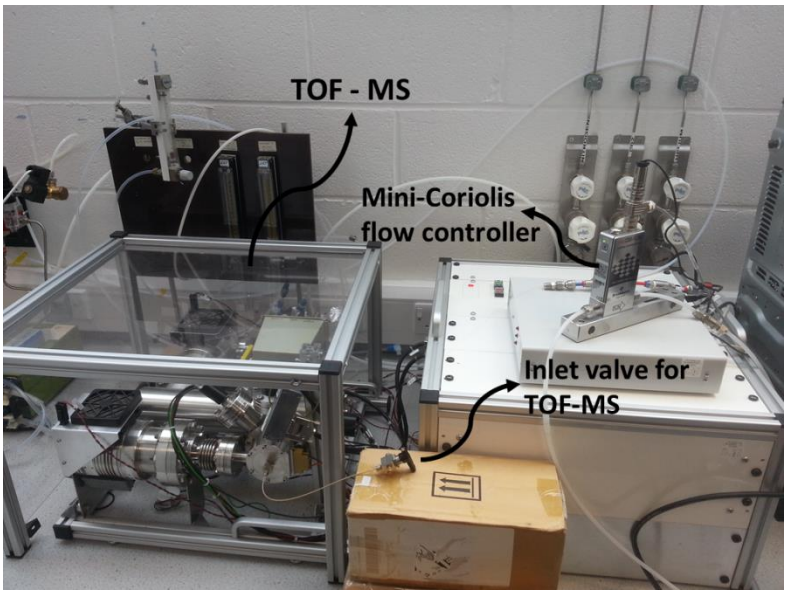

Figure 3.12: The Coriflow TM-13 and the TOF-MS

3.3. Analytical characterisation techniques

This section describes the analytical techniques applied for characterisation of the solid materials that were used throughout this research. Focus was concentrated on textural, chemical and dielectric properties of the sorbents, aiming at evaluating their CO_2 adsorption and desorption performance. As a result, the properties that directly affect the TSA and MSA processes were chosen to be investigated. Initially, CO_2 adsorption capacity using thermo-gravimetric analysis (TGA) was conducted in order to examine if the selected sorbent was a good candidate for the CO_2 capture process (Section 3.3.1). In addition, Brunauer, Emmett and Teller (BET) analysis, examining the surface area and the porosity of the materials, was also undertaken, providing information on the porous network and CO_2 adsorption mechanism (Section 3.3.2). Moreover, the chemical texture of each material was also of interest and as a result, elemental analysis (CHN analysis) was conducted (Section 3.3.3). Lastly, dielectric properties of each material were calculated, since accurate evaluation of these properties provides with valuable information to properly incorporate the material into the MSA heating process (Section 3.3.5). Each aforementioned property was investigated before and after the TSA and MSA experiments, in order to examine the effect of the cyclic heating processes to the materials, which would help to predict the life span of each sorbent.

3.3.1. Thermogravimetric analysis (TGA)

TGA is a characterisation method during which the amount and rate of weight change in a material is monitored, either as a function of increasing temperature, or isothermally as a function of time. A TGA instrument usually consists of a sample pan that is placed in a furnace, supported by a precision balance. During the heating or cooling of the pan, depending on the experiment, the sample's mass is recorded while a purge gas flow creates and controls the sample environment. This gas is either an inert or a reactive gas that passes through the sample and is responsible for its weight change (Perkin Elmer, 2010).

CO_2 adsorption capacity analyses were conducted using a TA Instruments Q500 Thermogravimetric Analyser (TGA) in a controlled gas flowing environment, in order to validate that the selected sorbents are good candidates for CO_2 capture. This instrument has a weight precision of ±0.01% and a temperature precision of ±0.1°C.

The weight increase observed in the samples is attributed to the adsorption of the CO_2 onto each sample. The initial weight of the sample was ~20mg. Prior to CO_2 adsorption experiment, the samples were preconditioned and dried at 100°C using a purge gas flow of N_2 at 5 ml/min for 30 minutes. Then, the adsorption temperature was elevated and stabilised at the target temperature, namely 35°C for 30 minutes at atmospheric pressure, followed by a switch of the flowing gas to 90% CO_2 at 100 ml/min (balanced with N_2), in order to investigate the samples' CO_2 adsorption capacity. The weight increase related to CO_2 adsorption was monitored as a function of time at constant temperature (35°C) and concentration of CO_2 at atmospheric pressure. The adsorption step lasted for 2 hours to allow sufficient time for the capture process to equilibrate. Subsequently, the temperature was increased to 70°C and the gas was shifted back to a N_2 flow of 5ml/min for 1 hour, in order to allow CO_2 desorption to occur. It is worth mentioning that this CO_2 desorption procedure does not simulate the actual technology used at an industrial scale application, however, it is considered an established practice in a laboratory-scaled analysis, as reported in published work (Essaki et al., 2005; Olivares-Marin et al., 2010).

3.3.2. BET surface area and DFT pore size analysis

The amount adsorbed is mainly affected by the surface area and porosity of the solid adsorbent, influencing the quality and utility of the sorbent and as a result those physical properties need to be extensively investigated. Knowledge of surface area and especially porosity is often an important key in understanding the formation, structure, and potential application of the sorbent material. In order to examine the surface area and the porosity of the sample material, gas adsorption analysis is commonly used. This analysis takes place by exposing the solid sample to gases or vapors within a range of conditions and evaluating either the sample's volume or its weight change, measuring the so-called material's adsorption isotherm. In theory, depending on the type of adsorbent/absorbate and intermolecular interactions between material's surface and the gas, different-shaped of isotherms can be formed. Figure 3.13 shows the modern IUPAC classification of adsorption isotherms, also known as Brunauer, Deming, Deming and Teller (BDDT) classification, identifying six different broad categories:

- Type I: Steep initial region due to very strong adsorption forces, indicating strong adsorbent microporosity (monolayer adsorption only). Moreover, a

limiting value (plateau) is also evident, due to filled pores, essentially implying that there are relatively small – or no - external surfaces.

- Type II: At first, the rounded knee indicates approximate location of monolayer formation, whereas the low slope region in the middle of isotherm indicates the existence of some multilayers. Lastly, absence of hysteresis indicates adsorption on and desorption from a non-porous or macroporous adsorbent with strong adsorbate-adsorbent interactions (unrestricted monolayer-multilayer adsorption).
- Type III: The lack of knee represents a non-porous or macroporous adsorbent with extremely weak adsorbate-adsorbent interaction.
- Type IV: At first, the rounded knee indicates approximate location of monolayer formation, whereas the low slope region in the middle of isotherm indicates the existence of some multilayers. Moreover, hysteresis indicates capillary condensation in meso and macropores.
- Type V: Adsorption isotherm with hysteresis, while pores are evident in the mesopore range. The lack of knee represents extremely weak adsorbate-adsorbent interaction.
- Type VI: Stepped isotherm, rarely encountered

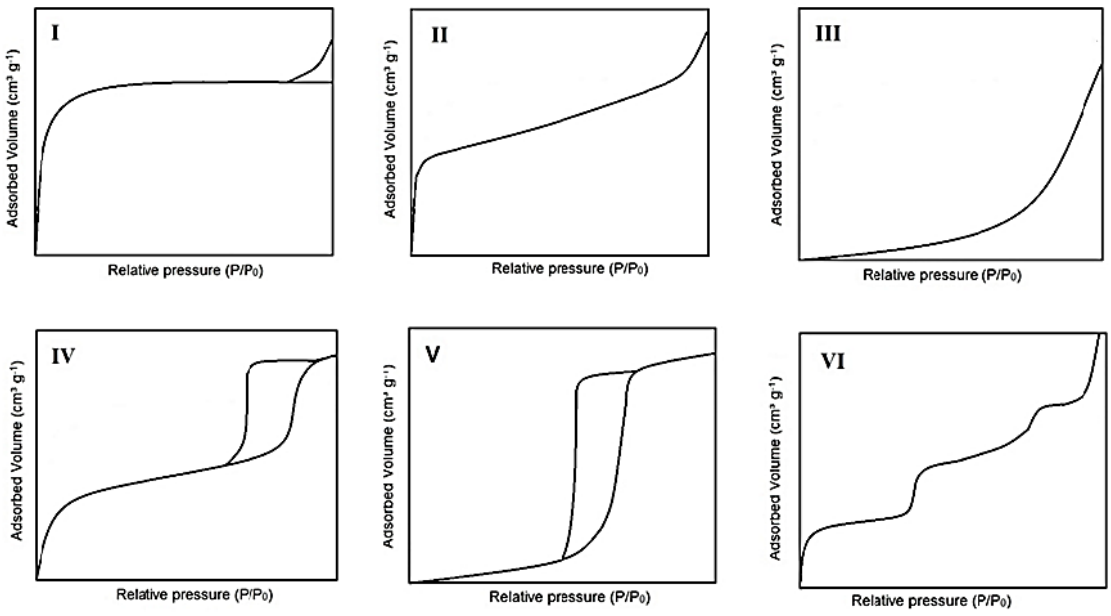

Figure 3.13: IUPAC classification of adsorption isotherms (Balbuena et al., 1993)

Adsorption isotherms (Figure 3.13) help to extract important information about the sorbent material, such as surface area and pore size distribution. Isotherm models, such

as Langmuir, Brunauer, Emmett and Teller (BET), Dubinin Radushkevich method (DR), Temkin adsorption isotherm and Freundlich models, are used to interpret the adsorption isotherms. In this work, the BET model was used, since it is the most accepted model for analysis of the physical adsorption of gases on porous carbons. From the above categories, BET can only be applied to type I, II, IV and VI. BET equation can be expressed as:

$$\frac{P}{V(P^0-P)} = \frac{1}{V_m c} + \frac{(c-1)}{V_m c}\frac{P}{P^0} \tag{3.6}$$

Where V is the volume of gas adsorbed at pressure P, P^0 is the saturated pressure of adsorbing gas at a particular temperature, V_m is the volume of gas adsorbed to form a monolayer on the surface, known as the monolayer volume. Moreover c is expressed by the following equation:

$$c = \exp[\frac{H_a - H_L}{RT}] \tag{3.7}$$

where H_a is the enthalpy of adsorption of the gas on the solid, H_L is the heat produced on forming the second and higher layers, R is the ideal gas constant and T is the temperature (Brunauer et al., 1938).

In addition, adsorption isotherms can also be utilised for pore size analyses. Density Functional Theory (DFT) method was used in this research since it is a common model for microporous materials (Shaw, 1998). DFT describes the gas adsorption process at the fluid-solid interface. Applying DFT to the experimental adsorption isotherms (Figure 3.13), both micro- and meso-porosity can be determined as a continuous distribution of pore volume with respect to pore size. Seaton et al. (1989) were the first to propose that the DFT model provides a more reasoned and versatile approach in order to calculate the pore structure parameters, compared to methods that were used until then. Unlike conventional methods, DFT provides a continuous distribution, with smooth transition between regions and all data are used. Although DFT is not preferred for complex disordered pore structures, it has computational advantage over molecular simulation for simple fluids and pore shapes like slits, spheres, or cylinders (Ogbuka, 2013).

The amount of sample used for the above analyses was approximately 0.5g. Sample preparation involved degassing the samples overnight (15 hours) at 100°C. For both analyses, the sample under investigation was exposed to N_2 at its liquid state (77 K). The BET equation applies at a relative pressure range (P/P_0) of $0.05 < P/P_0 < 0.3$ and the samples were subjected to a 90-point BET surface area analysis, and full adsorption isotherms were collected for all samples. BET surface area and DFT pore size analyses were conducted for all the materials used in this research, using the Gemini VII 2390, provided by Micromeritics, with an accuracy <±0.5% (measured by the manufacturer).

As seen in Figure 3.14, the Gemini instrument consists of two gas reservoirs (A), filled with equal amount of the desired adsorptive (usually N_2), which is dosed into the sample and balance tubes. During gas adsorption from the sample, the pressure tends to decrease in the sample tube. Consequently, a transducer (B) is used to monitor the desired pressure, while causing a fast response servo valve (C) to hold the pressure constant. A second pressure transducer (D) detects any pressure difference between the two tubes and causes another servo valve (E) to equilibrate the pressure in both tubes. Another transducer (F) monitors the pressure between the two reservoirs to determine the amount of gas adsorbed on the sample.

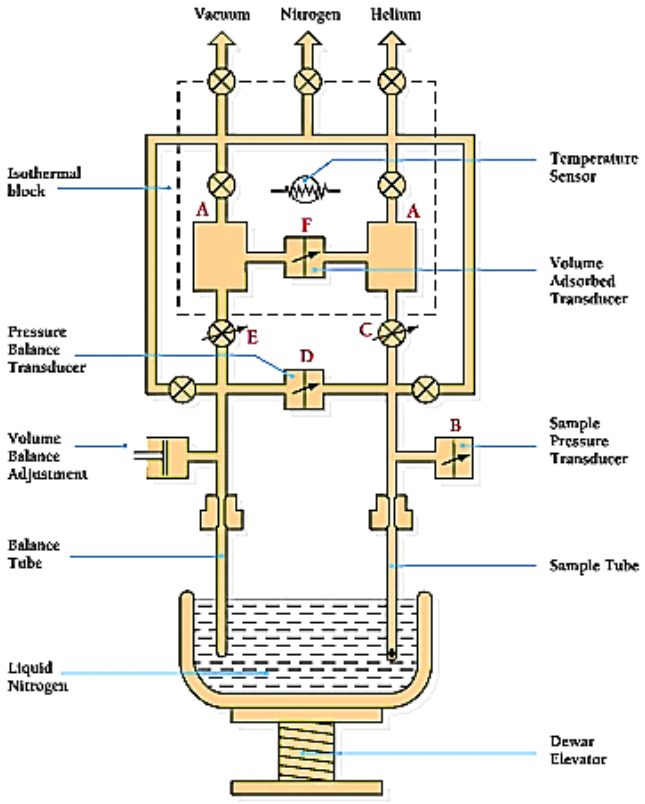

Figure 3.14: The Gemini instrument used for the BET and DFT analysis (Micromeritics Gemini VII brochure, 2014)

3.3.3. Elemental analysis

Elemental analysis is used to determine the amount of an element in a compound, usually expressed as a weight percentage. This analysis offers the possibility to determine the empirical formula of a compound, which is the formula that presents the proportions of the elements found in it (Etherington et al., 2001). There are various experimental ways to determine elemental compositions, however, the most frequent type of elemental analysis is the carbon, hydrogen, and nitrogen (CHN) analysis (Thompson, 2008). CHN analysis was conducted by the department of Engineering and Physical Sciences (EPS) of Heriot-Watt University using the Exeter CE-440 Elemental Analyser. The accuracy of the instrument is ±0.15%, while the sample size is typically 1-5mg.

At first, the sample is weighed to one millionth of a gram inside a small tin capsule, which is placed into the analyser's furnace (combustion tube) at 950ºC. At this temperature, tin oxide is formed after combustion at an oxygen-rich environment, resulting in a temperature increase to well above 1800ºC. Under those conditions, vaporization of the sample takes place, followed by complete combustion forming CO_2, N_2, N_xO_y, H_2O and other by-products. Halogens, sulfur, phosphorus, and other undesirable by-products are removed using chemicals inside the combustion tube. Subsequently, the sample gases flow through a reduction tube, removing any unused oxygen and converting NO_x to N_2. Then these gases are homogeneously mixed in a mixing chamber under constant pressure and temperature. Lastly, a small amount of this mixture flows through a series of high-precision thermal conductivity detectors, each containing a pair of thermal conductivity cells, where the quantity of CO_2, H_2O, N_2 and He carrier gas, is recorded. Combining these readings and the weight of sample used, %C, %H, %N are calculated.

3.3.4. Dielectric properties

In microwave processes, the main parameter that affects the heating efficiency of a material is its dielectric properties, as mentioned in Section 2.2.2. There are various ways to measure those properties, namely capacitor, transmission line, cavity resonator and open cavity methods, with the cavity resonator method (resonant measurements) being the most frequently used.

Two types of resonant measurements are commonly in practice, namely perturbation and low loss measurement methods. The first method is applicable for all permittivity, medium to high loss and magnetic materials measurements, whereas the second is applied to low loss materials using larger samples. However, the perturbation method is widely used, utilizing a TM cavity geometry, presented in Figure 3.15. Attention is centered on the TM_{010} mode, since it is the most useful mode for dielectric properties measurement. The tests were completed by the Centre for High Frequency Engineering, in Cardiff University, using the TM_{010} Mode at 2.50 GHz.

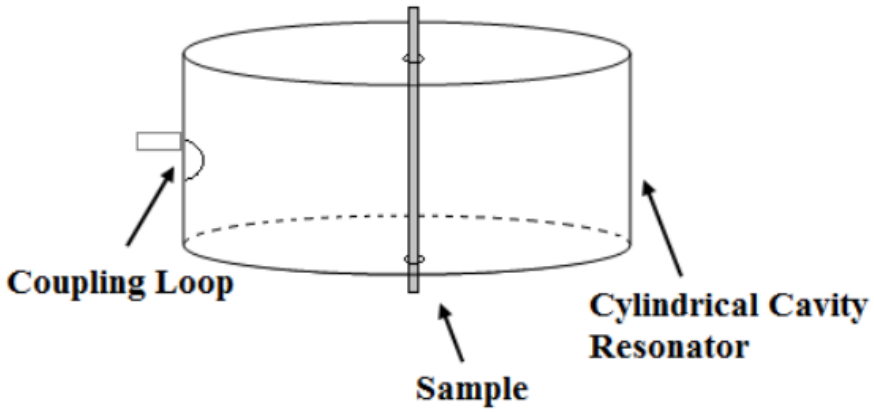

Figure 3.15: The TM cavity geometry

In this method, the first step for estimating the dielectric properties of a material is to measure the quality factor (Q-factor) - the frequency to bandwidth ratio of the resonator - and the resonant frequency (f_0) of the empty cavity, here referred to as 'blank' (Figure 3.16).

Then, the measurement is repeated after filling the cavity with the tested material, which as seen in Figure 3.15, is positioned at the centre of the cavity (the rod-shaped solid sample). The samples were placed in standard Eppendorf tubes and placed on-axis in a 2.5 GHz TM010 cylindrical cavity (Figure 3.17). Three samples were prepared for each material, each of nominal volume of approximately 200 μl and the results were normalised as per mg of sorbent. Placing the sample in the cavity results in changes in the field, shifting the 'blank' resonant frequency or Q-factor (Q).

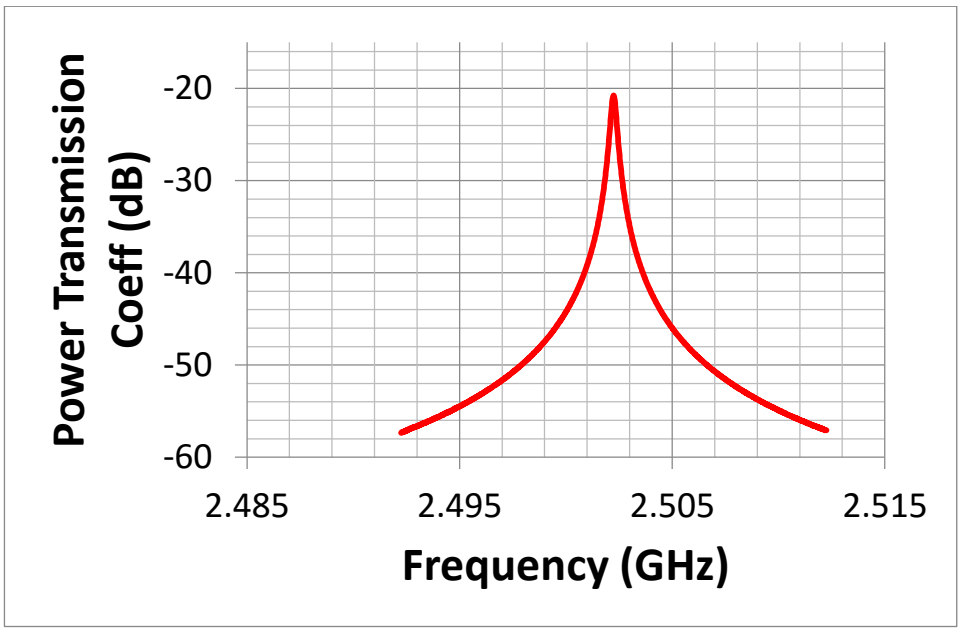

Figure 3.16: The blank measurement

The tested materials' properties can be calculated from the changes in resonant frequency and Q-factor compared to the 'blank' measurements, determining the relative permittivity (ε_r') and the loss factor (ε_r'') from the following equations:

$$\varepsilon_r' - 1 \approx \frac{2*V_{eff}}{V_s} * \frac{\Delta f_0}{f_0} \tag{3.8}$$

$$\varepsilon_r'' \approx \frac{V_{eff}}{V_s} * \frac{\Delta f_B}{f_0} \tag{3.9}$$

$$Q = \frac{f_0}{f_B} \tag{3.10}$$

Where Δf_0 is the change in resonant frequency, f_B is the bandwidth, Δf_B is the change in bandwidth, V_{eff} is the effective cavity volume and V_s is the sample volume.

In addition, according to Pointing's Theorem, the average microwave absorbed power P_{abs} per unit volume (W/m^3) is proportionally related with the dielectric properties of the material and the magnitude of the internal electric field ($|E|$ in V/m) and can be expressed by:

$$P_{abs} = 2\pi f \varepsilon_0 \varepsilon_r'' \, |E|^2 \quad (3.11)$$

where f is the microwave frequency (Hz). Here, it should be mentioned that it has been assumed that the power is uniform throughout the volume and that thermal equilibrium has been reached (Hill, 2000).

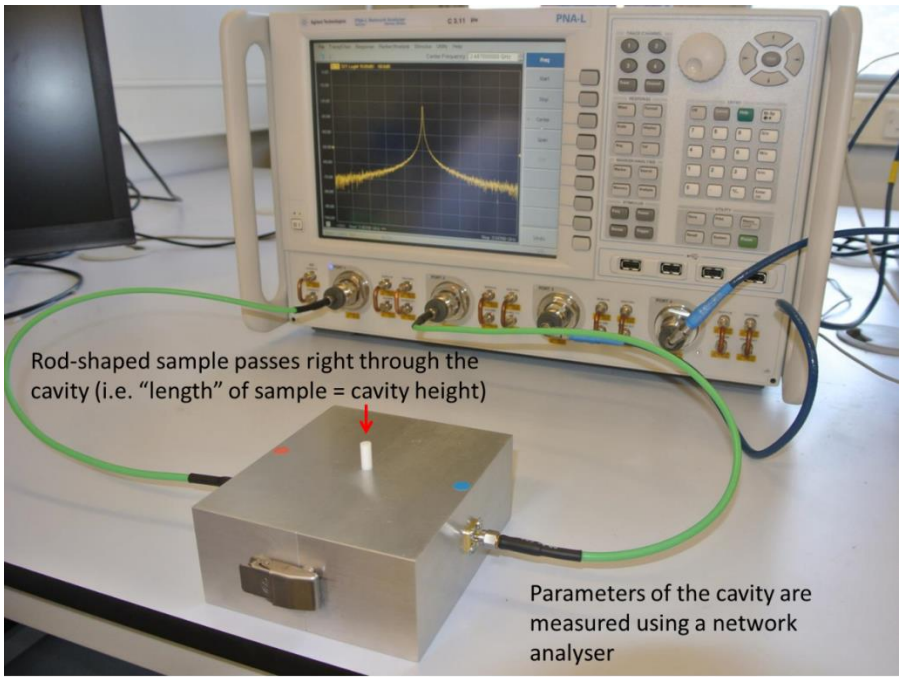

Figure 3.17: Complete layout of the dielectric properties measurement equipment

3.4. MSA/TSA process

All the CO_2 adsorption/desorption experiments were conducted using the lab-scale setup shown in Figures 3.18 and 3.19. The setup includes all the equipment and instrumentation presented in this chapter, namely a fixed-packed bed column (length l_r = 250 mm, outside diameter OD_r = 30 mm, inner diameter ID_r = 10 mm, packed bed diameter d_b = 20 mm) fabricated from Pyrex glass, equipped with a grade 1 (90–150 μm) sintered disk. The microwave system consisted of an 800W microwave source, equipped with a 2.45GHz magnetron and a modified cavity (Sharp), as shown in Figure 3.19. The fixed-bed temperature was determined by an IRP (Optris CTfast CT LT 25F) which measured the AC bed temperature from the top of the reactor through a zinc selenide (ZnSe) window. The IR pyrometer was also connected to a PID controller (Eurotherm 3504) during microwave heating (MW), in order to control the power needed to reach the specific target temperature. Experiments for examination of the

conventional heating (CH) desorption were conducted using a 144W heating tape, provided by Omega, with total length of 60cm and width of 2cm, placed in such a way to completely cover the AC bed reactor externally, while the temperature was monitored using the IRP once again. Energy consumption measurements were determined using a plug-in device that was constantly measuring the power consumed by each individual electrical instrument, provided by Eco-Eye. Moreover, a full monitor equipped with a 13mm split CT Clamp, display and Transmitter, MMC Card and a USB cable was assembled to log live electricity usage from the display and save it to the PC.

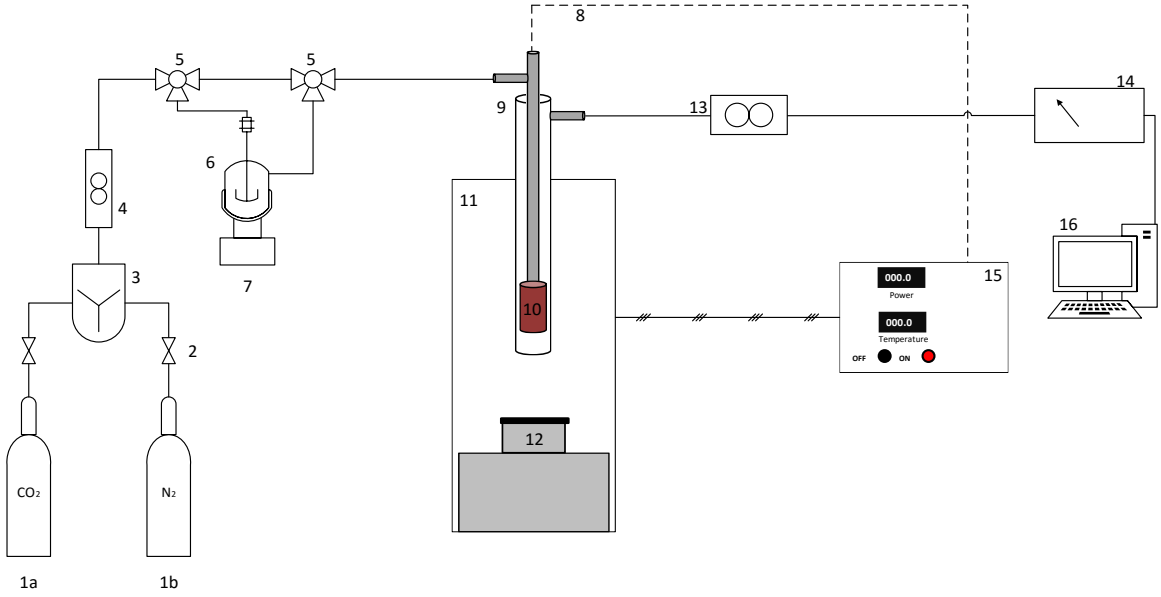

Figure 3.18: Schematic representation of the experimental rig, 1a. Gas cylinder – CO_2, 1b. Gas cylinder – N_2, 2. Two-way valves, 3. Gas mixer, 4. Mass flow controller, 5. Three-way valves, 6. Bubbler filled with water, 7. Electric heating plate, 8. IR Pyrometer, 9. Glass reactor, 10. Sorbent bed, 11. MW Cavity, 12. Magnetron, 13. Mass flow meter, 14. Mass spectrometer (TOF-MS), 15. PID Temperature and Power controller, 16. PC

Gas volumetric flow rate variations, occurring in the fixed bed as a consequence of CO_2 adsorption/desorption, were monitored by a mass flow controller, El Flow Bronkhorst 201-CV, placed at the exit of the adsorption column, and digitally interfaced with the PC unit. Moreover, CO_2 and N_2 concentrations were continuously measured by the TOF-MS and the data were acquired and analysed using Hiden QGA Pro software.

A gas mixture containing CO_2 and N_2 in various partial pressures was produced using an Omega FL-6GP-41ST-41ST-41ST gas mixer, generating a constant total flow of 100 ml/min or 150ml/min (parameter 1). The second parameter examined was the CO_2 concentration in the feed gas, namely 5%, 15%, 40% (vol.) CO_2 balanced with N_2.

These three different concentrations were chosen as they simulate real exhaust gas streams from a gas fired power plant, a coal-fired power plant and a cement industry respectively.

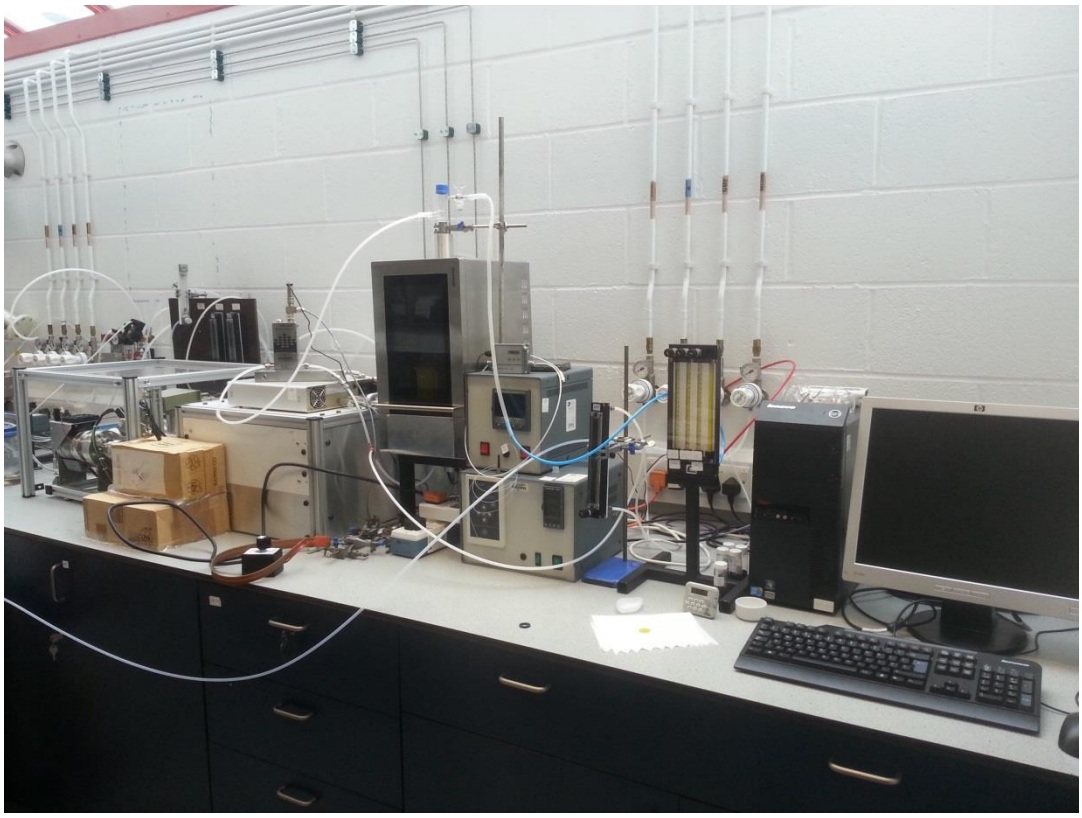

Figure 3.19: Photo of the experimental rig

The next parameter that was investigated was the effect of the moisture for the adsorption/desorption steps, since the high water levels present in the exhaust flue gas of any of the above processes result in additional implications in the adsorption and desorption processes (Webley and Zhang, 2014). As a result, for the purposes of the wet conditions experiments, the method of the dew-point generation was followed during the adsorption step. In order to generate high relative humidity in a gas mixture, the gas stream is passed over a heated water bath, from which the water evaporates into the stream. For this purpose, a Pyrex glass bubbler filled with 1L of water was used. The bubbler was placed on an electric heater, controlling the temperature of the water at around 55°C, thus creating a moisture content of ~10%. The last parameter that was reported was the desorption temperature; a comparison between MSA and TSA took place at two different temperatures, namely 70°C and 130°C, taking into consideration

that a higher temperature than 130°C may have resulted in decomposition of some samples' impregnation.

3.5. Sorbent materials and experimental nomenclature

3.5.1. Solid sorbents

This section presents the materials used in this study, according to the sorbents selection criteria discussed in Section 2.1.4. This research focuses solely on low-temperature solid adsorbents (<200°C), since the temperature of the flue gas to be treated lies between 40 and 80°C (Drage et al., 2006). Six different materials were used, five of them being carbon-based and one being a silica-based material. The first aim of using these sorbents was to investigate various process parameters and decide on the critical conditions that could result in an intensified MSA process, compared to TSA. As a result, a well-characterised microporous granular activated carbon (GAC) was used as the reference material, since it was reported to present high CO_2 adsorption potential, has not undergone any treatment, can be found in abundance and has desirable dielectric properties. After deciding on the critical conditions and important parameters for MSA (Chapter 4), a material investigation took place studying the importance of raw material, adsorbent shape and surface modifications (Chapter 5). Five materials were chosen for this investigation - four of which are carbon based with the last one being silica-based - in order to compare with the performance of GAC. Those sorbent materials present different properties in terms of functionalities (NH_3 impregnation) and forms - powder, granular and pellets - for the carbon-based ones, while the silica combines form and surface modifications, since it is a powdered form amine impregnated (TEPA) material.

The materials used in this research include:

a. Carbon based sorbent materials:
    - Microporous granular activated carbon (GAC) from palm shell, obtained by NORIT, used as the reference sample.
    - Activated carbon, obtained by Desotec:
        i. Pellet form, from coconut shell, with product name Organosorb 10-CO (Org).

ii. Powder form, obtained after grinding the original Organosorb (OrgP)

- Granular AC from almond shells (AS), obtained from Instituto Nacional del Carbón (INCAR, Oviedo, Spain):
  iii. Parent sample, referred to as GKAS;
  iv. GKAS – N800, treated with ammonia, introducing basic functionalities on the parent sample's surface, resulting in better CO_2 adsorption capacities as reported at INCAR.

b. Silica-based sorbent materials, obtained from Rey Juan Carlos University, Madrid, Spain
   - SBA-15-TEPA (30): Mesoporous silica, impregnated with tetraethylenepentamine (TEPA), resulting in considerable CO_2 uptake, previously examined at Rey Juan Carlos University. However, slow desorption rates as well as a slow but steady loss of adsorption capacity were reported with continuous-cyclic use due to TEPA evaporation.

3.5.2. *Experimental nomenclature*

Here, it should be noted that the experiments reported in the adsorption figures described in Chapters 4 and 5, follow a MaterialCO_2Dry/WetFlow nomenclature; for example, in the case of GAC, with a total volumetric flow rate of 100ml/min at wet gas conditions and 40% CO_2 (vol.), the name of the experiment would equivalently be written as GAC40W100.

Similarly for the desorption experiments, the pattern followed was CO_2Dry/WetFlowCH/MWT_{des}. For example, in the case of regenerating the material with microwave heating, using a purge gas flow rate of 100ml/min, previously (during adsorption) mixed with 40% CO_2 (vol.), at dry conditions and at $T_{des} = 70°C$, the name of the experiment would accordingly be: 40D100MW70.

3.6. Fixed-bed dynamic adsorption/desorption experiments

The experimental work in the fixed bed reactor aimed at evaluating (i) the CO_2 dynamic adsorption capacity of the studied samples and how it is affected under wet gas conditions and total flow rate, (ii) the differences between MSA and TSA with regards to regeneration efficiency, desorption kinetics and energy consumption, and (iii) the effect of consecutive adsorption/desorption cycles, on the textural properties of the AC. In this regard, continuous adsorption/desorption tests were conducted as described in the next sections.

For both experimental procedures (MSA and TSA), the reactor was packed with 5g of material, previously heated overnight at 100°C to remove any moisture content. The overall experimental cycle consisted of 6 steps, as described below.

Step 1 - Purging: Prior to adsorption, a purge step was flown for 30mins, using 200ml/min of N_2, in order to create a N_2-rich atmosphere conditions without impurities, as determined by the TOF-MS.

Step 2a - Adsorption: Adsorption runs were performed by feeding the fixed bed reactor with a gas mixture of CO_2 and N_2 at ambient conditions (T=25°C and P=1atm), simulating each time a different scenario; a combination matrix of three different CO_2 concentrations in the gas mixture (5%, 15%, 40% vol.), two flow rates (100ml/min and 150ml/min) both in the presence and absence of moisture resulted in 12 distinct experiments that were conducted for the adsorption process. The breakthrough curves, presented in the next chapters, were obtained from this step using the TOF-MS (Section 3.2.4) and are used to calculate the equilibrium CO_2 adsorbed amount q_{eq} ($g_{CO_2} ads./ g_{sorb}$). The CO_2 loading in the bed can be determined by a dynamic mass balance, which requires numerical integration of the data:

$$q_{eq} = \frac{F_{CO_2}^{in} * \rho_{CO_2}}{m} \int_0^{t_{eq}} \left(1 - \frac{C_{CO_2}^{out}(t)}{C_{CO_2}^{in}}\right) dt \quad (3.12)$$

Where $\rho_{CO_2} = 1.842\ kg/m^3$ represents CO_2 density, evaluated at 20°C and 1bar, while m is the total mass of the AC used (g). Moreover, $C_{CO_2}^{out}(t)/C_{CO_2}^{in}$ represents the time evolution of CO_2 in terms of the ratio of the volumetric flow rate of CO_2 at the bed outlet relative to that in the feed and $F_{CO_2}^{in}$ the total volumetric flow rate of CO_2 in the reactor feed.

Equation 3.12 estimates the total number of moles of CO_2 retained by the column during the adsorption step and can be calculated using a graphical method explained below, that makes use of the outlet CO_2 concentration and the feed flow-rate. This method avoids the need to examine the variation of the molar CO_2 flow-rate at the exit of the bed; it simply calculates the total mass retained by the column as a percentage (ratio of the adsorbed area to the total area on a graph of CO_2 concentration, % v/v, versus time, min) of the total mass that enters the system (Garcia et al., 2011).

Figure 3.20 shows the area that needs to be integrated in order to calculate the amount of CO_2 adsorbed by the sorbent. This area is divided in two sub-areas, namely A and B that need to be added in order to integrate from t_0 to t_{eq}. Calculating the sub-area A (A_A) is simple since it is rectangular in shape, with length equal to t_1-t_0 and height equal to 100%:

$$A_A = (t_1 - t_o) * 100\% \tag{3.13}$$

However, sub-area B (A_B) was calculated using the trapezoidal rule, a numerical method developed to simplify the integral. The trapezoidal rule is based on the Newton-Cotes formula that if one approximates the integrand by an n^{th} order polynomial, then the integral of the function is approximated by the integral of that n^{th} order polynomial (Kaw et al, 2012). Integrating polynomials is simple and is based on the calculus formula:

$$\int_a^b x^n dx = \left(\frac{b^{n+1} - a^{n+1}}{n+1}\right), n \neq 1 \tag{3.14}$$

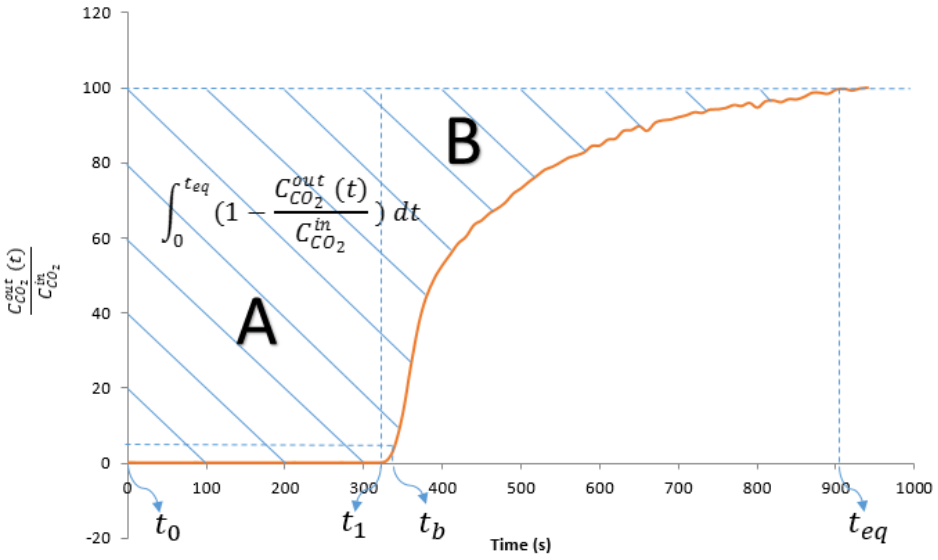

Figure 3.20: Analysis of the area calculated for the adsorption step

So approximating the integral

$$I = \int_a^b f(x)dx \tag{3.15}$$

to find the value of the above integral, one assumes

$$f(x) \approx f_n(x) \tag{3.16}$$

where

$$f_n(x) = a_0 + a_1x + \cdots + a_{n-1}x^{n-1} + a_nx^n \tag{3.17}$$

where $f_n(x)$ is a n^{th} order polynomial. The trapezoidal rule assumes $n = 1$, that is, approximating the integral by a linear polynomial (straight line),

$$\int_a^b f(x)dx \approx \int_a^b f_1(x)dx$$

$$= \int_a^b (a_0 + a_1x)dx = a_0(b-a) + a_1(\frac{b^2-a^2}{2}) \tag{3.18}$$

Assuming $(a, f(a))$ and $b, f(b))$ as the two points to approximate $f(x)$ by a straight line from a to b,

$$f(a) = f_1(a) = a_0 + a_1a \tag{3.19}$$

$$f(b) = f_1(b) = a_0 + a_1b \tag{3.20}$$

Solving the above two equations for a_1 and a_0,

$$a_1 = \frac{f(b)-f(a)}{b-a}$$

$$a_0 = \frac{f(a)b-f(b)a}{b-a} \tag{3.21}$$

Hence from Equation (3.18) it can be derived

$$\int_a^b f(x)dx \approx \frac{f(a)b-f(b)a}{b-a}(b-a) + \frac{f(b)-f(a)}{b-a}\frac{b^2-a^2}{2} \tag{3.22}$$

$$= (b-a)\left(\frac{f(a)+f(b)}{2}\right) \tag{3.23}$$

Applying the above generic example to the sub-area B (Figure 3.21), the integral can be approximated by using n trapezoids added together according to the equation:

$$A_B = \sum(C_{n+1} - C_n)\left(\frac{t_n+t_{n+1}}{2}\right) \tag{3.24}$$

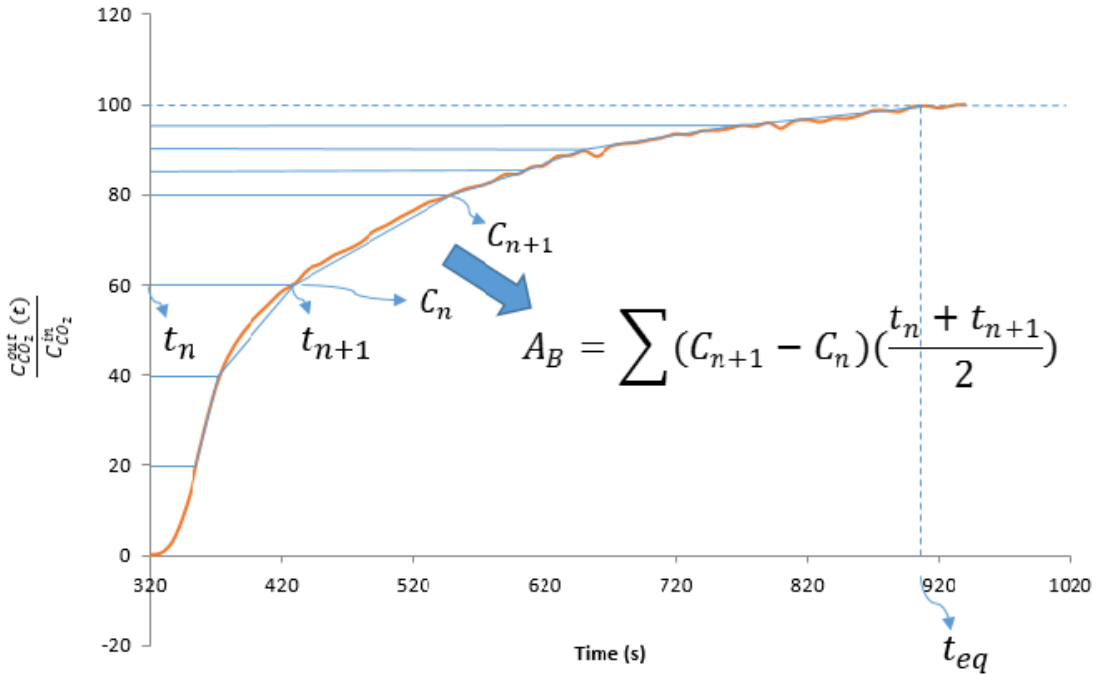

Figure 3.21: Calculation of the sub-area B using the trapezoidal model for integration

Consequently, using equations 3.13 and 3.24, the total area of the breakthrough curve can be calculated from equation 3.25:

$$A = A_A + A_B = (t_1 - t_o) * 100\% + \sum(C_{n+1} - C_n)(\frac{t_n + t_{n+1}}{2}) \quad (3.25)$$

Step 2b - Blank experiments: The behavior of the separation system without the sorbent material (blank experiments) was also tested. The corrections due to the late response of the TOF-MS were obtained with a blank experiment carried out using an empty reactor for each experiment. Therefore, corrected adsorption capacity of the solid adsorbents (A') can be calculated by subtracting the adsorption capacity between the adsorption experiment (A) and the blank experiment (A_{bl}), as seen in Figure 3.22.

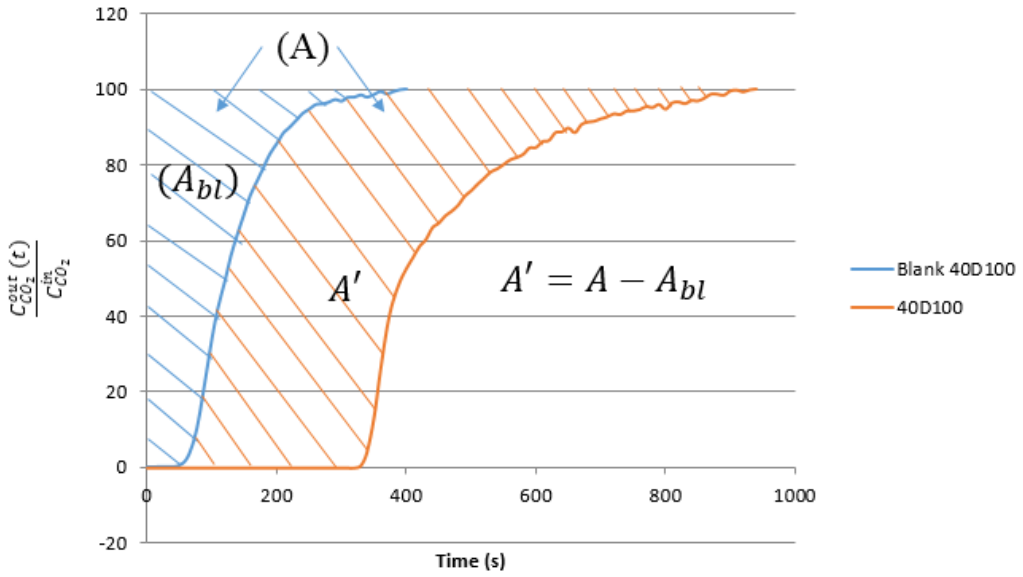

Figure 3.22: Example of a blank experiment during the adsorption step using 40% (vol.) CO_2 and 100ml/min (balance N_2)

As a result, the corrected area can be determined from equation 3.26:

$$A' = A - A_{bl} \quad (3.26)$$

Step 3 - Purging: After the completion of the adsorption step, another purge step takes place using high N_2 flow (>250ml/min), aiming at cleaning the TOF-MS capillary line from any residual CO_2. The gas stream does not go through the reactor, to avoid initialisation of CO_2 desorption.

Step 4a - Desorption: Regeneration of the sorbent bed takes place, either using the multimode microwave system for MSA, or the heating tape for TSA, taking into consideration three variables, namely the volumetric total flow rate and the gas condition, according to the adsorption step, and the desorption temperature, as explained above. Similarly to the adsorption step, the total specific amount of CO_2 desorbed from the studied solid sorbents (q_{des}) was obtained for both heating processes from the desorption profiles, applying a simple material balance, calculating the area under the desorption curve:

$$q_{des} = \int_0^{t^{0.5}} \frac{F_{tot}^{out}(t) * \rho_{CO_2}}{m} C_{CO_2}^{out}(t)\ dt \tag{3.27}$$

Where $t^{0.5}$ represents the time required to complete the desorption process, based upon the fact that the lowest detectable limit of the TOF-MS is 0.5% CO_2 (vol.). Moreover, F_{tot}^{out} is the total volumetric flow, measured from the mini-coriolis flow controller at the exit of the reactor.

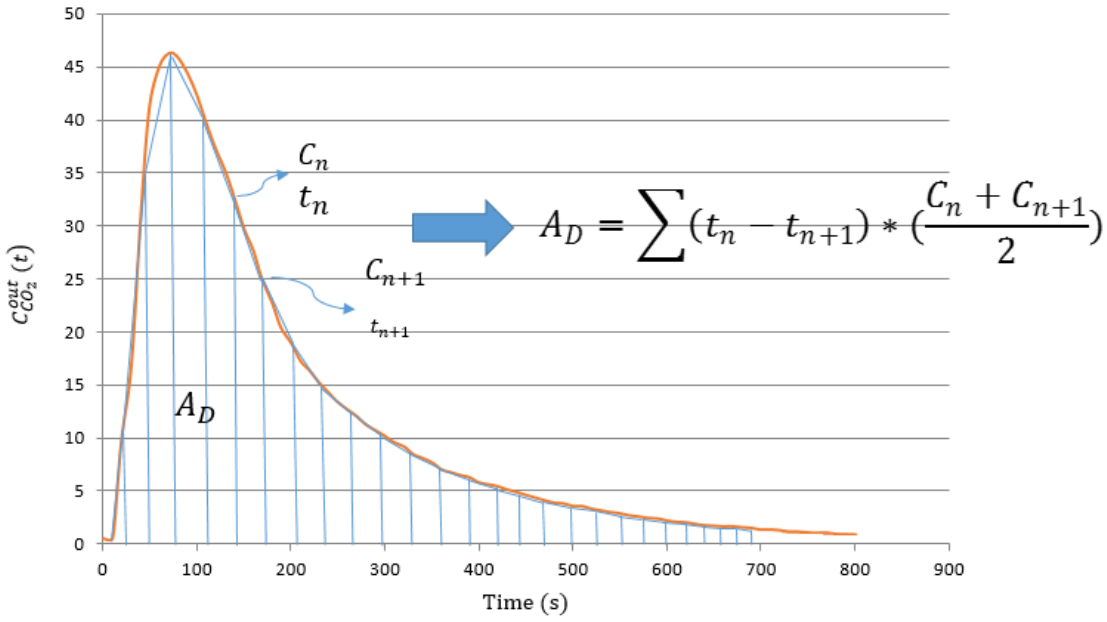

Figure 3.23: Calculation of the area under the desorption curve, A_D, using the trapezoidal model for integration

Similarly to the adsorption step, the area under the curve (A_D) was integrated using the trapezoidal rule (Figure 3.23) as follows:

$$A_D = \sum(t_n - t_{n+1}) * (\frac{C_n + C_{n+1}}{2}) \quad (3.28)$$

Step 4b - Blank experiments: Once again, the need to subtract the area that is created due to the late response of the TOF-MS is important. CO_2 flow was switched off, creating a desorption curve until the CO_2 was flushed out of the reactor due to the continuous N_2 flow. The final amount of CO_2 desorbed (A'_D) can be calculated by the following equation:

$$A'_D = A_D - A_{D,bl} \quad (3.29)$$

Where, $A_{D,bl}$ is the amount of CO_2 calculated from the blank experiment using the trapezoidal rule, as seen in Figure 3.24.

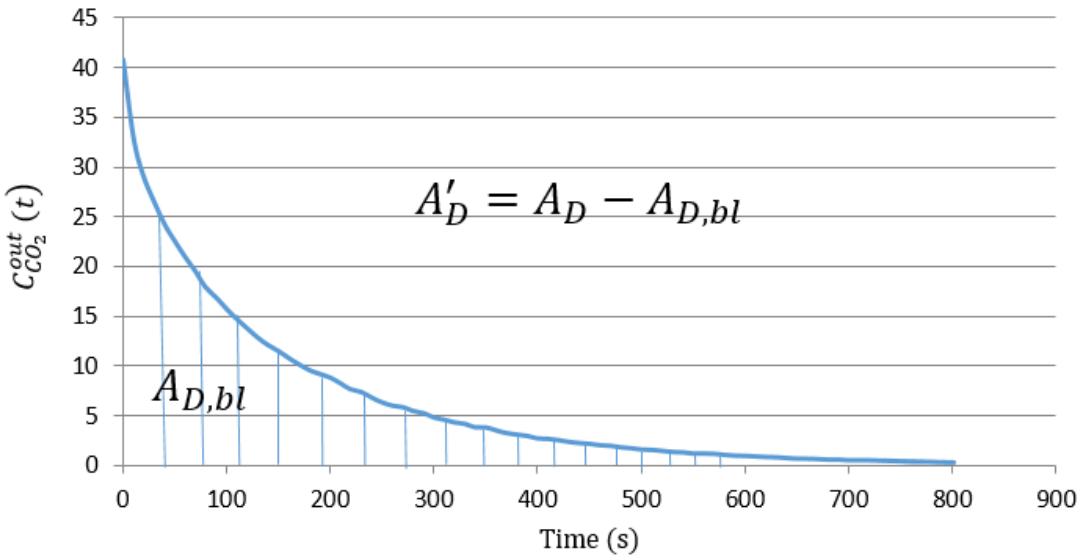

Figure 3.24: Example of a blank experiment during the desorption step using 40% (vol.) CO_2 and 100ml/min (balance N_2)

Step 5 – cool down: After the end of the desorption step, another purge step under N_2 conditions was followed for 30mins, in order to cool down the reactor and remove any residual CO_2 from the gas lines. Then, in the case of materials' cycle-ability investigation, the complete procedure is repeated, starting from step 1.

References

Balbuena, P.B. and Gubbins, K. (1993) 'Theoretical interpretation of adsorption behavior of simple fluids in slit pores', Langmuir, vol. 9, pp. 1801-1814

Balsamo, M., Silvestre-Albero, A., Silvestre-Albero, J., Erto, A., Rodriguez-Reinoso, F. and Lancia, A. (2014) *'Assessment of CO_2 adsorption capacity on activated carbons by a combination of batch and dynamic tests'*, Langmuir, vol. 30, pp. 5840–5848, DOI: 10.1021/la500780h

Bogdal, D. (2006) *'Microwave Assisted Organic Synthesis. One Hundred Reaction Procedures'*, Tetrahedron Organic Chemistry Series; Elsevier: Amsterdam, vol. 25;

Brunauer, S., Emmett, P.H. and Teller, E. (1938) '*Adsorption of Gases in Multimolecular Layers'*, American Chemical Society, vol. 60, pp. 309-319

Carmody, O., Frost, R., Xi, Y. and Kokot, S. (2007) '*Surface characterisation of selected sorbent materials for common hydrocarbon fuels*', Surface Science, vol. 601(9), pp. 2066-2076

Cherbanski, R. and Molga, E. (2009) '*Intensification of desorption process by use of microwaves-an overview of possible applications and industrial perspectives'*, Chemical Engineering and Processing, vol. 48, pp. 48-58

De Witt, D.P. and Nutter, G.D. (1988) '*Theory and Practice of Radiation Thermometry'*, John Wiley & Son, New York, ISBN 0-471-61018-6

Drage, T.C., Arenillas, A., Smith, K. and Snape, C.E. (2006) '*Comparison of pre- and post-combustion CO_2 adsorbent technologies'* 8th International Conference on Greenhouse Gas Control Technologies, Trondheim / Norway, 19 – 22 June

Gaal, P.S. (1999) '*Thermal conductivity and thermal expansion*' 12th 24th, CRC Press, Pennsylvania

Garcia, S., Gil, M.V., Martin, C.F., Pis, J.J., Rubiera, F. and Pevida, C. (2011) *'Breakthrough adsorption study of a commercial activated carbon for pre-combustion CO_2 capture'*, Chemical engineering journal, vol. 171, pp. 549-556

Gary Ong, K.C. and Akbarnezhad, A. (2014) *'Microwave-Assisted Concrete Technology: Production, Demolition and Recycling'*, Technology & Engineering

Hart-Smith, G. and Blanksby, S. (2012) *'Mass Analysis'*, Mass Spectrometry in Polymer Chemistry, pp. 5-32

Hashisho, Z. (2007) '*Microwave-swing adsorption for the capture and recovery, or destruction for a more sustainable use of organic vapors'*, PhD thesis, University of Illinois at Urbana-Champaign

He, X.D., Li, Y.B., Wang, L.D., Sun, Y. and Zhang, S. (2009) '*High emissivity coatings for high temperature application: Progress and prospect*', Thin Solid Films, vol. 517, pp. 5120-5129

Jana, S., Das, S., Ghosh, C., Maity, A. and Pradhan, M. (2015) *'Halloysite Nanotubes Capturing Isotope Selective Atmospheric CO2',* Scientific Reports vol. 5:8711, pp. 1-8, DOI: 10.1038/srep08711

Kaw, A. and Kalu, E. (2012) 'Numerical methods with applications', autarkaw.com (Standard Copyright Licence), 2nd Edition

Kazachkin, D., Nishimura, Y., Irle, S., Feng, X., Vidic, R. and Borguet, E. (2009) *'Temperature and pressure dependence of molecular adsorption on single wall carbon nanotubes and the existence of an ''adsorption/desorption pressure gap'*, Carbon, vol. 48, pp. 1867 – 1875, DOI: 10.1016/j.carbon.2009.11.018

Knaebel KS (1990) *'A"How-To" Guide for Adsorber Design'*, Adsorption Research, Inc., Dublin, Ohio.

Leonelli, C. and Veronesi, P. (2015) *'Microwave Reactors for Chemical Synthesis and Biofuels Preparation'* Production of Biofuels and Chemicals with Microwave, Biofuels and Biorefineries 3, DOI 10.1007/978-94-017-9612-5_2

Ling, J., Ntiamoah, A., Xiao, P., Xu, D., Webley, P. and Zhai, Y. (2014) *'Overview of CO_2 Capture from Flue Gas Streams by Vacuum Pressure Swing Adsorption Technology'*, Austin Journal of Chemical Engineering, Volume 1 Issue 2, pp. 1-7

Menendez, J., Arenillas, A., Fidalgo, B., Fernandez, Y., Zubizarreta, L., Calvo, E. and Bermudez, J.M. (2010) '*Microwave heating processes involving carbon materials'*, Fuel Processing Technology, vol. 91, pp. 1-8

Menendez, J.A., Menendez, E.M., Garcia, A., Parra, J.B. and Pis, J.J. (1999) '*Thermal treatment of active carbons: a comparison between microwave and electric heating'*, Journal of Microwave Power and Electromagnetic Energy, vol. 34(3), pp. 137–43

Ogbuka, C.P. (2013) '*Development of solid adsorbent materials for CO_2 capture*', PhD thesis, University of Nottingham

Olivares-Marín, M., Drage, T.C. and Maroto-Valer, M.M. (2010) '*Novel lithium-based sorbents from fly ashes for CO_2 capture at high temperatures'*, International Journal of Greenhouse Gas Control, Vol. 4(4), pp. 623-629, DOI: 10.1016/j.ijggc.2009.12.015

Requena-Pérez, M.E., Pedreño-Molina, J.L., Monzó-Cabrera, J. and Díaz-Morcillo, A. (2005) '*Multimode Cavity Efficiency Optimization by optimum load location: experimental approach*', IEEE Transactions on Microwave Theory and Techniques, Vol. 53, pp. 2838-2845

Richardson, J.F., Harker, J.H. and Backhurst, J.R. (2002) '*Chemical Engineering: Particle Technology and Separation Processes*', vol. II, fifth ed., Butterworth-Heinemann, Oxford

Rousseau, R.W. (1987) '*Handbook of Separation Process Technology'*, Wiley

Seaton, N.A., Walton, J., Quirke, N. (1989) '*A new analysis method for the determination of the pore-size distribution of porous carbons from nitrogen adsorption measurements'*, Carbon, vol. 27, pp.853–861.

Shaw, D.J. (1998) '*Introduction to Colloid and Surface Chemistry*', 4th ed., Butterworth Heinemann, Oxford

Stefanidis, G., Muñoz, A. N., Sturm, G. and Stankiewicz, A. (2014) '*A helicopter view of microwave application to chemical processes: reactions, separations, and equipment concepts*', Rev Chem Eng, DOI 10.1515/revce-2013-0033

Wharton, Y. (2012) *'Microwave flow chemistry: Faster, cleaner, greener, safer'*, Speciality Chemicals Magazine, pp. 27-28'

Chapter 4 – Process parameters in MSA/TSA

This chapter discusses the results obtained from a series of experiments using a granular activated carbon (GAC), provided from Norit (GAC NORIT GCN3070). Initially, characterisation studies of the parent material are discussed, followed by a detailed comparison of MSA and TSA in terms of desorption efficiency, kinetics and energy consumption, according to the parameters explained in Section 3.4. GAC was used as a reference material against the materials that will be presented in Chapter 5. As a result, a full study, covering and combining all the parameters produced from a total of 48 experiments, is presented, aiming at identifying the best experimental conditions for an efficient regeneration process in terms of CO_2 recovery amount, time required and energy spent during regeneration. Lastly, the possibility to re-use the specific material in a recurring process without damaging its properties is examined, studying its changes in textural characteristics, CO_2 adsorption capacity and dielectric properties after 25 consecutive adsorption/desorption cycles.

4.1. Characterisation of GAC

Prior to the commencement of the experimental work, a complete characterisation study of the GAC material was undertaken, focusing on textural, chemical and dielectric properties. Textural properties included surface area (BET), total pore volume and size (DFT) and CO_2 adsorption capacity (TGA); chemical properties included elemental analysis regarding CHN content, while dielectric properties included resonant measurements using a TM_{010} mode, as explained in Section 3.3. Moreover, the penetration depth and the absorbed power potential were also calculated, using equations from Section 2.2.6. The results are presented in Table 4.1 and are discussed in this section.

Table 4.1: Textural, chemical and dielectric properties of parent GAC

	Textural			Chemical	Dielectric				
Material	**S_{BET} m^2/g**	**Total Pore Vol. (Vp) cm^2/g**	**TGA CO_2 uptake (% w/w) at 25°C**	**C (%)**	ε_r'	ε_r''	**tan delta (tan δ)**	**Dp (cm)**	**P_{abs} (%)**
GAC	946.7	0.62	11.7	90.85	15.2	6.6	0.44	2.2	89

Figure 4.1 shows the weight change of the GAC monitored by the TGA. It is evident that during the drying step the weight of the sample was reduced by 8%, allowing enough time to degasify the sample, making sure that all the moisture has evaporated prior to the CO_2 adsorption step. After switching from N_2 flow to a gas mixture of 90% (vol.) CO_2 flow and 10% N_2, an increase in terms of weight change was observed, for which the weight of the GAC was increased by 10.7% from its initial 91.8%. This actually means that a total of 11.7% (w/w) increase, in other words 2.65mmol CO_2 per gram of sorbent, was observed for the GAC at 35°C.

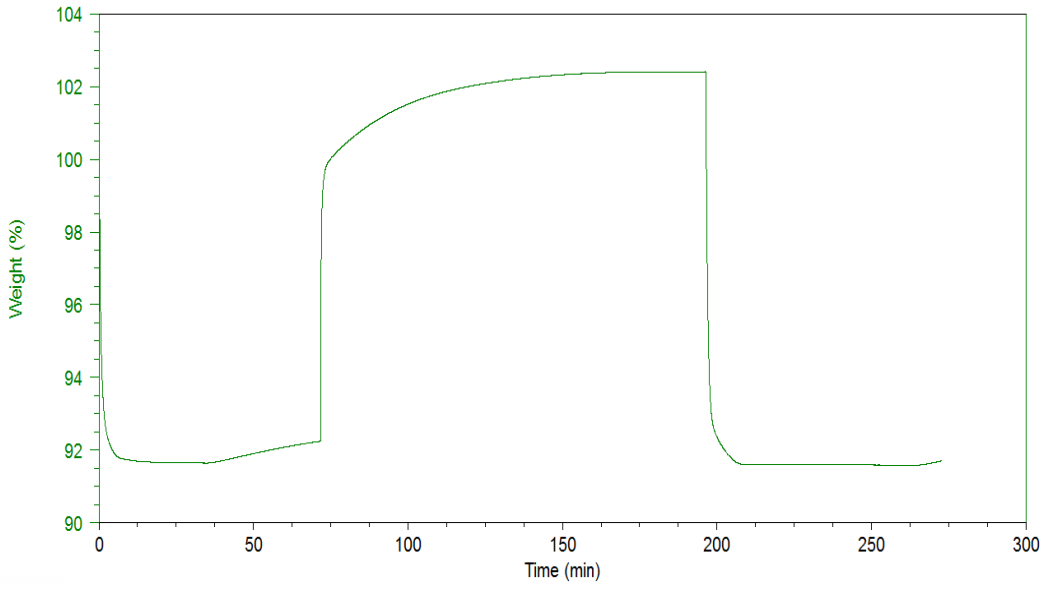

Figure 4.1: TGA CO_2 adsorption/desorption test using the parent GAC at 35°C

Next, a study on the surface area and porous characteristics took place. Figure 4.2 shows the typical adsorption (red line)/desorption (blue line) isotherm of N_2 at 77 K for GAC, which corresponds to the type I isotherm according to the IUPAC classification (IUPAC, 1985) described in Section 3.3.1. These isotherms are typically associated

with a microporous structure, with their exposed surface residing almost entirely inside those micropores. Once the micropores are filled with adsorbate, little or no external surface is left for further adsorption. The particle size of the GAC was 210-595μm (30-70 mesh, 93%), the BET surface area was 953 m²/g, while the total pore volume (V_p) was 0.62 cm^2/g. Furthermore, CHN analysis showed an expectedly high amount of carbon (C) inside the GAC, namely 90.9%.

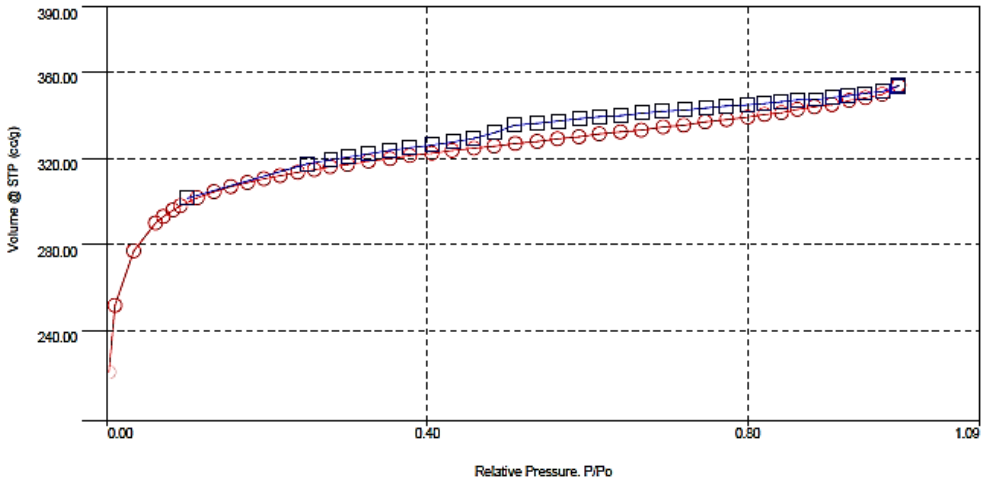

Figure 4.2: N_2 adsorption/desorption isotherm of the granular AC

Lastly, the dielectric properties of the GAC sorbent were assessed. Figure 4.3 presents the difference in resonant frequency (Δf_0) and transmitted power (Δf_B) for the parent sample at 2.45GHz (f_0), compared to the blank measurement, described in Section 3.3.5. Comparing Figures 3.16 and 4.3, Δf_0 and Δf_B can be calculated. Moreover, equations 3.8, 3.9 and 2.3 were used to calculate the loss tangent. The effective cavity volume V_{eff} and the sample volume used in those equations were: $V_{eff} = 71ml$ and V_s = 0.2ml. Tan δ value was calculated to be tan δ=0.44, while the penetration depth was 2.2cm, both being typical values for activated carbon (Menéndez et al., 2009). The P_{abs} reported in Table 4.1 represents the heating efficiency calibrated per mg of GAC and was equal to 89%, indicating an excellent transformation of microwave energy to heat.

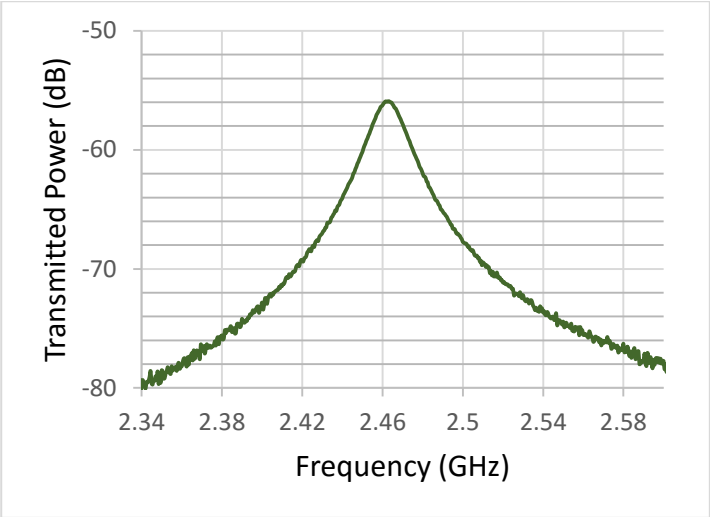

Figure 4.3: Difference in resonant frequency and transmitted power for the parent GAC at 2.45GHz

4.2. CO_2 adsorption studies

Prior to investigating and comparing the two desorption methods, namely MSA and TSA, it is necessary to calculate the amount of CO_2 adsorbed in the GAC. Moreover, examining the effect of (a) CO_2 concentration in the gas mixture, (b) total flow rate of the feed gas and (c) existence or absence of moisture in the feed gas, are of high importance, since these parameters will directly affect the desorption performance as well. As a result, CO_2 capture experiments were conducted as the first step to test the GAC using the lab-scale rig presented in Chapter 3 (Section 3.4).

Table 4.2: CO_2 adsorbed from GAC for various conditions

CO_2 Concentration (vol. %)	Gas condition	F_{tot}^{in} (ml/min)	q_{ads} (g)	g_{co2ads}/g_{sorb}	% (g_{co2ads}/g_{sorb})	$mmol_{CO2}/g_{sorb}$
40%	Dry	100	0.39	0.078	7.8	1.78
		150	0.44	0.088	8.8	2.01
	Wet	100	0.44	0.088	8.8	2.01
		150	0.51	0.102	10.2	2.32
15%	Dry	100	0.15	0.030	3.0	0.69
		150	0.21	0.042	4.2	0.96
	Wet	100	0.19	0.038	3.8	0.87
		150	0.24	0.048	4.8	1.11
5%	Dry	100	0.11	0.022	2.2	0.52
		150	0.13	0.025	2.5	0.57
	Wet	100	0.14	0.027	2.7	0.62
		150	0.17	0.033	3.3	0.75

The dynamic response of the gas–solid adsorption system was followed by recording the CO_2 outlet concentration at the exit of the reactor as a function of time by using the TOF-MS (Section 3.2.4), in order to obtain the so-called breakthrough curves (Figures 4.5, 4.7 and 4.9). Specifically, the time-dependent CO_2 amount adsorbed was expressed in terms of the ratio of the CO_2 concentration at the bed outlet relative to that in the feed ($C_{CO_2}^{out}(t)/C_{CO_2}^{in}$). In addition, N_2 concentration was almost constant during all adsorption tests ($C_{N_2}^{out}(t)/C_{N_2}^{in}$ = 1), indicating that N_2 adsorption on the AC can be considered negligible, under the investigated experimental conditions. Finally, all the adsorption experiments were conducted four times and an average of each measurement was considered. Consequently, the error estimation of the results was calculated to be on the range of ±2%, as shown by the error bars in the following figures (Figures 4.4, 4.6 and 4.8). Table 4.2 summarises the results that will be discussed in Section 4.2.1-4.2.3

4.2.1. Effect of CO_2 concentration in the CO_2/N_2 binary mixture

Figures 4.5, 4.7 and 4.9 present the breakthrough curves obtained for GAC at ambient temperature and pressure using three different CO_2 concentrations, at the inlet of the reactor ($C_{CO_2}^{in}$= 40%, 15% and 5% vol. respectively), as a function of total volumetric flow rate and wet/dry condition of feed gas. It is noticeable that while CO_2 is being adsorbed on the carbon, during the first moments of the adsorption step, it is not detected at the reactor outlet from the TOF-MS and only when the breakthrough time, t_b, (which is the time needed for $C_{CO_2}^{out}(t)/C_{CO_2}^{in}$ = 0.05) is reached, CO_2 becomes detectable in the outlet gas stream (Plaza et al., 2010). Moreover, for each flow rate and feed gas condition, the curves become steeper as the $C_{CO_2}^{in}$ increases, likely due to an increase in the mass transfer rate (Balsamo et al., 2010). Furthermore, the characteristic breakthrough time and the equilibrium time (t_{eq}) decrease as $C_{CO_2}^{in}$ increases regardless the flow rate and the moisture presence, even if the differences reduce in the case of the wet feed gas.

Figures 4.4, 4.6 and 4.8 present the total amount of CO_2 adsorbed from GAC during the adsorption step. It is evident that as the CO_2 concentration in the feed gas increases, the

total CO_2 amount adsorbed increases as well; the highest adsorbed amount was observed for the case of 40% (vol.) CO_2 in the gas feed and was calculated to increase from 0.39 to 0.51g per 5g of GAC. This means that for this specific feed concentration mixture, the amount calculated was close to the one predicted and reported from the TGA experiments (~11%), namely 8-10% per gram of GAC. This result was expected, since the GAC experiments were conducted with a 90% (vol.) CO_2 concentration (balanced with N_2), as reported in Section 3.3.1. However, in the cases of low CO_2 concentration in the mixture, the amount adsorbed decreased significantly, showing an important deviation from the expected saturation values; it is notable that in the case of 15% (vol.) CO_2 in the inlet, only 0.15-0.24g, or in other words 3%-5% per gram of GAC, were adsorbed, while in the case of 5% (vol.) CO_2 the decrease was even more obvious, concluding to only 0.1-0.16g, or 2%-3% (wt.) per gram of GAC to be adsorbed from the bed. This can be explained by Henry's law according to which, adsorption is proportional to the partial pressure of CO_2 (P_{CO_2}), expressed by the following equation:

$$X = K_H P_{CO_2} \tag{4.1}$$

where X is the surface coverage and K_H is Henry's adsorption constant (Smit et al., 2014).

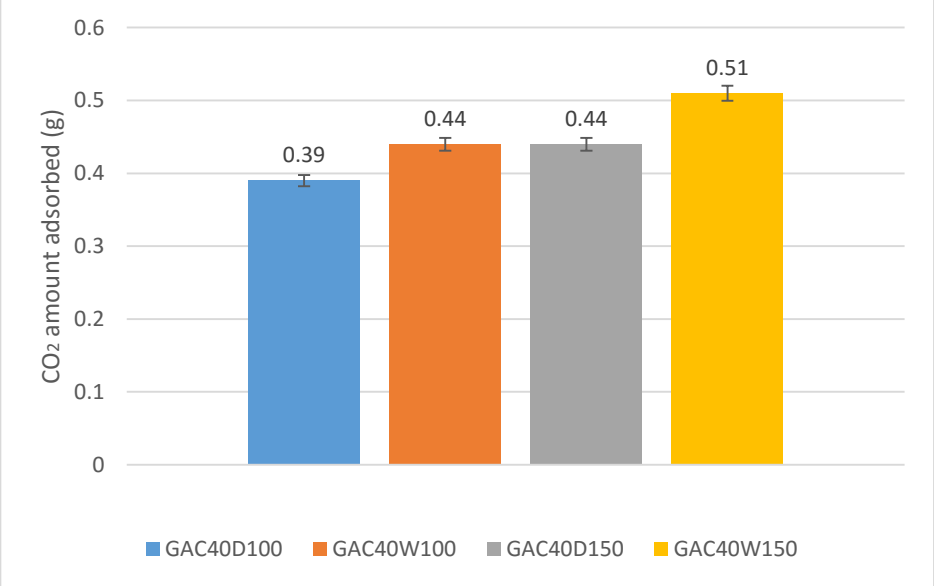

Figure 4.4: Amount of CO_2 adsorbed onto the GAC from a 40/60 CO_2/N_2 binary mixture at 25°C and 1bar, for 4 different parameters

However, one important factor to be taken into consideration is that a continuous CO_2 adsorption/desorption system measures the dynamic adsorption, instead of the static adsorption capacity. The dynamic adsorption capacity takes into account that only a part of the bed, namely the equilibrium zone (EZ) is saturated, whereas the mass transfer zone (MTZ) is only moderately saturated (Qu et al., 2009). In addition, another zone with fresh solid sorbent may be present, completely adsorbate-free, if the unit works under a fixed adsorption time. In contrast, the static adsorption capacity values derive from the weight change of the adsorbent, leaving it for several hours (or days) under controlled conditions in terms of partial pressure or relative humidity and at a certain temperature.

The static adsorption capacity can be a great indication for the maximum saturation perspectives of a sorbent; however, when dealing with industrial applications, the dynamic adsorption capacity should be taken into consideration (Wu, 2004). As a result, this research will only report the static adsorption capacity for characterisation purposes, while the dynamic capacity will be used to compare samples and conditions throughout.

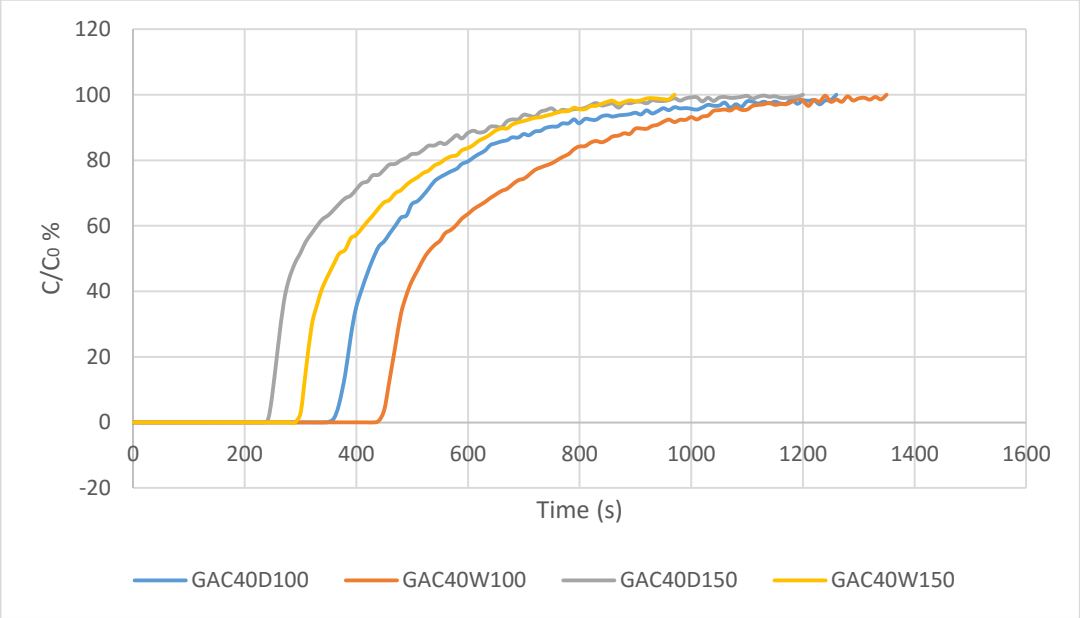

Figure 4.5: Breakthrough curves obtained from a 40/60 CO_2/N_2 binary mixture at 25°C and 1bar, comparing flow rates and dry/wet gas conditions

4.2.2. Effect of total flow rate

The next parameter that was investigated is the effect of the total flow rate of the binary mixture in the inlet of the reactor. This is a very important parameter, since it directly affects the dimensions, especially the diameter, of the reactor vessel, playing a crucial role to the total cost of the process. Moreover, it also affects the pressure drop inside the reactor in a proportional relation, meaning that as the total flow rate increases, the pressure drop increases as well. For the purposes of this research, two different flows were used, namely $F_{tot}^{1} = 100ml/min$ and $F_{tot}^{2} = 150ml/min$. F_{tot}^{1} was selected considering that the lowest detection values for the Coriflow TM-13 instrument (instrument range for N_2 flow: 70ml/min to 700ml/min). Furthermore, F_{tot}^{2} was selected taking into consideration that initial testing of the rig showed that during MSA desorption, the flow was possible to reach >600ml/min for an inert flow of N_2>150ml/min. As a result, considering that the maximum detectable flow of the Coriflow TM-13 instrument is 700ml/min, the total flow rate was limited to 150ml/min. These two flow rates can be converted to gas velocities, since the diameter of the bed is known (d_b=10mm) and correspond to 1.27m/min and 2m/min respectively.

A flow rate increase is systematically accompanied by a slight increase of the amount adsorbed (Gritti et al., 2005). This can be proven by the mass transfer correlation introduced by Sherwood, Pigford and Wilke (McGraw-Hill, 1974), which can be applied to adsorbates of both gaseous and liquid form. The correlation employs the Colburn-Chilton j-Factor and the Reynolds number (equation 3.2). The j-factor is determined by equation 4.2:

$$j_d = \left(\frac{k}{v_s}\right) * Sc^{0.667} \tag{4.2}$$

Where Sc is the Schmidt number, a dimensionless number used to characterize fluid flows in which there are simultaneous momentum and mass diffusion convection processes and is defined by:

$$Sc = \frac{\mu_d}{\rho D_{AB}} \tag{4.3}$$

Where D_{AB} is the diffusion coefficient of A to B. As a result, the mass transfer correlation can be determined by:

$$j_d = 1.17 * Re^{-0.415} \quad (4.4)$$

Combining equations 3.2, 4.2, 4.3 and 4.4 and solving for the mass transfer coefficient (k):

$$k = \frac{1.17 v_s (\frac{\rho v_s d}{\mu})^{-0.415}}{(\frac{\mu}{\rho D_{AB}})^{0.667}} \quad (4.5)$$

It can be seen from equation 4.5 that $k \sim u_s^{0.585}$, which means that a 10-fold velocity increase would lead to a 4-fold increase of the mass transfer coefficient. Consequently, an increase from 1.27m/min to 2m/min would lead to an increase of 64% of the mass transfer coefficient.

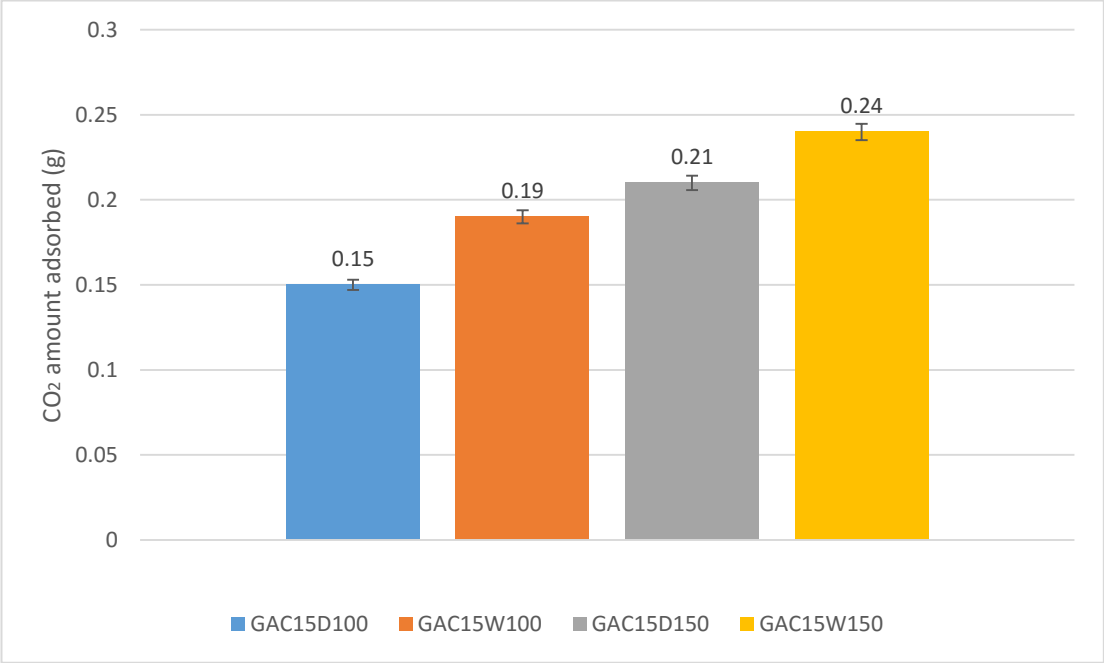

Figure 4.6: Amount of CO_2 adsorbed onto the GAC from a 15/85 CO_2/N_2 binary mixture at 25°C and 1bar, for 4 different parameters

It is evident that, for every CO_2 concentration in the inlet, the characteristic breakthrough time t_b decreases as the total volumetric flow rate (F_{tot}^{in}) increases, even if the differences reduce when comparing wet flue gas conditions. As expected, it can be

observed that there is a monotonic shift of the whole breakthrough curve towards lower times as the total flow rate increases, meaning that the CO_2 adsorption rates increase proportionally with the increase of the flow. Moreover, the equilibrium time (t_{eq}), defined as when CO_2 concentrations at the bed inlet and outlet are practically equal, is reached 3.5mins faster in the case of the dry gas, whereas in wet gas conditions, the t_{eq} is reached ~8mins faster. However, it is notable that the CO_2 adsorption capacity increases in all cases (Figures 4.4, 4.6 and 4.8); for a dry 40/60 CO_2/N_2 gas mixture, the CO_2 adsorption capacity increased from 0.39 to 0.44 g_{CO_2} (from 8% to 9% per g of GAC), whereas for a dry 15/85 CO_2/N_2 mixture, the CO_2 adsorption capacity was $0.21g_{CO_2}$ (4.1% w/w ratio) at 150ml/min, being significantly increased compared to $0.15g_{CO_2}$ at 100ml/min (3% w/w ratio) representing a rise of 40%. Furthermore, when 5% CO_2 were introduced inside the gas mixture, a rise in CO_2 adsorption capacity was observed as well, from 0.1 to 0.12g per g of GAC.

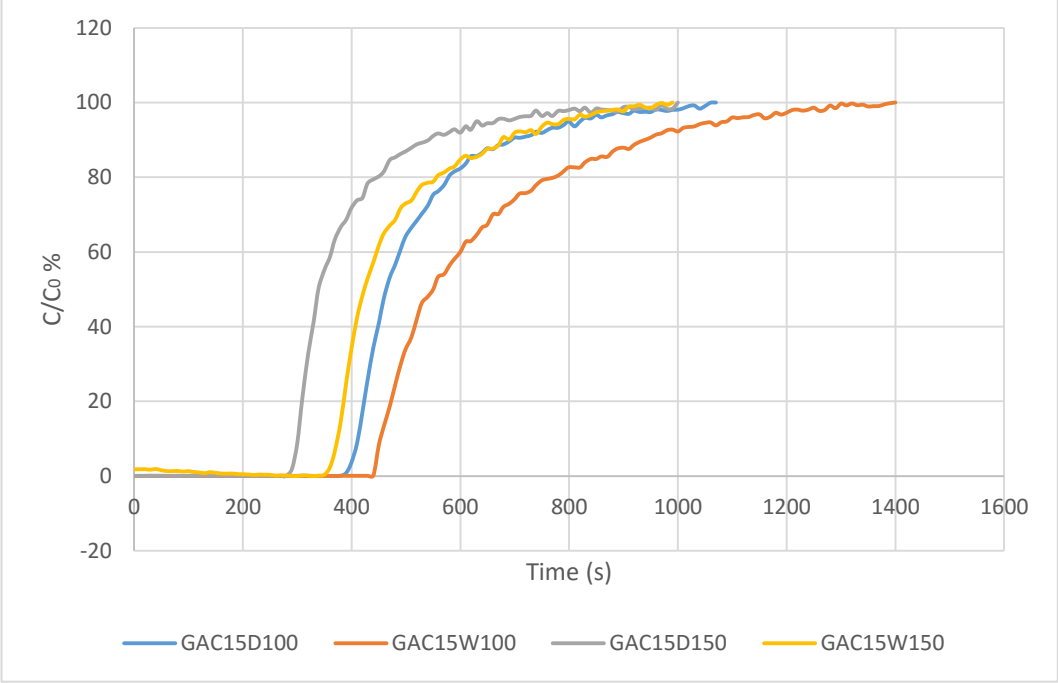

Figure 4.7: Breakthrough curves obtained from a 15/85 CO_2/N_2 binary mixture at 25°C and 1bar, comparing flow rates and dry/wet gas conditions

Considering the case of the wet binary gas mixture, the same trend was observed; the CO_2 adsorption capacity was increased in every case that the total volumetric flow rate was increased; $0.51g_{CO_2}$ (10.2% w/w ratio) from $0.44g_{CO_2}$ (8.8% w/w ratio), equal to a 16% increase in the case of 40% CO_2 in the feed gas as seen in Figure 4.4, $0.24g_{CO_2}$ (4.8% w/w ratio) from $0.19g_{CO_2}$ (3.9% w/w ratio) representing a rise of 23% in the case

of 15% CO_2 (Figure 4.6). The same increase rate was also observed for the case of 5% CO_2 where, from $0.135 g_{CO_2}$ it increased to a maximum of $0.165 g_{CO_2}$, representing a 22% rise of CO_2 adsorbed (Figure 4.8).

4.2.3. Effect of moisture content

In general, activated carbon is known for its hydrophobic character and as such, the presence of moisture does not affect its CO_2 adsorption capacity (de Ridder, 2012). One reason for that is that the separation principle of carbon sorbents is based on kinetic separation, and as a result, a fast adsorption gas like CO_2 is hardly affected by a slow adsorption gas, such as water vapour (Dong et al., 2011). Interestingly enough, a ~10% of moisture in a binary gas mixture of CO_2 and N_2 seems to enhance the CO_2 adsorption capacity on that particular GAC. The CO_2 adsorption capacity in the case of 40/60 gas mixture (Figure 4.4) was increased by as much as 16% when 150ml/min were used (from $0.44 g_{CO_2}$ to $0.51 g_{CO_2}$), while for 100ml/min there was an increase of 13%, from $0.39 g_{CO_2}$ to $0.44 g_{CO_2}$. It is notable that, the highest increase was once again observed for the case of 15% CO_2 in the gas mixture (Figure 4.6); $0.19 g_{CO_2}$ (3.9% w/w ratio) from $0.15 g_{CO_2}$ (3% w/w ratio) for 100ml/min, resulting in a significant 25% rise. However, when a higher total flow rate of 150ml/min was introduced into the reactor, the increase was smaller, from $0.21 g_{CO_2}$ (4.1% w/w ratio) to $0.24 g_{CO_2}$ (4.8% w/w ratio) - namely 17%. For the case of 5% CO_2 into the gas mixture (Figure 4.8), the increase was also quite significant, since a 23% rise of CO_2 amount adsorbed onto the GAC for a total flow of 100ml/min was detected (~$0.13 g_{CO_2}$ from 0.107), whereas for 150ml/min the rise was 22% ($0.165 g_{CO_2}$ from $0.135 g_{CO_2}$).

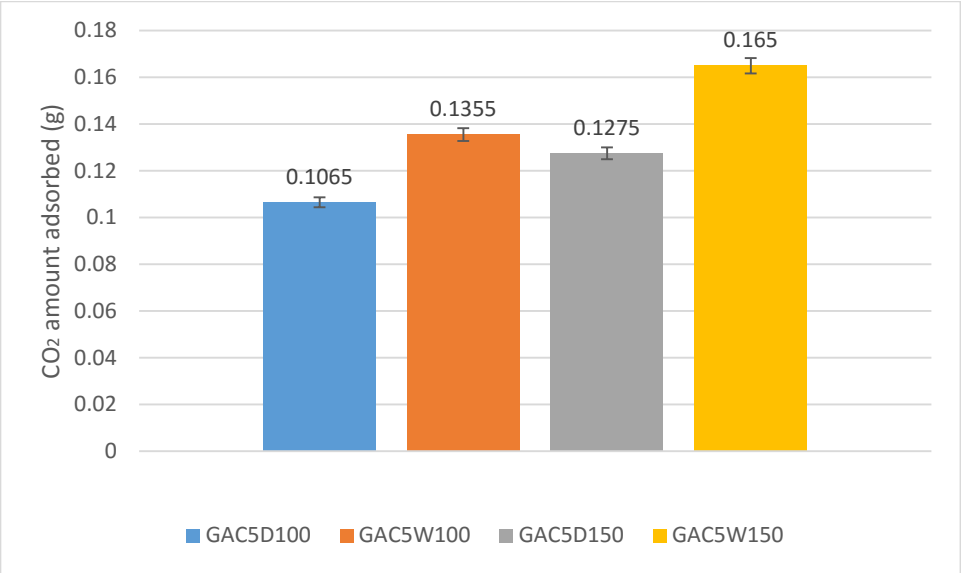

Figure 4.8: Amount of CO_2 adsorbed onto the GAC from a 5/95 CO_2/N_2 binary mixture at 25°C and 1bar, for 4 different parameters

This rise of the CO_2 adsorption capacity when introducing water vapour inside the binary gas mixture, when using GAC as an adsorbent, does not follow any of the previous literature studies suggesting that activated carbon is not influenced by the presence of moisture (Songolzadeh et al., 2012). This may be attributed to the fact that the total flow rate of the feed increased due to the vapour created during the moisture formation and as it was shown in the previous section, an increase in the total flow rate enhances the total amount of CO_2 adsorbed.

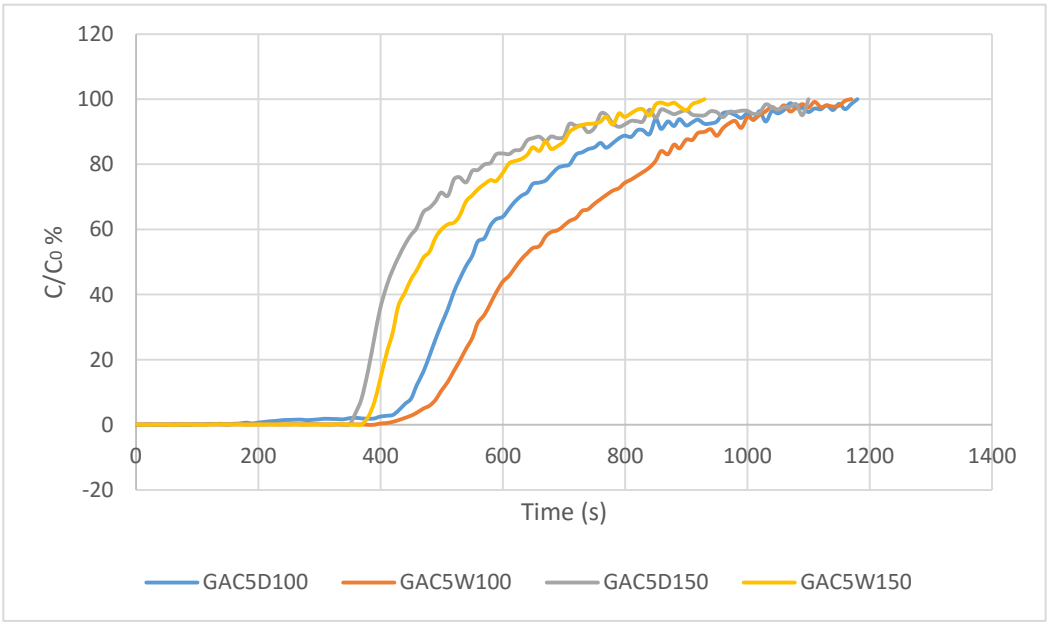

Figure 4.9: Breakthrough curves obtained from a 5/95 CO_2/N_2 binary mixture at 25°C and 1bar, comparing flow rates and dry/wet gas conditions

4.3. Comparison of MSA/TSA heating rates

Prior to the desorption experiments, the GAC heating rates were examined, comparing microwave (MW) and conventional (CH) heating in the presence of 100ml/min N_2 flow. Figures 4.10 and 4.11 show those rates, comparing MW with CH heating at 70°C and 130°C. It is clear that MW heating offers a faster process for the specific material compared to CH. In the case of MW the desired temperature is reached relatively fast, since only 40 seconds are needed for the bed to reach 70°C, whereas 3.5 minutes is the required time for 130°C MW heating. On the other hand, in the case of CH, a linear heating process is observed; the heating tape heats the Pyrex glass wall of the reactor, which passes the heat to the AC bed via conduction. This results in a long heating process (7 min for heating at 70°C and 15 min for 130°C) and more heat losses without the advantage of the rapid initial heating step.

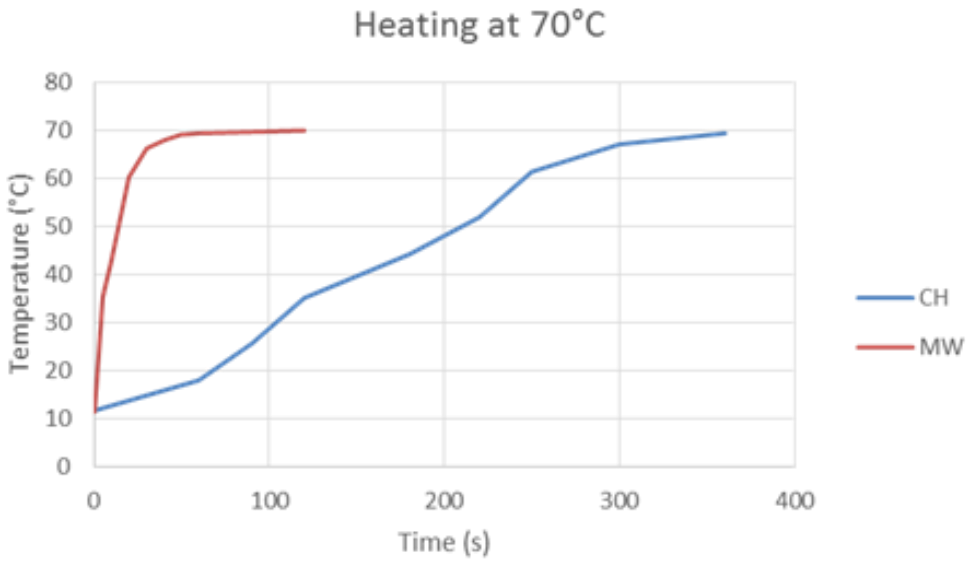

Figure 4.10: Heating rates process comparison of MW and CH for 70°C

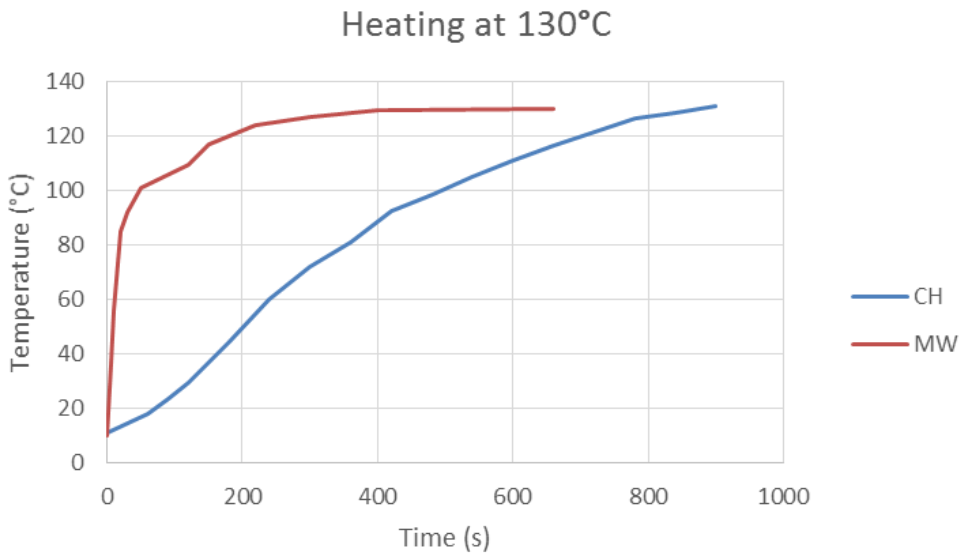

Figure 4.11: Heating rates process comparison of MW and CH for 130°C

Moreover, the rate of change in GAC temperature was compared for MW heating, as shown in Figure 4.12. The MW heating response demonstrates that the temperature increase rate declines as the temperature increases. This thermal response of the dry GAC during the MSA process is very promising because it indicates that the loss factor (ε'') of the adsorbent material does not increase with temperature. This means that a potential 'runaway effect', - in other words, the uncontrollable increase of the adsorbent's temperature, described in Section 2.2.7.1 - can be avoided when using GAC. The runaway effect would derive from a positive slope of the material's loss factor versus temperature (Metaxas and Meredith, 1983), which is not the case for this adsorbent. As a result, the rate of temperature change versus temperature of the sorbent is used here as an indicator for possible thermal runaway (Hashisho, 2007) and these rates are reported in Figure 4.12. It is clear that the temperature change rate is decreasing as the sorbent bed is heated, meaning that the loss factor of the GAC does not increase with temperature and as such, the runaway effect is avoided.

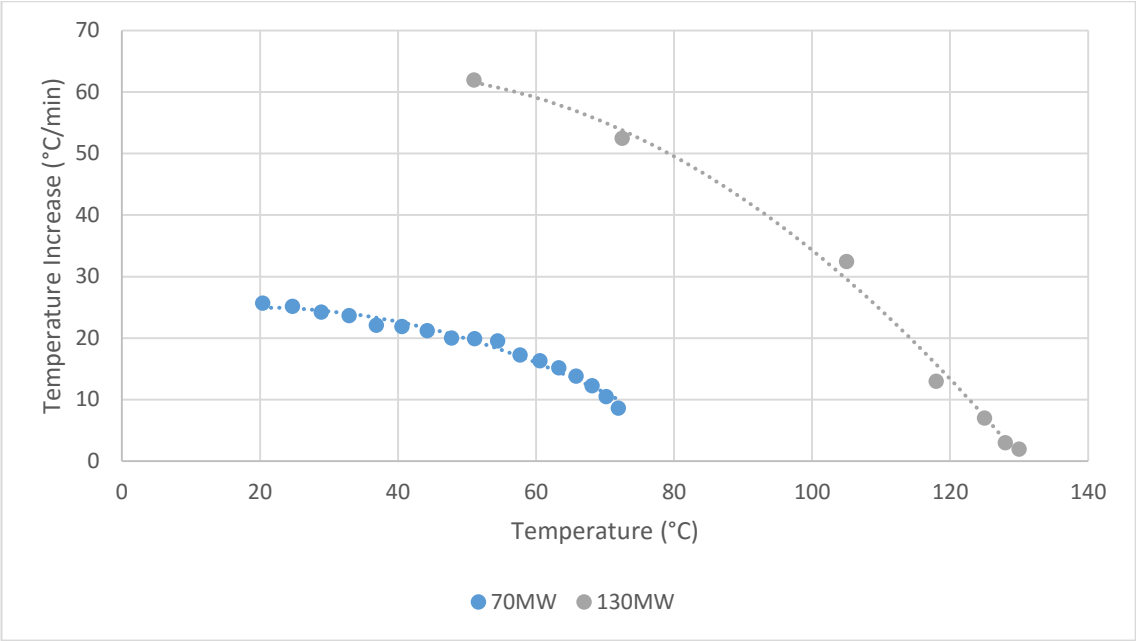

Figure 4.12: Heating rates for MW at 70°C and 130°C

As explained in Section 3.3.5, the average absorption of microwave power (also known as heating potential), P_{abs}, is associated with the frequency used during the application, the dielectric properties of the material and the strength of the electric field of the microwave energy, described from equation 3.11 (Metaxas and Meredith, 1983). This equation, combined with the rate of change of the sorbent's temperature and differentiated it with respect to temperature, provides an estimation of the loss factor change with temperature:

$$\frac{d\varepsilon_r''}{dT} = \frac{\rho C_p}{\omega \varepsilon_0 |E|^2} \frac{d}{dT}\left(\frac{\Delta T}{\Delta t}\right) \tag{4.6}$$

From the above equation, it is expected the loss factor of the GAC to decrease with increasing temperature. As a result, the effect of thermal runaway is unlikely in this occasion, being in agreement with other studies in the field of MSA processes (Hashisho, 2007).

Another important observation was that at the end of the microwave application, while the temperature of the GAC bed was 70°C, the temperature of the glass reactor wall was 40°C, or 80°C in the case of heating to 130°C. This can be attributed to the fact that glass is a microwave transparent material that cannot be heated under microwave irradiation, since it lets the waves pass through it, as discussed in Section 3.2.1.

However, the temperature of the reactor continued to increase to 60°C - 65°C (and 110°C - 120°C respectively) even after stopping the MW heating, presumably due to conductive heating from the hot bed to the reactor's walls.

4.4. CO_2 Desorption studies

The main focus of this research is the regeneration process that follows the CO_2 adsorption step. As explained in Chapter 2, two desorption technologies are typically applied in laboratory and/or industrial CCS applications nowadays, namely PSA and TSA. However, they are not considered to be the optimum pathways for CO_2 adsorption technology for reasons mentioned in Section 2.1.5. Accordingly, research towards the development of rapid thermal processes avoiding the disadvantages that PSA and TSA present is required. This study presents and analyses a relatively new approach for CO_2 capture, namely Microwave Swing Adsorption (MSA) technology, a process that is proposed in order to decrease the overall energy penalty by faster, more efficient and less energy intensive heating of the sorbents.

Utilisation of microwave energy for heating processes has been known for a long time, and the development of microwave ovens has more than 60 years of history. Previous studies on microwave assisted desorption applications showed that electromagnetic energy may be an appropriate alternative to conventional thermal heating, minimising energy losses and process time, as discussed in Section 2.2.9. However, the concept of using microwave energy in CCS applications to replace the conventional TSA and/or PSA processes is quite new and has not been studied before. As a result, further investigation is needed in order to prove that MSA can intensify CO_2 desorption process, since the post-combustion capture and regeneration process utilises larger CO_2 concentrations and lower temperatures (50-150°C) than the ones previously studied.

The effects of microwave regeneration of sorbent materials can vary depending on various process parameters, such as applied power, mass of saturated adsorbent, purge gas flow rate, irradiation and gas impurities such as moisture content. In this chapter, experimental studies of GAC CO_2 desorption comparing MSA and TSA technologies have been conducted. In order to intensify the regeneration process, the MSA process should primarily ensure that:

(a) The highest possible degree of desorption of the adsorbed compound is achieved (regeneration efficiency). Therefore, the regeneration of the solid sorbent is the first parameter investigated, comparing the amount of CO_2 desorbed against the previously adsorbed amount (4.4.2).

(b) A straightforward and efficient separation step of the adsorbed compound from the solid sorbent is possible, leading to a time and energy effective process (Shah et al., 2013). Thus, CO_2 desorption rates and energy consumption during the process are examined (Sections 4.4.3 and 4.4.4)

(c) The least possible textural erosion and mechanical destruction of adsorbent takes place, contributing to re-utilisation of the specific material. As a result, the possibility to re-use the GAC sample even after 25 consecutive MSA/TSA cycles is also investigated, as shown in this chapter (Section 4.6).

Furthermore, examination of the moisture impact during microwave heating is also important, since water vapour is also present in the flue gas mixture. Here, it should be noted that all the desorption experiments were conducted four times and an average of each measurement was considered. Consequently, the error estimation of the results was calculated to be on the range of ±2%, as shown by the error bars in the following figures.

4.4.1. Desorption profiles

Figures 4.13a-d to 4.15a-d present the CO_2 outlet concentration ($[CO_2]$) profiles during CO_2 desorption via MSA and TSA as a function of time (seconds) using two different temperatures, namely 70°C and 130°C. It is clear that there are two different outlet concentration patterns; MSA follows the *log-normal distribution*, while TSA results fits in the *Rayleigh distribution*. The log-normal distribution, sometimes also known as Galton distribution, is a probability distribution whose logarithm has a normal distribution. It is only applicable when the quantity of interest (in this case CO_2 outlet concentration) is positive, since log(x) exists only when x is positive. The following equation can be applied to the MSA profiles, according to the log-normal distribution:

$$[CO_2]_{MSA} = \frac{1}{\sigma t\sqrt{2\pi}}\, e^{-(lnt-\mu)^2/2\sigma^2} \tag{4.7}$$

where σ is the scale parameter (σ≈0.25) and μ is location parameter (μ=0).

Similarly, the Rayleigh distribution, named after William Strutt, Lord Rayleigh, is the distribution of the magnitude of a two-dimensional random vector whose coordinates are independent, identically distributed, mean 0 normal variables (Kundu and Raqab, 2004). The equation that describes the Rayleigh distribution and can be applied to the TSA desorption profiles is the following:

$$[CO_2]_{TSA} = \frac{t}{\sigma^2} e^{-t^2/(2\sigma^2)} \quad (4.8)$$

Where σ is again the scale parameter (σ lies between 2 and 3 for the TSA profiles).

All the MSA profiles show that the maximum [CO_2] is reached relatively fast, meaning that most of the adsorbed CO_2 is quickly desorbed, due to the rapid heating of the sorbent, breaking the van der Waals bonds between adsorbent and adsorbate within seconds from the beginning of the application. However, it is quite noticeable that there are differences between the profiles depending on the CO_2 concentration during the adsorption step. These differences can be explained taking into consideration that the amount of CO_2 inside the pores of the GAC to be desorbed varies for each case, as shown in Section 4.2. The characteristic peak of the $[CO_2]_{out}$ during the MSA process is almost equal (in the case of 40% CO_2) or higher (in the cases of 15 and 5%) to the concentration of CO_2 in the binary mixture during the adsorption step. On the other hand, it is important to note that during the TSA process, this peak does not reach the $[CO_2]_{in}$ for the cases of $[CO_2]_{in}$ =40% and 15% and as a matter of fact it is notably lower than half compared to the MSA process. However, in the case of $[CO_2]_{in}$ = 5%, the peak during TSA exceeds $[CO_2]_{out}$ = 5%, which is a very important result when dealing with low CO_2 concentration, as in the case of a gas-fired power plant (Section 2.1.2.2). MSA, though, achieves an even greater $[CO_2]_{out}$ peak, between 10% and 18% depending on the parameters examined.

40% CO_2

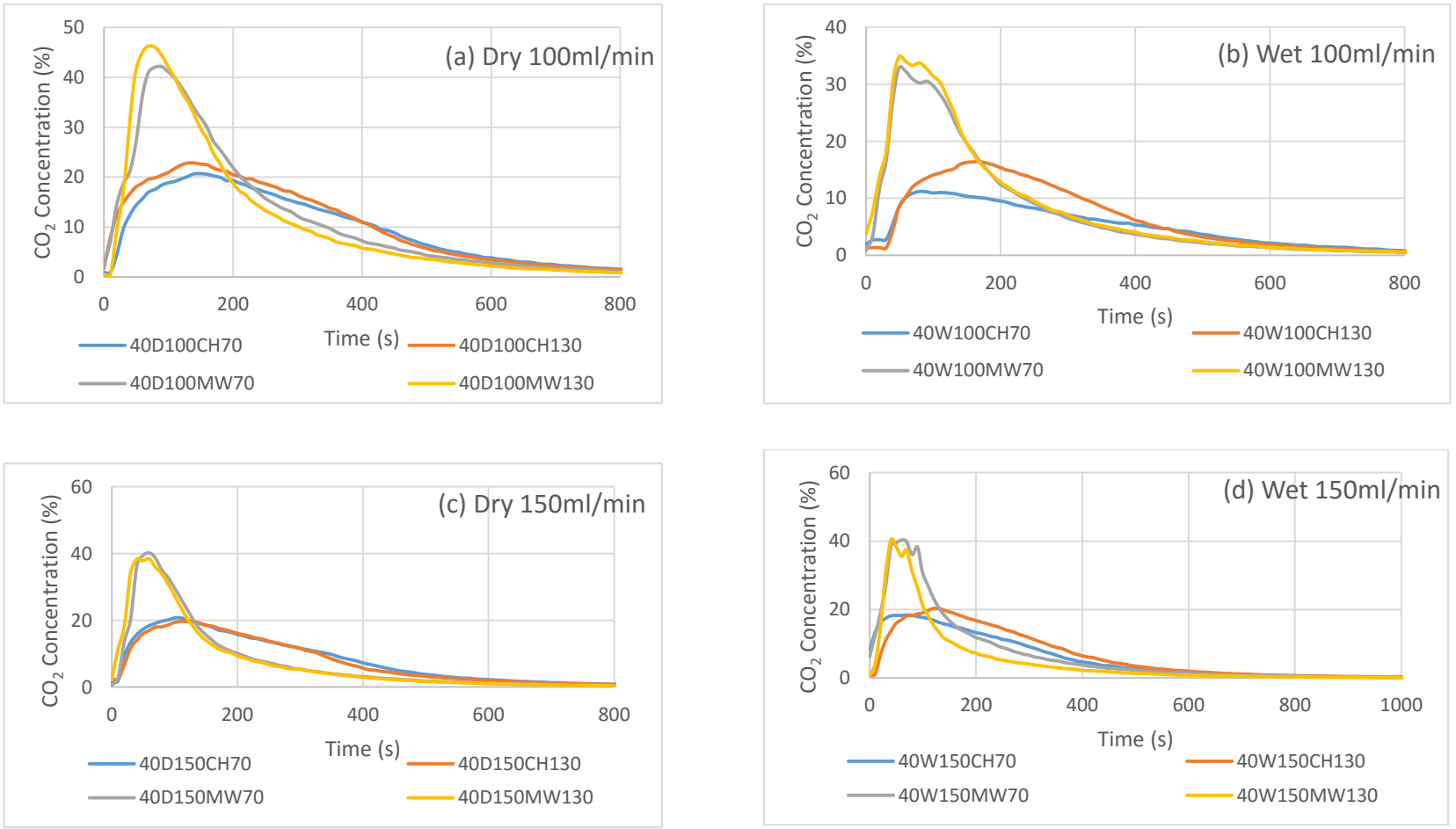

Figure 4.13a-d: Time dependent CO_2 outlet concentration profiles during GAC regeneration at 70°C and 130°C via MSA and TSA

Another significant difference is that the maximum $[CO_2]_{out}$ (curves' peaks) is reached much faster for the cases of MSA compared to TSA; in the case of $[CO_2]_{in}$ = 40%, the desorption peak was reached after 40-50 seconds in the MSA mode, whereas almost 3 minutes were needed for the TSA mode (Figure 4.13). The same trend is noticeable for the cases of $[CO_2]_{in}$ = 15% and 5%, where the peak during MSA is reached significantly faster compared to TSA (Figures 4.14 and 4.15). As a result, combining the facts that the peak of $[CO_2]_{out}$ is double in the case of MSA while it is reached clearly faster (1/3 of the time needed) compared to the TSA mode, it is clear that microwaves have the ability to intensify the process in terms of CO_2 desorption kinetics. Another important point is that in the case of TSA, there is a proportional relation between desorption time and CO_2 amount previously adsorbed. This was expected since the rate of desorption of an adsorbate (R_{des}) is proportional to the concentration of the adsorbed species (N), as seen in equation 4.9:

$$R_{des} = k_{des} N^x \tag{4.9}$$

Where x is the kinetic order of desorption (in this case $x = 1$) and k_{des} is the rate constant for the desorption process expressed in an Arrhenius form:

$$k_{des} = A exp(-\frac{E_a^{des}}{RT}) \tag{4.10}$$

Where A is the pre-exponential factor, E_a^{des} is the desorption activation energy, R is the ideal gas constant and T is the desorption temperature.

Comparing the TSA desorption profiles for the different $[CO_2]_{in}$, it can be seen that the $[CO_2]_{out}$ peak is reached after ~150 seconds when 40% of CO_2 was previously introduced, while in the case of 15% CO_2 this time increased to ~180-200 seconds. An even higher rise was noticed for the 5% CO_2, where the desorption peak was reached after almost 250 seconds. This is extremely important for the cases of low CO_2 concentrations in the exhaust gas mixtures, since it actually means that the desorption process takes longer time to start when operated with TSA technology.

15% CO_2

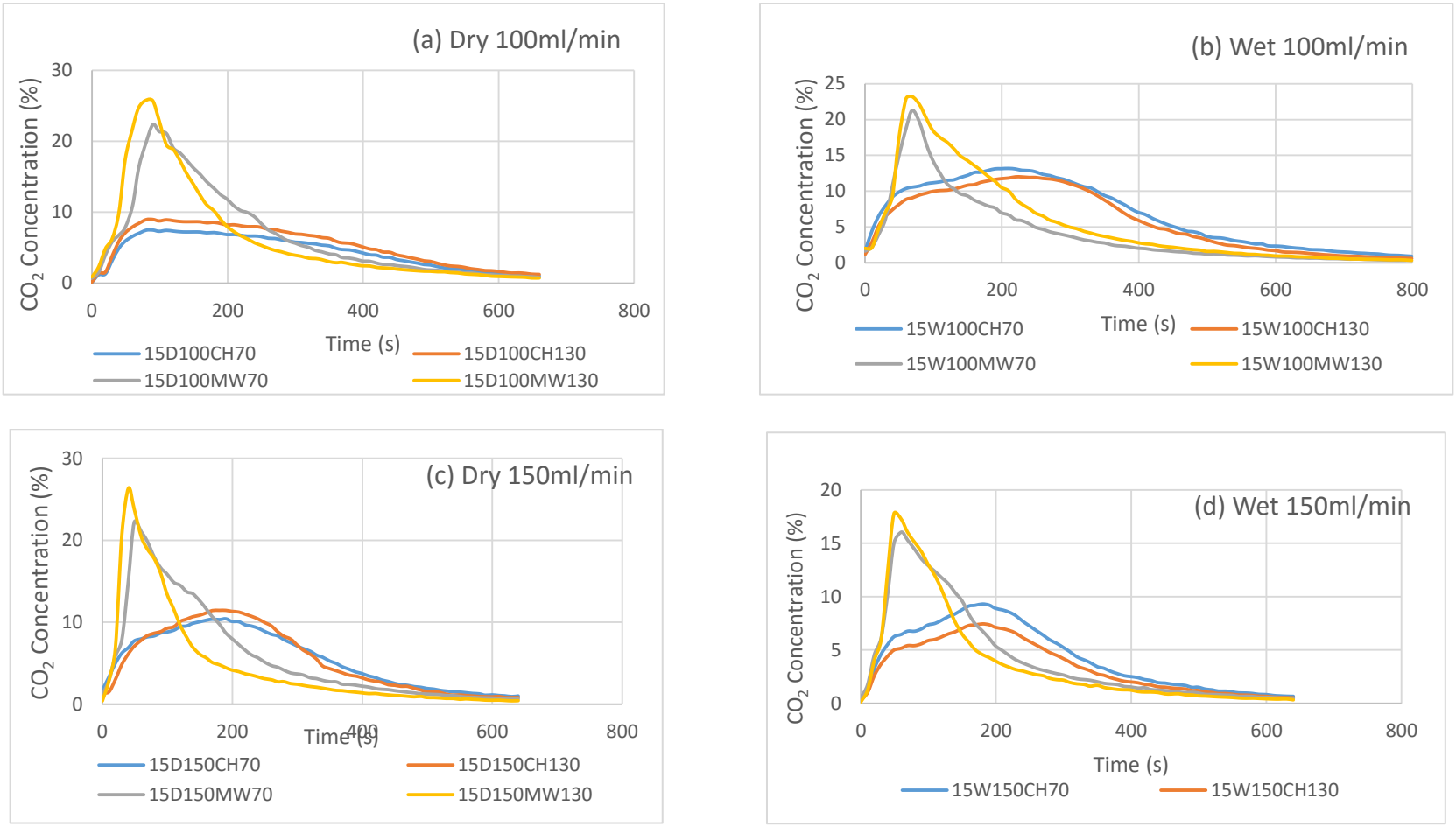

Figure 4.14a-d: Time dependent CO_2 outlet concentration profiles during AC regeneration at 70°C and 130°C via MSA and TSA

However, this is not the case for the MSA process, where the amount of energy needed for the desorption to initiate is supplied directly into the material, due to the nature of microwave heating discussed in section 2.2.9. As a result, the desorption peak during the MSA process lies between 60 and 90s for all $[CO_2]_{in.}$

It is worth mentioning that the wet conditions seem to affect the desorption process as well. In the case of a wet binary mixture of $[CO_2]_{in}$ = 40% during adsorption, the desorption profiles were different for both flow rates; specifically, the peaks were considerably lower and they were not clearly formed, slightly deviating from the expected distribution (Figure 4.13b). This abnormality was mostly evident during the MSA heating process and can be attributed to the fact that the dielectric properties of the material changed significantly when introducing moisture into the gas mixture, resulting in a higher amount of power absorbed during the regeneration process, due to the polar nature of H_2O as seen in section 2.2.4. This resulted in the presence of two adjacent $[CO_2]_{out}$ maxima, resulting from the pulse operation mode of the microwave, as explained in section 3.2.2.

However, this abnormality is not visible in the cases of smaller CO_2 amounts adsorbed. This was expected, since the amount of moisture inside the GAC is proportional to the amount of CO_2 adsorbed, and hence, when using a smaller concentration of CO_2 during the adsorption step, the amount of water held from the GAC did not create any irregularity in the desorption profiles.

Another clear difference between the two distribution patterns is the long tail that can be observed in the TSA process for every case. This tail suggests that the residual CO_2 desorption takes place slowly, due to a driving force reduction (in this case ΔT) (Balsamo et al., 2013), while in the case of MSA, the curve reaches an asymptote more rapidly, indicating that almost all the CO_2 is desorbed immediately after irradiating the AC bed with electromagnetic energy.

5% CO_2

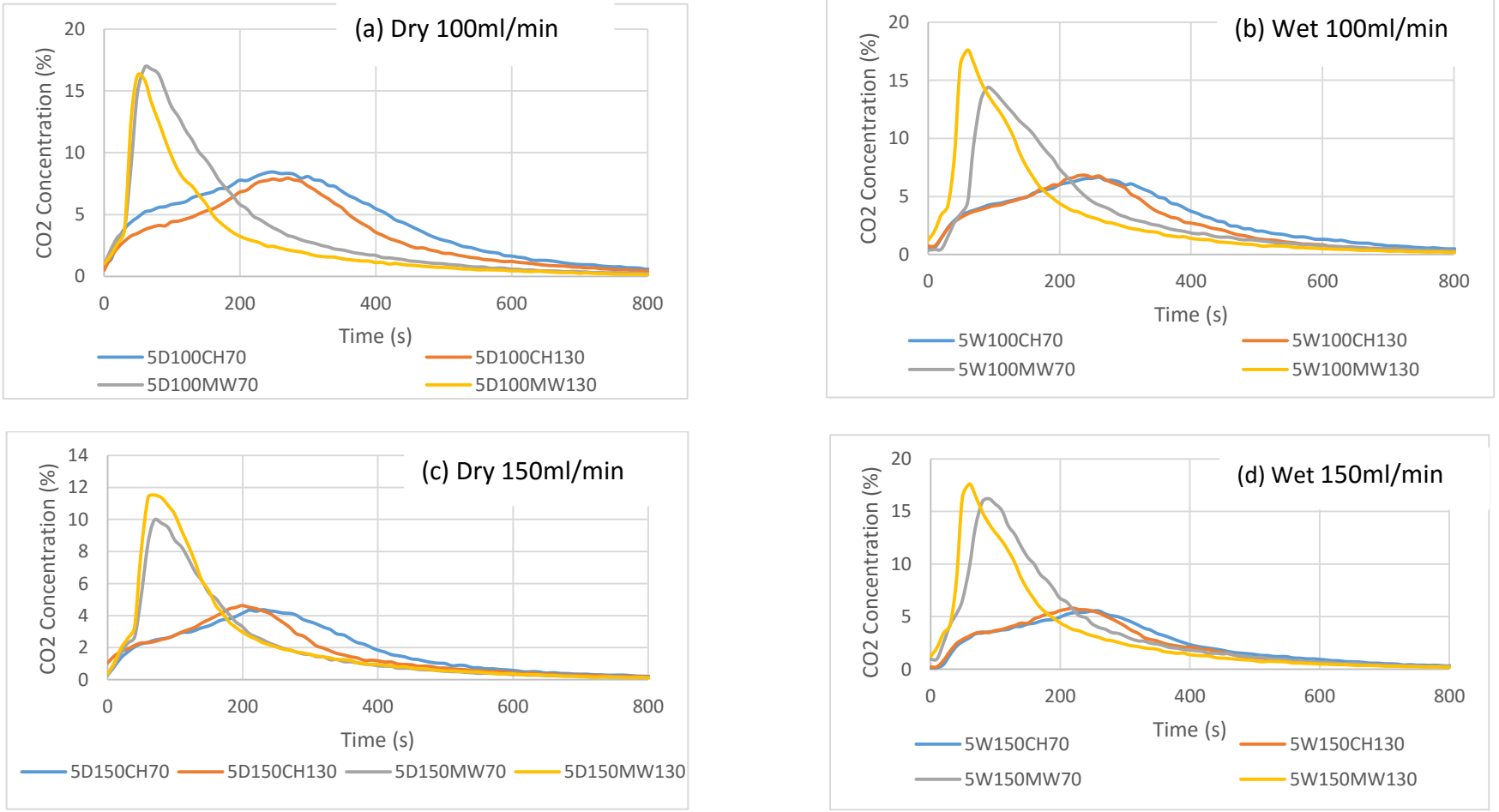

Figure 4.15a-d: Time dependent CO_2 outlet concentration profiles during AC regeneration at 70°C and 130°C via MSA and TSA

Furthermore, CO_2 desorption profiles were also quantitatively examined in order to investigate the best experimental conditions for an intensified regeneration process. Attention was mainly payed to CO_2 recovery amount, time required for the desorption process for a given regeneration level and energy consumed per kg of sorbent, the latter being a critical factor for the feasibility of a CO_2 capture plant. As a result, in the next Sections (4.4.2-4.4.4), the effects of heating method, heating temperature, flow rate, gas condition and $[CO_2]_{in}$ on the regeneration efficiency, desorption kinetics and energy consumption are discussed. Moreover, a thermal distribution map of the bed reactor is presented (Section 4.5) followed by an investigation of the possibility of re-using the GAC for 25 consecutive cycles (Section 4.6).

4.4.2. Regeneration efficiency

For the purposes of this study, desorption efficiency was the first parameter selected to evaluate the regeneration performance of GAC when comparing the two different heating technologies, MSA and TSA. Desorption efficiency (n_{des}) is defined by the ratio of amount of CO_2 released during regeneration to total CO_2 amount previously adsorbed by the GAC bed and can be calculated by the following equation:

$$n_{des} = \frac{Q_{des}}{Q_{ads}} * 100\% \quad (4.11)$$

Initially, the case of $[CO_2]_{in}$ =40% was examined and the results are presented in Figures 4.16 and 4.17. It is obvious that MSA intensified the desorption process in terms of GAC regeneration efficiency, since n_{des} is higher for every case that microwaves were utilised. The temperature increase does not seem to play an important role in the desorbed amount, since similar trends are reported for both 70°C and 130°C. However, it can be concluded that when using a higher temperature, the regeneration efficiency increased. This increment, though, is not large enough to justify a heating process at a higher temperature, which would lead to higher cost due to the increased energy consumption, as discussed in Section 4.4.4.

On the other hand, it is clear that the most influential factor was the gas condition during the adsorption step; both TSA and MSA processes report lower regeneration efficiencies in the cases of wet gas previously adsorbed. This could be associated with

the fact that CO_2 is faster adsorbed than H_2O, which comes second, blocking the pores on the surface, as mentioned in Section 4.2.3. As a result, H_2O acts as a superficial cover, not allowing the CO_2 molecules to diffuse to the outside of the pores when a heating process is applied. As can be seen from Figures 4.16 and 4.17 there is a huge decrease in the $n_{des,}$ especially when TSA is used; at 70°C desorption, n_{des} decreases from 66% to 32% for 100ml/min N_2 (carrier gas) flow rate and from 68% to 52% for 150ml/min. Furthermore, even when the GAC was heated at 130°C, the same trend was evident; a radical decrease from 79% to 38% for 100ml/min N_2 and from 70% to 40% for 150ml/min. These values are well below the desirable values for a large scale process, where desorption efficiencies of >80% are needed in order for the capture process to be economically feasible (Su et al., 2014).

MSA was expected to present better results, since water is very well known for its excellent dielectric properties due to its polar nature. A more efficient heating process was forecasted, which would consequently lead to higher amounts of CO_2 released from the sorbent. The experiments conducted proved the above point but not in a desirable level; regeneration efficiency is clearly improved when MSA is applied, as seen in Figures 4.16 and 4.17. When heating at 70°C, an increase from TSA's 32% to 53% for 100ml/min N_2 flow and from 52% to 66% for 150ml/min N_2 flow was evident. Moreover, in the case of 130°C, MSA managed to enhance n_{des} from 38% to 55% and from 40% to 64%, respectively. However, it is quite clear that these numbers are still well below the target of 80% of a real scale process, which in fact was reached using MSA under dry gas conditions at 70°C and 130°C and 100ml/min N_2 flow.

Lastly, the increase in the N_2 carrier gas flow rate does not significantly affect the regeneration efficiency, however an interesting trend is reported; when increasing from 100ml/min to 150ml/min, there is a small improvement in the efficiency in the case of TSA, whereas this change seems to affect negatively the MSA process for the dry gas, contrary to the wet gas conditions, where a positive effect is reported. The CO_2 molecules are detached from the solid sorbent due to the temperature increase; however, they are blocked under the superficial H_2O adsorbed and as a result an additional driving force is needed, which in this case is the increased velocity of the carrier gas.

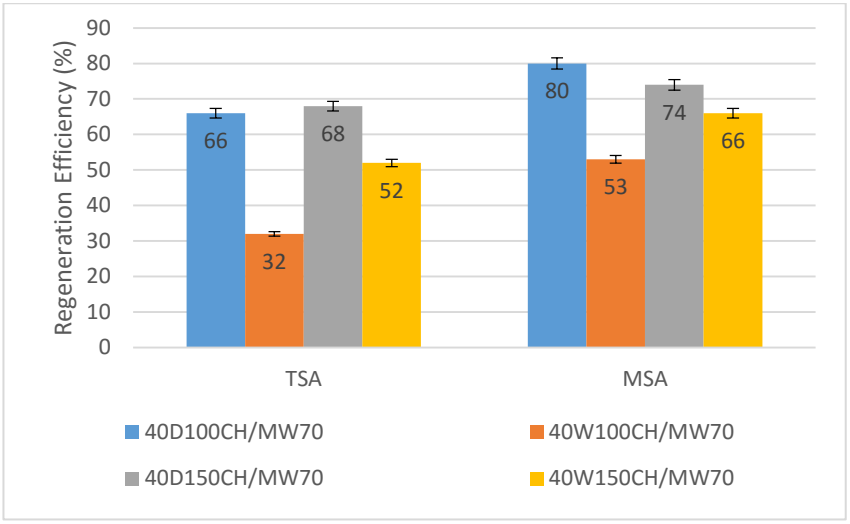

Figure 4.16: ($[CO_2]_{in}$ =40%) Comparison of the regeneration efficiency for MSA and TSA at 70°C

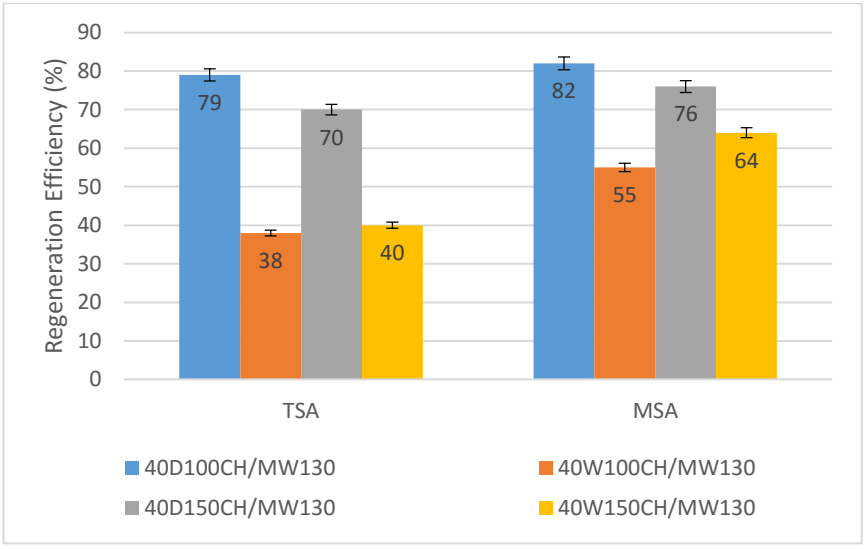

Figure 4.17: ($[CO_2]_{in}$ =40%) Comparison of the regeneration efficiency for MSA and TSA at 130°C

Similar trends were reported in the case of $[CO_2]_{in}$ =15%; however, each case individually resulted in better regeneration efficiencies compared to the previous outcomes. The results presented in Figures 4.18 and 4.19 demonstrate that the regeneration efficiency increased in all cases when MW was applied, as a consequence of the fast heating of the sorbent, as explained in Section 4.4.1. It is also evident that lower flow rates and dry gas conditions result in higher desorption efficiencies, whereas the increase in temperature from 70°C to 130°C did not seem to play an important role. Specifically, the highest desorption efficiency during TSA, when heating either at 70°C or 130°C, was observed when 100ml/min and dry gas conditions were used, namely

80%. MW improved this value to a maximum of 91% (~13% increase) in the case of 70°C and to 88% for 130°C desorption, which were also the highest values of all cases.

It is also worth mentioning, that the lowest desorption efficiencies were once again calculated for the wet gas conditions, namely 70%-73% at 70°C and 71% at 130°C for TSA. However, experimental tests under the MSA process showed an improvement in those efficiencies as well, resulting in much higher amount of CO_2 desorbed from the GAC. When heating at 70°C, using 100ml/min a 83% efficiency was reached, while this amount decreased for a higher purge flow rate (150ml/min) to 77%. Accordingly, when heating at 130°C, using 100ml/min the desorption efficiency improved from 71% to 82%, while for 150ml/min the rise was smaller, from 71% to 76%. It can be concluded that for $[CO_2]_{in}$ =15%, MSA managed to increase the regeneration efficiency of the GAC over the acceptable limits of 80%; considering all parameters reported, while TSA reports an average of ~74%, MSA intensified the desorption process leading to an increase regarding n_{des} to an average of 84%.

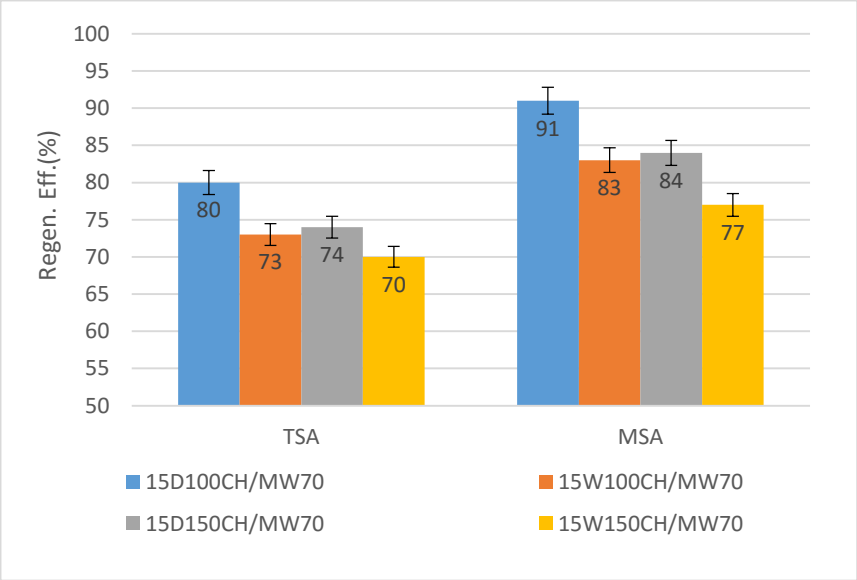

Figure 4.18: ($[CO_2]_{in}$ =15%) Comparison of the regeneration efficiency for MSA and TSA at 70°C

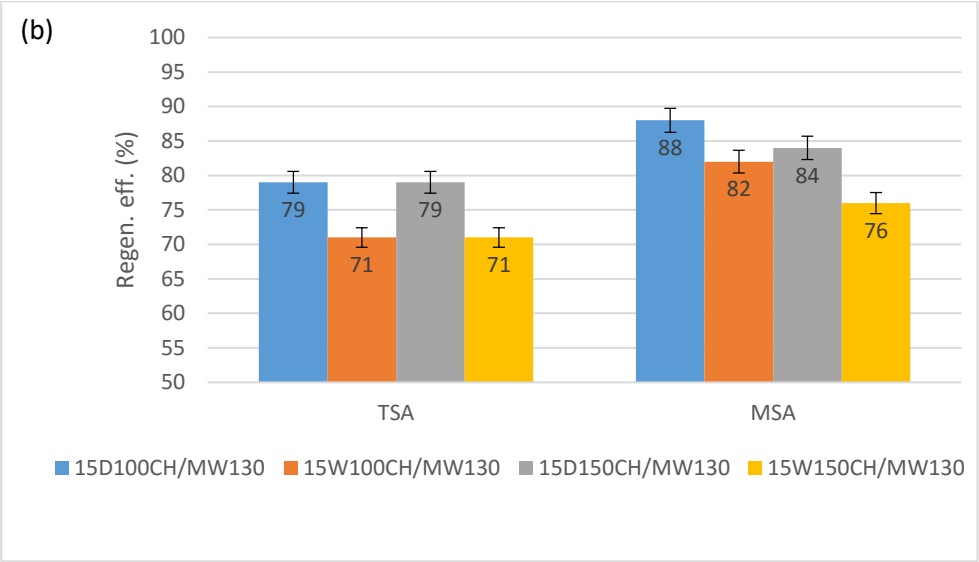

Figure 4.19: ($[CO_2]_{in}$ =15%) Comparison of the regeneration efficiency for MSA and TSA at 130°C

Lastly, $[CO_2]_{in}$ =5% (simulating the CO_2 partial pressure in the flue gas of a gas-fired power plant) was examined, which also showed similar trends with the previous outcomes for each individual case (Figures 4.20 and 4.21). However, comparing the regeneration efficiency for each CO_2 concentration, the trend was not as expected; n_{des} using TSA process for $[CO_2]_{in}$ =40% averaged ~55% for 70°C and ~58% for 130°C, which increased vastly for $[CO_2]_{in}$ =15%, namely ~74% for both temperatures. Same trend was followed for the MSA process, where from 68% and 70%, n_{des} reached an average of 84% for both temperatures. This trend was expected to continue when decreasing the amount of CO_2 in the gas binary mixture during the adsorption step, namely $[CO_2]_{in}$ =5%. Nonetheless, TSA resulted in an average of 61% for 70°C and 70% for 130°C, while MSA reported an average of 74% for both temperatures. This means that the optimum concentration of CO_2 lies between 5% and 40%, for which the regeneration efficiency can practically be close or over the limits of 80%, is 15%.

As expected, the lowest desorption efficiencies were reported for the wet gas conditions, namely 57%-60% (for 100ml/min and 150ml/min, respectively) at 70°C and 62%-67% at 130°C for TSA. MSA process managed to increase those efficiencies as well; when heating at 70°C, using 100ml/min a 66% was possible, while this amount increased for a higher purge flow rate (150ml/min) to 68%.

Accordingly, when heating at 130°C, using 100ml/min the desorption efficiency improved to 70%, while for 150ml/min the rise was smaller, reaching 75%.

Interestingly enough, the temperature increase played a more important role than in the previous cases, since when the GAC was heated at 130°C it showed a greater regeneration efficiency compared to 70°C. This can be explained taking into consideration that in the case of $[CO_2]_{in}$ =5%, the adsorbed amount was much lower than in the other cases, as shown in Section 4.2 (2.5 $g_{CO2}/g_{sorbent}$ compared to 9.2 and 4.5 $g_{CO2}/g_{sorbent}$ for 40 and 15% vol. CO_2 in the gas mixture, respectively). This would mean that CO_2 needed a higher driving force (temperature difference) in order to be detached and diffused from the pores of the GAC and as such better regeneration efficiencies are reported for 130°C compared to 70°C. An efficiency average of ~61% was calculated for TSA at 70°C, which was increased to 70% at 130°C. Similarly, when MSA was applied, the average regeneration efficiency increased from ~70% to 76%.

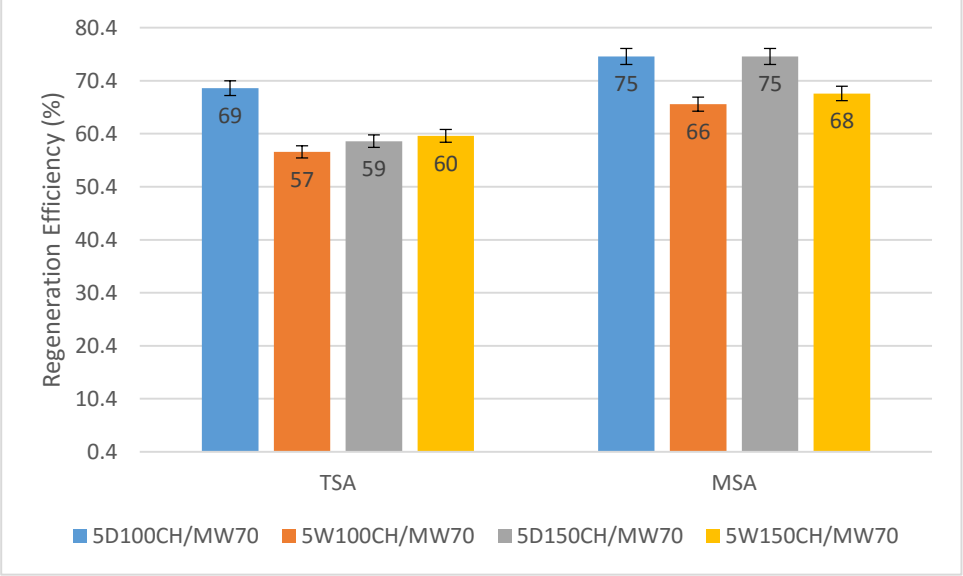

Figure 4.20: ($[CO_2]_{in}$ =5%) Comparison of the regeneration efficiency for MSA and TSA at 70°C

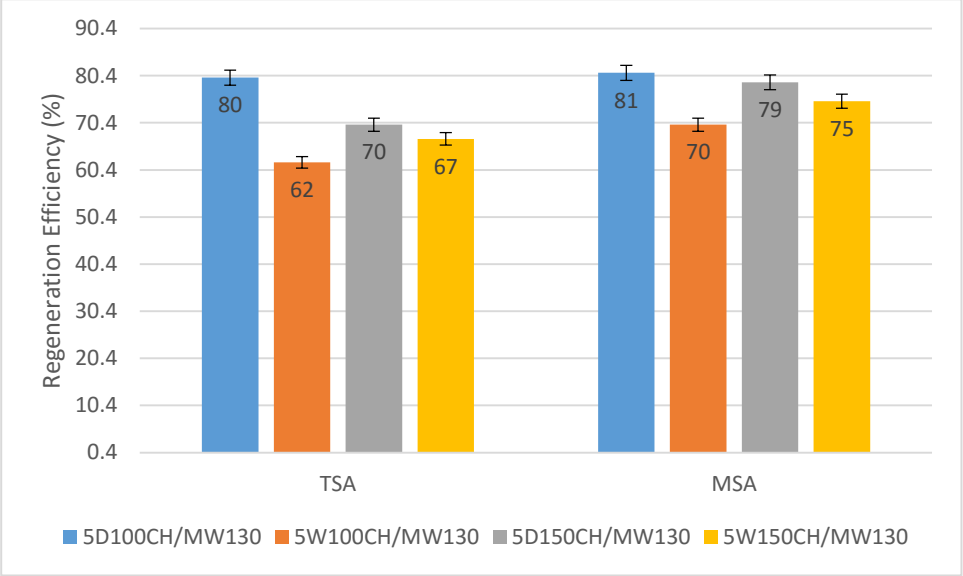

Figure 4.21: ($[CO_2]_{in}$ =5%) Comparison of the regeneration efficiency for MSA and TSA at 130°C

It can be concluded that MSA improved the regeneration efficiency of the studied GAC, compared to TSA. However, the values obtained were not as high as expected, especially in the case of wet gas conditions, and only some of them were equal or higher than 80%, which is the lowest acceptable limit for the feasibility of a real scale CO_2 capture unit. This result was not expected, taking into consideration the excellent dielectric nature of H_2O. One possible reason that could explain the above statement is that, MSA has the disadvantage of temperature non-uniformity inside the target object, in this case sorbent bed. This non-uniformity can be influenced by various parameters, such as material characteristics, frequency used and bed geometry. The latter can vastly affect the temperature distribution inside the reactor, contributing to a highly non-uniform heating of the total bed. As a result, temperature distribution profiles (heat maps) are shown and discussed in Section 4.5.

4.4.3. Desorption kinetics

One crucial parameter for the economics of the CO_2 capture process is the desorption kinetics, in other words how fast CO_2 is desorbed from the GAC. As previously explained, TSA is favourable compared to PSA in terms of regeneration efficiency of the solid sorbent, however it presents disadvantages with regards to the time needed for the desorption to be completed. MSA can lead to intensified desorption kinetics taking advantage of the fast heating rates that occur during the process. In this sub-section, a comparison between TSA and MSA, using the experimental data is presented.

Here it should be noted that considering the shape of desorbing profiles (Figures 4.13-4.15), it can be predicted that a higher desorption time contributes to a more effective GAC regeneration resulting in a higher CO_2 percentage recovery, but this would possibly lead to higher energy consumption and larger desorption times. For this reason, four different desorption times (t_{50}, t_{70}, t_{90}, t_{95},) were examined, trying to find a balance between the above statements, in order to create an integrated desorption process. Each desorption time describes a different CO_2 percentage of the total desorbed amount, e.g. t_{70} corresponds to a 70% of total CO_2 recovered by desorption.

Regarding the effect of the regeneration method followed, as clearly seen from Figures 4.13-4.15, the desorption profiles become narrower and higher for MSA compared to TSA, and thus denoting a faster desorption process. Figures 4.22 to 4.27 express this time decrease (%) for MSA technology compared to TSA, providing some interesting results. Initially, it is evident that for every case the regeneration is highly intensified for the case of 50% desorption. It is interesting that as the desorption process continues, the time difference between TSA and MSA becomes smaller. This effect can also be proven by the desorption profiles (4.14-4.16), where in the case of MSA the peak of $[CO_2]_{out}$ is reached significantly faster (1/3 of the time needed) compared to TSA. Moreover, this maximum amount of $[CO_2]_{out}$ is also 2 times higher than in the case of TSA, meaning that during the initial step of the desorption process (from $[CO_2]_{out} = 0$ to $[CO_2]_{out} = [CO_2]_{out,max}$) MSA is significantly favoured compared to TSA. However, the long tails presented in the MSA profiles denote that the rest of the desorption process is slow and does not significantly change when changing regeneration technology, since the tails are also present for TSA. As a result, the larger amount of CO_2 is desorbed from the GAC, the smaller differences in desorption rates between MSA and TSA are observed.

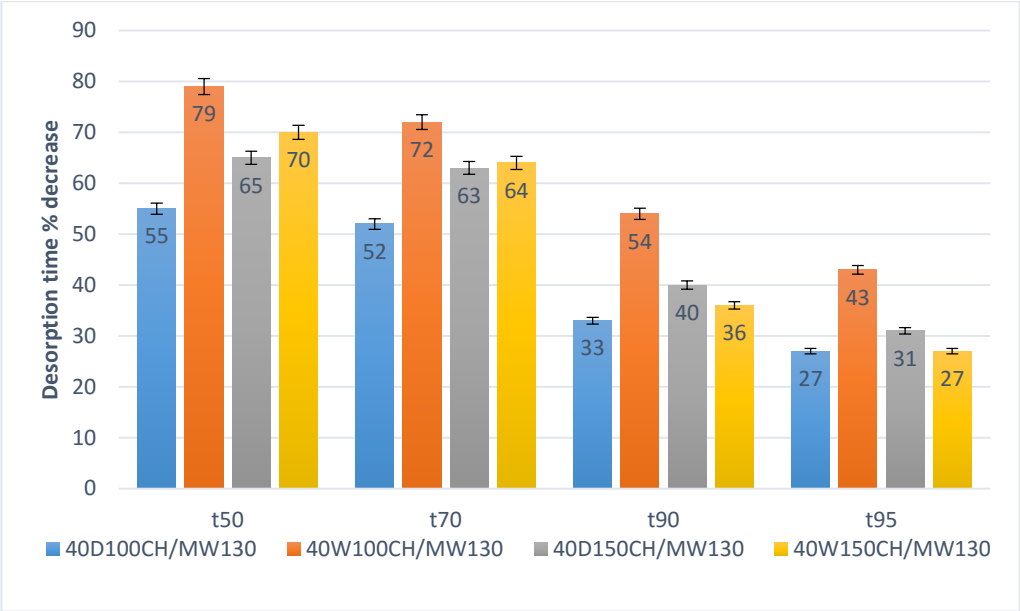

Figure 4.22: Desorption time % decrease for $[CO_2]_{in}$ =40% at 70°C

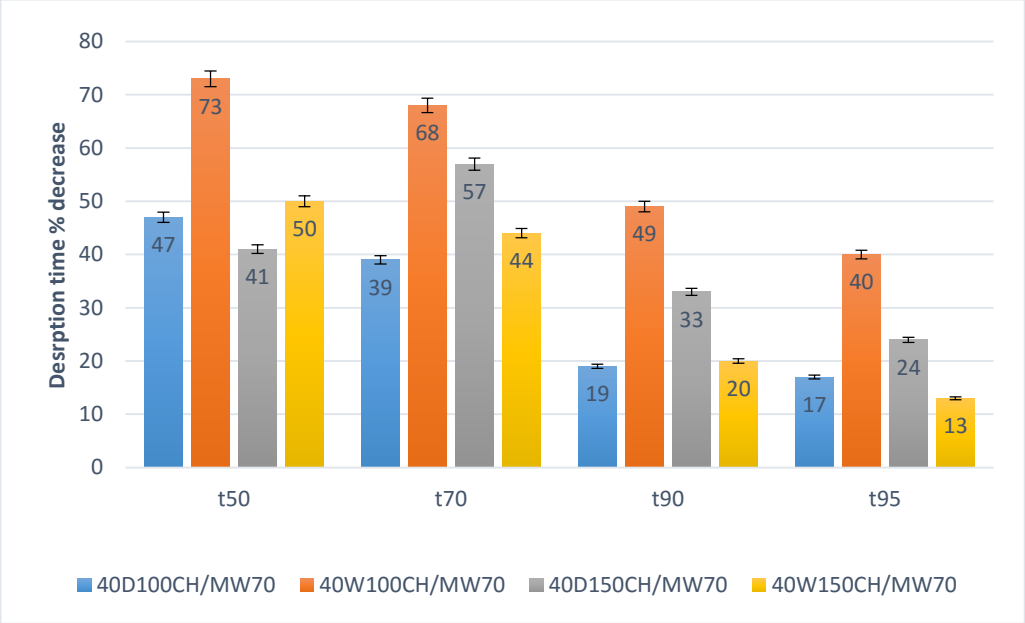

Figure 4.23: Desorption time % decrease for $[CO_2]_{in}$ =40% at 130°C

Figures 4.22 and 4.23 demonstrate the case of $[CO_2]_{in}$ = 40%, for which a huge decline in the regeneration time for 50% desorption was observed, since the MSA is reported to be 2-5 times faster compared to TSA. Interestingly enough, the highest decrease was observed for the wet gas conditions, namely a 79% and 70% decrease was attainable when heating at 70°C using 100 and 150ml/min of N_2 flow, respectively. This supports

the statement that the moisture content inside the gas favours the MSA process. As previously reported (Section 2.2.7.2), the presence of moisture enhances the heating of the sorbent, since microwaves are not only absorbed from the GAC, but also from the water molecules attached on the surface of the material.

Looking at the larger CO_2 amounts desorbed (t_{70} to t_{95}), it is clear that for both heating temperatures the trend remains the same. MSA improves the desorption kinetics, decreasing the amount of time needed, while the highest decline is reported for wet gas conditions at 100ml/min of N_2 flow. However, t_{95} decreases when using MSA only for an average of ~30% for 70°C and almost 23% for 130°C. It is evident that the larger the regeneration time, the higher the regeneration efficiency. However, rapid regeneration processes are usually preferred, resulting in an equilibrium between adsorption and desorption rates and lower amount of energy consumed as well. In continuous large scale industrial applications, adsorption is usually considered complete after reaching the breakthrough time, which in the case of GAC lies between 4 and 7 mins (Figures 4.5, 4.7 and 4.9). As a result, a desorption process that does not exceed a total of 7 min – ideally <4min - is preferred in this case, leading to compromises against the amount of CO_2 desorbed; 50% of CO_2 desorbed is on the other hand not the optimum solution since this would mean that the GAC pores would remain half full with CO_2 after regeneration, which would lead to a decrease in the sorbent's CO_2 adsorption capacity in the next cycle. As a result it is believed that a good compromise between time and desorbed amount would be a 70% desorption. This is in agreement with other studies reported by Balsamo (2013) and Webley (2014), where they examined t_{50}, t_{70}, t_{80} and t_{90} with regards to CO_2 recovery amount, time required for the desorption process (at a fixed regeneration level) and CO_2 mean concentration in the desorbing flow, concluding that a 70-80% desorption level provides optimum results via TSA and microwave-assisted PSA respectively.

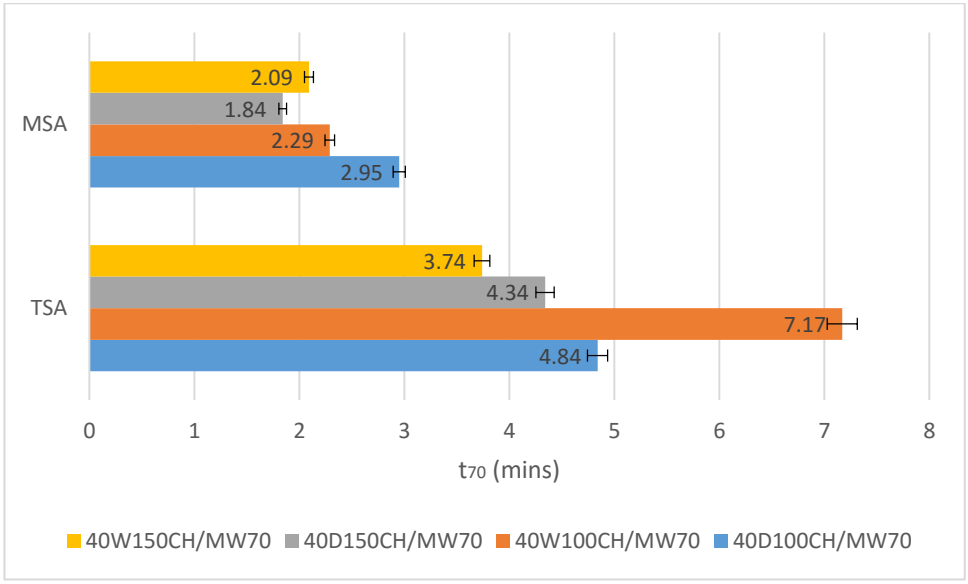

Figure 4.24: Comparison of t_{70} for MSA and TSA when heating at 70°C for $[\mathbf{CO_2}]_{in}$ = 40%

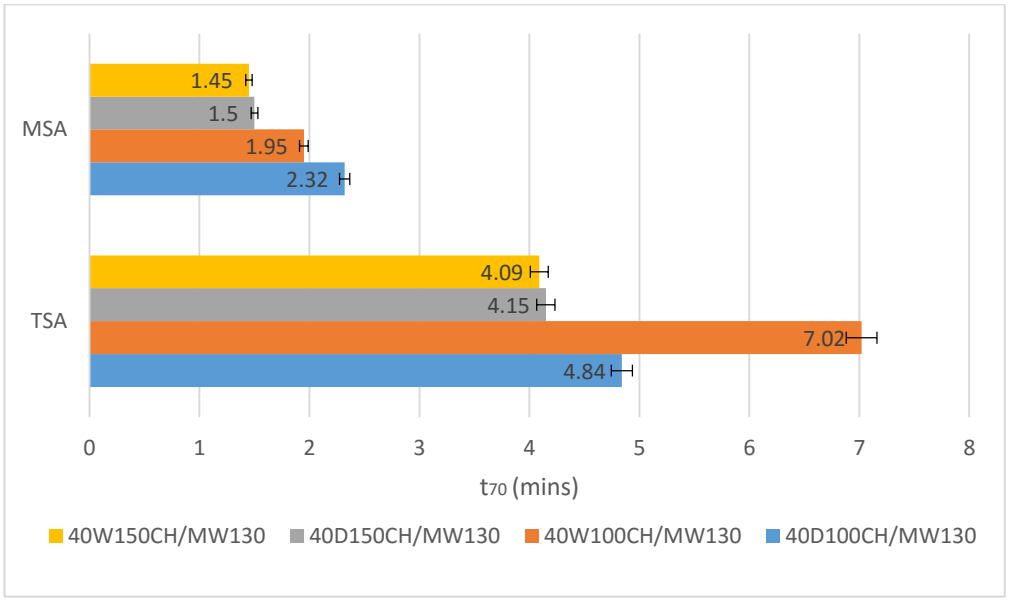

Figure 4.25: Comparison of t_{70} for MSA and TSA when heating at 130°C for $[\mathbf{CO_2}]_{in}$ = 40%

Figures 4.24 and 4.25 present a direct comparison of the 70% CO_2 desorbed in terms of time between MSA and TSA for two different temperatures, 70°C and 130°C. It is clear that TSA is a more time-consuming process, needing an average of 4.3 minutes to reach t_{70} when heating at 70°C, while the increase in temperature to 130°C did not seem to play an important role. More importantly, in the case of wet gas at 100ml/min N_2 flow, t_{70} increases to ~7.2 minutes for 70°C and to ~7 minutes for 130°C, which denotes an

extremely slow desorption process due to the influence of the water adsorbed as discussed in Section 4.4.2. Nevertheless, MSA intensified the CO_2 desorption kinetics for the wet gas conditions, by managing to decrease the time needed by as much as 70%, resulting in a t_{70} process that took an average of 2 minutes to be accomplished. The above figures also show an inversely proportional relation between desorption rate and purge gas flow rate, meaning that as the N_2 flow rate increases, t_{70} decreases. However, this decrease in time was proportionally evident for both TSA and MSA cases and as a result they cannot be associated with the desorption technology used; an increase in the gas velocity through the AC bed is seemingly associated to larger mass transfer coefficients, due to driving force increase.

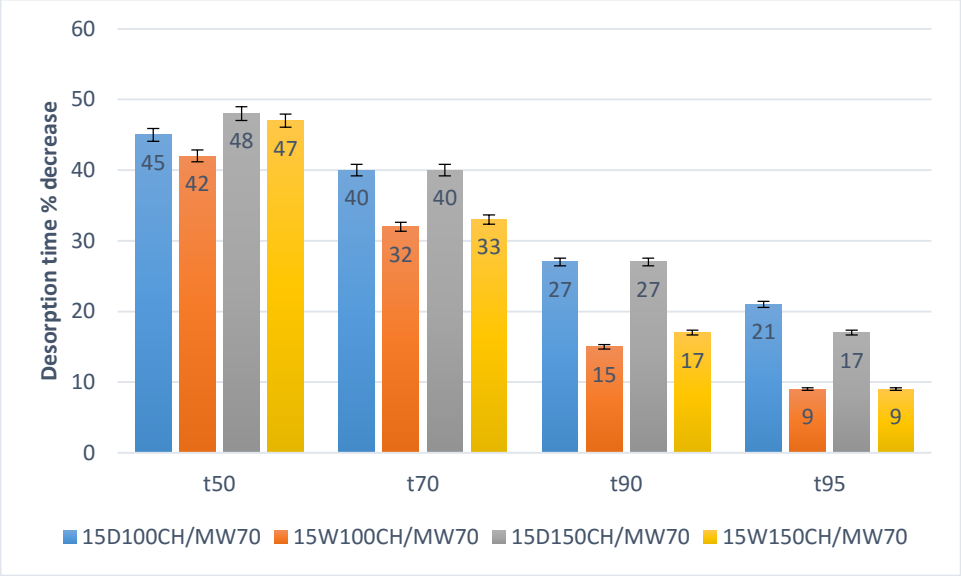

Figure 4.26: Desorption time % decrease for $[\boldsymbol{CO_2}]_{in}$ =15% at 70°C

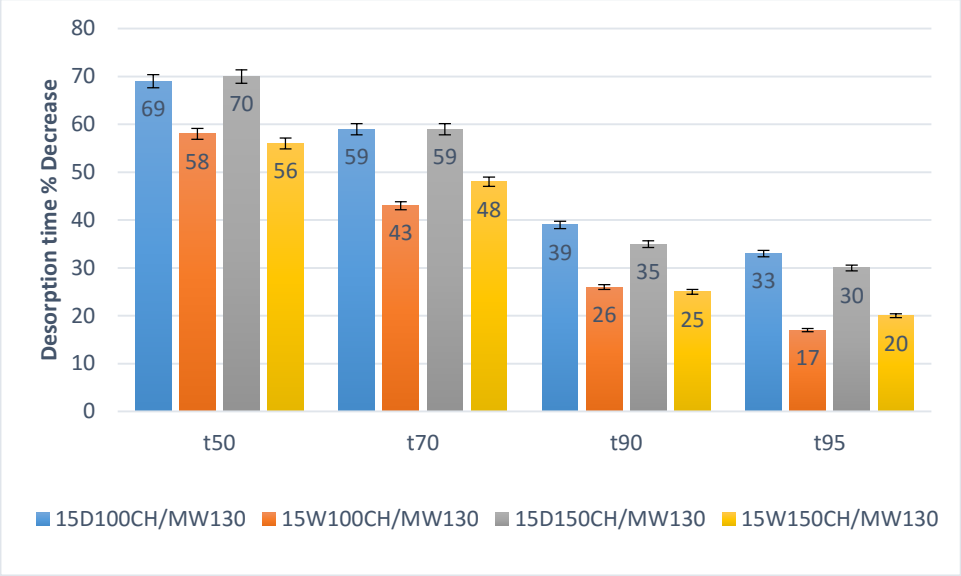

Figure 4.27: Desorption time % decrease for $[CO_2]_{in}$ =15% at 130°C

Figures 4.26 and 4.27 show the decrease in desorption time (%) in the case of $[CO_2]_{in}$=15% in relation with the amount of CO_2 desorbed for 70°C and 130°C respectively. Similar to the case of $[CO_2]_{in}$=40%, the desorption kinetics tend to be similar as the regeneration amount increases, especially for the case of wet gas conditions where MSA managed to intensify the process by only 9% for 70°C and 18% for 130°C. However, it is clear that once again t_{70} could work as a good compromise between amount desorbed and time consumed, with the MSA process being able to significantly decrease t_{70} as well.

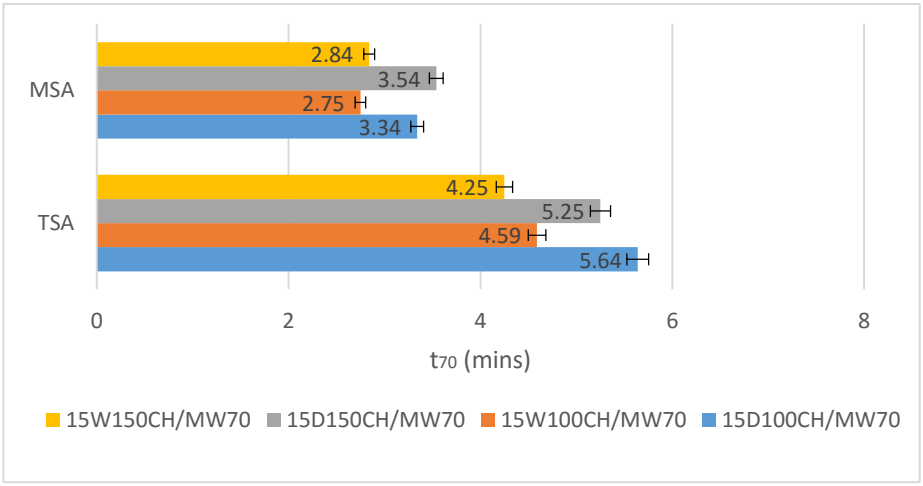

Figure 4.28: Comparison of t_{70} for MSA and TSA when heating at 70°C for $[CO_2]_{in}$ = 15%

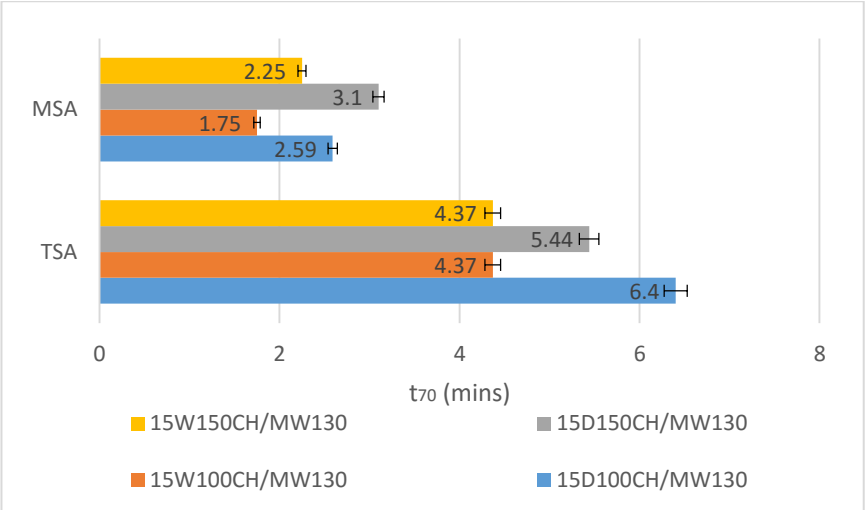

Figure 4.29: Comparison of t_{70} for MSA and TSA when heating at 130°C for $[\mathbf{CO_2}]_{in}$ = 15%

In all cases, the time needed to obtain the desired CO_2 recovery percentage (t_{70}) monotonically decreases when using MW, being also further decreased with both desorption temperature and N_2 purge flow rate increase, as observed in Figures 4.28 and 4.29. More specifically, TSA process lies between 4 and 6 minutes, while MSA reduces this time to 2-3.5 minutes, representing a reduction of 40-60%. This becomes even clearer in the case of heating up to 130°C; t_{70} was reduced by as much as 60% for the dry conditions, whereas for the wet conditions the decrease was equal to ~45%. It is also worth mentioning that for every wet gas experiment, the t_{70} was significantly lower than in the case of dry gas conditions; this could be attributed to the fact that, as reported in Section 4.4.2, the desorption efficiency of the wet gas simulation was lower, meaning that less amount of CO_2 was desorbed. As a result, it is reasonable to expect a faster desorption process when less amount of CO_2 is desorbed.

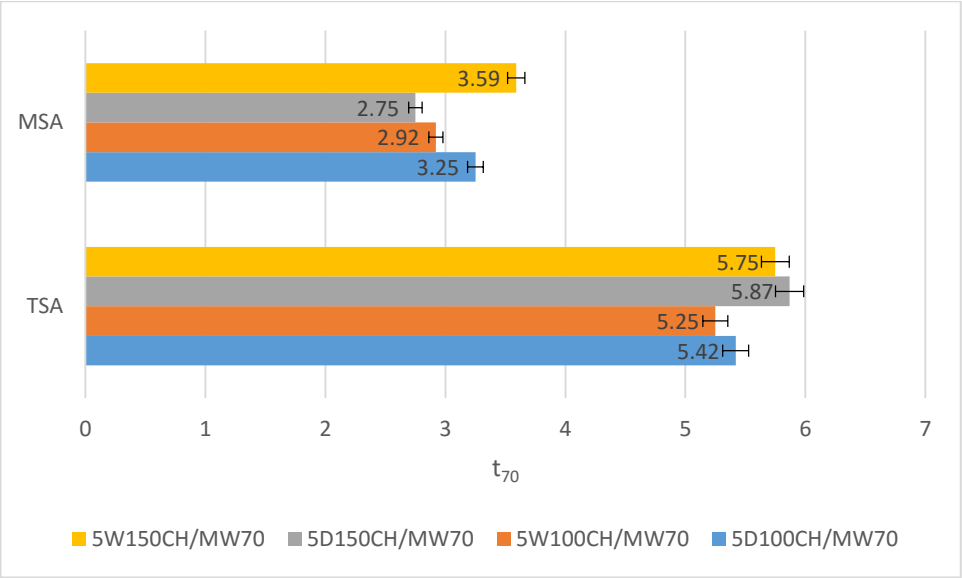

Figure 4.30: Comparison of t_{70} for MSA and TSA when heating at 70°C for $[\mathbf{CO_2}]_{in}$ = 5%

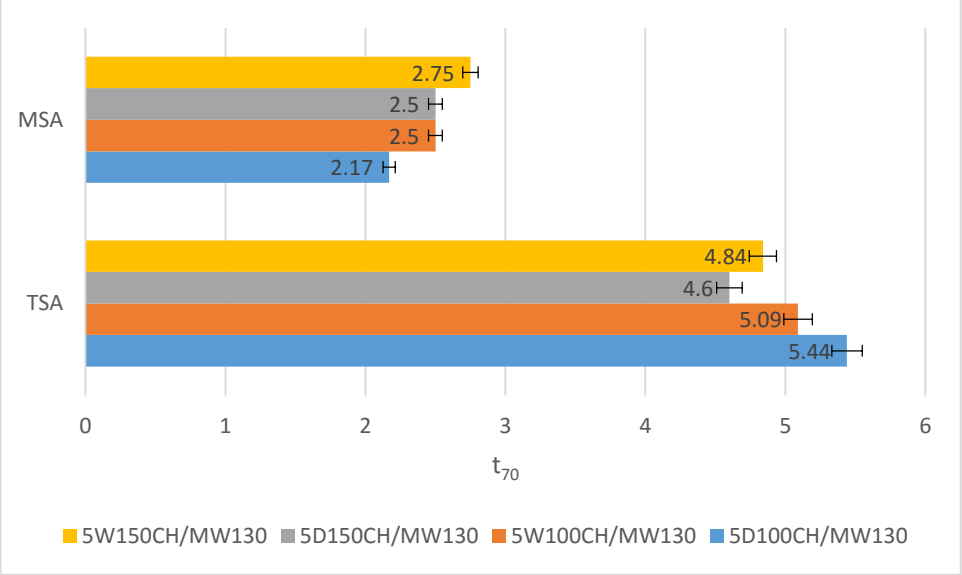

Figure 4.31: Comparison of t_{70} for MSA and TSA when heating at 130°C for $[\mathbf{CO_2}]_{in}$ = 5%

The last case examined was for the $[CO_2]_{in}$ =5%, which provided the same trends as before (Figures 4.30 and 4.31). In this case, only t_{70} is presented, since it was already proven that a 70% desorption is a good compromise between CO_2 amount recovered and time needed. Once again, MSA was able to intensify the regeneration process, resulting in a desorption time decrease of approximately 40% for both 70°C and 130°C heating. More specifically, the TSA process for 70% desorption in the dry conditions is completed after 4.8-5.8 minutes, whereas in the case of MSA, only 2.2 to 3.2 minutes are needed, depending on the regeneration temperature. Moreover, wet conditions

experiments showed the same trends, with a decrease from an average of 5.2 to 2.9 minutes, corresponding to a 45% decrease.

This section investigated the effect of TSA and MSA on the CO_2 desorption kinetics. Initially, 4 different desorption times were reported, each indicating a different desorption percentage of CO_2. This evaluation helped to determine the best regeneration conditions, deciding on a suitable compromise between CO_2 amount recovery and desorption time. As a result, 70% recovery was selected as the optimum choice, for which a comparison between MSA and TSA was presented. It was proven that MSA managed to reduce the time needed for 70% desorption to take place by as much as 45%, which, as seen in the next section (Section 4.4.4), is an important factor for the economics of the CO_2 capture process.

4.4.4. Energy consumption

Another important parameter to take into consideration for the intensification of the GAC regeneration is the energy consumption during the desorption step, as it is directly associated with the energy penalties that are imposed to the power plants. In general, it is clear that the energy consumption is proportional to the regeneration temperature and the amount of sorbent needed, as can be seen by equation 4.12:

$$P = \frac{m * C_p * \Delta T}{t} \quad (4.12)$$

Where ΔT ($\Delta T = T_{des} - T_{amb}$) is the temperature difference between desorption (T_{des}) and ambient temperature (T_{amb}), C_p is the thermal conductivity of the sorbent material and t is the time needed for the desired desorption to take place. However, considering that in MW the energy is transferred from the inside to the outside of the material as microwaves propagate through molecular interactions between the material and the electromagnetic field, resulting in a much more efficient heating process, it is reasonable to expect a much lower energy consumption for MSA. In this case, only $t = t_{70}$ is considered, which accounts for a 70% CO_2 desorption as explained in Section 4.4.3, as the energy consumed is directly associated with the desorption time. As a result, in order to keep consistency regarding the parameters compared, the E_{70} is examined, accounting for the energy needed to achieve a 70% desorption.

Figures 4.32 and 4.33 present the E_{70} consumed during the regeneration process of GAC that was previously saturated using $[CO_2]_{in}$ =40% heating to 70°C and 130°C, respectively. As expected, MSA achieved an important decrease in the energy consumed during the desorption step. It is clear that, for every set of experiments E_{70} was reduced by at least 70%, with the best result deriving from the wet gas conditions. Specifically, when the dry conditions were applied, a decrease from 0.68 to 0.37 and from 0.55 to ~0.26 kWh/kg_{sorb} during desorption at 70°C for 100ml/min and 150ml/min N_2 flow respectively, was reported. This decline was also evident for the wet gas case, where instead of 0.65 and 0.53 kWh/kg_{sorb}, only ~0.25 kWh/kg_{sorb} were consumed. A similar trend is evident when heating to 130°C; however, greater amounts of energy were recorded for both MSA and TSA, as expected. An average of 0.67 kWh/kg_{sorb} was recorded for 70°C desorption, whereas this amount reached 1.01 kWh/kg_{sorb} when heating at 130°C for the TSA process. Similarly during MSA, the E_{70} increased from ~0.3 kWh/kg_{sorb} to 0.35 kWh/kg_{sorb}.

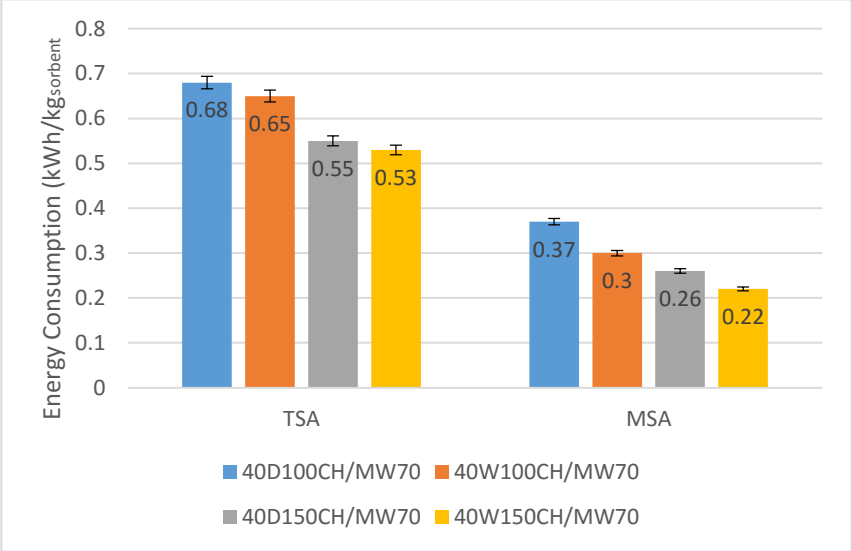

Figure 4.32: Energy consumption during GAC regeneration at 70°C for $[CO_2]_{in}$ =40%

Another interesting trend derives from the relation between E_{70} and carrier gas (N_2) volumetric flow rate; for both processes, an inverse proportionality between those factors was evident. Precisely, an increase from 100ml/min to 150ml/min resulted in ~15% decrease in the energy consumed during regeneration. This decrease was even higher in the case of wet gas, where for the TSA application reached a 25% decrease, a similar decrease was recorded for MSA as well. This trend was to be expected, since as described in Section 4.4.3, the increase of the flow reduces the desorption time.

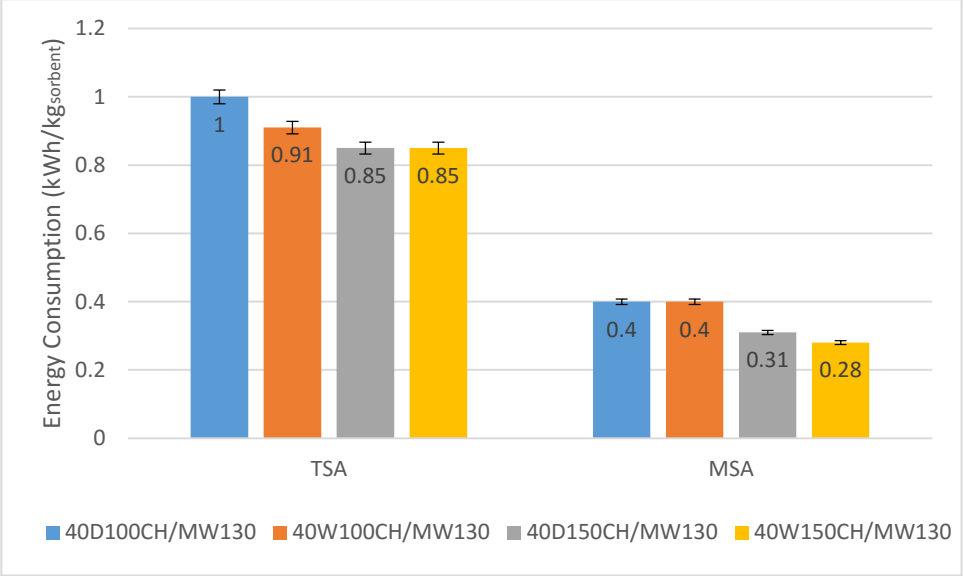

Figure 4.33: Energy consumption during GAC regeneration at 130°C for $[CO_2]_{in}$ =40%

Similar conclusions were observed for $[CO_2]_{in}$ =15%. As reported in Figure 4.34 in the case of 70°C desorption, an average of ~0.6 kWh/kg_{sorb} were needed to regenerate 70% of the total desorbed amount (E_{70}) for TSA technology. On the other hand, when MSA was applied, a significant reduction of ~40% was possible, reducing the amount of energy needed to an average of 0.38 kWh/kg_{sorb}. The same trend was observed when the desorption took place at 130°C (Figure 4.35), where the reduction was even greater; an average of ~1.05 kWh/kg_{sorb} was needed for TSA, whereas the consumption during MSA decreased to only ~0.42 kWh/kg_{sorb}, resulting in a ~60% reduction. However, it is quite interesting to point out that, the E_{70} for $[CO_2]_{in}$ =15% was higher for both TSA and MSA for every case examined, compared to $[CO_2]_{in}$ =40% . This can be explained by taking into consideration that in the case of $[CO_2]_{in}$ =40%, the CO_2 molecules are desorbed faster as seen in Section 4.4.3, compared to $[CO_2]_{in}$ =15%, reducing the amount of energy needed as well.

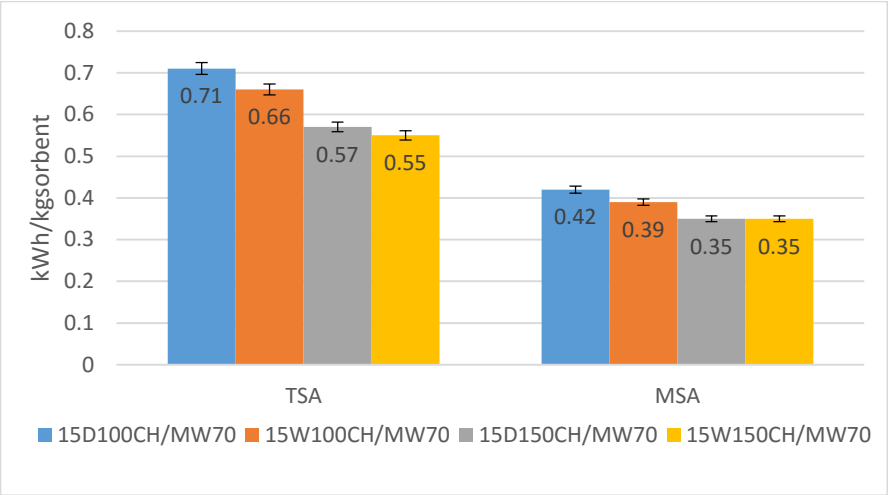

Figure 4.34: Energy consumption during GAC regeneration at 70°C for $[CO_2]_{in}$ =15%

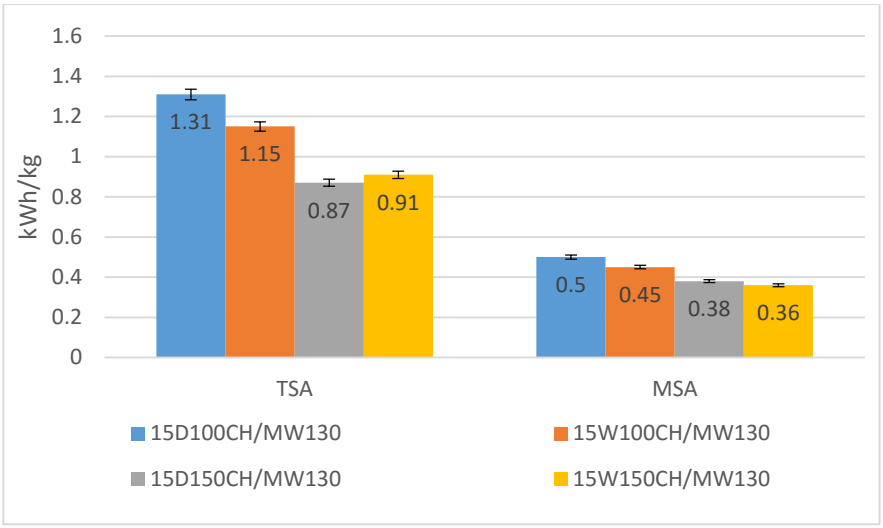

Figure 4.35: Energy consumption during GAC regeneration at 130°C for $[CO_2]_{in}$ =15%

Lastly, the E_{70} for the case of $[CO_2]_{in}$ =5% was examined. Once again, the MSA process clearly achieved an important reduction in the energy spent for the regeneration of the GAC. Figures 4.36 and 4.37 report the comparison between the two modes for 70°C and 130°C, respectively. It is clear that in the case of 70°C desorption, an average of ~0.76 kWh/kg_{sorb} were needed to regenerate 70% of the total CO_2 previously adsorbed (E_{70}) for TSA technology. On the other hand, during MSA application, a vast reduction of ~55% was possible, reducing the amount of energy needed to an average of 0.35 kWh/kg_{sorb}. The same trend was observed when heating up to 130°C; an average of ~1.1 kWh/kg_{sorb} was needed for TSA, whereas the consumption during MSA decreased to only ~0.47 kWh/kg_{sorb}, resulting in a 60% reduction. However, once again, the E_{70} for $[CO_2]_{in}$ =5% was higher for both TSA and MSA for every case examined, compared

to $[CO_2]_{in}$ =40% and $[CO_2]_{in}$ =15%. This was also expected, since the desorption times for $[CO_2]_{in}$ =5% for each case were higher compared to $[CO_2]_{in}$ =40% and $[CO_2]_{in}$ =15% (Section 4.4.3).

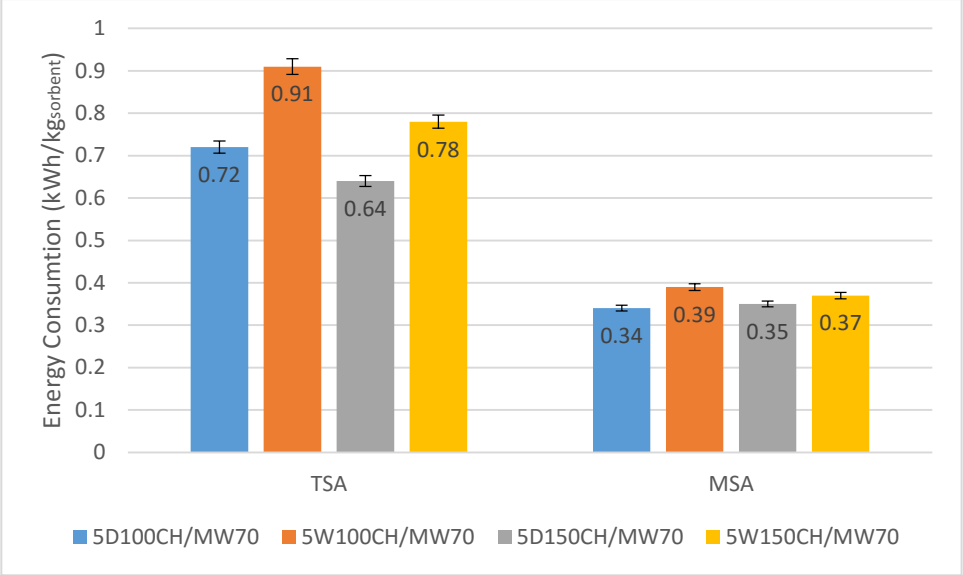

Figure 4.36: Energy consumption during GAC regeneration at 70°C for $[CO_2]_{in}$ =5%

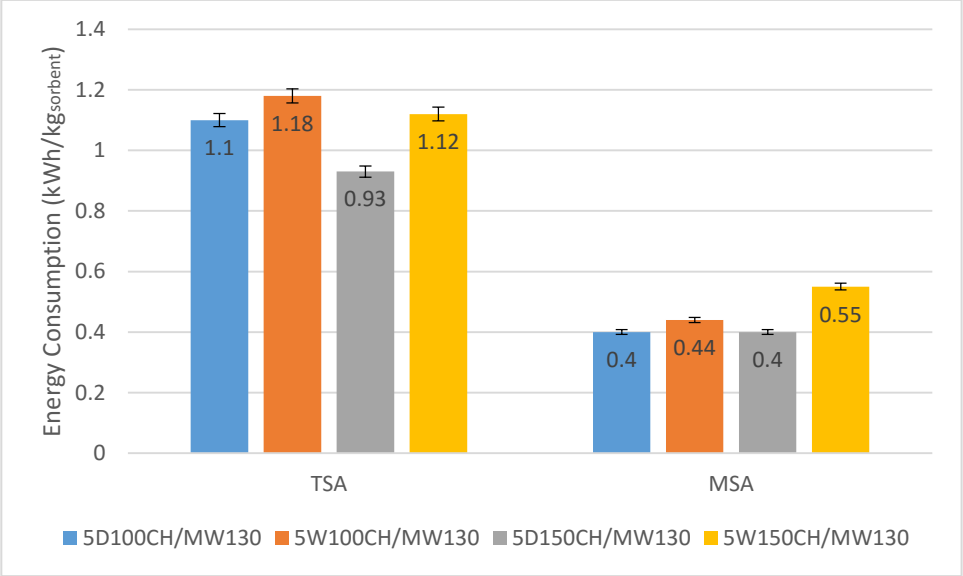

Figure 4.37: Energy consumption during GAC regeneration at 130°C for $[CO_2]_{in}$ =5%

The above results were to be expected since, as discussed in Chapter 2 (Section 2.2.9), the main difference between TSA and MSA is the way in which heat is generated and consequently absorbed from the solid sorbent inside the bed. In TSA, the heat source (in this case the heating tape discussed in Section 3.4) is located outside the GAC bed and the bed is heated by conduction and convection, resulting in increased heat losses.

Moreover, a significant temperature gradient is established in the GAC bed, until conditions of steady state are reached. On the other hand, during MSA, energy is transferred through the material electro-magnetically, not as a thermal heat flux. Therefore, the rate of heating is not limited and the uniformity of heat distribution is generally improved. Microwave energy is supplied directly to the carbon particles that convert this energy to heat, according to the following approximation:

$$P_D = 55.61 * 10^{-14} E^2 f \varepsilon' tan\delta \quad (4.13)$$

Where P_D is the power dissipation. Microwave desorption process is not limited by the thermal conductivity of the vessel, resulting in an instantaneous localized heating of the GAC bed. Specifically for CO_2 desorption, the direct absorption of energy, in contrast to the indirect supply of heat by thermal conduction, by the adsorbent enables a much faster process (as seen in Section 4.4.3) resulting in sufficient regeneration at lower process temperatures (Section 4.4.2). Consequently this results in energy savings, as seen above, making the desorption process more efficient and cost-effective.

In this section, the energy consumed during MSA and TSA processes was compared. Initially, a relation between flow rate and energy consumption was proven, since for every case, the E_{70} was decreased with increasing carrier gas flow rate (N_2). Furthermore, it is also clear that there is a relation between E_{70} and amount adsorbed during the adsorption step; when comparing the above three different cases, a decline in amount of energy consumed per kg of sorbent was evident with increasing $[CO_2]_{in}$. This trend was expected, since as examined in Section 4.4.3, the desorption time was also decreasing with increasing $[CO_2]_{in}$. **Most importantly, it was proven that MSA is a more energy efficient process, compared to TSA. It was reported that an average of only ~15-25% of the energy consumed during TSA is needed for MSA for the same conditions and regeneration temperature. Same trends appeared for 70°C and 130°C, however $E_{70}^{70°C}$ was considerably lower compared to $E_{70}^{130°C}$. As a result, taking into consideration that the regeneration efficiency and the desorption kinetics were not considerably improved by a temperature increase, combining it with the fact that a higher energy consumption is reported, it can be concluded that 130°C desorption may be classified as more energy intensive compared to 70°C, making it unfavourable for the GAC desorption process.**

4.5. Temperature Distribution

Until now, this research has proven that microwave irradiation was able to enhance the CO_2 desorption process from the GAC, by increasing its regeneration efficiency and desorption rates as well as decreasing the amount of energy needed for this step, compared to TSA application. However, some unexpected trends were reported, especially in the case of the regeneration efficiency, which for some cases was expected to be higher. One reason for not achieving the expected amount of CO_2 desorbed could possibly be attributed to the most significant drawback of a microwave application, known as the non-uniform temperature distribution inside the target object. This non-uniformity has also been observed by many researchers for various microwave processes as well (Ho et al., 1992, Vadivambal et al., 2010). This non-uniform heating is created from the possible presence of standing waves originated from transmission and reflection from interfaces, resulting in a non-uniform distribution of microwave energy. Factors that affect this non-uniformity can be the dielectric properties of the material (dielectric loss and penetration depth), as well as bed thickness, shape and size (Kelen et al., 2006). A previous research from Sakai and Wang (2004) confirmed that the dielectric properties play an important role in the temperature distribution. Moreover, parameters such as bed shape and size were studied by Gunasekaran and Yang (2007) reaching to the conclusion that it is not only the material itself that influences the heating uniformity but also its formed geometry. Furthermore, they reported that other important factors regarding temperature distribution include pulsating ratio and microwave processing time and concluded that a pulsed operation of microwave heating, which is the case in this research, results in a more uniform heating compared to continuous mode microwave heating. Lastly, Funawatashi and Suzuki (2003) divided the factors affecting non-uniform heating into two categories with regards to the object's size. It was concluded that for smaller size objects ($<500cm^3$), standing wave is dominant as interaction between transmission and reflection waves takes place within the object. In contrast, in the case of larger objects in terms of size the rapid decay of incident wave is the primary cause for the non-uniform heating (Hossan et al., 2010).

In order to estimate the importance of this effect, a temperature distribution (heat map) of the material bed is necessary. However, a precise temperature measurement inside a microwave oven has been identified as a very difficult task; the IRP used throughout the

experimental work is not able to provide accurate data for this objective, as it only measures the temperature of the surface of the bed. Moreover, other temperature measurement tools (e.g. thermocouples) were not possible to be used for reasons explained in Section 3.2.3. As a result, an optical sensor was used during microwave heating, which was placed in various heights (y-axis) inside the reactor bed with an increment of 1cm. Regarding the measurements in the x-axis (diameter), 3 measurements were recorded, namely 2 on each boundary (walls) and one in the centre. This creates a 2 dimensional matrix of 18 measurements that were repeated 5 times in order to minimise the human error and average values are presented below. All the measurements were taken after the PID controller reached a steady state – equilibrium condition, meaning that the microwave system was not further heating the sample, providing enough power only to maintain the output temperature.

Figures 4.38 and 4.39 show the temperature distribution maps of the GAC bed when MW was applied at 70°C and 130°C, respectively. In both cases, the highest temperature is recorded at the centre line of the reactor; in the case of 70°C, the GAC bed reached a maximum of 78°C in the centre of the reactor, whereas in the case of 130°C the temperature went up to 143°C. The lowest temperatures were recorded on the surface of the bed (height h_b = 5cm), namely 60°C and 112°C. Between the surface and the centre of the bed, a linear temperature distribution is evident for both cases. However, there is a clear difference in the temperature diffusion pattern at the basis of the bed, where when heated to 70°C, the basis of the bed has almost the same temperature as the surface, creating a symmetric distribution. On the other hand, this symmetry is not evident when heating to 130°C, since the temperature on the basis is around 125°C, lower compared to the centre but higher compared to the surface.

From the heat maps, it can be concluded that temperature control during microwave heating is certainly a difficult task, since temperature gradients from 60 to 80°C and from 110 to 143°C were reported when heating this particular GAC to 70°C and 130°C. Even if the GAC presents excellent dielectric properties as seen in Section 4.1, it is still heated in a non-uniform way. This means that the geometry of the bed influences the temperature distribution as well, as it will be reported in Chapter 5 (Section 5.3.2.5).

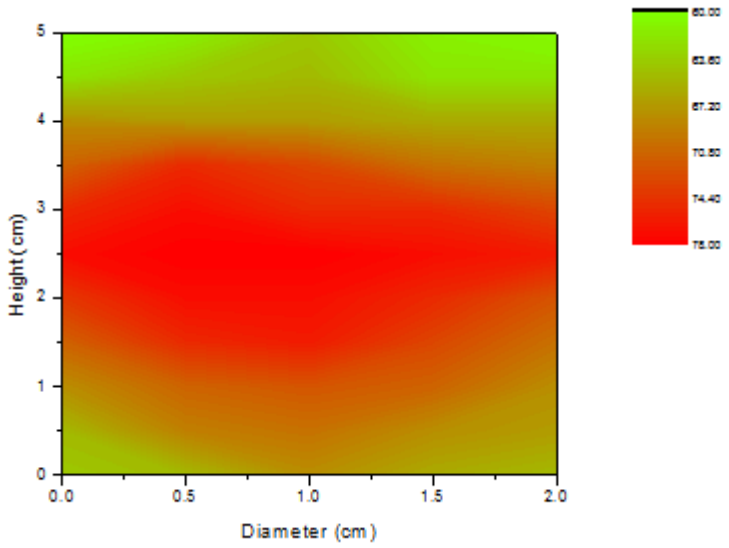

Figure 4.38: Heat map of the GAC bed when heated at 70°C with MSA

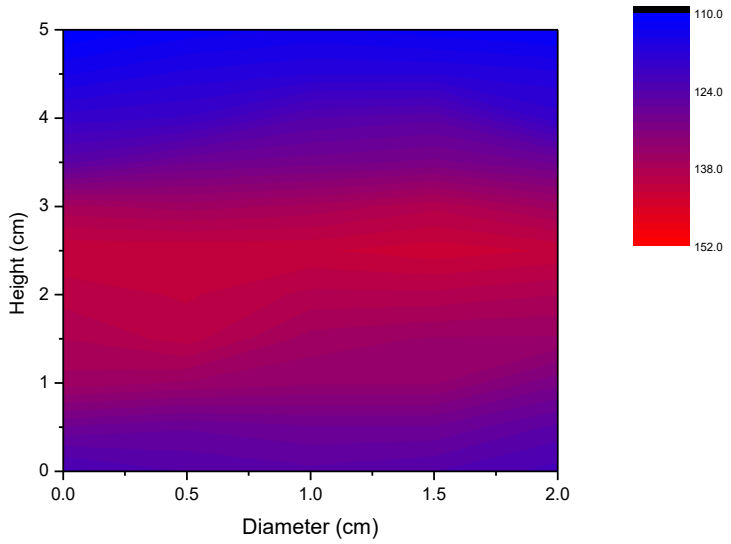

Figure 4.39: Heat map of the GAC bed when heated at 130°C with MSA

4.6. GAC cyclic process and strength

One parameter that greatly affects the economics of the CO_2 capture process by adsorption technologies is the re-use of the solid sorbent (Drage et al., 2012). In order to examine the stability of the sorbent in cyclic conditions, a continuous cyclic operation of CO_2 adsorption/desorption was examined. A total of 25 cycles were completed and the sorbent was examined in terms of its surface area, pore size and CO_2 adsorption capacity under the same conditions used during the initial characterisation (Section 4.1).

The results would help to interpret whether the specific GAC is influenced by consecutive MSA or TSA processes. The same procedure as for a single cycle (Section 3.6) was followed. It is important to note that since it was not feasible to complete 25 cycles in one day, the sample remained inside the reactor under inert conditions, created from a 50ml/min N_2 flow while the process was not in operation (overnight). Table 4.3 summarises the results from this study, comparing GAC's textural, chemical and dielectric properties after 25 MSA or TSA cycles with the parent GAC and the results are discussed below.

Table 4.3: Textural, chemical and dielectric properties of parent and reused (25 MSA or TSA cycles) GAC

Material	S_{BET} m^2/g	Total Pore Vol (V_p) cm^2/g	C (%)	TGA CO_2 uptake (% w/w) at 25°C	ε_r'	ε_r''	tan delta (tan δ)	D_p (cm)	P_{abs} (%)
GAC	946.7	0.62	90.9	11.7	15.2	6.6	0.44	2.2	89
GAC after 25 MSA cycles	340.7	0.45	89.1	11.4	18.9	9.2	0.49	1.8	93
GAC after 25 TSA cycles	292.4	0.42	84.9	11.1	16.6	8.2	0.50	1.9	92

It is observed that both processes do not affect significantly the maximum amount of CO_2 adsorbed. However, after 25 cycles of MSA, the CO_2 adsorption capacity is higher (11.4% w/w) than in the case of 25 TSA cycles (11.1% w/w). Even if the difference between the two is not so significant, an important trend is evident which may provide a prediction of how the material would respond after >25 cycles. Figure 4.40 shows the evolution of the CO_2 adsorption capacity as a function of number of cycles. It is clear that GAC's CO_2 adsorption capacity decreases linearly when MSA process is applied by an average rate of 0.4% per cycle.

On the other hand, in the case of TSA, there are two distinct patterns; at first (0-10 cycles) the decrease rate is similar to the MSA one, however there is a significant change after the 10^{th} cycle, where the CO_2 adsorption capacity decrease rate becomes 1.3% per cycle.

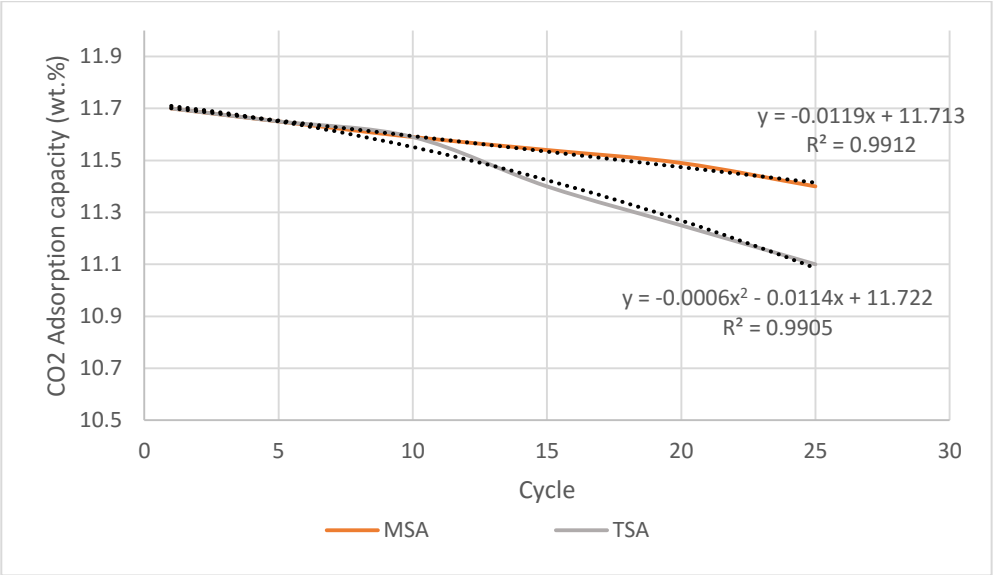

Figure 4.40: CO_2 adsorption capacity (% wt.) of GAC after consecutive adsorption/desorption cycles via MSA and TSA

Conventional thermal heating of GAC after successive adsorption and regeneration cycles decreases the CO_2 adsorption capacity significantly, which is attributed to the adverse changes in the adsorbent physical structure (Dehdashti et al., 2010), meaning that specific surface areas and micropore volumes slightly decreased after consecutive cyclic heating (Ania et al., 2007). Consequently, BET surface area and pore volume studies have been undertaken in order to prove the above statement. As can be seen in Table 4.3, an abrupt decrease in the BET surface areas of the regenerated samples was observed. BET surface area values declined significantly after consecutive regeneration cycles, ending in 65% lower than those of the parent GAC. This effect was more evident during the TSA process, since the apparent BET surface area of GAC fell to 296m^2/g (67% decrease) after 25 cycles, compared to 348m^2/g (61% decrease) when using MSA. In addition, the total pore volume of the sorbent was also lower after regeneration, namely 0.45 and 0.42cm^2/g for MSA and TSA respectively, compared to 0.6cm^2/g for the parent GAC, proving that some destruction of the pore network is apparent. Some destruction and collapse of the porous network is observed for both processes, which would have an immediate effect on the efficiency of the process, resulting in the aforementioned decrease in CO_2 adsorption capacity, pore volume and BET surface area. When regeneration is performed by TSA, the micropore volume decrease is accompanied by a downward shift to pores of narrower sizes, suggesting that desorption under conventional heating could result in some blocking effects at the entrance of the pores.

In contrast, in the case of MSA, a slower and gradual fall is observed, proving that pores blockage, specific surface areas and micropore volumes reduction occur to a lesser extent compared to TSA, being in agreement with previous studies (Ania et al., 2005).

Finally, it can be observed that after 25 MSA or TSA cycles, the dielectric properties of GAC were improved, resulting in higher loss tangent values, namely 0.49 and 0.5 for MSA and TSA cyclic processes, respectively. This increase had also an effect on the microwave power absorption potential of the sobent (P_{abs}), possibly due to the change of the porosity network and the decrease of the void space of the material, as will be discussed in Section 5.1.2; it was found that P_{abs} increased after 25 cycles of both MW and CH heating from 89% to 93% and 92% respectively, suggesting that the microwave energy absorption, and consequently the heating efficiency, improves with increasing number of cycles. However, the penetration depth decreased to 1.8 and 1.9cm respectively, which was to be expected from equation 2.9 (Section 2.2.6).

4.7. Conclusions

In this chapter, the results obtained from a series of experiments using a granular activated carbon (GAC) were presented. To begin with, characterisation studies of the parent material in terms of CO_2 adsorption capacity, dielectric properties, BET and elemental analysis were discussed. Next, the adsorption step was presented, trying to investigate the effect of various parameters, such as CO_2 concentration inside the binary gas mixture (40%, 15% and 5% vol. CO_2 – balance N_2), total feed gas flow rate and moisture (~10%) presence. It is concluded that as the CO_2 concentration in the feed gas increases, the total CO_2 amount adsorbed (dynamic adsorption capacity) increases as well, since, according to the Henry's law, adsorption is proportional to the partial pressure of the adsorbed gas (in this case CO_2). Moreover, one interesting factor was that, a ~10% of moisture in the binary gas mixture of CO_2 and N_2 seems to enhance the CO_2 adsorption capacity on this particular GAC; due to the introduction of H_2O vapors, the total flow rate of the feed gas was increased, resulting in better adsorption performance of the GAC. Furthermore, it was proven that an increase in the total flow results in increased amount of CO_2 adsorbed; a mass transfer correlation was used to

prove that an increase from 1.27m/min to 2m/min would lead to an increase of ~65% of the mass transfer coefficient, favouring the CO_2 adsorption process.

After completion of the adsorption tests, desorption experimental results were presented and described; initially, a comparison between MSA and TSA in terms of heating rates was produced. This comparison proved that MSA has the ability to heat the GAC at a faster pace to the required temperature, compared to TSA. Moreover, it was also shown that there is no risk of thermal runaway when using this material, since the heating rate was decreasing with increasing temperature. Subsequently, desorption studies were discussed, focusing on three parameters that helped evaluating and comparing the two processes, namely regeneration efficiency, desorption kinetics and energy consumption per kg of sorbent used. Since GAC was used as a reference material against the materials that are presented in the next chapters, a full study, covering and combining all the parameters produced from a total of 48 experiments, was presented. Those experiments proved that MSA enhanced the regeneration efficiency of the GAC, compared to TSA. However, the values obtained were not as high as expected, especially in the case of wet gas conditions, and only some of them were equal or higher than 80%, which is the lowest acceptable limit for the feasibility of a real scale CO_2 capture unit. One possible reason is that, MSA has the disadvantage of temperature non-uniformity inside the sorbent bed. This non-uniformity can be influenced by various parameters, such as material properties, frequency and bed geometry. As a result, temperature distribution was also examined for the GAC bed. These thermal maps showed that even if the T_{av} is equal to the target temperature, its distribution was not uniform; the higher temperatures were observed in the centre of the sample, whereas the lowest values were recorded for the surface of the bed. This temperature non-uniformity was attributed to the nature of the multimode microwave heating and has a number of possible causes such as inherent electromagnetic field non-uniformity due to cavity design, heat losses and/or inhomogeneity of the sample and shape, size and dielectric properties of the sample being heated.

Regeneration efficiency was followed by a comparison of CO_2 desorption kinetics during MSA and TSA. Initially, four different desorption times were reported, each indicating a different CO_2 recovery percentage. This evaluation helped to determine the best regeneration conditions, deciding on a suitable compromise between CO_2 amount

recovery and desorption time. As a result 70% recovery was selected as the optimum choice, for which a comparison between MSA and TSA was presented, since the desorption rates need to be in equilibrium with the adsorption rates for any continuous separation process. It was proven that MSA managed to reduce the time needed by as much as 45%, which, was an important factor for the economics of the CO_2 capture process, since it directly affects the energy consumption. Furthermore, the influence of the moisture content in the feed gas mixture was also discussed. It was proven that in the case of MSA, moisture deposited on the surface of the material affects the heating process in a positive way, since a faster desorption process was observed, compared to the dry conditions. This was to be expected, since H_2O, being a dipole, is a very good microwave absorber, enhancing the heating process resulting in energy savings as well.

Energy consumption was also compared for the case of 70% CO_2 desorption and at the beginning, an inverse relation with the total carrier gas flow rate was reported. Furthermore, it was also clear that there is an inversely proportional relationship between energy consumed and amount adsorbed during the adsorption step. Most importantly, it was proven that MSA is a more energy efficient process, compared to TSA. It was reported that an average of only ~30-50% of the energy consumed during TSA is needed for MSA for the same conditions and regeneration temperature. The decrease in energy consumption during the MSA process can initially be attributed to the fact that MSA is a faster process compared to TSA. Secondly, microwave heating mechanism is inherently different compared to conventional heating via conduction and convection. During TSA heat losses, resistances in heat transfer due to the reactor and temperature gradients are observed, whereas during MSA microwaves are directly absorbed from the GAC, transforming electromagnetic energy to heat instantly. The latter mechanism results in a more efficient and volumetric heating, compared to the TSA process. Same trends appeared for every temperature investigated, however $E_{70}^{70^{\circ}C}$ was considerably lower compared to $E_{70}^{130^{\circ}C}$. As a result, taking into consideration that the regeneration efficiency and the desorption kinetics were not considerably improved by a temperature increase, combining it with the fact that a higher energy consumption is reported, it can be concluded that 130°C desorption may be classified as more energy intensive compared to 70°C, making it unfavourable for the GAC desorption process.

Lastly, the possibility to use the specific material in a cyclic process was examined and as a result the stability of the sorbent in cyclic CO_2 adsorption/desorption conditions was studied. The textural and dielectric properties of the material were measured before and after 25 cycles of MSA or TSA. It was reported that the regenerated GAC presented an increased tan δ value, resulting in improved microwave power absorbed and heating efficiency compared to the parent sample as the cycles increased. Moreover, BET surface area analyses suggested that the porous structure and the surface area of the material are affected by both heating processes, however, the decrease is more evident in the case of TSA. Pores blockage, specific surface areas and micropore volumes reduction occur to a lesser extent when using MSA, compared to TSA. Nevertheless, the CO_2 adsorption capacity of the sorbent is not drastically affected by the textural changes for both processes, although the decrease is more pronounced when TSA is applied. The above observations lead to the conclusion that MSA has the potential to be used in a cyclic process without significant destruction of the GAC sorbent and without affecting its CO_2 adsorption potential significantly.

References

Ania, C. O., Menendez, J. A., Parra, J. B. and Pis, J. J. (2005) '*Effect of microwave and conventional regeneration on the microporous and mesoporous network and on the adsorptive capacity of activated carbons*', Microporous and Mesoporous Materials, Vol. 85, pp. 7-15, DOI 10.1016/j.micromeso.2005.06.013

Ania, C. O., Menendez, J. A., Parra, J. B. and Pis, J. J. (2007) '*Microwave assisted regeneration of activated carbons loaded with pharmaceuticals*' Water Resources, Vol. 41 (15), pp. 3299-3306

Balsamo, M.; Budinova, T.; Erto, A.; Lancia, A.; Petrova, B.; Petrov, N.; Tsyntsarski, B. (2013) '*CO_2 adsorption onto synthetic activated carbon: Kinetic, thermodynamic and regeneration studies*', Separation and Purification Technology, vol. 116, pp. 214–221

Bradshaw, S.M., van Vyk, E.J. and de Swardt, J.B. (1998) '*Microwave heating principles and the application to the regeneration of granular activated carbon*', The Journal of The South African Institute of Mining and Metallurgy, July/August, pp. 201-212

Cherbanski, R. and Molga, E. (2009) '*Intensification of desorption processes by use of microwaves-An overview of possible applications and industrial perspectives*' Chemical Engineering Processes, Vol. 48, pp. 48-58, DOI 10.1016/j.cep.2008.01.004

de Ridder, D.J. (2012) '*Adsorption of organic micropollutants onto activated carbon and zeolites*', Water Management *Academic Press*

Dong, X., Zhang, J., Li, G., Xiao, P., Webley, P. and Zhai, Y.C. (2011) '*Effect of water vapor from power station flue gas on CO_2 capture by vacuum swing adsorption with activated carbon*' Journal of Fuel Chemistry and Technology, Vol. 39 (3), pp. 169-174, DOI 10.1016/S1872-5813(11)60016-9

Drage, T. C., Trevor C., Snape, C., Stevens, L.A., Wood, J., Wang, J., Cooper, I., Dawson, R., Guo, X., Satterleyf, C. and Irons, R. (2012) '*Materials challenges for the*

development of solid sorbents for post-combustion carbon capture' Journal of Materials Chemistry, Vol. 22, pp. 2815–2823

Essaki, K., Kato, M. and Uemoto, H. (2005) '*Influence of temperature and CO_2 concentration on the CO_2 absorption properties of lithium silicate pellets'*, Journal of materials science, Vol. 40, pp. 5017–5019

Etherington, K., Rodger, A. and Hemming, P. (2001) *'CHN microanalysis-a technique for the 21st century?'*, Lab-Plus-Iinternational, pp. 26-27

Funawatashi, Y. and Suzuki, T. (2003) '*Numerical analysis of microwave heating of a dielectric*', Heat Transfer – Asian Res., Vol. 32 (3), pp. 227–236

Gritti, F. and Guiochon, G. (2005) '*Effect of the flow rate on the measurement of adsorption data by dynamic frontal analysis'*, Journal of chromatography A, vol. 1069 (1), pp. 31-42. DOI:10.1016/j.chroma.2004.08.129

Gunasekaran, S. and Yang, H. (2007) '*Effect of experimental parameters on temperature distribution during continuous and pulsed microwave heating*', Journal of Food Engineering, Vol. 78 (4), pp. 1452–1456

Hashisho, Z. (2007) '*Microwave-swing adsorption for the capture and recovery, or destruction for a more sustainable use of organic vapors'*, PhD thesis, University of Illinois at Urbana-Champaign

Hill, M.J. (2000) '*The microwave palaeointensity technique and its application to lava*' Ph.D. Dissertation, University of Liverpool, UK

Ho, Y.C. and Yam, K.L. (1992) '*Effect of metal shielding on microwave heating uniformity of a cylindrical food model*', Journal of Food Processing and Preservation, Vol. 16(5), pp. 337−359

Hossan, M., Byun, D. and Dutta, P. (2010) *'Analysis of microwave heating for cylindrical shaped objects'*, International Journal of Heat and Mass Transfer, Vol. 53, pp. 5129–5138, doi:10.1016/j.ijheatmasstransfer.2010.07.051

IUPAC, International Union of Pure and Applied Chemistry (1985) '*Reporting physisorption data for gas/solid systems'*, Pure & Appl. Chem., Vol. 57, No. 4, pp. 603-619

Johnson, D.L., Skamser, D.J. and Spotz, M.S. (1993) '*Temperature gradients in microwave processing: Boon and bane*', Ceramic Transactions: Microwave Theory and Applications in Materials Processing II, Vol. 36, pp. 133-145

Kato, M., Essaki, K., Nakagawa, K., Maezawa, Y., Takeda, S., Kogo, R. and Hagiwara, Y. (2003) '*Novel CO_2 Absorbents Using Lithium-Containing Oxides'*, Applied ceramic technology, Vol. 2 (6), pp. 467-475, DOI: 10.1111/j.1744-7402.2005.02047.x

Kelen, A., Ress, S., Nagy, T., Pallai, E. and Pintye-Hodi, K. (2006) '*Mapping of temperature distribution in pharmaceutical microwave vacuum drying*', Powder Technology, Vol. 162 (2), pp. 133–137

Kundua, D. and Raqabb, M.Z. (2005) *'Generalized Rayleigh distribution: different methods of estimations'*, Computational Statistics & Data Analysis, vol. 49, pp. 187 – 200, DOI:10.1016/j.csda.2004.05.008

Lindstrom, P., Tierney, J., Wathey, B. and Wsetman, J. (2001) '*Microwave assisted organic synthesis – a review*' Tetrahedron, Vol. *57* (45), pp. 9225-9283; DOI: 0.1016/S0040-4020(01)00906-1

McKetta, J.J. and Cunningham, W.A. (1978) '*Encyclopedia of Chemical Processing and Design*', Marcel Dekker, New York, vol. 6, pp. 292–310

Menéndez, J.A., Arenillas, A., Fidalgo, B., Fernández, Y., Zubizarreta, L., Calvo, E.G. and Bermúdez, J.M. (2010) *'Microwave heating processes involving carbon materials'*, Fuel Processing Technology, vol. 91, pp. 1–8

Metaxas, A.C. and Meredith, R.J. (1983) '*Industrial Microwave Heating*', Peter Peregrinus Ltd., ISBN 0906048893, London, UK

Olivares-Marín, M., Drage, T.C. and Maroto-Valer, M.M. (2010) '*Novel lithium-based sorbents from fly ashes for CO_2 capture at high temperatures'*, International Journal of Greenhouse Gas Control, Vol. 4(4), pp. 623-629, DOI: 10.1016/j.ijggc.2009.12.015

Plaza, M.G., García, S., Rubiera, F., Pis, J.J. and Pevida, C. (2010) *'Post-Combustion CO_2 Capture with a Commercial Activated Carbon: Comparison of Different Regeneration Strategies'*, Chemical Engineering Journal, vol. 163, pp. 41–47, doi:10.1016/j.cej.2010.07.030

Qu, Y., Sun, J., Li, F., Zhang, C. and Zhou, Q. (2009) '*The Determination of Dynamic Adsorption Curve, Adsorption Capacity and Breakthrough Capacity of Powdered Activated Carbon for Perfluorooctanoic Acid elimination from Water'*, Bioinformatics and Biomedical Engineering, PP. 1-3, DOI: 10.1109/ICBBE.2009.5163588

Rashidi, N.A., Yusup, S. and Loong, L.H. (2013) '*Kinetic Studies on Carbon Dioxide Capture using Activated Carbon*', Chemical Engineering Transactions, Vol. 35, pp. 361-366, DOI: 10.3303/CET1335060

Sakai, N., Wang, C. (2004) '*An analysis of temperature distribution in microwave heating of foods with non-uniform dielectric properties'*, Journal of Chemical Engineering, Vol. 37 (7), pp. 858–862

Shah, I.K., PRE, P. and Alappat, B.J. (2013) *'Steam Regeneration of Adsorbents: An Experimental and Technical Review',* Chemical Science Transactions, vol. 2(4), pp. 1078-1088, DOI:10.7598/cst2013.545

Smit, B., Reimer, J.R., Oldenberg, C.M. and Bourg, I.C. (2014) '*Introduction to Carbon Capture and Sequestration'*, Imperial College Press, London, UK

Songolzadeh, M., Takht Ravanchi, M. and Soleimani, M. (2012) '*Carbon dioxide capture and storage: a general review on adsorbents*', World Academy of Science, Engineering and Technology, Vol. 70, pp. 225–232

Su, S., Thiruvenkatachari, R., Yu, X. and Jin, Y. (2014) '*Site Trials of Novel CO_2 Capture Technology at Delta Electricity'* Final Report CSIRO Energy, May

Thompson, .M (2008) *'CHNS Elemental Analysers'*, The Royal Society of Chemistry, pp. 35-36

Vadivambal, R. and Jayas, D.S. (2010) '*Non-uniform temperature distribution during microwave heating of food materials−a review'*, Food and Bioprocess Technology, Vol. 3(2), pp. 161−171

Webley, P. and Zhang, J. (2014) '*Microwave assisted vacuum regeneration for CO_2 capture from wet flue gas*', Adsorption 2014, Vol. 20, pp. 201-210; DOI 10.1007/s10450-013-9563-y

Wu, J. (2004) '*Modeling adsorption of organic compounds on activated carbon A multivariate approach'*, PhD thesis, Umeå University, Umea, Sweden

Chapter 5 – Material parameters in MSA/TSA

In the previous chapter, the process parameters for the TSA and MSA technologies were discussed for a carbon based material (GAC). Following the conclusions that MSA can intensify the CO_2 desorption process at 70% CO_2 recovery as the optimum choice, this chapter focuses on the study of different adsorbent material, highlighting the importance of raw material, adsorbent shape and surface modifications in the desorption process. Five materials were chosen for this investigation - four of which are carbon based, with the last one being a lithium based silica - in order to compare with the performance of the reference material, GAC, described in Chapter 4. The selected materials are presented in Table 5.1; they present different properties in terms of functionalities (NH_3 impregnation) and forms - powder, granular and pellets - for the carbon-based sorbents, while the silica material combines form and surface modification, since it is a powdered form impregnated with amine (TEPA) material.

Table 5.1: Solid sorbents selected for study in Chapter 5

Sorbent name	Provider	Raw material	Shape	Particle size (mm)	Treatment
GKAS	CSIC (Spain)	Almond shells AC	Granules	0.7-0.9	-
GKAS-N	CSIC (Spain)	Almond shells AC	Granules	0.7-0.9	NH_3 modified surface
Org	Desotec (Belgium)	Coconut shells AC	Granules	2-4	-
OrgP	Desotec (Belgium)	Coconut shells AC	Powder	0.06	Grinded Org
SBA TEPA	Rey Juan Carlos University (Spain)	Silica SBA-15	Powder	0.04	30% TEPA impregnation

Firstly, characterisation studies of the materials are presented, including textural properties that describe how they affect the bed design, and dielectric properties. A comparison of MSA and TSA modes follows, taking into account only the most influential parameters derived from Chapter 4, namely the importance of anhydrous or wet conditions as well as the desorption temperature varies, while the total flow rate and the $[CO_2]_{in}$ will remain constant throughout. As a result, a study including a total of 40 experiments (eight experiments per sample) are discussed, aiming at identifying the

influence of adsorbent and bed shape as well as surface modifications on the CO_2 desorption process when using MSA.

5.1. Materials Characterisation

The first objective of this chapter is to identify the effect of adsorbent shape on the adsorption/desorption of the MSA system. Sorbent materials are usually divided into four basic categories according to their physical properties, shape and surface chemical modifications, which are briefly described below:

i. Granular adsorbents

Granular adsorbents are relatively smaller in terms of particle size compared to pelletized materials. They are commonly used for both liquid/solid (water treatment and components separation in a flow system) and gas/solid applications (deodorising and VOC removal, including CO_2 capture processes) and their size vary according to the process; for example, water/liquid applications utilise granular sorbents of 6x10 (3.3x2.0 mm), 8x16 (2.4x1.2 mm), 12x30 (1.7x0.6 mm), or 20x50 (0.8x0.3 mm) mesh size while in air/vapour applications a bigger particle size is used (4x6 – 4.76x3.36 mm, 4x8 – 4.76x2.38 mm or 4x10 – 4.76x2.00mm). In this chapter, two different granular sorbent materials are compared in terms of adsorption and MSA/TSA performances, namely GKAS and GKAS-N800, as seen in Table 5.1. These sorbents are carbon based materials produced by the Instituto Nacional del Carbón (CSIC). Almond shells were used as raw material for both samples, with GKAS-N800 samples (being referred as GKAS-N in this chapter) undergoing an amination process that included heat treatment with gaseous ammonia (NH_3). The original objective of this process was to introduce basic N_2 functionalities onto the GKAS activated carbon, in order to enhance CO_2 adsorption potential, as will be discussed in Section 5.2. This research focuses on the effect of these N_2 functionalities on the MSA/TSA desorption processes.

ii. Pelletized adsorbents

Pelletized (or extruded) sorbent materials are most commonly found in cylindrical forms with diameters varying from 0.8 to 45 mm. Typical applications include air/gas purification processes (gas/solid separation technologies), since they present low pressure drop as the gas passes through the sorbent bed. Moreover, they are well known

for their high mechanical strength that could enhance the possibility of reusing the samples and low dust content (Sarkar and Bose, 1997). Pelletized or extruded activated carbons (pressed pellets) are predominantly produced from mixing pulverised charcoal or anthracite with a suitable binder, being extruded at high pressure in order to form their cylindrical shape. In this research, pelletized activated carbon, provided by Desotec (Belgium) with product name Organosorb 10-CO (referred to as Org in this chapter), was utilised. Org was produced from coconut shells, with particle size between 2.8 and 4.75 (accounting for 93%) and is commonly used to remove low boiling organic solvents and odours from air and gas. However, its large surface area (1140m^2/g), micropore volume and hardness (96%) make this sorbent suitable for exhaust gases treatment as well, VOC capture including CO_2 and SO_2 desulphurisation processes.

iii. Powdered adsorbents

The most common sorbent materials in powder form (or fine granules) present an average diameter between 0.15 and 0.25 mm, being significantly smaller compared to pellets and granules. In general, powder materials can be defined in various ways, but most commonly they are referred to as materials that consist of at least 90% (% w/w) of particles with a size less than 0.5mm (35 mesh). Powdered materials are usually fabricated from crushed or ground particles, with the vast majority (95–100%) of which passing through a 50 to 80 mesh sieve. In this occasion, Desotec Org (referred to as OrgP in this chapter) was used to produce the powdered adsorbent; OrgP was prepared by grinding the original Org pellet, using a Fritsch Pulverisette 2 mortar grinder, producing a sorbent with a size that is predominantly less than 0.075mm (sieve number 200) .

iv. Impregnated adsorbents

Impregnated sorbent materials can be found in any of the above forms, namely powders, granules or pellets. Chemical modification of the surface of solid sorbents has been the centre of attention with the most common scenarios including basic organic group (amines) and inorganic metal oxides (alkali metal or alkali-earth metal) being of particular interest (Samanta et al., 2011). The interaction between the acidic CO_2 molecules and modified basic active sites on the surface enhances the performance of the sorbent in terms of CO_2 adsorption capacity through the formation of covalent

bonding (Yu et al., 2012). In the last section of this chapter (Section 5.4), a mesoporous silica based material is investigated, namely SBA TEPA produced from impregnating SBA-15 with Tetraethylenepentamine (TEPA). Those samples were prepared and characterised at Rey Juan Carlos University in Madrid, Spain.

Prior to the commencement of the experimental work, all the materials were characterised in terms of chemical composition, textural and dielectric properties. The results are presented in the following sections.

5.1.1. Textural and chemical properties

In order to evaluate the CO_2 adsorption capacity of the sorbent materials mentioned in the previous section (Section 5.1), as well as their desorption performance during MSA and TSA processes, a number of parameters should be taken into consideration, including surface area, pore volume, CHN elemental analysis, CO_2 adsorption capacity and surface treatment, as discussed in Section 3.3. Another important parameter introduced in this section is the bed (or bulk) density. In simple terms, the bed density (ρ_b) is the mass of the adsorbent in a specific volume and can be calculated from the following equation:

$$\rho_b = \frac{m_{ads}}{V_t} \tag{5.1}$$

where m_{ads} is the mass of the adsorbent and V_t is the total volume of the bed The bed density is an important parameter that can lead to estimations regarding the shape of the bed and should not be confused with the apparent density of the bed (ρ_{ap}). The apparent density of a packed bed corresponds to the density measured after vibrating the granules in a way to minimize void spaces between particles (Totten et al., 2004). Typical ρ_{ap} values vary between 250 to 650 kg/m³ for the case of packing with activated carbons. On the other hand, the bed density is the density of the material loaded into an adsorber column or container, and is used for adsorber sizing in gas and liquid phase applications. Typically, it accounts for 90 to 91% of the apparent density and as a result it is usually calculated from the following equation:

$$\rho_b = 0.9 * \rho_{ap} \tag{5.2}$$

As it will be discussed later, the shape of the bed influences the temperature distribution during MSA, leading to different temperature gradients for every case. In this research, the parameter that defines the shape of the bed is the height since it is the only parameter that can change (the diameter remains constant $d_b = 20mm$), according to the aforementioned bed density. Bed shape is also related to bed porosity, another important factor when dealing with packed bed reactors. Bed porosity can be affected by the packing mode, the ratio between column to particle diameter ($^{D}/_{d_p}$), the particle shape and size distribution and of course bed height, according to Klerk (2003) and Zou et al. (1995). It should not be confused with the void fraction (ε) which is a measure of the void spaces in the material, and is expressed as a fraction of the volume of voids over the total volume, between 0 and 1, or as a percentage between 0 and 100% and can be estimated from:

$$\varepsilon = \frac{V_{void}}{V_t} \tag{5.3}$$

Where V_{void} is the void volume of the bed and is defined as

$$V_{void} = V_t - V_{ads} \tag{5.4}$$

As a result, equation 5.3 can also be written as:

$$\varepsilon = \frac{V_t - V_{ads}}{V_t} \tag{5.5}$$

which results in $\varepsilon = 1 - \frac{V_{ads}}{V_t}$ (5.6)

Taking into consideration that $= {}^{M}/_{\rho}$, then equation 5.6 can be transformed to

$$\varepsilon = 1 - \frac{\rho_b}{\rho_{ads}} \tag{5.7}$$

Where ρ_{ads} describes the particle density, which is the mass of adsorbent per volume occupied by the particle. It can be concluded that the void fraction depends on the density of the sorbent and the density of the sorbent bed.

Table 5.2 summarises the properties of the materials used in this chapter. GAC is also included in this table for comparison reasons. Moreover, the bed volume and density are also included for each case, calculated from the above equations.

Table 5.2: Chemical analysis and textural characterisation of the samples

Sorbent	g used	Treatment	S_{BET} m^2/g	Total Pore Vol (V_p) cm^2/g	C (%)	H (%)	N(%)	Bed height h_b (cm)	Bed Volume (V_b) cm^3	Bed Density (ρ_b) kg/m^3	TGA CO_2 uptake (% w/w) at 25C
GAC	5	Parent material	946	0.6	90.8	0.3	0.2	5.5	44.22	113.08	11.7
GAC (CH)	5	Parent material	292.4	0.42	84.8	0.3	0.2	5.5	44.22	113.08	11.1
GAC (MW)	5	Parent material	340.7	0.45	89.1	0.1	0.2	5.5	44.22	113.08	11.4
GKAS	1.6	-	21	0.01	91.0	2.0	0.4	1.6	12.87	124.33	6.9
GKAS-N	1.6	NH_3 Modified surface	326	0.24	89.2	0.6	4.5	1.8	14.47	110.58	9.6
Org	5	-	1140	0.55	89.1	0.4	0.4	5.3	42.61	117.35	5.7
OrgP	5	Powder Org	1050	0.48	89.2	0.4	0.4	4.4	35.37	141.37	5.5
SBA TEPA	1.4	30% TEPA Impregn.	294	0.53	15.4	-	9.0	4.2	33.77	41.46	7.4

It is clear that all the carbon-based samples consist of >88% carbon, while the rest is shared between hydrogen and nitrogen. Moreover, it is interesting that they present similar bed densities, which implies that the temperature distribution of the bed during MSA will be uniform, since the shape of the bed is identical for each case. However, the penetration depth of the microwave irradiation should also be taken into account for each individual case and this will be discussed in Section 5.1.2.

It is interesting to note that the GAC samples present the highest CO_2 adsorption capacity, compared to the other carbon based materials when tested in the thermogravimetric analyser. This capacity remains high and above 10% even in the case of the reused GAC for both 25 cycles of MSA and TSA (11.4% and 11.1% respectively). It is also evident that the GAC samples demonstrate the highest pore volume ($0.6cm^2/g$), while the highest BET surface area is shown in the case of Org and OrgP. However, these samples present the lowest CO_2 adsorption capacity, since only a 5.5-5.7% (w/w) weight uptake was reported. An interesting case is that of the SBA TEPA, which even if it presents a significant CO_2 uptake (7.4% w/w), its bed density is significantly lower than that of the carbon based sorbents. This factor is expected to

play an important role in the volumetric heating of the bed during the regeneration process, as well as in the bed sizing during scaling up studies.

5.1.2. Dielectric properties

In addition to the textural and chemical properties of a sorbent material, a crucial parameter in microwave heating is also its dielectric properties, since they indicate the energy coupling of a material with the electromagnetic field leading to an estimation of its heating potential (Metaxas et al., 1983; Schubert et al., 1995), as reported previously in Section 3.3.5. As a result, three important parameters were evaluated in order to clarify the dielectric properties of the sorbent materials being in consistency with Chapter 4, following the equations of Section 3.3.5. The parameters evaluated are the tan delta (tan δ) value, the penetration depth (D_p) and the heating efficiency (or microwave power absorption potential) per mg of sample. Similarly to Chapter 4, the dielectric properties were measured in collaboration with University of Cardiff, using an on-axis TM010 cylindrical cavity at 2.5 GHz. The results of the dielectric measurements are reported in Table 5.3, from which useful conclusions can be drawn.

As mentioned in Section 2.2.6 that the ability of a material to convert electromagnetic energy to thermal energy is inversely proportional to its penetration depth ($tan\ \delta \sim {}^{1}/_{D_p}$), the $D_p$values were reported for each sorbent. It is clear that the above connection between tan δ value and penetration depth is valid, resulting in very high D_p values for the silica based sorbents and in very low values for the carbon based materials. The penetration depth, along with the shape and the void spaces of the bed, are responsible for the uniform or non-uniform temperature distribution inside the sorbent bed, as discussed later in this chapter. Furthermore, it is interesting to note that the highest tan δ values were reported for the GAC sample, while this value was increased after 25 cycles of TSA or MSA, as reported in Section 4.6. The lowest values were reported for the case of SBA TEPA, which could possibly mean that they are not microwave absorbent materials and that they will not be heated under electromagnetic irradiation. However, this outcome should be ascertained from the following power absorption graph (Figure 5.1). Looking at the carbon based sorbents, variations in the tan δ values can be noted; specifically, it is evident that for the GKAS and the Org sorbents the values reported are much lower than that of the GAC, namely 0.13 and

0.15 respectively. However, when measuring the dielectric properties of the sample modified with NH_3 functionalities, GKAS-N, the tan δ value almost tripled to 0.34. Moreover, when looking at the OrgP, which is the grinded powder deriving from Org, the tan δ value increased to 0.23. This is a very interesting result, considering that the samples' chemical composition is almost identical (>89% of carbon inside the samples), indicating that the shape of the material plays an important role on its dielectric properties.

Table 5.3: Dielectric properties of the sorbents used in this research. GAC CH/MW: Samples that have undergone 25 TSA/MSA cycles, respectively, GKAS (CH)/(MW): GKAS samples that have undergone 4 TSA/MSA cycles, respectively, GKAS-N (CH)/(MW): GKAS-N samples that have undergone 4 TSA/MSA cycles, respectively, Df_0: change in resonant frequency, Df_B: change in unloaded 3dB bandwidth, ε_r': relative permittivity, ε_r'': loss factor, D_p: penetration depth

Material	Average Mass (mg)	Df_0	Df_B	ε_r'	ε_r''	tan delta	D_p (cm)
GAC	119	50	47	15.2	6.68	0.44	2.2
GAC CH	115	55	58	16.62	8.24	0.5	1.9
GAC MW	125	63	65	18.9	9.23	0.49	1.8
GKAS	100	9	3	3.56	0.43	0.13	13.5
GKAS (CH)	102	10	4	3.84	0.57	0.15	13.2
GKAS (MW)	99	10	4	3.84	0.57	0.15	13.2
GKAS-N	104	46	33	14.07	4.69	0.34	3.1
GKAS-N (CH)	105	49	36	14.92	5.12	0.35	2.9
GKAS-N (MW)	109	52	45	15.77	6.39	0.41	2.4
Org	149	167	49	48.43	6.96	0.15	3.8
OrgP	149	88	42	26	5.97	0.23	3.3
SBA TEPA	64	6.2	0.11	2.77	0.02	0.01	400

Another important parameter with regards to the dielectric properties of the material is the microwave power % absorption, or else heating efficiency. This parameter will help to validate the above results, helping to understand which samples have the potential to be heated effectively under electromagnetic irradiation. Figure 5.1 describes the heating efficiency per mg of the samples used in this research. It is clear that the carbon based samples are heated much more efficiently compared to the silica based sorbent. Specifically, SBA TEPA presents a heating efficiency of 2% respectively, which means that this material is not suitable for microwave applications. On the other hand, most of the carbon based sorbents demonstrate excellent heating efficiencies, higher than 85%, classifying them as exceptional microwave absorbents. However, the GKAS sample presents unexpectedly low heating potential that does not exceed 18%. Nevertheless, it is apparent that the GKAS sample presents higher microwave heating efficiencies after

4 cycles of TSA or MSA, namely 20% and 26%, respectively. This phenomenon was also evident in the case of GAC, as explained in Section 4.6, as well as in the case of GKAS-N, for which the initial efficiency was 83% increasing to 85% and 90% after 4 cycles of TSA and MSA respectively. These results are in accordance with the aforementioned data about tan δ, validating the sorbents' microwave heating potential.

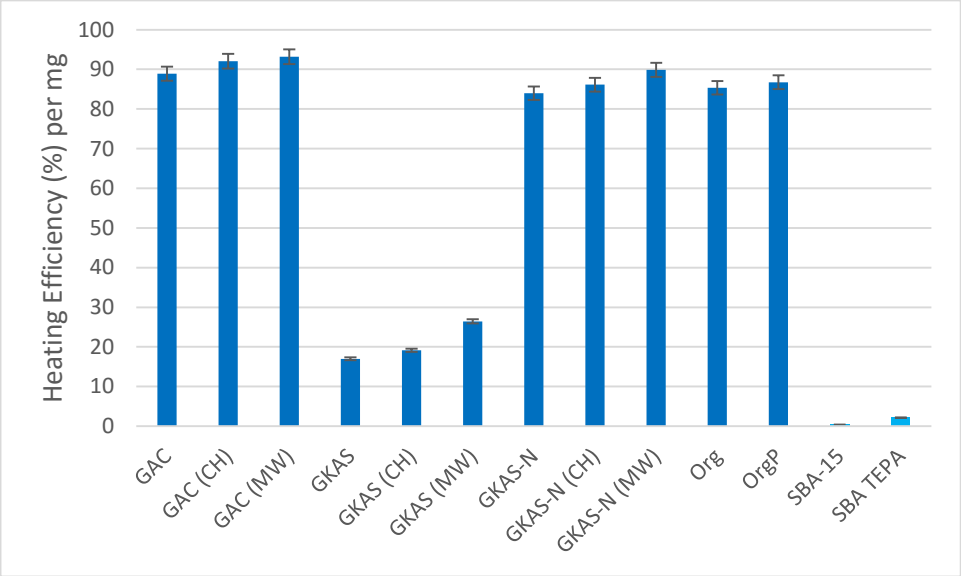

Figure 5.1: Heating Efficiency (%) per mg of sorbent. The carbon based materials are highlighted in dark blue, whereas the lithium based silicas are in light blue

One reason that could possibly explain this abnormality with the GKAS sample is that it possesses limited transport pores (total pore volume V_p = 0.01 cm^2/g, as reported in Table 5.2). As Ho et al. (2003) pointed out, solid materials usually present various porosity-related challenges affecting their mechanical, chemical, electrical and thermal properties. In general, the presence of porosity is expected to decrease the conductivity of the system; the extend depends on the fraction of porosity. However, in the case of microwave heating the above relation is more complex; various modelling theories have been introduced as an attempt to predict the connection between porosity and dielectric constant, including the Maxwell-Wagner-Sillars, Bruggeman-Hanai and Looyenga treatments (Lestreiz et al., 1998). Each theory depends on the distribution and shape of the voids, however these modelling attempts are beyond the aims and objectives of this research. Indicatively and in order to show the complexity of the study, the Maxwell-Wagner-Sillars model can be expressed by the following equation of Volume Average Theory (VAT):

$$\varepsilon_{eff} = (1 - P) * \varepsilon'_r + P * \varepsilon_i \quad (5.8)$$

Where $P = {V_{por}}/{V_t}$, with V_{por} being the volume of the pores, ε_{eff} the effective dielectric constant and ε_i the dielectric constant value (Bouledjnib et al., 2010).

Moreover, in the case of GKAS-N, another effect contributes to its efficient heating compared to GKAS, when using MSA; the NH_3 surface functionalities of the specific sample enhance the efficiency of the heating, compared to GKAS, resulting in increased microwave absorption efficiency. The molecular geometry of NH_3 is trigonal pyramidal, resulting in a vector sum of the three H-N bond dipole moments (u_{HN} = 1.33 D) of 1.47, as seen in Figure 5.2. This means that the NH_3 molecule is polar, which as discussed in Section 2.2.4 significantly affects the MW heating process, since the electric field component of the microwaves forces induced dipoles to rotate with the alternating field. This molecular movement produces friction among the rotating molecules and the energy is subsequently dispersed as heat.

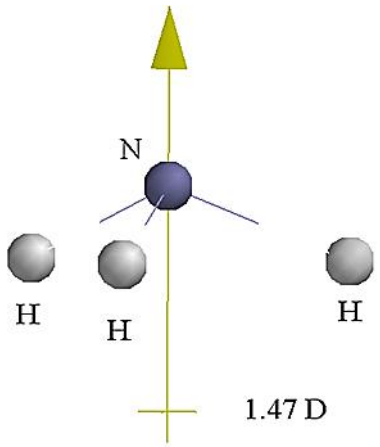

Figure 5.2: NH_3 molecular geometry

5.2. GKAS & GKAS-N800

Up to this point, this research focused on the GAC which was a carbon-based material but with no surface modifications. Therefore, a reasonable next step is to test a modified AC that has previously shown enhanced CO_2 adsorption uptake compared to its parent sample, into the TSA and MSA rigs. The main purpose of this study is to examine if the chemical modifications of the surface of the sorbent would play a role on the microwave absorption ability, leading to an enhanced desorption step.

Chemical impregnation of carbon-based sorbents has received significant attention for the CO_2 adsorption process (Yu et al., 2010). It is based on the principles of CO_2 chemical absorption (chemisorption) using aqueous amine solutions, where CO_2 reacts with primary or secondary amines and forms carbamates (Caplow, 1968 and Crooks et al., 1989). To overcome the issues deriving from this technology, such as high energy demand especially during the desorption process and equipment corrosion, while maintaining high CO_2 adsorption capacity and selectivity, hybrid solid sorbents have been developed by impregnation of solid supports with amines (Xu et al., 2003, Satyapal et al., 2001, Maroto-Valer et al., 2005, Maroto-Valer et al., 2008, Plaza et al., 2007 and Plaza et al., 2008). Nonetheless, Plaza et al. (2007) reported that this technique does not work well with microporous sorbent materials, since the amines tend to block the access to the pores network of the AC, partially eliminating the positive effect of their improved surface chemistry, leading to reduced CO_2 adsorption potential. Furthermore, other drawbacks of amine surface modification of solid sorbents include: high volatility, potential degradation in oxygen environment, leaching and deactivation in the existence of sulphur components in the flue gas (Plaza et al., 2009).

However, Plaza et al. (2011) reported that apart from amine impregnation, there are other ways to enhance the adsorption of the acidic CO_2, namely by introducing basic functionalities on the AC; the molecule of CO_2 behaves as an electron acceptor (weak Lewis acid) able to interact with electron-donors, such as nitrogen surface groups. There are various ways to insert nitrogen functionalities onto the sorbent, such as pyrolysis of N-containing polymers (Drage et al., 2007, Pevida et al. 2008 and Zhao et al., 2010), chemical reaction (Gray et al., 2004 and Zhao et al., 2010) or heat treatment with ammonia gas in the presence or absence of oxygen (usually referred to as ammoxidation and amination respectively) (Jansen et al., 1994, Pevida et al., 2008, Plaza et al., 2009, Plaza et al., 2010, Plaza et al, 2010 and Przepiórski et al., 2004). For the purposes of this research, amination was selected as the pathway to modify the surface of the AC, since it has already been proven that this technique enhances the CO_2 adsorption, according to Plaza et al. (2011). Specifically, they reported that amination resulted in effective introduction of stable N_2 heteroatoms into the carbon matrix promoting the development of a basic AC with increased delocalised electrons, while simultaneously it promotes the narrow microporosity of the AC, enhancing CO_2 adsorption potential.

As a result, two different carbon-based solid sorbents were evaluated in the present section, the first being the parent sample (GKAS), while the second one being the nitrogen modified sorbent (GKAS-N). These sorbents were obtained from almond shells and were produced in Spain during a collaboration with the Instituto Nacional del Carbón (CSIC). The particle size of the raw material was measured to be between 1 and 3 mm and was carbonised under N_2 flow at 873 K. Later, the carbonised product gave rise to two different samples; the first sample was produced by physical activation with 10 cm^3/min of CO_2 flow up to a 40% of burn off at 973 K, obtaining the sample referred to as GKAS. The second sample, referred to as GKAS-N, was the nitrogen modified sorbent and was obtained by treating the carbonised material with ammonia (NH_3) at 1073 K for 2 h.

5.2.1. Adsorption

Figure 5.3 shows the CO_2 breakthrough curves of the aforementioned carbons, GKAS and GKAS-N, at ambient temperature and pressure for a feed consisting of 15% vol. CO_2 (85% N_2), at a total flow rate of 100ml/min. These experiments were carried out to evaluate the performance of the selected sorbent materials and compare them with GAC using conditions that simulate that of a flue gas stream and as a result, the moisture content was also taken into account. The letter D expresses the dry conditions of the feed gas, while the letter W is used when wet gas conditions were examined, as previously explained in Section 3.7. The time-dependent evolution of the effluent CO_2 molar fraction (y-axis represents the normalised value $C_{CO_2}^{out}(t)/C_{CO_2}^{in}$) is presented. Initially, all the CO_2 that enters the reactor is adsorbed by the sorbent separating it from the N_2 that exits the bed. After three to six minutes, depending on the sorbent and the conditions used, the mass transfer zone approaches the bed outlet and some CO_2 molecules start to be detected in the effluent stream by the TOF-MS. It is interesting that GKAS curves present shorter breakthrough times, t_b, (which is the time needed for $C_{CO_2}^{out}(t)/C_{CO_2}^{in}$ = 0.05), compared to GKAS-N for each condition; specifically, for the dry feed gas experiments t_b equals with 210 seconds for GKAS, while in the case of GKAS-N it increases to 245 seconds. The same trend is evident for the wet feed gas adsorption, namely t_b increases from 295 to 340 seconds. The sorbent bed then reaches

equilibrium conditions and becomes saturated as the effluent concentration equals that of the feed ($C_{CO_2}^{out}(t) / C_{CO_2}^{in} = 1$). The curves corresponding to the GKAS sorbent are broader in shape, compared to the ones representing GKAS-N that are steeper, which suggests that increased mass transfer resistance is present due to the limited transport pores that it possesses (GKAS: V_p=0.01 cm^2/g, as reported in Table 5.2). Combining the longer breakthrough times with the lower mass transfer resistance, it can be concluded that GKAS-N presents better adsorption performance compared to GKAS, which is in accordance with previous studies (Plaza et al., 2011).

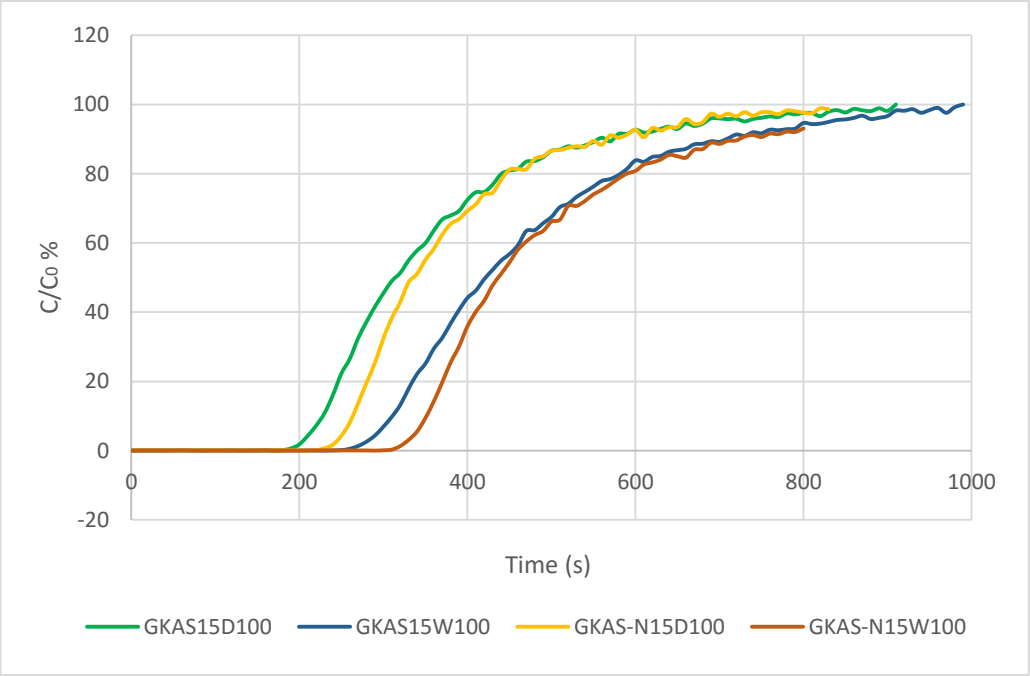

Figure 5.3: Breakthrough curves obtained from a 15/85 CO_2/N_2 binary mixture at 25°C and 1bar, comparing GKAS and GKAS-N at dry and wet gas conditions

Figure 5.4 summarises the CO_2 amount adsorbed for both samples under dry and wet feed gas conditions. As previously reported (Section 4.2) the CO_2 breakthrough capacities are below the corresponding values obtained from the thermogravimetric analyses that were presented in Section 5.1.1, due to the conceptual difference between static and dynamic adsorption potential discussed in Section 4.2.1. Moreover, the reported amount adsorbed is subjacent to the case of pure CO_2 flow, due to the reduced CO_2 partial pressure in the feed gas mixture. Nevertheless, GKAS and especially GKAS-N still present a significant CO_2 adsorption capacity. As expected, GKAS-N showed higher CO_2 dynamic adsorption capacity, compared to GKAS: in particular, 0.1 g of CO_2 were adsorbed per 1.6 g of GKAS-N under dry feed gas conditions,

corresponding to a weight uptake of 6.25% (w/w), which is an enhanced performance compared to GKAS which under the same operating conditions presented a 5.1% (w/w) weight increase (0.08 g of CO_2 per 1.6 g of sorbent). The GKAS-N sorbent showed an enhanced performance under wet feed gas conditions as well, following the same trends reported for GAC in Chapter 4 (Section 4.2.3). It is noticeable that both samples increased their CO_2 dynamic adsorption capacities, however the amount adsorbed from GKAS was still lower than GKAS-N. Specifically, the weight increase was enhanced from 5.1% to 5.6% and from 6.25% to 7.35% for GKAS and GKAS-N, respectively.

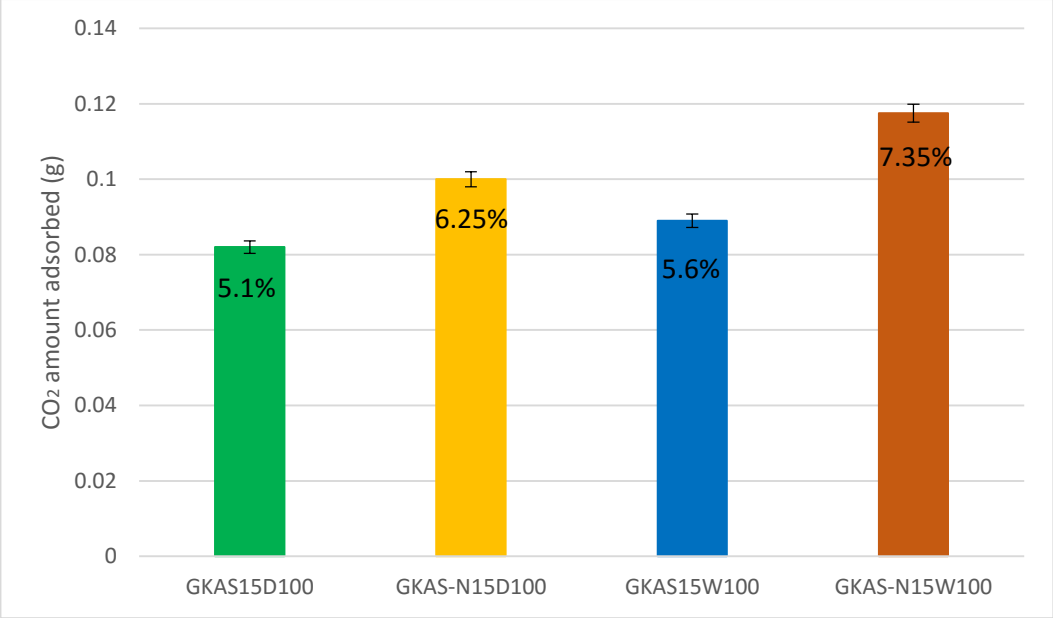

Figure 5.4: Amount of CO_2 adsorbed onto the GKAS and GKAS-N from a 15/85 CO_2/N_2 binary mixture at 25°C and 1bar, for dry and wet gas conditions

5.2.2. Desorption

After reaching equilibrium conditions ($C/C_0 = 1$) during adsorption, desorption step was conducted for the GKAS and GKAS-N, under a 100ml/min N_2 purge gas flow examining two temperatures, namely 70°C and 130°C in order to compare TSA and MSA processes. The effect of dry and wet gas conditions was examined as well.

5.2.2.1. Desorption profiles

Figures 5.5 and 5.6 present the CO_2 outlet concentration profiles for GKAS during CO_2 desorption via MSA and TSA as a function of time (seconds) using two different temperatures, namely 70°C and 130°C and two different gas conditions, dry and wet

respectively. Unlike the case of GAC, it is clear that there are no distinct differences in the CO_2 outlet distribution between TSA and MSA. The advantages of the MSA distribution described in Chapter 4 including the rapid peak of $[CO_2]_{out}$ within seconds and the initial high heating rates, as well as the absence of a long tail towards longer desorption times are not evident in the case of GKAS. Here, both desorption modes present similar $[CO_2]$ peaks and long tails, indicating that the heating rates of the two modes are identical, contrary to the case of GAC.

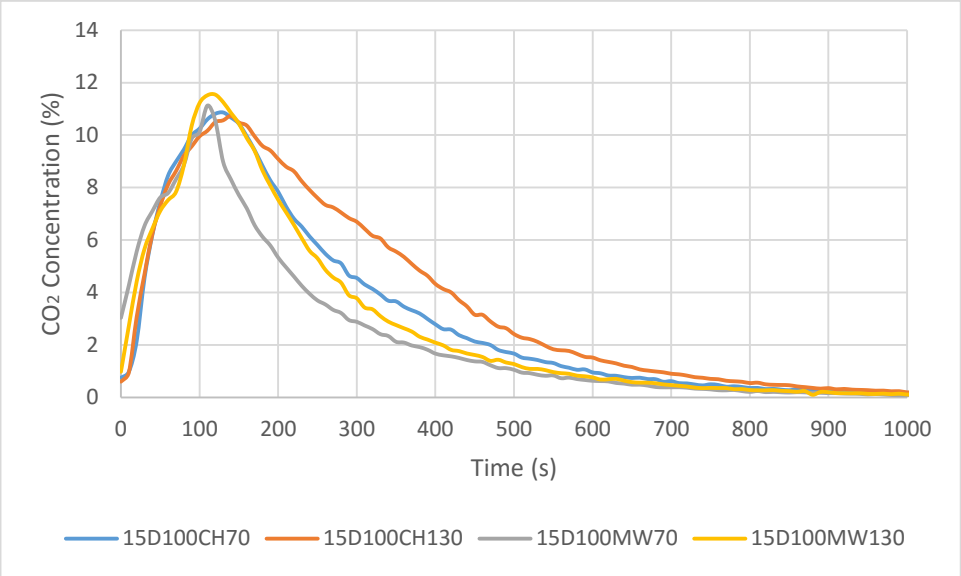

Figure 5.5: Time dependent CO_2 outlet concentration profiles during GKAS regeneration at 70°C and 130°C for dry gas conditions via MSA and TSA

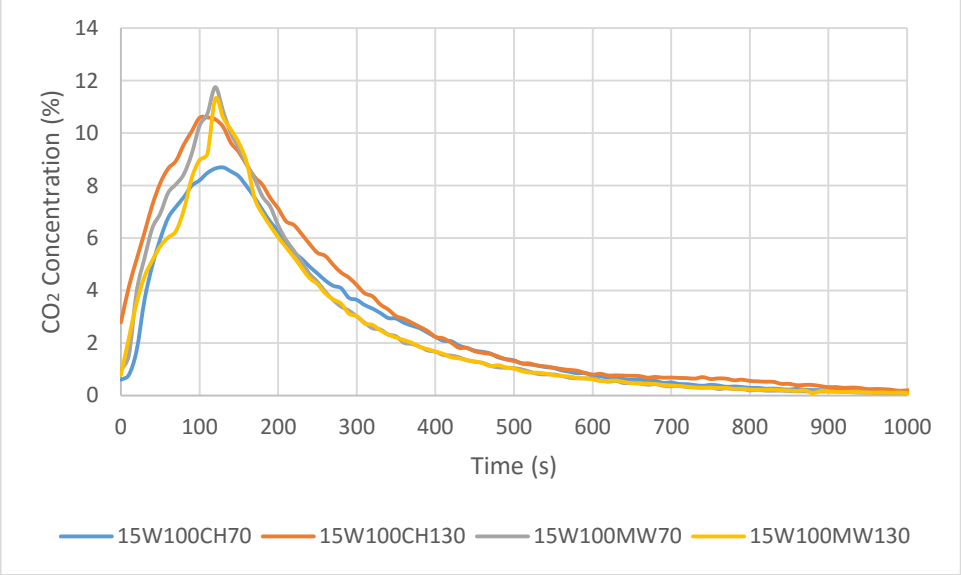

Figure 5.6: Time dependent CO_2 outlet concentration profiles during GKAS regeneration at 70°C and 130°C for wet gas conditions via MSA and TSA

As a result, it is also interesting to evaluate the heating rates throughout the desorption experiment for the TSA and MSA modes presented in Figure 5.7, in order to validate the above assumption. At first, the thermal response of GKAS during the MSA process looks promising, since it indicates that the loss factor of the adsorbent material does not increase with temperature, as in the case of GAC (Section 4.3). This means that the 'runaway effect', can be avoided for the case of GKAS as well, since the slope of the sorbent's heating rates versus temperature, is not positive. However, it is also clear that the rates are different than in the case of GAC. At the beginning of the process, GAC presented extremely high heating rates, 25°C/min and 60°C/min for 70°C and 130°C respectively, leading to the initial rapid CO_2 desorption described from the high peak in the desorption graphs. In contrast, this was not the case for GKAS, for which initially the heating rate was 7°C/min and 10°C/min for 70°C and 130°C, respectively, for the MSA process. Even if these rates were higher than in the TSA case (2°C/min and 5°C/min, respectively), they did not result in a different heating process, since the difference is not noteworthy, thus generating similar desorption graphs. Looking at Section 5.1.2, this effect could simply be attributed to the non-favourable dielectric properties of GKAS; this material presented the lowest microwave absorption potential (14%), compared to the other carbon based materials and as a result, no distinct differences in the performance of MSA compared to TSA were to be expected.

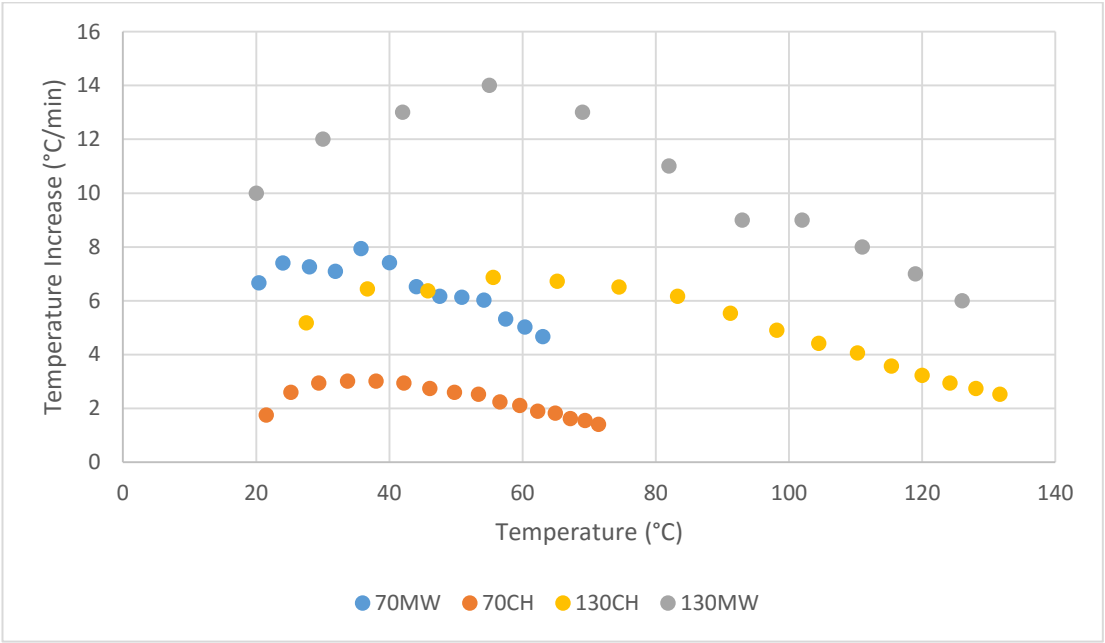

Figure 5.7: Heating rates of GKAS for MW and CH at 70°C and 130°C

On the other hand, GKAS-N presented quite distinct dielectric properties (85% microwave absorption efficiency), compared to GKAS, mainly due to the polar nature of the NH_3 surface functionalities, as reported in Section 5.1.2. As a result, GKAS-N presented clearly different trends during CO_2 desorption via MSA and TSA, as seen in Figures 5.8 and 5.9, similar to the trends reported for the GAC sample; the maximum $[CO_2]_{out}$ is clearly higher during the MSA process compared to TSA, meaning that most of the adsorbed CO_2 is quickly desorbed, due to the rapid heating of the sorbent, similar to GAC. However, it is interesting to note that, unlike the GAC case, the peaks of TSA and MSA appear at approximately the same time period, namely after 80-100 seconds, depending on the gas conditions. It is also worth mentioning that the introduction of moisture seems to affect the desorption process as well since the peaks were considerably lower compared to the dry gas conditions; specifically, a 10-15% reduction in the curves' peaks is apparent for both TSA and MSA for each temperature used. However, in order to assess the full performance of GKAS and GKAS-N, the regeneration efficiency, desorption kinetics and energy consumption parameters should be taken into consideration.

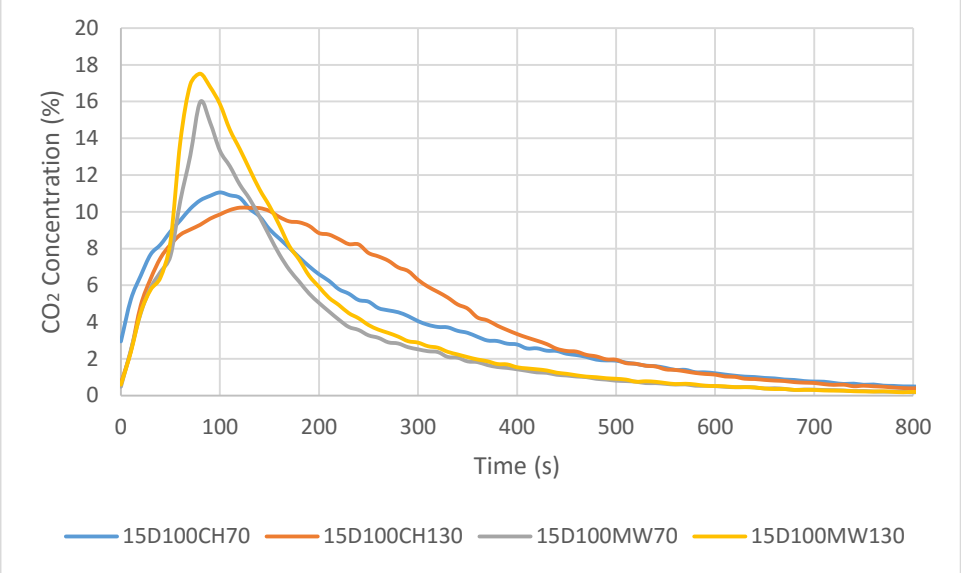

Figure 5.8: Time dependent CO_2 outlet concentration profiles during GKAS-N regeneration at 70°C and 130°C for dry gas conditions via MSA and TSA

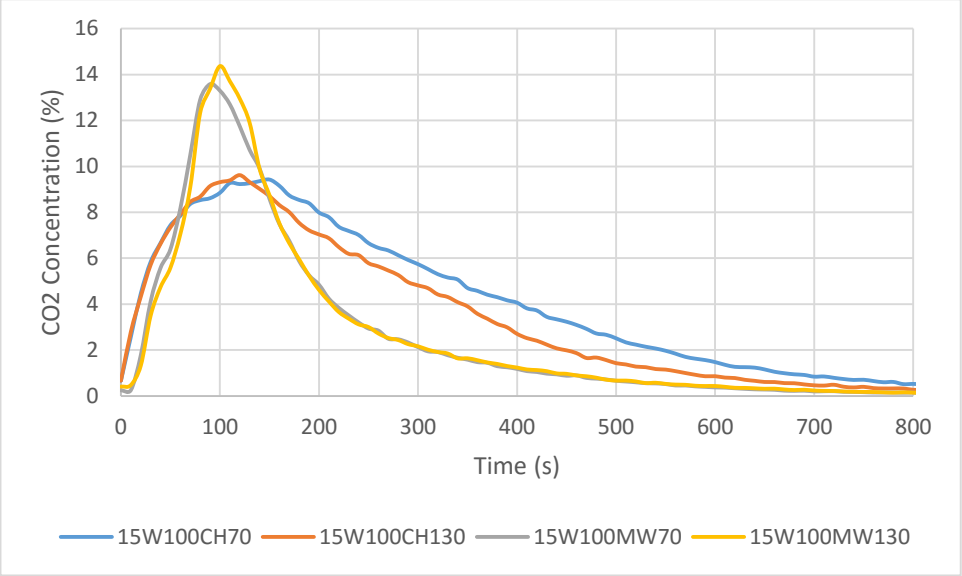

Figure 5.9: Time dependent CO_2 outlet concentration profiles during GKAS-N regeneration at 70°C and 130°C for wet gas conditions via MSA and TSA

5.2.2.2. Regeneration efficiency

Initially, the regeneration efficiency of GKAS and GKAS-N during MSA and TSA is discussed. Figures 5.10 and 5.11 show the performance of both sorbents, previously loaded with CO_2 from a 15% (vol.) gas mixture (balance N_2), during desorption, including both dry and wet gas conditions at 70°C and 130°C. It is clear that for both sorbents MSA resulted in an increase of the total regeneration efficiency of the materials. This is an interesting result, especially for the case of GKAS, since it was shown in the previous section (Section 5.2.2.1) that the desorption profiles in the MSA mode did not show any distinct differences compared to TSA. However, here it is evident that MSA enhanced its regeneration efficiency; for the case of dry gas conditions, an increase from 85% to 91% and from 83% to 90% for 70°C and 130°C respectively was reported. Moreover, when using wet gas conditions during the adsorption step, the regeneration efficiency of the sorbent decreased significantly for TSA from 85% to 63% and from 83% to 67% for 70°C and 130°C, respectively. Nevertheless, MSA managed to improve TSA's regeneration efficiencies, resulting in an increase to 71% and 82%, respectively. It is worth mentioning that the increase in temperature did not play an important role for dry gas conditions. On the other hand, there is an important difference in the regeneration efficiency during MSA mode when increasing the temperature under wet conditions, namely a significant increase from 71% to 82%. This was to be expected since, as discussed in Section 4.2.3, H_2O blocks

the pores on the surface – acting as a superficial cover -, not allowing the CO_2 molecules to diffuse to the outside of the pores when a heating process is applied. As a result, a higher temperature enhances the quick evaporation of the H_2O molecules, allowing more CO_2 to be desorbed and diffused through the pores of GKAS-N, hence increasing the regeneration efficiency.

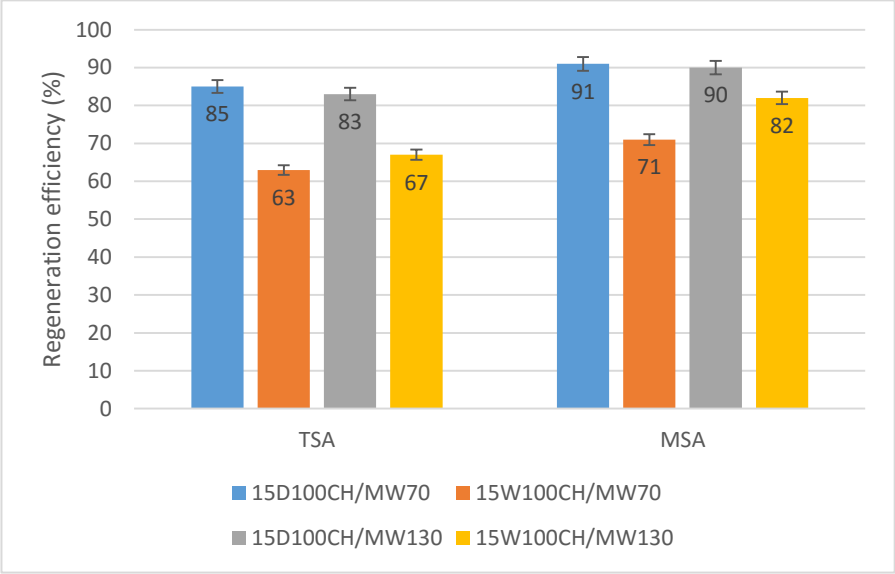

Figure 5.10: Comparison of the regeneration efficiency of GKAS for MSA and TSA at 70°C and 130°C at dry/wet gas conditions

Similar trends were reported for GKAS-N, as seen in Figure 5.11. However, even if this sorbent is heated more efficiently during MSA compared to GKAS, due to its enhanced dielectric properties (Section 5.1.2), the regeneration efficiency of the sorbent follows the exact same trends, indicating that it is not the heating process, but the heating mechanism that is important during CO_2 desorption. It is evident that for the case of dry gas conditions, an increase from 85% to 92% and to 91% for 70°C and 130°C, respectively, was observed, being very close to the results presented for GKAS, within the error deviation of the experiments (±2.5%). Furthermore, for the case of wet gas conditions during the adsorption step, the regeneration efficiency of the sorbent decreased significantly during TSA mode from 85% to 63% and 61% for 70°C and 130°C, respectively. Once again, MSA improved TSA's regeneration efficiencies, resulting in an increase to 73% for both temperatures. It is also worth mentioning that even if MSA managed to enhance the CO_2 desorption process in terms of regeneration efficiency of the sorbent, it did not manage to reach the 80% limit for the wet gas conditions that was set as the target efficiency in Chapter 4.

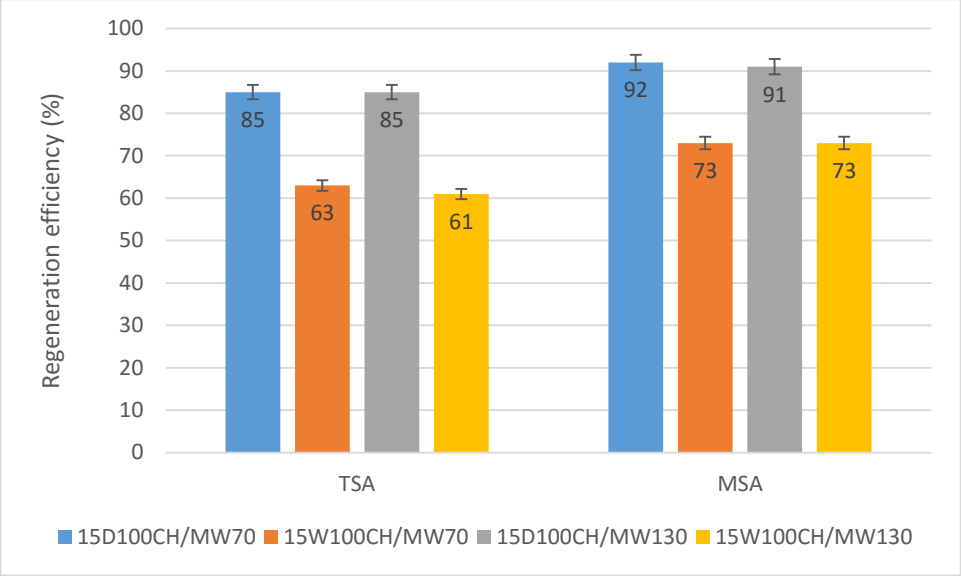

Figure 5.11: Comparison of the regeneration efficiency of GKAS-N for MSA and TSA at 70°C and 130°C at dry/wet gas conditions

5.2.2.3. Desorption kinetics

The next parameter that is investigated in this section is the CO_2 desorption kinetics when using GKAS and GKAS-N comparing MSA and TSA modes. In Section 5.2.2.1 it was reported that GKAS presented similar desorption profiles for both MSA and TSA, which was not the case for GKAS-N, for which the two profiles were distinctly similar compared to GAC. This information demonstrated an initial assumption based on the CO_2 desorption profiles that the desorption rates would be almost identical in the case of GKAS, when comparing the two heating processes. Figure 5.12 shows the comparison of desorption rates for GKAS during MSA and TSA, taking into consideration the time needed for 70% of CO_2 desorption to take place (t_{70}). It is apparent that there is some time reduction when using the MSA technology compared to TSA mode. Specifically, in the case of dry gas conditions, t_{70} decreased from 4.5 to 4.2 minutes and from 4 to 3.8 minutes for 70°C and 130°C, respectively. However, this reduction is not significantly different from an expected error (±2%, as explained in section 4.4) to justify the use of MSA technology for this sorbent. On the other hand, the most noticeable reduction occurred in the case of wet gas conditions, reducing the time needed by 30% (from 5.25 to 3.67 and from 4.25 to 3.1 minutes for 70°C and 130°C respectively) for both temperatures. This means that in the presence of moisture in the exhaust gas, MSA process is more efficient compared to TSA, having also in

mind that the regeneration efficiency achieved is higher during the MSA as shown in Section 5.2.2.2.

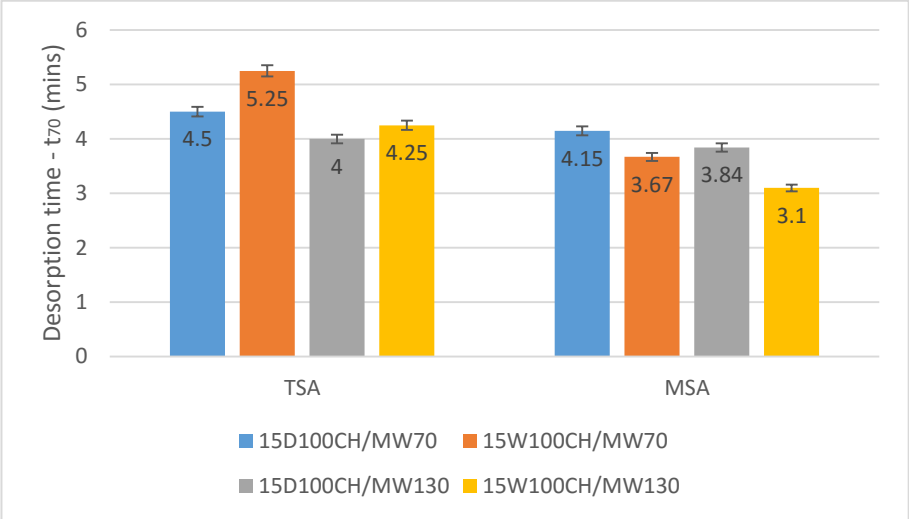

Figure 5.12: Comparison of t_{70} for MSA and TSA using GKAS when heating at 70°C for dry/wet gas conditions

Figure 5.13 presents the comparison between MSA and TSA in terms of desorption time needed (t_{70}) when using GKAS-N as sorbent. The differences between MW and CH heating mechanisms are clear and the process is significantly less time-consuming for every case examined, following a similar trend to GAC. Precisely, an average of 4.5 minutes are needed to reach t_{70} for desorption under TSA when using dry gas conditions, while in the presence of moisture t_{70} increased for both 70°C and 130°C. In contrast, MSA intensified the CO_2 desorption kinetics for both dry and wet gas experiments, by managing to decrease t_{70} efficiently for every case examined; specifically, for the dry gas experiments, the time was reduced by as much as 35%, from 4.6 to 2.9 and 2.8 minutes for 70°C and 130°C, respectively. More importantly, the greatest decline in desorption time was evident for the wet gas experiments, where the decrease reached 45%, reducing t_{70} from 5.25 and 4.8 to 2.8 and 2.9 for 70 and 130°C, respectively.

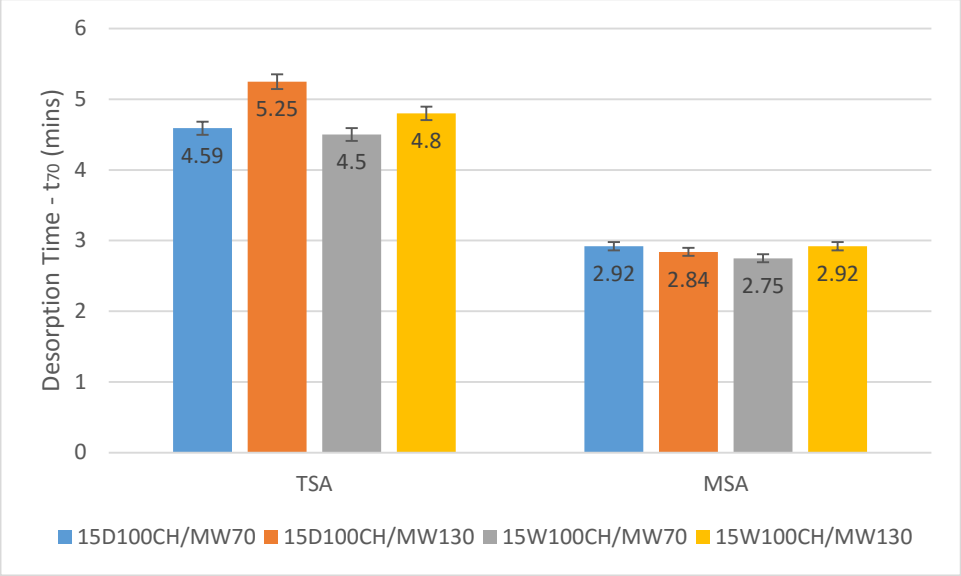

Figure 5.13: Comparison of t_{70} for MSA and TSA using GKAS-N when heating at 70°C for dry/wet gas conditions

5.2.2.4. Energy consumption

The last parameter that was used in order to examine the performance of GKAS and GKAS-N during MSA and TSA desorption is the energy spent during this step. Similarly to Section 4.4.4., only E = E_{70} was considered, which accounts for the energy required for a 70% CO_2 desorption, in order to keep consistency with regards to the parameters compared. Since the energy consumed is directly associated with the desorption time (equation 4.12), it should be expected that the GKAS sample would present a lower performance in terms of energy efficiency compared to GKAS-N and GAC. Figure 5.14 presents the results obtained for GKAS during CO_2 desorption at 70°C and 130°C for dry/wet gas conditions and it is evident that the amount of energy consumed is higher than that of GAC (Section 4.4.4) for both TSA and MSA. In this instance, a clear trend is observed, resulting in higher consumptions with the increase in temperature and the switch to wet gas conditions. Specifically, when using TSA as desorption method and dry gas conditions, the energy consumed increases from 1.74kWh/kg to 2.6kWh/kg when increasing the temperature from 70°C to 130°C, respectively. A similar increase is evident for the wet gas conditions, where the consumption is even higher, escalating from 2.15 to 2.7kWh/kg. Analogous trends can be observed for the MSA mode, however, in this scenario the energy consumed is proportionally lower; a 25% decrease (from 1.74 to 1.3 kWh/kg) in the energy needed for 70% CO_2 desorption is reported in the case of dry gas conditions when heating at 70°C, while this reduction is less in the case of 130°C (20%, from 2.6 to 2.1kWh/kg).

The benefits of MSA are reduced even more in the case of wet gas conditions, where even if MSA still manages to cut down the amount of energy consumed, it does not exceed 17% - from 2.15 to 1.76kWh/kg and from 2.7 to 2.25kWh/kg for 70°C and 130°C, respectively.

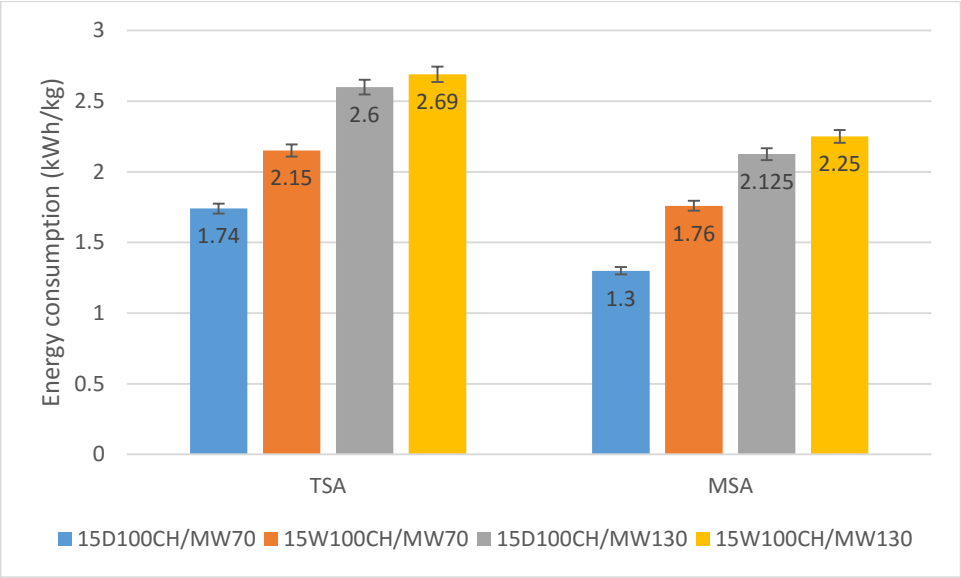

Figure 5.14: Energy consumption during GKAS regeneration at 70°C and 130°C for dry/wet gas conditions

Figure 5.15 presents the E_{70} consumed during the regeneration process of GKAS-N that was previously saturated using $[CO_2]_{in}$ =15% heating to 70°C and 130°C, respectively. As expected, contrary to the case of GKAS, MSA achieved an important decrease in the energy consumed during the desorption step, making GKAS-N a more competitive adsorbent than GKAS; it is clear that, for every set of experiments E_{70} was reduced by at least 37%, with the best results deriving from the desorption at 130°C. Specifically, it was observed that when the GKAS-N sample was regenerated at 70°C, a decrease from 1.26 to 0.8 (37%) and from 1.4 to ~0.85 kWh/kg_{sorb} (40%) during desorption under dry and wet gas conditions, respectively. This decline was even more pronounced in the case of 130°C desorption, where instead of 1.96 and 1.97 kWh/kg_{sorb}, only ~0.97 kWh/kg_{sorb} were consumed, accounting for a significant decrease that exceeds 50%.

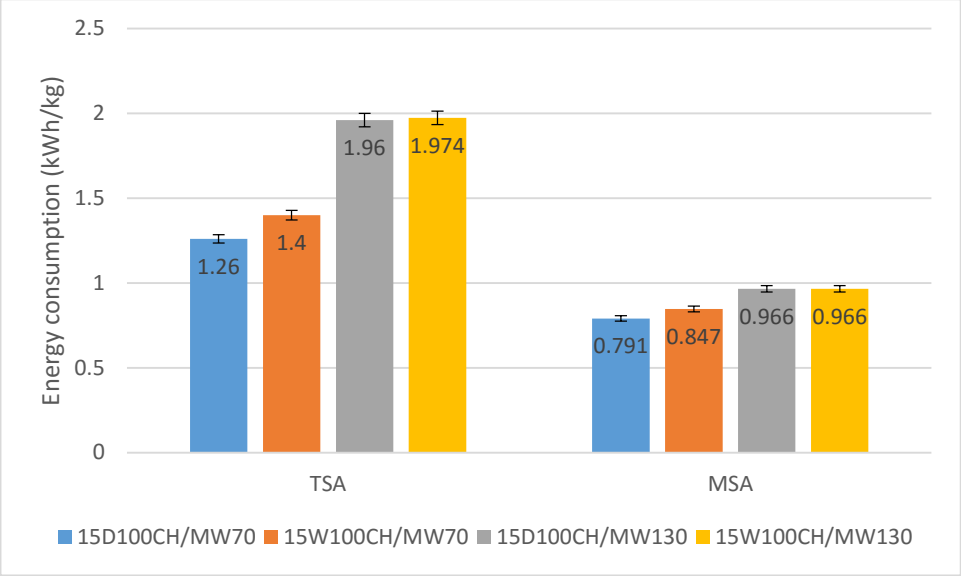

Figure 5.15: Energy consumption during GKAS-N regeneration at 70°C and 130°C for dry/wet gas conditions

5.2.3. Conclusions for GKAS and GKAS-N

In this section, the performance of two carbon based sorbents for CO_2 capture and regeneration under TSA and MSA was evaluated. The first sample, GKAS, was produced from raw biomass, almond shells, whereas the second sample, GKAS-N derived from GKAS after introducing some basic N_2 functionalities on the surface by impregnation with NH_3. The aim of this chapter was to evaluate the performance of those sorbents, trying to examine possible relations between NH_3 impregnation and microwave heating processes. It was shown that unexpectedly the GKAS sample did not present desirable dielectric properties, which greatly affected its performance during MSA. Accordingly, the low microwave power absorption potential of GKAS influenced its regeneration process and as a result the desorption profiles generated from MSA and TSA were almost identical. However, MSA managed to enhance the regeneration efficiency of GKAS due to the direct heating of the sample from the MW, resulting in efficiencies higher than 90% in the case of dry gas conditions and 73-81% for wet gas. Moreover, the desorption kinetics were also intensified from the microwave heating, with the most noticeable result occurring in the case of wet gas conditions, reducing the time needed by 30%. Furthermore, an energy consumption reduction was evident as well, decreasing the energy needed by 25% and 17% for dry and wet gas conditions respectively.

On the other hand, GKAS-N presented a higher CO_2 adsorption uptake compared to GKAS to begin with, due to the presence of transfer pores, resulting in lower mass transfer resistance. Moreover, it also showed distinctly different desorption profiles under MSA mode, taking advantage of the fast heating rates due to its excellent dielectric nature. One possible reason that the MW is enhanced compared to GKAS could be the presence of NH_3 groups on the surface of the material; as discussed in Section 5.1.2, the NH_3 molecule is polar, thus the dipoles rotate with alternating field during MW and as such this friction is dispersed as heat. Consequently, regeneration efficiencies, desorption kinetics and energy requirements were improved compared to the case of GKAS.

However, even if MSA managed to intensify the desorption process for both materials, the comparison of the performance of GKAS and GKAS-N with GAC is not promising for various reasons; the only values that both GKAS and GKAS-N are comparable against GAC is related with the regeneration efficiency. However, it should be taken into account that GAC presents a higher CO_2 adsorption capacity (~10.8% compared to 6.9% and 9.6% for GKAS and GKAS-N, respectively). Nonetheless, comparing the dynamic adsorption potential, GAC seems to be favoured in processes that include high CO_2 partial pressures, while when dealing with low partial pressures (as in the case of post-combustion CO_2 capture), GKAS and GKAS-N seem to be advantageous. In terms of desorption kinetics, it is clear that GKAS is the weakest sorbent material between those three, since it presents an average of 3.5mins, whereas only 3 and 2.8mins are needed for GAC and GKAS-N respectively.

As a result, it can be concluded that the pore volume of a material plays a critical role in the desorption process when using MSA, with the existence of large pore volume inside a sorbent enhancing the MW. Moreover, the introduction of NH_3 to the material is another parameter that affects the MSA process, since the use of a polar element enhances the heating and consequently its desorption performance.

5.3. Desotec Organosorb

The next materials that were tested in the TSA and MSA rigs were obtained from Desotec (Belgium) and the aim was to clarify the connection between the shape of the

sorbent particles and their desorption properties, comparing MSA and TSA. As a result, two different AC – large granules and powder - produced from the same precursor were used. In general, large granules or pellets of AC are preferred when dealing with high pressure operations or when high volumetric adsorption capacity is needed (Craven et al., 2014). Desotec Organosorb 10-CO (2.80-4.75 mm), referred to as Org, is a coconut shell based granular activated carbon commonly used to remove low boiling organic solvents and odours from air and gas. However, its large surface area ($1140 m^2/g$) and pore volume ($0.55 cm^2/g$), reported in Table 5.2, make this sorbent suitable for exhaust gases treatment as well, including CO_2, VOC capture and SO_2 desulphurisation processes.

On the other hand, powdered AC (PAC) are commonly used by water treatment plants on either a full time basis or as needed for taste and odor control or removal of organic chemicals. Raw precursors for the production of PAC include organic materials with high carbon content such as coal, lignite or wood and its apparent density ranges between 0.3 and 0.75 g/cm^3, depending on the precursor and production process (Najm et al., 1991). As a result, the second material used in this section, referred to as OrgP, was produced by grinding the Org using a Fritsch Pulverisette 2 mortar grinder until the solid mixture achieved homogeneity, creating fine powder passing through a 200 mesh sieve (0.075 mm).

5.3.1. Adsorption

Figure 5.16 presents the breakthrough curves obtained during the adsorption experiments using Org and OrgP at ambient temperature and pressure. The CO_2 concentration in the feed was $[CO_2]_{in}$ = 15%, with the balance being N_2, while the total gas flow rate was 100ml/min. Two feed gas conditions were reported, anhydrous and wet, with the wet case being simulated by injecting 10% moisture content, similar to Section 4.2.3. Following the error analysis in Chapter 4, the adsorption step was repeated four times, with the results presented being an average of those measurements, leading to a low deviation of ±2%, as seen by the error bars of Figure 5.17.

It is evident that, for both Org and OrgP, the characteristic breakthrough time t_b increases, when switching from dry to wet feed gas conditions. This is a first indication

that in the case of moisture addition, the CO_2 dynamic adsorption capacity is higher compared to the results for anhydrous conditions. As expected from the thermogravimetric analyses measurements, it can be observed that the OrgP curves are steeper compared to Org, meaning that mass transfer resistance is lower, but CO_2 adsorption amount is lower as well. This difference in steepness of the curves is more evident in the case of wet gas conditions. Moreover, the equilibrium time (t_{eq}), for which CO_2 concentrations at the bed inlet and outlet are practically equal, is reached 3 minutes faster in the case of OrgP under wet gas, whereas under dry gas conditions, the t_{eq} for both sorbents is almost equal. One reason that explains this phenomenon is associated with the shape of the sorbent; OrgP, being a fine powder, tends to agglomerate when adding moisture to the gas mixture, prior to its CO_2 saturation and as a result, equilibrium time is reached faster. On the other hand, in the case of Org, there is no sign of agglomeration, since there is enough space for the H_2O to be deposited between the large granular particles inside the material bed. This is in agreement with previous studies (Standish et al., 1991), where it was reported that at any initial moisture content, it is sensible to assume uniform mixing of the particles if the particle size is large (>1mm).

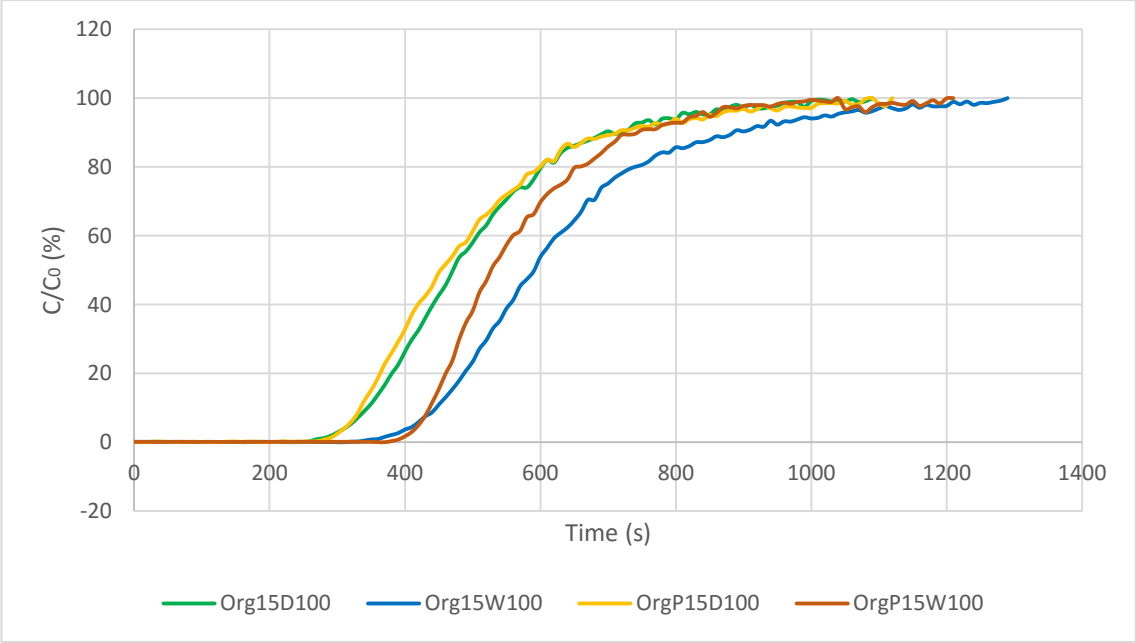

Figure 5.16: Breakthrough curves obtained from a 15/85 CO_2/N_2 binary mixture at 25°C and 1bar, comparing Org and OrgP at dry and wet gas conditions

Figure 5.17 presents the total amount of CO_2 adsorbed from Org and OrgP during the adsorption step. It is clear that for both dry and wet gas conditions, the amount of CO_2

adsorbed was higher in the case of Org. Specifically, the Org managed to adsorb 0.18 g of CO_2 under dry gas conditions, while this amount increased for the wet gas to 0.21g. On the other hand, OrgP showed a poor performance during adsorption, ending with only 0.15 and 0.17 g of CO_2 adsorbed for the dry and wet gas conditions respectively. This effect could be attributed to the fact that, as mentioned in Section 5.1, a granular sorbent with large particle size takes advantage of the fact that no channeling, fluidizing, or bypassing takes place when a fluid passes through; large granules create a solid structure where migration of the adsorbent particles or channel formation is avoided. On the other hand, a powder sorbent may generate a loose particle bed into the reactor, which could lead to fluid chanelling; this would result in an uneven distribution of the fluid into the adsorbent bed while a vast amount of sorbent would not be utilised. As a result, the CO_2 adsorption capacity of OrgP would reasonably be lower than in the case of Org. Interestingly enough, a ~10% of moisture into a binary gas mixture of CO_2 and N_2 seems to enhance the CO_2 adsorption capacity of both Org and OrgP, for the same reasons as in the case of GAC, GKAS and GKAS-N. The CO_2 adsorption capacity in the case of Org was increased by as much as 17% (from $0.18 g_{CO_2}$ to $0.21 g_{CO_2}$), while for OrgP the increase was lower, from $0.15 g_{CO_2}$ to $0.17 g_{CO_2}$, accounting for a 13% rise.

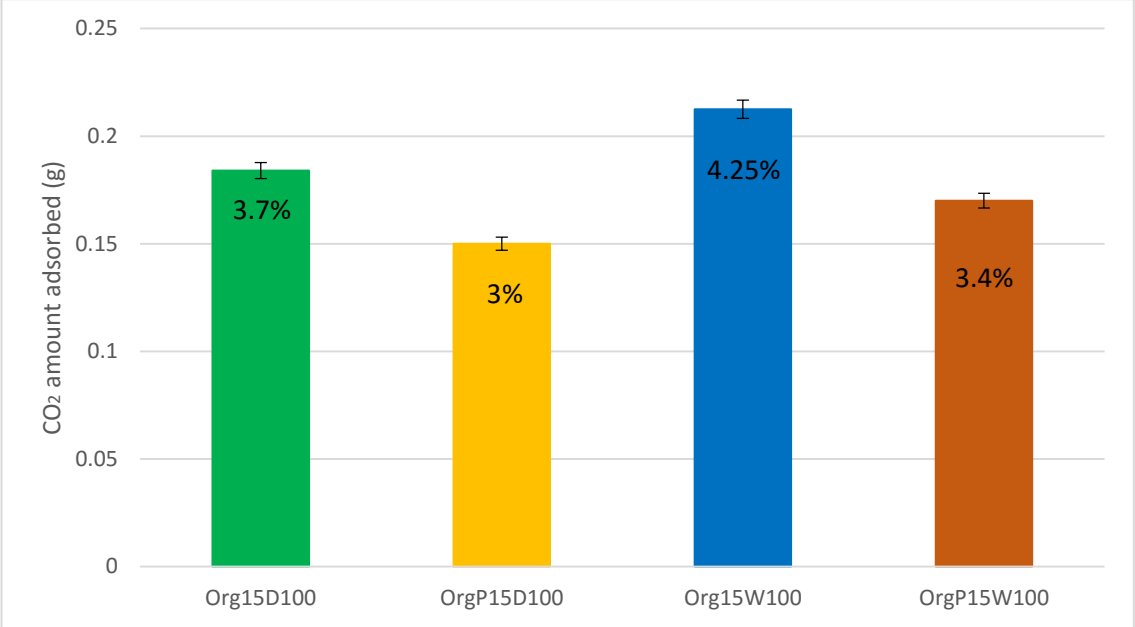

Figure 5.17: Amount of CO_2 adsorbed onto the Org and OrgP from a 15/85 CO_2/N_2 binary mixture at 25°C and 1bar, for dry and wet gas conditions

5.3.2. Desorption

After reaching equilibrium conditions ($C/C_0 = 1$) during adsorption process, desorption step was conducted for the Org and OrgP, following the same procedure as in the previous materials. N_2 purge gas flow was set to 100ml/min and two temperatures were selected, namely 70°C and 130°C in order to compare TSA and MSA processes. The effect of dry and wet gas conditions are also discussed.

5.3.2.1. Desorption profiles

Figures 5.18 to 5.21 present the $[CO_2]_{out}$ profiles during CO_2 desorption from Org and OrgP via MSA and TSA modes as a function of time (seconds) using two different temperatures, namely 70°C and 130°C. Similar to the GAC desorption profiles, it is noticeable that there are two different outlet concentration patterns, MSA following the *log-normal distribution*, while TSA profiles are described by the *Rayleigh distribution*.

As discussed in Section 5.1.2., Org and OrgP present almost identical dielectric properties, including microwave absorption potential, with GAC and GKAS-N. As a result, since Org and OrgP are excellent microwave absorbers, it was expected that the MSA CO_2 desorption profiles as well as the heating rates would be proportionally similar with the previous cases. Truly, once again the most important difference derived from the aforementioned distributions is that in the case of MSA the maximum $[CO_2]_{out}$ (curves' peak) is reached distinctively faster compared to TSA mode. This means that most of the adsorbed CO_2 is quickly desorbed, due to the rapid heating of the sorbent, suggesting that the dissipation of CO_2 through the pores of Org and OrgP is favoured by microwave heating. It is remarkable that during MSA the $[CO_2]_{out}$ peak is reached after ~50 seconds for both Org and OrgP, regardless dry/wet gas conditions or desorption temperature, taking advantage of the high initial heating rates that microwave heating can provide, as in the case of GAC discussed in Section 4.3. On the other hand, a smooth desorption profile is evident for the case of TSA, where the desorption rates are clearly lower compared to MSA. It is noticeable that the maximum $[CO_2]_{out}$ is reached much later compared to MSA, due to the different heating mechanism during the two processes, discussed in Section 2.2.9; in both materials, the desorption peak in the TSA mode was reached after 200 seconds (>3mins). The same trend is evident with varying desorption temperature and gas conditions.

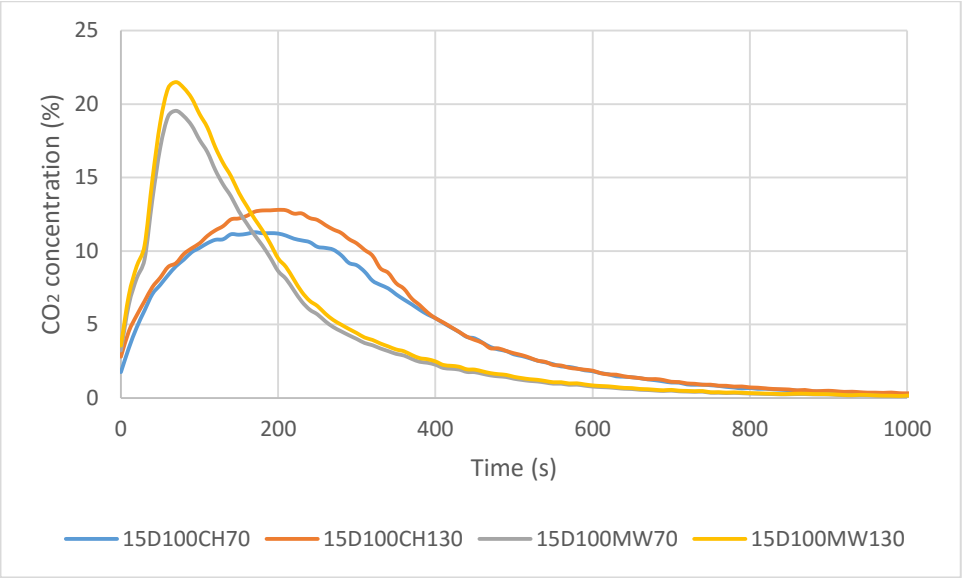

Figure 5.18: Time dependent CO_2 outlet concentration profiles during Org regeneration at 70°C and 130°C for dry gas conditions via MSA and TSA

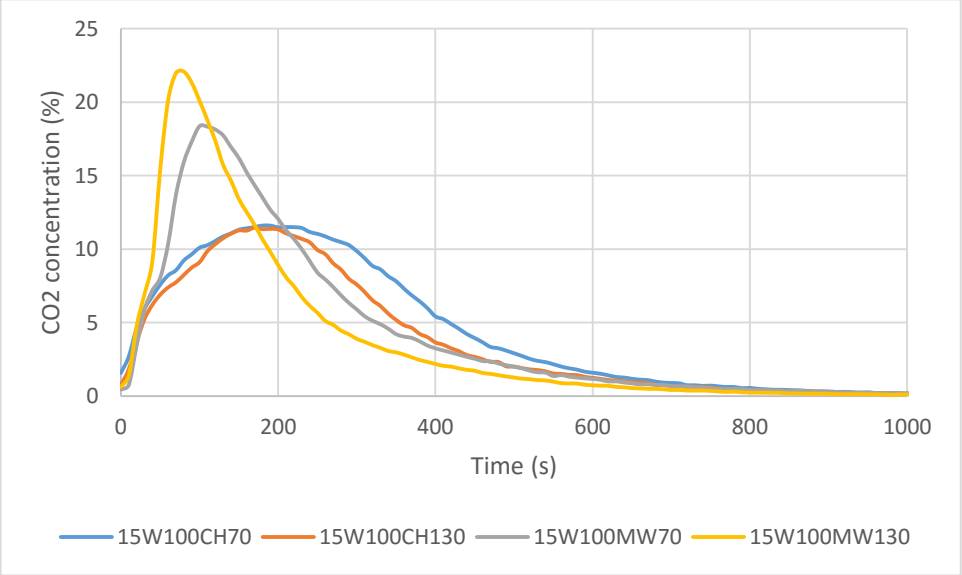

Figure 5.19: Time dependent CO_2 outlet concentration profiles during Org regeneration at 70°C and 130°C for wet gas conditions via MSA and TSA

As a result, combining the facts that the peak of $[CO_2]_{out}$ is considerably higher in the case of MSA while it is reached clearly faster (1/4 of the time needed) compared to the TSA mode, it is evident that microwaves have the ability to intensify the CO_2 desorption process for both Org and OrgP. Taking advantage of the excellent dielectric characteristics that these two materials present (Table 5.3), the CO_2 molecules attached onto the surface of the sorbents are rapidly detached due to the fast heating during

MSA, compared to TSA. However, further analysis of regeneration efficiency, desorption kinetics and energy consumption will follow in order to confirm the above statement.

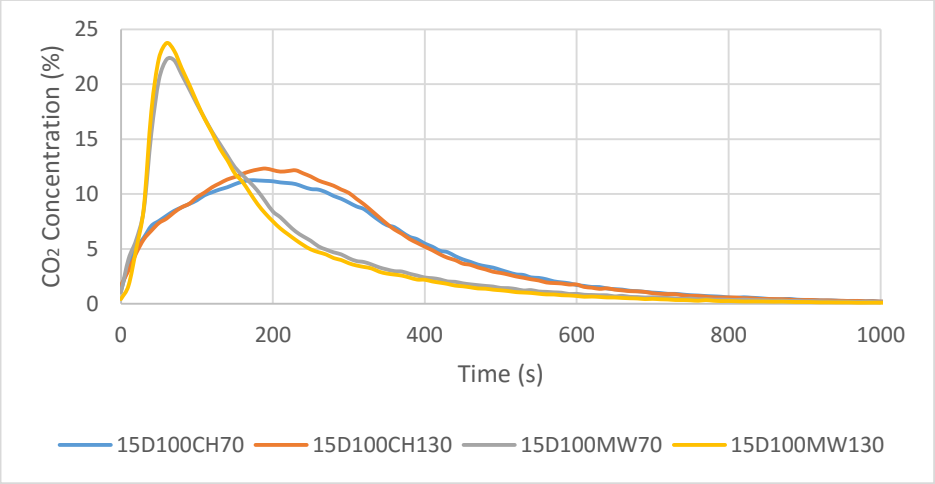

Figure 5.20: Time dependent CO_2 outlet concentration profiles during OrgP regeneration at 70°C and 130°C for dry gas conditions via MSA and TSA

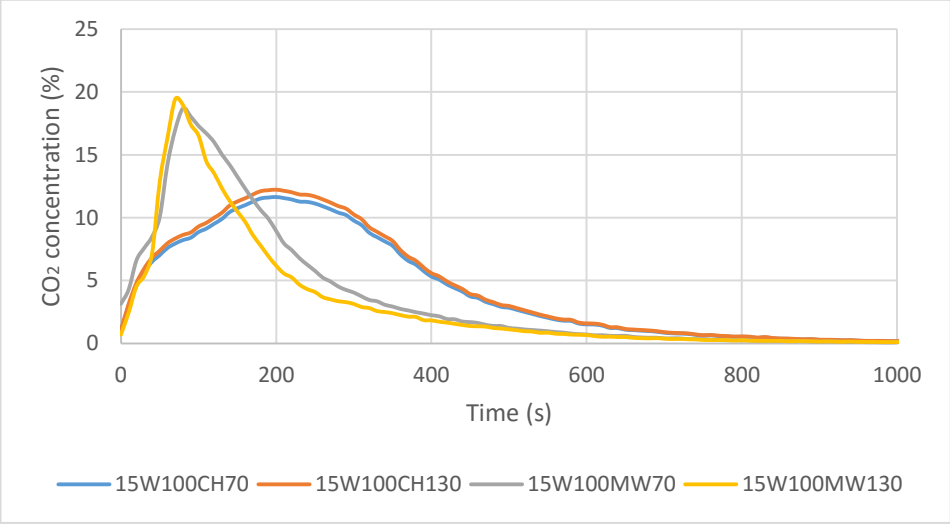

Figure 5.21: Time dependent CO_2 outlet concentration profiles during OrgP regeneration at 70°C and 130°C for wet gas conditions via MSA and TSA

5.3.2.2. Regeneration efficiency

The first parameter under investigation for the performance of Org and OrgP under TSA and MSA was their regeneration efficiency. The equations used were described in Section 4.4.2.

It is obvious that MSA intensified the desorption process in terms of Org/OrgP regeneration efficiency, since n_{des} is higher for every case when microwaves were utilised. One interesting observation is that the temperature increase does not seem to play a significant role in the regeneration performance, since similar trends are reported for both 70°C and 130°C. However, it can be concluded that when using a higher temperature, the regeneration efficiency increased. This increment, though, is not large enough to justify a heating process at a higher temperature, which would lead to higher cost due to the increased energy consumption, as will be discussed in Section 5.3.2.4.

On the other hand, it is clear that the most influential factor was the dry/wet gas condition during the adsorption step; specifically, both TSA and MSA processes report lower regeneration efficiencies in the cases of wet gas previously adsorbed. As can be seen from Figures 5.22 (Org) and 5.23 (OrgP), there is a huge decrease in the $n_{des,}$ when TSA is used when introducing wet feed gas; at 70°C desorption, n_{des} decreases from 81% to 66% for Org and from 88% to 69% for OrgP. Moreover, even when the sorbent materials were heated at 130°C, the same trend was evident; a radical decrease from 80% to 72% for Org and from 94% to 74% for OrgP. These values are well below the desirable values for a large scale process, where desorption efficiencies of >80% are needed in order for the capture process to be economically feasible, as explained in Section 4.4.2. However, experimental tests under the MSA process showed a radical improvement in those efficiencies as well, resulting in much higher amount of CO_2 desorbed from the Org/OrgP, being eventually comparable with the values obtained during dry gas conditions; for heating at 70°C, 88% was possible, while this amount increased further to 94% when heating at 130°C. In the case of OrgP, the desorption efficiency improved from 69% to 92% and from 74% to 89% for 70°C and 130°C desorption respectively, under wet conditions.

In addition, the highest desorption efficiencies were reported for the dry gas conditions, as expected; Org showed a total of 81% and 80% CO_2 desorbed during 70°C and 130°C TSA heating, respectively, while OrgP presented a better performance resulting in 88% and 94% regeneration efficiency. MSA process managed to boost those efficiencies as well; when heating at 70°C, a 88% was possible for the Org material, while this amount increased for higher temperature to 94%. Accordingly, when using OrgP, the desorption efficiency improved to 94% and 97% for 70°C and 130°C, respectively.

It can be concluded that MSA managed to increase the regeneration efficiency of both Org and OrgP, resulting in higher efficiencies compared to GAC. In the case of dry gas conditions, TSA shows very good results for the Org and OrgP sorbents, since an average of 81% and 91%, respectively, was reported, while the corresponding value of GAC was 77%. The values of Org/OrgP and GAC were fairly similar in the MSA mode, namely 85-90%. However, in the case of wet gas, the performance of Org/OrgP was exceptionally better compared to GAC; an average of 90% was reported for Org/OrgP, while GAC's regeneration efficiency under the same conditions was slightly below 80% (~79.5%).

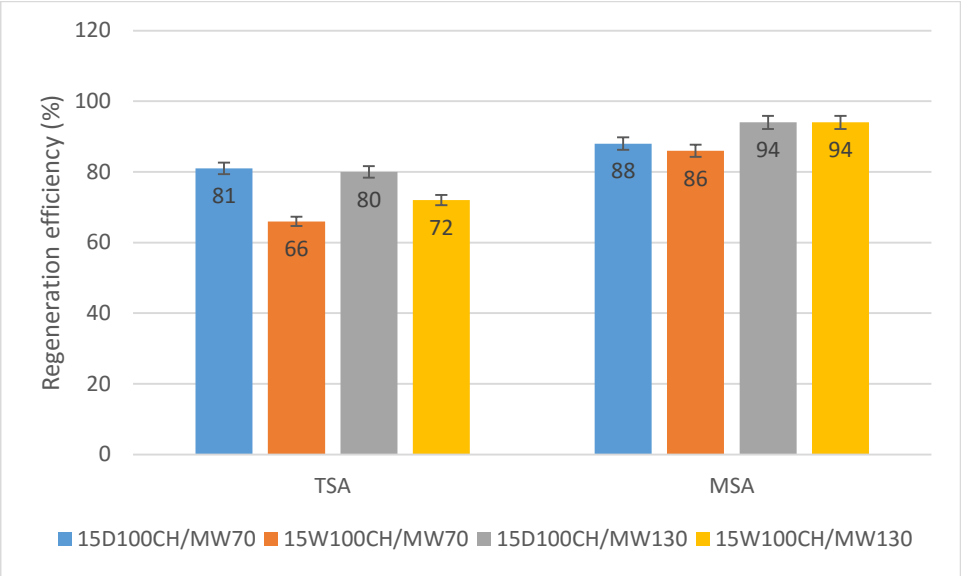

Figure 5.22: Comparison of the regeneration efficiency of Org for MSA and TSA at 70°C and 130°C at dry/wet gas conditions

The reasons for the above results are due to the differences in the way moisture was distributed in the samples; firstly, fine powders and small granules (<1mm) present strong cohesive forces between particles, tending to agglomerate when mixing with moisture content. In this form, the moisture is similar to bound water and it is difficult to remove with microwave energy (Standish et al., 1991). Another reason for the better performance of the large granules is associated with the differences in permeabilities. During microwave heating of granular materials, moisture movement to the surface occurs by both liquid and vapour mass flow. For low permeability, which is the case for small particles (GAC and OrgP), vapour pressure can build up inside the fixed bed and water droplets can be expelled, a phenomenon referred to as liquid pumping ensues (Perkin, 1983). As a result, it is reasonable to point out that in the case of a wet flue

gas, sorbents with large particle sizes (large granules >1mm, or pellets) may be preferred (Standish et al., 1988).

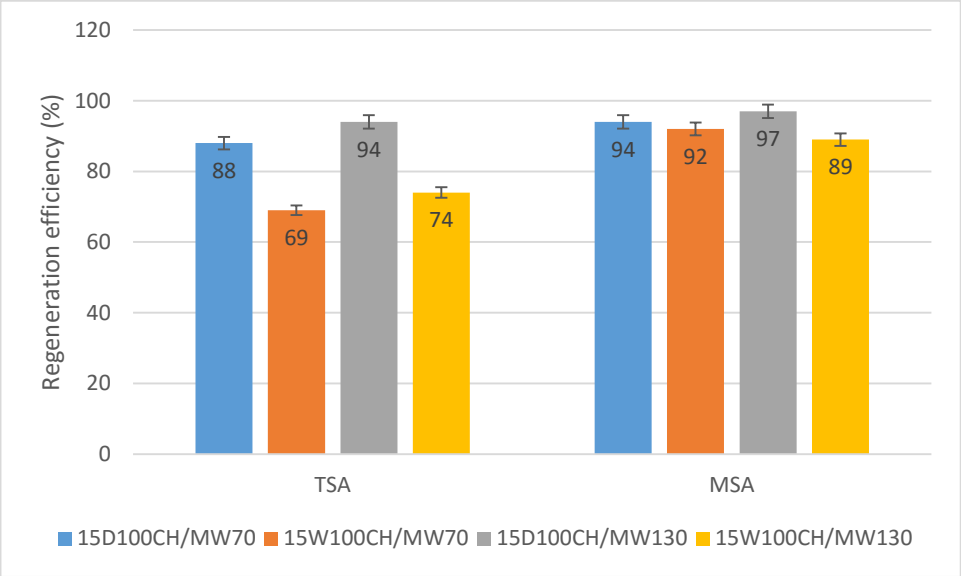

Figure 5.23: Comparison of the regeneration efficiency of OrgP for MSA and TSA at 70°C and 130°C at dry/wet gas conditions

5.3.2.3. Desorption kinetics

The next parameter that was investigated was the desorption kinetics of Org and OrgP during MSA and TSA. As discussed in Section 4.4.3, 70% recovery was selected as the optimum desorption condition, balancing between energy consumption and time needed for the desorption to be accomplished. As a result a comparison of t_{70}, i.e. the time needed for 70% CO_2 recovery, between MSA and TSA modes are presented next.

The following figures (Figure 5.24 and 5.25) present a direct comparison of the t_{70} between MSA and TSA for two different temperatures, 70°C and 130°C for both dry and wet gas conditions. Specifically, Figure 5.24 presents the results obtained from desorption experiments using Org, while 5.23 describes the t_{70} comparison for the case of OrgP. It is clear that TSA is a more time-consuming process, needing an average of ~5.0 minutes to reach t_{70} when heating at 70°C, while the increase in temperature to 130°C did not seem to play an important role, since t_{70} only decreased to an average of ~4.9 minutes. This suggests that CO_2 is desorbed at lower temperatures, before reaching 130°C, being in agreement with previous studies (Plaza et al., 2011), where it was reported that TSA at 100°C was sufficient to achieve full regeneration of the

activated carbon. This is an important observation for the process, since the use of a lower temperature during desorption is directly associated with lower energy consumption. In contrary, MSA intensified the CO_2 desorption kinetics for both dry and wet gas conditions, by managing to decrease the time needed by as much as 48%, resulting in a t_{70} process that took an average of 2.6 minutes to be accomplished for OrgP, being in agreement with the observations reported for the CO_2 desorption profiles in Section 5.3.2.1. It is interesting to point out that even though MSA managed to accelerate the CO_2 desorption process from Org as well, the decrease in t_{70} was smaller compared to OrgP; Figure 5.24 shows that an average of 2.9 minutes were needed in the case of OrgP, resulting in a 35% reduction, 13% less than Org. This can be associated to the differences in the size of the bed formed for Org and OrgP, combined with the different penetration depth that they possess (Tables 5.2 and 5.3); materials with high values of loss factor are characterised by lower values of penetration depth, meaning that microwaves can totally be absorbed within the outer layers of the material (Bogdal, 2005). For example, in the case of OrgP (with penetration depth of 3.2cm), the total microwave power is absorbed faster while the waves penetrate the material, compared to Org (with penetration depth of 3.8cm). As a result heat is generated faster in the case of OrgP and is then transferred to the rest of the bed via conduction. A smaller bed size (diameter: 2cm and height: 4.4cm), compared to Org (diameter: 2cm and height 5.5cm) also enhances the heating via conduction resulting in faster heating rates for OrgP, as seen when comparing Figures 5.24 and 5.25.

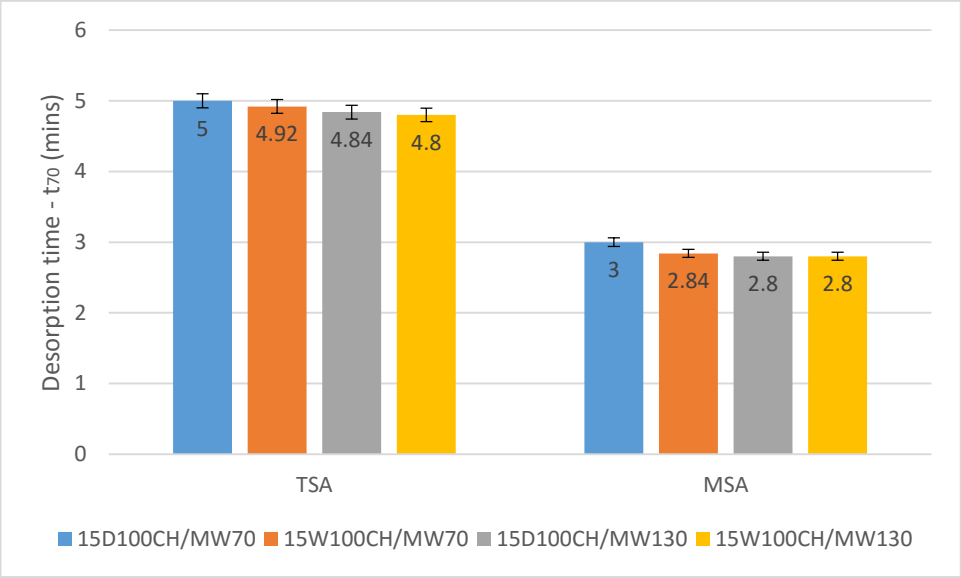

Figure 5.24: Comparison of t_{70} for MSA and TSA using Org when heating at 70°C for dry/wet gas conditions

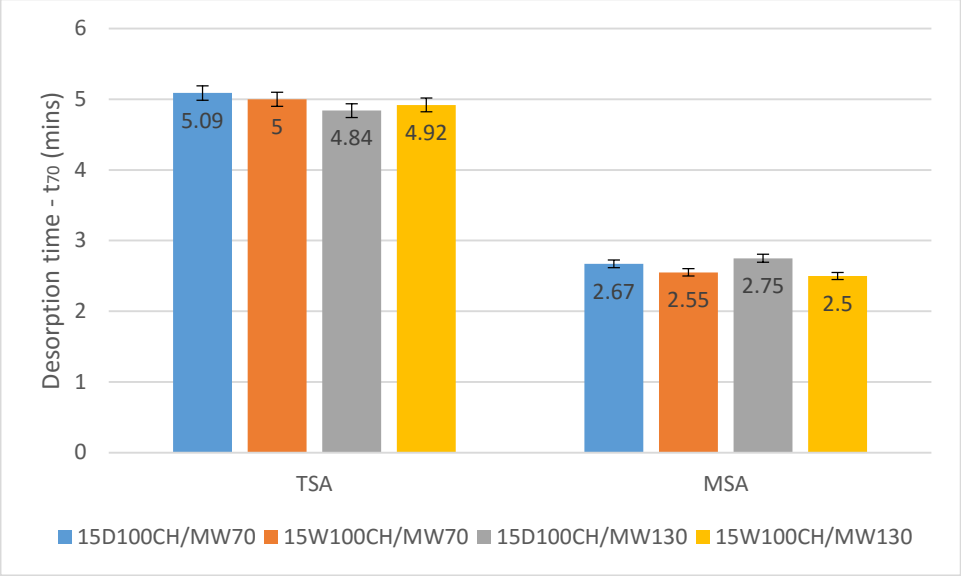

Figure 5.25: Comparison of t_{70} for MSA and TSA using OrgP when heating at 70°C for dry/wet gas conditions

5.3.2.4. Energy consumption

The last parameter under investigation for the comparison of TSA and MSA is the energy consumption during the regeneration of Org and OrgP. As explained in Section 4.4.4, the energy consumption is directly associated with the thermal and dielectric properties of the material and as a result it is forecasted that MSA would lead to lower consumption compared to TSA in this scenario. Moreover, taking into consideration the relation between material density, porous structure and size with microwave absorption previously discussed (Sections 5.1.2, 5.2.3 and 5.3.2.2), it can also be expected that the Org and OrgP adsorbents would present very promising results with regards to energy consumption measurements, compared to GKAS and GKAS-N.

Figures 5.26 and 5.27 describe the comparison of energy usage (kWh/kg) between TSA and MSA for two different temperatures (70°C and 130°C) and dry/wet gas conditions, for Org and OrgP, respectively. As expected, MSA achieved an important decrease in the energy consumed during the desorption step (E_{70}); it is clear that for every set of experiments E_{70} was reduced by at least 35%, with the best result deriving from the 130°C desorption temperature. Specifically, when an output temperature of 70°C was selected, a decrease from 0.63 to 0.33 kWh/kg_{sorb} and from 0.62 to ~0.4 kWh/kg_{sorb} during desorption for dry and wet gas conditions, respectively, was reported. This decline was even more radical in the case of 130°C, where instead of 0.97 and 0.9 kWh/kg_{sorb}, only ~0.44 and 0.5 kWh/kg_{sorb} were consumed. Similar values were

reported when using OrgP (Figure 5.27), with the variation of the values being in the range of the error possibility. This was to be expected, since Org and OrgP have the same C composition, derived from the same precursors, with the only difference being the particle size and shape. However, it is clear that the shape and size of the material do not alter the energy consumption during the CO_2 desorption step either for TSA or for MSA mode.

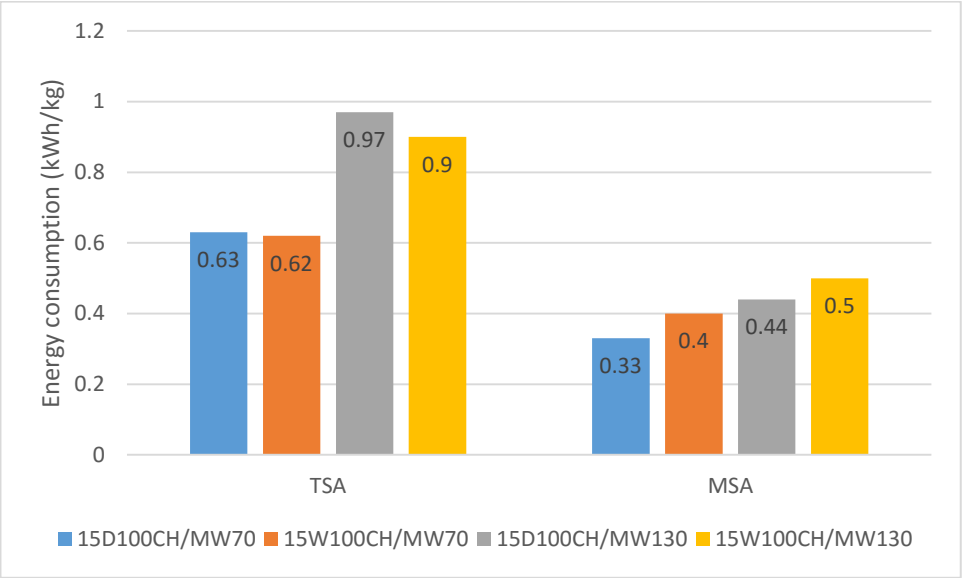

Figure 5.26: Energy consumption during Org regeneration at 70°C and 130°C for dry/wet gas conditions

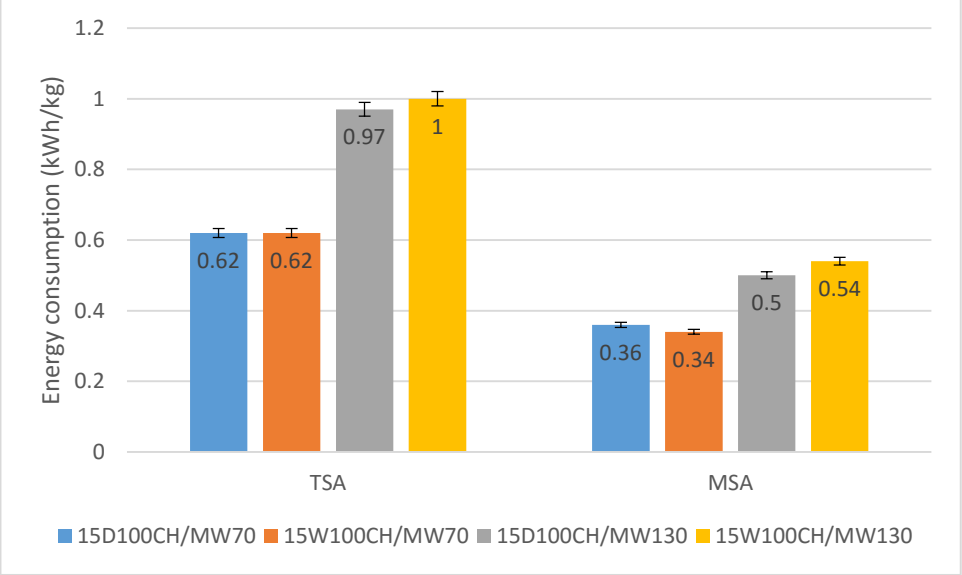

Figure 5.27: Energy consumption during OrgP regeneration at 70°C and 130°C for dry/wet gas conditions

5.3.2.5. Temperature distribution

As discussed in Section 4.5, the temperature distribution inside the bed reactor is an important factor to be considered when dealing with microwave applications. The temperature uniformity of a bed mainly depends on the material's dielectric properties, with the most influential parameter being the penetration depth, and on the bed's geometry, which is formed according to the material's shape and density. For this case, Org and OrgP generated different bed geometries, not in terms of shape (which remained cylindrical), but in terms of bed's height as discussed in Section 5.3.2.3, which directly affects the distribution of the temperature inside the bed, as seen in Figures 5.28 and 5.29. In all cases, the highest temperature was recorded at the centre line of the cylinder; in the case of 70°C, the Org and OrgP beds reached a maximum of 85°C in the centre of the cylinder, whereas in the case of 130°C the temperature went up to 152°C and 142°C for Org and OrgP, respectively. The lowest temperatures were recorded on the surface of the bed (height = 5cm), 60°C and 108°C for Org, whereas for OrgP 75°C 123°C. However, even if the patterns followed are the same for both Org and OrgP with regards to the hottest and coldest spots, it is clear that in the case of OrgP (higher density leading to lower bed height) the temperature difference inside the bed is smaller than in the case of Org; OrgP presents a ΔT_{bed} of 10°C when the target temperature is 70°C (ΔT_{bed} = 20°C when heating at 130°C), while in the case of Org the ΔT_{bed} increases to 25°C (44°C when heating at 130°C). Between the surface and the centre of the bed, a linear temperature distribution is evident for both cases.

As previously discussed, another important parameter influencing the temperature distribution of the bed during microwave heating is the penetration depth of the target material. In microwave heating, due to the penetrative power of microwaves, heat can be generated from within the material itself as a result of the absorption of microwave energy by the material directly. The penetration depth varies among materials and among different geometries, resulting in different temperature distributions inside the bulk of the sorbent materials (Gupta and Wung, 2007). Comparing the heating of the GAC fine granules with the large granules of Org, it is clear that in the case of GAC the highest temperatures recorded were lower, namely 78°C and 143°C for heating at 70°C and 130°C respectively. This can associated to the difference in D_p values of both samples, reported in Section 5.1.2 ($D_{P_{Org}} = 3.8cm$ while $D_{P_{GAC}} = 2.2cm$). This means that the microwave penetration into the Org sample is not limited on its outer layer but

continues further to the core of the bed, while in the case of GAC the energy penetrating inside the bed cylinder is reduced faster. In other words, GAC has the ability to absorb microwave power faster than Org and OrgP, transforming it to heat that then is dispersed into the rest of the material by conduction. This results in significantly less temperature difference inside the bulk of the bed for GAC compared to Org and OrgP.

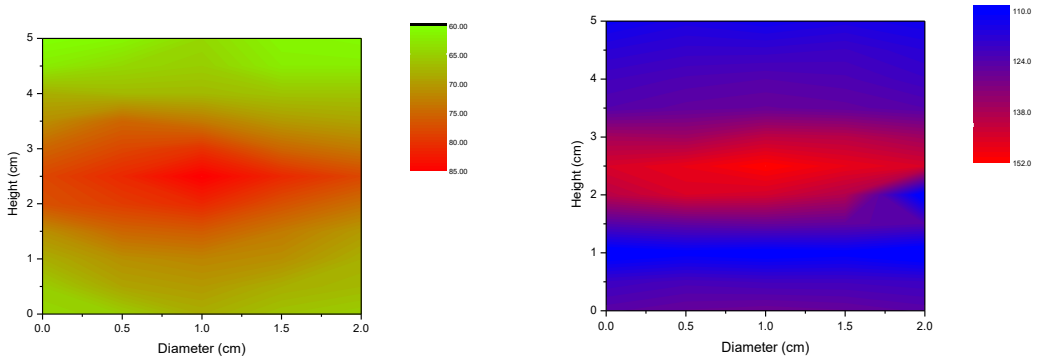

Figure 5.28: Heat map of the Org bed when heated with MSA at (a) 70°C and (b) 130°C

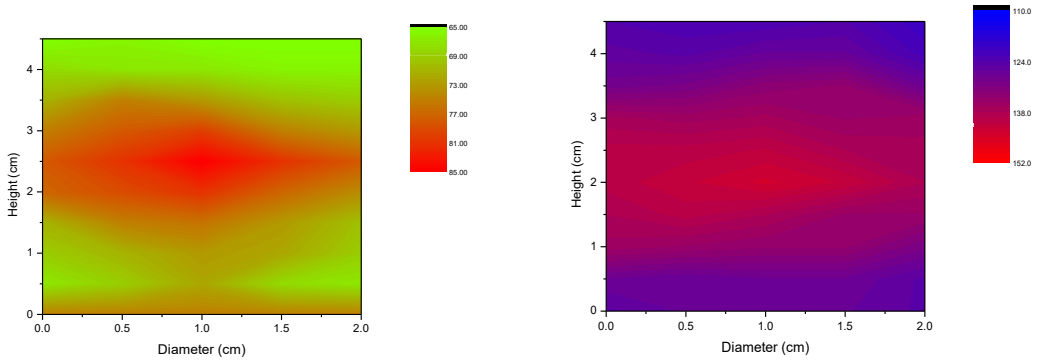

Figure 5.29: Heat map of the OrgP bed when heated with MSA at (a) 70°C and (b) 130°C

From the above heat maps, it can be concluded that predicting temperature distribution during microwave heating is a difficult task and is certainly affected by the dimensions of the target object, since temperature gradients from 60°C to 80°C and from 110°C to 150°C were reported when heating Org and OrgP to 70°C and 130°C. Even if these materials present excellent dielectric properties as seen in Section 5.1.2, they are still heated in a non-uniform way. Prediction models of temperature distribution for different geometries and bed sizes is an important field of study that is also suggested in the future work chapter (Section 6.2)

5.3.3. Conclusions for Org and OrgP

In this section, the performance of another two carbon based sorbents for CO_2 capture and regeneration under TSA and MSA was evaluated. The first sample, Org, was composed by large granules, whereas the second sample, OrgP derived from grinding the Org granules to form a powdered activated carbon. The aim of this study was to evaluate the performance of those sorbents, trying to examine possible relations between the shape of the sorbent and MSA. It was shown that both samples presented excellent dielectric properties, close to the ones reported for GAC in Chapter 4. As a result, MSA managed to intensify the CO_2 desorption process in the cases of Org and OrgP, in terms of regeneration efficiency, kinetics and energy consumption, compared to TSA, due to their excellent dielectric nature that enables high heating rates and efficient heating of the bulk.

However, the density of the samples was different, resulting in the creation of a different shaped sorbent bed packing inside the reactor, with the OrgP being more compact shaped compared to Org. This compact packing, combined with the smaller penetration depth of OrgP, resulted in a better temperature distribution inside the bed when heating it with MSA, compared to both Org and GAC. Moreover, a comparison of the desorption kinetics showed that materials of the same nature but with lower penetration depth can present higher desorption rates, since their heating rates are higher, due to their ability of absorbing the microwaves faster (OrgP). As a result, it can be concluded that fine granules (<1mm), or powder materials are favoured by the microwave heating, since they create a more compact sorbent bed that is heated faster and more uniformly, compared to a structure that consists of large granules (>1mm) or pellets.

On the other hand, in the case of wet gas applications, large granules or pellets should be considered as better candidates, compared of powdered materials, since the moisture content seems to affect both adsorption and MW desorption processes; during adsorption, a fine powder tends to agglomerate when adding moisture to the gas mixture, prior to its CO_2 saturation and as a result, equilibrium time is reached faster. On the other hand, in the case of larger particles, there is no sign of agglomeration, since there is enough space for the H_2O to be deposited between the large granular particles inside the material bed. Furthermore, in the case of MSA regeneration, apart

from the difficulty in regenerating an agglomerated material, another reason for the better performance of the large granules is associated with the differences in permeabilities. During microwave heating of granular materials, moisture movement to the surface occurs by both liquid and vapour mass flow. For low permeability, which is the case for small particles (GAC and OrgP), vapour pressure can build up inside the fixed bed and water droplets can be expelled, affecting the CO_2 desorption regeneration efficiency of the sample. As a result, it is safe to point out that in the case of a wet flue gas, sorbents with large particle sizes (large granules >1mm, or pellets) may be preferred.

5.4. Silica based materials

Previous sections have focused on carbon-based materials for CO_2 capture evaluated using TSA and MSA systems for the desorption step. These materials, along with zeolites, present a remarkable CO_2 adsorption capacity at low temperature applications (Arenillas et al., 2005; Wahby et al., 2010). However, van der Vaart et al. (2000) and Siriwardane et al. (2001) reported that this dynamic adsorption potential decreases significantly for processes with low CO_2 partial pressures, as proven in Section 4.2.1 as well. As a result, there is a need to investigate other materials that could potentially overcome the aforementioned barriers. Sanz-Perez et al. (2013) suggested the use of hybrid organic–inorganic materials produced from incorporation of organic groups to an inorganic matrix, such as mesostructured silicas, taking advantage of their excellent structural properties (Xu et al., 2003, Harlick and Sayari, 2007). As a result, this section focuses on a different adsorbent, namely a silica based material (SBA TEPA), which was produced and characterised in Rey Juan Carlos University, Spain, being part of a scientific collaboration. Its organic nature was generated by impregnating the calcined SBA-15 with tetraethylenepentamine (TEPA, = 0.998 g/mL), by wet impregnation, producing 2 g of SBA TEPA. Due to the TEPA's degradation at elevated temperatures (>120°C), regeneration of the material is only undertaken at mild temperatures (50-100°C). As a result, only one temperature was examined in this case, namely 70°C. The main objective of this section is to evaluate the possibility of using MSA for the regeneration of SBA TEPA, an adsorbent that has already shown excellent capture potential (Sanz-Perez et al., 2013), in order to enhance the CO_2 desorption process.

Table 5.4: Results obtained from TSA experiments using SBA TEPA under dry and wet feed gas conditions

Parameter	CO_2 adsorbed (g)	CO_2 adsorption per g_{sorb}(%)	Regeneration efficiency (%)	t_{70} (mins)	E_{70} (kWh/kg)
15D100CH70	0.12	8.6	88.24	7.4	3.32
15W100CH70	0.138	9.9	81.4	8.25	3.78

Table 5.4 summarises the results obtained from TSA experiments using SBA TEPA under dry and wet feed gas conditions. It is clear that this sorbent presents very good CO_2 dynamic adsorption potential, namely 8.6% and ~10% per g of sorbent for dry and wet gas, respectively, indicating that moisture had a positive effect on CO_2 capture. This result is in accordance with previous studies (Sanz-Perez et al., 2013), where it is stated that a rise in the sorbent's CO_2 capture capacity is expected under a wet adsorption feed gas mixture compared to dry gas conditions due to the development of carbonate and bicarbonate that results in doubling the 0.5 CO_2/N molar ratio, reported for anhydrous conditions (formation of carbamate). After the completion of the adsorption step, desorption under TSA was evaluated. It was reported that SBA TEPA presents very high regeneration efficiency, especially when dry gas is used, namely 88% when heating to 70°C. However, it is also evident that it presents poor desorption kinetics, since a total of 7.43 and 8.25 minutes are needed for 70% of desorption to take place, resulting in a 60% more time-consuming process, compared to the carbon based sorbents. Moreover, the energy use (E_{70}) is also higher than all the other cases investigated in this research, since 3.3kWh/kg and 3.8kWh/kg are consumed during 70% regeneration for dry and wet gas conditions, respectively.

The poor performance during regeneration of SBA TEPA under TSA mode can also be seen in Figure 5.30. The desorption profile of SBA TEPA is quite different compared to the profiles of the carbon based sorbents examined in this research, since it does not follow neither the log-normal nor the Rayleigh distributions; the $[CO_2]_{out}$ desorption peak occurs after 100 seconds, which was to be expected according to previous results reported before, however the desorption seems to come to an abrupt end immediately after this peak. As a result, there is a quick decrease in the amount of $[CO_2]_{out}$, which after ~200 seconds stabilizes and returns to the tail reported for the carbon based

sorbents. Nonetheless, this tail does not reach an asymptote even after 1000 seconds, with the regeneration being continued at very low levels of $[CO_2]_{out}$.

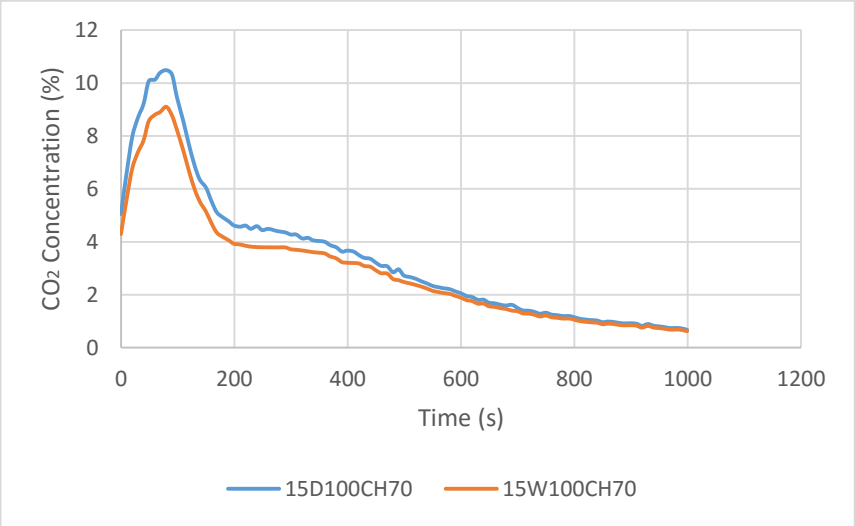

Figure 5.30: Time dependent CO_2 outlet concentration profiles during SBA TEPA regeneration at 70°C for dry/wet gas conditions TSA

As a result, the reasonable next step with regards to SBA TEPA research is to examine new pathways for its regeneration. Based on the results of MSA that were reported in this study, one interesting desorption technology that could possibly intensify the regeneration process of SBA TEPA is microwave heating. However, as reported in Section 5.1.2, SBA TEPA is a very poor dielectric material with almost zero microwave absorption potential. Nonetheless, one possible mechanism to overcome this barrier could be by mixing the sorbent material with a microwave susceptible material such as silicon carbide (SiC), as explained in Section 2.2.9. Consequently, fine powder of SiC was purchased from Sigma-Aldrich with particle size of 37-74 μm.

Three different attempts were studied, namely mixing SBA TEPA with SiC in three different weight proportions, namely 1:1, 1:2 and 1:3 and the heating rates at MSA mode with a target temperature of 70°C are reported in Figure 5.31. It is apparent that when using SBA TEPA without mixing it with SiC, the sorbent bed is not heated at all, increasing its temperature from 19°C to only 22°C after 6 minutes of MW heating. It is also clear that the more quantity of SiC used, the easier it gets to heat the bed, with the best performance reported in the case of mixing SBA TEPA with SiC at a 1:3 (w/w) ratio. However, even in this case, the bed is not heated to 70°C, which was the output temperature, but it only reaches ~60°C after 6 minutes of heating. This outcome is still

not desirable, having in mind that the carbon based sorbents were heated to 70°C after only ~1 minute of MW, as reported in Section 4.3. As a result, no MSA experiments were conducted in this case, however this could potentially be an interesting field of research for future studies.

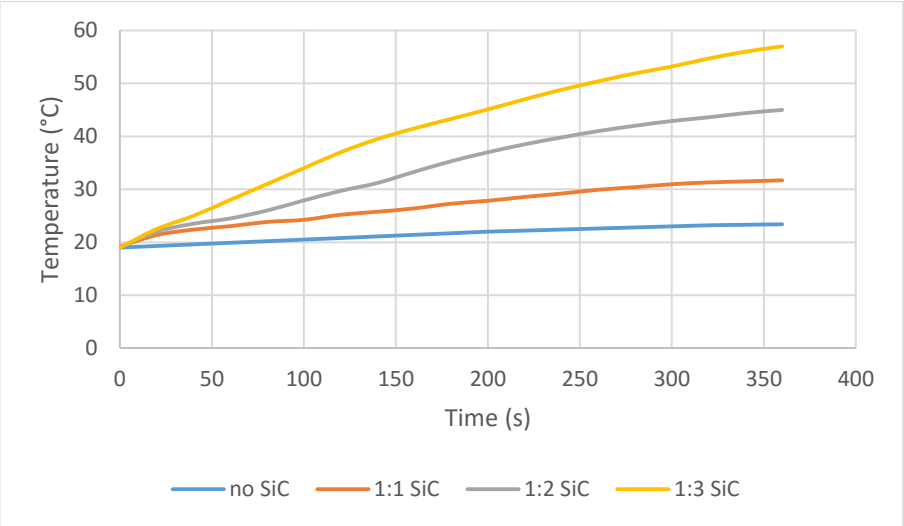

Figure 5.31: Heating rates process comparison of MW and CH for 70°

5.5. Conclusions

In this chapter, the performance of four carbon based and one silica based sorbents for CO_2 capture and regeneration under TSA and MSA was evaluated. The aim of this chapter was to relate the performance of those sorbents with physical, textural or chemical properties. As a result, sorbents that presented different geometries (large granules, such as Org and powders such as OrgP and SBA TEPA) and different chemical functionalities (basic NH_3 modified sorbents, GKAS-N and TEPA impregnated SBA, SBA-TEPA) were chosen to be compared with the performance of GAC, used as the reference material from Chapter 4.

Firstly, the influence of basic functionalities on carbon based sorbents on the adsorption/desorption performance was examined. It was shown that the GKAS sample did not present desirable dielectric properties, which had a noticeable influence on its performance during MSA. This result was not expected since GKAS chemical analysis showed a similar composition with the other carbon based sorbents that presented excellent microwave absorption potential. One possible explanation of this result was

that GKAS possesses limited transport pores. In general, the higher the pore volume of a sorbent material, the lower its electrical conductivity, however, when microwave heating is applied this relation is more complex; as the electrical conductivity decreases, the penetration depth increases which means that microwaves can penetrate a bulk sample more efficiently. This can be attributed to the fact that there is appropriate space inside the bulk of the material which possibly favours the reflection of microwaves, thus increasing the propagation paths into the adsorbent, the extend depending on the fraction of porosity. As a result, the microwave absorption potential is proportional to the pore volume of the material, as seen for the case of GKAS-N, Org and OrgP.

As a result, it can be concluded that the pore volume of a material plays a critical role in the desorption process when using MSA. The existence of large pore volume inside a sorbent seems to enhance the MW, since it provides more space for the waves to be reflected, resulting in a more efficient microwave absorption. Moreover, the introduction of NH_3 to the material's surface is another parameter that affects the MSA process, since the use of a polar element enhances the heating and consequently its desorption performance. Furthermore, GKAS-N presented higher CO_2 adsorption capacities, compared to the non-impregnated samples. As a result impregnation may be preferred when dealing with low CO_2 partial pressures in the feed gas mixture.

Looking at the influence of the shape of the sorbent on MSA and TSA, the samples Org (large granules) and OrgP (powder produced from the grinding of Org) were evaluated. It was shown that both samples presented remarkable dielectric properties, close to the ones reported for GAC in Chapter 4. However, due to the difference in shape, the density of the bed was different. This resulted in the creation of a different shaped sorbent bed packing inside the reactor, with the OrgP being more compact shaped compared to Org. This compact packing resulted in a better temperature distribution inside the bed when heating it with MSA, compared to Org bed which presented extensive void spaces between the particles. As a result, it can be concluded that fine granules (<1mm), or powder materials are favoured by the microwave heating, since they create a more compact sorbent bed that is heated faster and more uniformly, compared to a structure that consists of large granules (>1mm) or pellets.

However, it was reported that MSA managed to intensify the CO_2 desorption process in both cases of Org and OrgP as well, compared to TSA, in terms of regeneration efficiency, kinetics and energy use. Both pelletized and powder materials showed excellent dielectric character and as a result the decision between those two shapes depends only on the application and the process parameters, namely pressure drop. However the low CO_2 static as well as dynamic adsorption capacities that Org and OrgP presented, is a factor that needs to be taken into account. One interesting future study could be the modification of Org and OrgP with NH_3 functionalities (as in the case of GKAS and GKAS-N) in order to enhance their CO_2 adsorption/desorption potential as happened in the case of GKAS, however this study is beyond the aims of this research.

However, in the case of wet gas applications, large granules or pellets should be considered as better candidates, compared to powdered materials, since the moisture content seems to affect both adsorption and MW desorption processes; during adsorption, a fine powder tends to agglomerate when adding moisture to the gas mixture, prior to its CO_2 saturation resulting in faster equilibrium times. On the other hand, in the case of larger particles (>1mm), there was no sign of agglomeration, since there is enough space for the H_2O to be deposited between the large granular particles inside the sorbent bed. Moreover, in the case of MSA regeneration, apart from the difficulty in regenerating an agglomerated material, another reason for the better performance of the large granules is associated with the differences in permeabilities. During microwave heating of granular materials, moisture movement to the surface occurs by both liquid and vapour mass flow. For low permeability, which is the case for small particles (GAC and OrgP), vapour pressure can build up inside the fixed bed and water droplets can be expelled, affecting the CO_2 desorption regeneration efficiency of the sample. As a result, it is safe to conclude that in the case of a wet flue gas, sorbents with large particle sizes (large granules >1mm, or pellets) may be preferred.

Finally, an impregnated silica based powder (SBA TEPA) was also selected for evaluation of MSA and TSA processes. This material was selected because it has been reported as an excellent CO_2 sorbent that can overcome the barriers set from the post-combustion process parameters, namely low CO_2 partial pressures and elevated temperatures. This sorbent showed very good results regarding CO_2 dynamic adsorption capacities, which were also enhanced by the presence of moisture. However,

the regeneration of this material is regarded as the crucial step for this sorbent, since the CO_2 desorption process is time- and energy-consuming when using TSA, compared to the carbon based sorbents. Unfortunately, SBA TEPA is not an efficient microwave absorbent and the packed bed was not heated effectively even after mixing the sorbent with a ratio of 1:3 with SiC, a material that presents excellent dielectric properties. As a result, the evaluation of MSA for this sorbent was not feasible.

References

Bogdal, D. (2006) *'Microwave Assisted Organic Synthesis. One Hundred Reaction Procedures'*, Tetrahedron Organic Chemistry Series; Elsevier: Amsterdam, vol. 25

Bouledjnib, L. and Sahli, S. (2010) '*Investigation Of Pores Influence on Dielectric Constant Value in Low k Materials Using Monte Carlo Method*', M. J. Condensed matter, vol. 12 (3), pp. 199-203

Caplow, M. (1968) '*Kinetics of carbamate formation and breakdown*', J. Am. Chem. Soc., vol. 90, pp. 6795–6803

Craven, J.M., Swithenbank, J., Sharifi, V.N., Peralta-Solorio, D., Kelsall, G. and Sage, P. (2014) '*Development of a novel solids feed system for high pressure gasification'* Fuel Processing Technololy, Vol. 119, pp. 32–40

Crooks, J.E. and Donnellan, J.P. (1989) '*Kinetics and mechanism of the reaction between carbon dioxide and amines in aqueous solution',* J. Chem. Soc., vol. 2, pp. 331–333

Drage, T.C., Arenillas, A., Smith, K.M., Pevida, C., Piippo, S. and Snape, C.E., (2007) '*Preparation of carbon dioxide adsorbents from the chemical activation of urea–formaldehyde and melamine–formaldehyde resins',* Fuel, vol. 86,pp. 22–31

Fan, Y. Z., Yang, H. B., Li, M. H. and Zou, G. T., (2009) '*Evaluation of the microwave absorption property of flake graphite',* Mater. Chem. Phys., vol. 115, pp. 696−698

Grande, C.A. and Rodrigues, A.E. (2008) '*Electric swing adsorption for CO_2 removal from flue gases',* International Journal of Greenhouse Gas Control, vol. 2, pp. 194–202

Gray, M.L., Soong, Y., Champagne, K.J., Baltrus, J., Stevens Jr, R.W., Toochinda, P. and Chuang, S.S.C. (2004) '*CO_2 capture by amine-enriched fly ash carbon sorbents'*, Separation and Purification Technology, vol. 35, pp. 31–36

Gupta, M. and Wong W. (2007) '*Microwaves and metals'*, John Wiley & Sons (Asia) Pte. Ltd, Singapore

Hartnett, J., Irvine, T., Cho Y. and Greene, G. (1999) '*Advances in Heat Transfer'*, Vol. 33, pp. 1-524, ISBN: 978-0-12-020033-7

Ho, P.S. (2003) '*Low Dielectric Constant Materials for IC Applications'*, Springer, Berlin, Germany

Jansen, R.J.J. and Bekkum, H. (1994) '*Amination and ammoxidation of activated carbons'*, Carbon, vol. 32, pp. 1507–1516

Lestreiz, B., Maazouz, A., Gerard, J.F., Sautereau, H., Boiteux, G., Seytre G. and Kranbuehl, G.E. (1998) *'Is the Maxwell–Sillars–Wagner model reliable for describing the dielectric properties of a core–shell particle–epoxy system?'* Polymer, vol. 39 (26), pp. 6733–6742

Li, G., Xie, T., Yang, S., Jin, J. and Jiang, J. (2012) '*Microwave Absorption Enhancement of Porous Carbon Fibers Compared with Carbon Nanofibers*', Journal of Physical Chemistry, vol. 116, pp. 9196−9201, dx.doi.org/10.1021/jp300050u |

Maroto-Valer, M.M., Lu, Z. Zhang, Y. and Tang, Z. (2008) '*Sorbents for CO_2 capture from high carbon fly ashe's*, Waste Management, vol. 28, pp. 2320–2328

Maroto-Valer, M.M., Tang, Z. and Zhang, Y. (2005) '*CO_2 capture by activated and impregnated anthracites'*, Fuel Processing Technologies, vol. 86, pp. 1487–1502

Metaxas, A.C. and Meredith, R.J. (1983) '*Industrial Microwave Heating'*, Peter Peregrinus Ltd., London, UK

Najm, I.N., Snoeyink, V.L., Lykins, B.W. and Adams, J.Q. (1991) '*Using Powdered Activated Carbon: A Critical Review'*, Journal of American Water Association, vol. 83 (1), pp. 65-76

Pappacena, K.E. (2008) '*Thermal properties of wood-derived silicon carbide and copper–silicon carbide composites'*, PhD Thesis, Northwestern University

Pevida, C., Drage, T.C. and Snape, C.E. (2008) '*Silica-templated melamine–formaldehyde resin derived adsorbents for CO_2 capture*', Carbon, vol. 46, pp. 1464–1474

Pevida, C., Plaza, M.G., Arias, B. Fermoso, J., Rubiera, F. and Pis, J.J. (2008) '*Surface modification of activated carbons for CO_2 capture'*, Applied Surface Science, vol. 254, pp. 7165–7172

Plaza, M.G., García, S., Rubiera, F., Pis, J.J. and Pevida C. (2011) '*Evaluation of ammonia modified and conventionally activated biomass based carbons as CO_2 adsorbents in postcombustion conditions'*, Separation and Purification Technology, vol. 80, pp. 96–104, doi:10.1016/j.seppur.2011.04.015

Plaza, M.G., Pevida, C., Arias, B., Fermoso, J., Arenillas, A., Rubiera, F. and Pis, (2008) '*Application of thermogravimetric analysis to the evaluation of aminated solid sorbents for CO_2 capture*', Journal of Thermal Analysis and Calorimetry., Vol. 92, pp. 601–606

Plaza, M.G., Pevida, C., Arias, B., Fermoso, J., Casal, M.D., Martín, C.F., Rubiera, F. and Pis, J.J. (2009) '*Development of low-cost biomass-based adsorbents for postcombustion CO_2 capture'*, Fuel, vol. 88, pp. 2442–2447

Plaza, M.G., Pevida, C., Martín, C.F., Fermoso, J., Pis, J.J. and Rubiera, F. (2010) '*Developing almond shells-derived activated carbons as CO_2 adsorbents'*, Separation and Purification Technology, vol. 71, pp. 102–106

Plaza, M.G., Rubiera, F., Pis, J.J. and Pevida, C. (2010) '*Ammoxidation of carbon materials for CO_2 capture*', Applied Surface Science, vol. 256, pp. 6843–6849

Przepiórski, J., Skrodzewicz, M. and Morawski, A.W. (2004) '*High temperature ammonia treatment of activated carbon for enhancement of CO_2 adsorption'*, Applied Surface Science, vol. 225, pp. 235–242

Radosz, M., Hu, X., Krutkramelis, K. and Shen, Y. (2008) '*Flue-gas carbon capture on carbonaceous sorbents: toward a low-cost multifunctional carbon filter for ''green'' energy producers'*, Industrial and Engineering Chemistry Research., vol. 47, pp. 3783–3794

Ribeiro, M., Neto, P. and Pinho, C. (2010) *'Mean porosity and pressure drop measurements in packed beds of monosized spheres: side wall effects'*, International Review of Chemical Engineering, vol. 2 (1), pp. 40–46

Sanz-Pérez, E.S., Olivares-Marín, M., Arencibiac, A., Sanz, R., Callejac, G. and Maroto-Valer, M.M. (2013) '*CO_2 adsorption performance of amino-functionalized SBA-15 under post-combustion conditions'*, International Journal of Greenhouse Gas Control, vol. 17, pp. 366–375, http://dx.doi.org/10.1016/j.ijggc.2013.05.011,

Sarkar, S.C. and Bose, A. (1997) *'Role of Activated Carbon Pellets in Carbon Dioxide Removal'*, Journal Energy Conservation Management, vol. 38, pp. 105-110

Satyapal, S., Filburn, T., Trela, J. and Strange, J. (2001) '*Performance and properties of a solid amine sorbent for carbon dioxide removal in space life support applications'*, Energy Fuels, vol. 15, 250–255

Schubert, H. and Regier M. (2005) '*The Microwave Processing of Foods'*, CRC Press Woodhead Publishing, Boca Raton, FL, USA

Siriwardane, R.V., Shen, M.-S., Fisher, E.P. and Poston, J.A. (2001) '*Adsorption of CO_2 on molecular sieves and activated carbon'*, Energy Fuels, vol. 15, pp. 279–284

Sjostrom, S. and Krutka, H., (2010) '*Evaluation of solid sorbents as a retrofit technology for CO_2 capture'*, Fuel, vol. 89, pp. 1298–1306

Standish, N., Worner, H.K. and Obuchowski, D.Y. (1991) '*Particle size effect in microwave heating of granular materials'*, Powder Technology, Vol. 66, pp. 225–230

Suzuki, M., (1993) '*Fundamentals of Adsorption'*, edition IV, Kodansha, Tokyo

Totten, G.E., Funatanim, K. and Xie, L. (2004) '*Handbook of metallurgical process design*' CRC Press

Xu, X., Song, C., Andrésen, J.M., Miller, B.G. and Scaroni, A.W. (2003) '*Preparation and characterization of novel CO_2 Molecular Basket adsorbents based on polymermodified mesoporous molecular sieve MCM-41'*, Microporous Mesoporous Materials, vol. 62, pp. 29–45

Yu, C.H., Huang, C.H. and Tan, C.S. (2012) '*A Review of CO_2 Capture by Absorption and Adsorption'*, Aerosol and Air Quality Research, vol. 12, pp. 745–769, doi: 10.4209/aaqr.2012.05.0132

Zhao, L., Baccile, N., Gross, S., Zhang, Y., Wei, W., Sun, Y., Antonietti, M. and Titirici, M.M. (2010) '*Sustainable nitrogen-doped carbonaceous materials from biomass derivatives'*, Carbon, vol. 48, pp. 3778–3787

Zhao, L., Bacsik, Z., Hedin, N., Wei, W., Sun, Y., Antonietti, M. and Titirici, M.M. (2010), '*Carbon dioxide capture on amine-rich carbonaceous materials derived from glucose'*, Chemistry and Sustainability., vol. 3, pp. 840–845

Zou, R. P. and Yu, A.B. (1995) *'The packing of spheres in a cylindrical container: the thickness effect'*, Chemical Engineering Science, vol. 50(9), pp. 1504-1507, doi:10.1016/0009-2509(94)00483-8

Chapter 6 – Conclusions and future work

This chapter summarises the results and conclusions derived from the experimental studies (Section 6.1). Suggestions for further work are presented in Section 6.2.

6.1. Conclusions

Carbon dioxide capture and storage (CCS) has been recognised as one of the most important technologies towards climate change mitigation, mostly due to the fact that fossil fuels are still predominant for energy production, with the International Energy Agency predicting that they will provide ~75% of the world's primary energy in 2040. There are three main pathways for CO_2 capture, namely post-combustion, pre-combustion and oxy-fuel combustion. This research focused on post-combustion capture technology, since it offers various advantages over the other technologies, the most important being that it can be retrofitted to existing plants. However, retrofitting has a significant impact in the efficiency of the power generation process, since additional energy and costs are associated with the operation of the capture plant. CO_2 capture process represents typically about 70% of the total cost of the CCS chain, and therefore, novel processes that may result in cost reductions compared to existing commercially available technologies are gaining support. The economic evaluation of a CO_2 capture system is often driven by energy demands and in adsorption technology this energy is particularly required for the desorption step. As a result, efficient regeneration systems ensuring multiple re-use of adsorbent materials, while consuming the least possible energy, are required.

To this end, this study presented and analysed a relatively new approach for CO_2 capture, namely Microwave Swing Adsorption (MSA). The aim of this research was to intensify the CO_2 desorption process from solid materials, focusing on improving the regeneration efficiency and kinetics as well as the energy spent during this step. The above aim was based on the hypothesis that the direct absorption of energy during microwave heating by the solid adsorbent, in contrast to the indirect supply of heat by thermal conduction, may enable a much faster process using a lower process temperature that would result in less energy consumption, compared to existing technologies (conventional TSA processes).

The effects of microwave regeneration of sorbent materials can vary depending on various parameters, dividing this research in two main sections, namely process parameters (Chapter 4) and materials' properties parameters (Chapter 5). In this regard, continuous adsorption/desorption tests were conducted in a lab scale MSA/TSA rig (described in Chapter 3), using solid materials with different properties.

At first, Chapter 4 presented the characterisation studies of GAC, a microporous granular activated carbon with no surface modifications operating as the reference material for this research, in terms of CO_2 adsorption capacity, dielectric properties, BET and elemental analysis. Moreover, the effects of feed gas flow rate and existence of moisture during the adsorption step were examined. Purge gas flow rate, desorption temperature, CO_2 concentration in the feed gas during adsorption and moisture content were the parameters examined during the regeneration step, in an attempt to reach to a conclusion regarding the optimum process parameters during desorption. Finally, re-utilisation of the specific material was also examined, reporting a comparison of the sorbent's properties before and after 25 consecutive MSA or TSA cycles.

With regards to the adsorption step, it was concluded that as the CO_2 concentration in the feed gas increases, the total CO_2 amount adsorbed (dynamic adsorption capacity) increases as well, since, according to the Henry's law, adsorption is proportional to the partial pressure of the adsorbed gas (in this case CO_2). Moreover, moisture content in the CO_2/N_2 binary mixture resulted in enhanced CO_2 adsorption performance; namely as a consequence of the introduction of H_2O vapors (~55°C), the total flow rate of the feed gas was increased, resulting in better adsorption performance of the GAC. Lastly, it was proven that an increase in the total flow results in increased amount of CO_2 adsorbed; a mass transfer correlation was used to prove that an increase from 1.27m/min to 2m/min would lead to an increase of ~65% of the mass transfer coefficient, favouring the CO_2 adsorption process.

Adsorption experiments were followed by experimental results from CO_2 desorption via MSA and TSA; initially, a comparison between MSA and TSA in terms of heating rates was produced. This comparison proved that microwaves have the potential to heat the bed at a faster pace to the desired desorption temperature, compared to conventional heating. Microwave heating mechanism is inherently different compared to conductive

(and convective) conventional TSA heating. During TSA heat losses, resistances in heat transfer due to the reactor and temperature gradients were observed, whereas during MSA microwaves are directly absorbed from the GAC, transforming electromagnetic energy to heat instantly. Furthermore, it was also shown that there is no risk of thermal runaway – an effect that may lead to failure of the desorption process damaging the rig - when using this material, since the heating rate was decreasing with increasing temperature. Subsequently, desorption studies were discussed, focusing on three parameters that helped evaluating the initial aim of the project, namely regeneration efficiency, desorption kinetics and energy usage. The analysis of the experimental data proved that the initial hypothesis was correct; MSA managed to intensify the CO_2 desorption process, leading to remarkable improvement of the parameters mentioned above.

Specifically, it was reported that MSA contributed to an increase in the regeneration efficiency of the GAC sample, compared to TSA. However, the values obtained were not as high as expected, especially in the case of wet gas conditions the regeneration efficiency did not manage to reach 80%, which is the lowest acceptable limit for the feasibility of a real scale CO_2 capture unit. This was attributed to the most important disadvantage of microwave heating, namely the non-uniformity in temperature distribution of the heated material. In fact, this non-uniformity can be influenced by various parameters, such as material properties, frequency and bed geometry and as a result, temperature distribution maps (heat maps) were generated for the GAC bed. These maps showed that even if the T_{av} was equal to the target temperature, its distribution was indeed not uniform; the higher temperatures were observed in the centre of the sample, whereas the lowest values were recorded on the surface of the bed.

Regeneration efficiency was followed by a comparison of CO_2 desorption kinetics during MSA and TSA. In order to determine the best regeneration conditions, deciding on a suitable compromise between CO_2 recovery amount and desorption kinetics, four different desorption times were initially reported, each indicating a different CO_2 recovery percentage. It was concluded that a 70% recovery is a feasible adjustment and as a result this compromise was used for the remaining of this research, keeping consistency regarding the comparison between MSA and TSA technologies. It was proven that MSA managed to reduce the time needed for 70% desorption to take place

by as much as 45%, which, was an important factor for the economics of the CO_2 capture process, since it directly affects the energy consumption. Furthermore, the influence of the moisture content in the feed gas mixture was also discussed. It was proven that in the case of MSA, moisture deposited on the surface of the material affects the heating process in a positive way, since a faster desorption process was observed, compared to the dry conditions. This was to be expected, since H_2O, being a dipole, is a very good microwave absorber, enhancing the heating process resulting in energy savings as well.

Energy consumption, was also compared for the case of 70% CO_2 recovery and it was proven that MSA is a more energy efficient process, compared to TSA. It was reported that an average of only 30-50% of the energy consumed during TSA is needed for MSA for the same conditions and regeneration temperature, justifying the project's initial hypothesis. Same trends appeared for every temperature investigated, however $E_{70}^{70^{\circ}C}$ was considerably lower compared to $E_{70}^{130^{\circ}C}$. As a result, taking into consideration that the regeneration efficiency and the desorption kinetics were not considerably improved by a temperature increase, it can be concluded that 70°C is an adequate desorption temperature for MSA processes.

Lastly, the possibility to use the specific material in a cyclic process was examined, taking into consideration its changes in textural characteristics, CO_2 adsorption capacity and dielectric properties after 25 consecutive adsorption/desorption cycles under MSA and TSA. BET analysis proved that pores blockage, specific surface areas and micropore volumes reduction occur to a lesser extent when using MSA, compared to TSA, after 25 cycles. However, the CO_2 adsorption capacity of the sorbent is not drastically affected by the textural changes for both processes, with the decrease being more significant when TSA is applied. The above observations lead to the conclusion that MSA has the potential to be used in a cyclic process without significant destruction of the GAC sorbent and without affecting its CO_2 adsorption potential significantly. As a result, it was concluded that MSA is a favorable technology for the case of re-utilisation of the sorbent in the CO_2 capture process.

Following the conclusions from Chapter 4, Chapter 5 focused on the study of the adsorbent parameters, highlighting the importance of raw material, adsorbent shape and

surface modifications in the economics of the desorption process. Hence, five materials were chosen for investigation - four of which were carbon based with the last one being a silica-based sorbent. The aim of this chapter was to relate the performance of those sorbents with their physical, textural and chemical properties. As a result, sorbents that presented different geometries (large granules, such as Org and powders such as OrgP and SBA TEPA) and different chemical functionalities (basic NH_3 modified sorbents, such as GKAS-N and TEPA impregnated silica sorbents, such as SBA TEPA) and have previously shown remarkable CO_2 static adsorption capacities were chosen. These materials were also tested at the MSA and TSA rigs, taking into account only the most influential parameters derived from Chapter 4; the importance of anhydrous or wet conditions as well as the desorption temperature varied, while the total flow rate and the $[CO_2]_{in}$ remained constant throughout.

Characterisation studies showed that the GKAS sample did not present desirable dielectric properties, which had a noticeable influence in its performance during MSA. A possible explanation may be that this sorbent presented a completely different porosity network compared to the other carbon based sorbents; according to numerous modelling theories (Maxwell-Wagner-Sillars, Bruggeman-Hanai and Looyenga), porosity plays an important role on the dielectric constant of a material and depends on the size, shape and distribution of pores as well as on the volume fraction of air. This factor influenced the MSA regeneration performance of GKAS and as a result the desorption profiles generated from MSA and TSA were almost identical, leading to similar desorption kinetic values. However, enhanced regeneration efficiency and reduced energy consumption during MSA compared to TSA, were to be observed. On the other hand, the GKAS-N sample (generated from modifying the surface of GKAS using NH_3) performed better as a CO_2 sorbent compared to GKAS, in terms of CO_2 adsorption potential, regeneration efficiency, desorption kinetics and energy efficiency. This performance was even more enhanced when using MSA instead of TSA, taking advantage of its excellent dielectric nature.

As a result, the existence of large pore volume inside a sorbent seems to enhance microwave heating, while the introduction of polar NH_3 to the material's surface is another parameter that affects positively the MSA process.

The next parameter that was investigated was the influence of the shape of the sorbent on the performance of MSA and TSA. As such, the samples Org (large granules) and OrgP (powder, grinded Org) were evaluated. Characterisation showed that both samples presented encouraging dielectric properties as well as microwave absorption potential. However, due to the differences in shape, the density of the bed varied, resulting in the creation of a different shaped bed packing inside the reactor, with the OrgP being more compact-shaped compared to Org. This compact packing resulted in a better temperature distribution inside the bed when heating it with MSA, compared to both Org (large granules) and GAC (fine granules). As a result, it can be concluded that materials with small particle size (powder form), are favoured by the microwave heating, since they create a more compact sorbent bed that is heated faster and more uniformly, compared to a structure that consists of large granules (>1mm) or pellets.

On the other hand, in the case of wet gas applications, large granules or pellets (Org) should be considered as better candidates, compared to powdered materials (OrgP), since the moisture content seems to affect both adsorption and MSA processes; during adsorption, a fine powder tends to agglomerate when adding moisture to the gas mixture, prior to its CO_2 saturation resulting in faster equilibrium times. On the other hand, in the case of larger particles (>1mm), there was no sign of agglomeration, since there is enough space for the H_2O to be deposited between the large granular particles inside the sorbent bed. Moreover, in the case of MSA regeneration, apart from the difficulty in regenerating an agglomerated material, another reason for the better performance of the large granules is associated with the differences in permeabilities. During microwave heating of granular materials, moisture movement to the surface occurs by both liquid and vapour mass flow. For low permeability, which is the case for small particles (GAC and OrgP), vapour pressure can build up inside the fixed bed and water droplets can be expelled, affecting the CO_2 desorption regeneration efficiency of the sample. As a result, it is safe to conclude that in the case of a wet flue gas, sorbents with large particle sizes (large granules >1mm, or pellets) may be preferred.

However, it was reported that MSA managed to intensify the CO_2 desorption process in both cases (Org and OrgP) compared to TSA in terms of regeneration efficiency, kinetics and energy use, since both materials showed excellent dielectric character. However the low CO_2 static as well as dynamic adsorption capacities that Org and OrgP

presented, is a factor that needs to be studied further. One interesting future study could be the modification of Org and OrgP with NH_3 functionalities (as in the case of GKAS and GKAS-N) in order to enhance their CO_2 adsorption/desorption potential, however this study is beyond the aims of this research.

The last material that was examined for MSA and TSA processes was an impregnated lithium based silica in powder form (SBA TEPA). The selection of this material was based on previous reports describing it as an excellent CO_2 sorbent that can overcome the barriers set from the post-combustion process parameters, namely low CO_2 partial pressures and elevated temperatures. This sorbent showed very good results regarding CO_2 dynamic adsorption capacities, which were also enhanced by the presence of moisture, being in accordance with previous evidence. However, the regeneration of this material is regarded as the decisive step for the use of this sorbent, since the CO_2 desorption process is time- and energy-consuming when using TSA, compared to the carbon based sorbents. Unfortunately, SBA TEPA is not an efficient microwave absorbent either and therefore the packed bed was not heated effectively even after mixing the sorbent with a ratio of 1:3 with SiC, a material that presents excellent dielectric properties. As a result, the evaluation of MSA for this sorbent was not feasible.

Taking into consideration the above discussion, it can be concluded that MSA has the potential to replace the TSA technology in the CO_2 capture process for every case studied in this research. MSA managed to intensify the performance of CO_2 desorption, in terms of sorbent's regeneration efficiency, desorption kinetics and energy consumption. Moreover, it was shown that consecutive MSA cycles do not destroy the sample, allowing the sorbent to last longer compared to TSA. Furthermore, lower desorption temperatures (70°C) can be applied when using MSA, having a significant effect on the economics of the process. Additionally, in order to increase the microwave heating efficiency, materials with increased porosity networks, leading to higher dielectric properties and microwave absorption capacities should be chosen. Lastly, in the presence of moisture in the exhaust gas, materials with larger size (pellets or large granules) need to be selected for an MSA process.

6.2. Recommendations for future work

As discussed above, the concept of MSA is not new, since microwave heating has been used in the past to regenerate various types of adsorbents, including silica gel, zeolites, activated carbons and polymeric adsorbents, mostly focusing on VOC removal or moisture drying. However, the use of microwave energy in the CO_2 capture technology to replace the conventional TSA and/or PSA processes is a quite unique approach and as a result there is a lot of research that needs to be done prior to commercialisation of this technology.

At first, one important point of interest for future research may be the properties of the sorbent material. This research focused only on basic surface modifications (NH_3 and TEPA), however, it would be interesting to investigate other impregnation pathways as well. Moreover, a deeper analysis on the dielectric properties of the materials and how they can be modified may optimise the microwave heating process further. As discussed in Chapter 5, it was evident that there is a connection between porosity and dielectric properties; various modelling theories have been introduced as an attempt to predict this correlation, including the Maxwell-Wagner-Sillars, Bruggeman-Hanai and Looyenga treatments. However, there is no model theory in the field of CO_2 separation using porous materials that are then regenerated via microwave heating. Furthermore, the possibility of introduction of a microwave susceptible material (such as SiC) inside a bed packed with a microwave reflective material may also be studied further.

Moreover, from an engineering point of view, it is well established that there are specific steps in order to move from the conceptual design to commercialisation, including research (lab scale), development, demonstration (pilot plant) and finally mature commercial technology. There are various reasons that still prevent the scalability of microwave technology to industrial applications; these include the effect of scale parameters (surface to volume ratio and heat loss effects), costly equipment, non-effective temperature/power and pressure control systems, changes in microwave absorption potential of the target object when scaling-up, narrow penetration depth of the radiation into the target object, non-precise prediction of process energy consumption from lab-scale microwave experiments and difficulties in forecasting the efficiency of the magnetron at high powers. As a result, there is a need for custom design for every process, which is also considerably different from the lab-scale

equipment (where typically a general-use multimode cavity is used) and the reproducibility of the results is difficult to be achieved taking into account only the lab-scale experiments (Tinga and Sutton, 1993). Consequently, a research project simulating large scale MSA plants, combined with a full techno-economic assessment of the proposed technology, may also be of interest.

Lately, there has been a lot of interest in simulating microwave heating applications inside multi-mode cavities for microwave heating applications using softwares such as COMSOL and ANSYS (Salvi et al., 2010, Santos et al., 2010, Pitchai, 2011). Computational studies can facilitate an initial prediction of temperature distributions for different geometries and reactor columns, as this is an important field of study that directly affects the efficient performance of the MSA process. Moreover, correlations between microwave heating performance and material textural characteristics may also need to be analytically studied. Furthermore, simulations may provide evidence of whether a process could be reproducible in a large scale system as well (Rosa et al., 2012). Moreover, process simulation tools, such as ASPEN HYSYS or ASPEN Plus, may also contribute to the prediction of the performance of MSA in a larger scale from a process perspective. These simulations, combined with experimental data that were presented in this thesis, may support scalability predictions of the MSA process in the CCS technology.

References

Bansal, N., Singh, J.P. and Schneider, H., (2009) '*Innovative Processing and Synthesis of Ceramics, Glasses and Composites VIII'*, John Wiley & Sons, Inc., Hoboken, New Jersey (2009), Vol. 166, DOI: 10.1002/9781118407820

De La Hoz, A., Alcázar, J., Carrillo, J., Herrero, M., Muñoz, J., Prieto, P., De Cózar, A. and Diaz-Ortiz, A., (2011) '*Reproducibility and Scalability of Microwave-Assisted Reactions'*, Microwave Heating, ISBN: 978-953-307-573-0, InTech

Donati, G. and Paludetto, R., (1997) '*Scale up of chemical reactors'*, Catalysis Today, Vol. 34, pp. 483-533

Pitchai, K., (2011) '*Electromagnetic and Heat Transfer Modeling of Microwave Heating in Domestic Ovens'*, PhD Thesis, University of Nebraska at Lincoln

Rosa, R., Veronesi, P. and Leonelli, C., (2013) '*Optimisation of Microwave-assisted rapid debinding of CIM parts in multi-mode applicators'*, Advanced Processing and Manufacturing Technologies for Structural and Multifunctional Materials VI, DOI: 10.1002/9781118217528

Salvi, D., Boldor, D., Ortego, J., Aita, G.M. and Sabliov, C.M., (2010) '*Numerical Modeling of Continuous Flow Microwave Heating: A Critical Comparison of COMSOL and ANSYS'*, Journal of Microwave Power and Electromagnetic Energy, Vol. 44 (4), pp. 187-197

Santos, T., Costa, L.C., Valente, M., Monteiro, J. and Sousa, J., (2010) '*3D Electromagnetic Field Simulation in Microwave Ovens: a Tool to Control Thermal Runaway'*, Excerpt from the Proceedings of the COMSOL Conference 2010 Paris

Tinga, W.R. and Sutton, W.H., (1993) '*Key issues in microwave processing, research and commercialization—an open forum'*, Microwaves: theory and application in materials processing II, American Ceramic Society, Westerville, Vol. 36, pp. 45–49

Appendix 1 – Dielectric properties

Method: Samples were placed in standard Eppendorf tubes and placed on-axis in a 2.5 GHz TM_{010} cylindrical cavity. Three samples were prepared for each material, each of nominal volume of approximately 200 µl. The error bars shown in the following graphs are those obtained by the standard errors of the three measurements. The silica based samples are much lower loss than the carbon samples and so are shown plotted on separate graphs to bring out the differences between them.

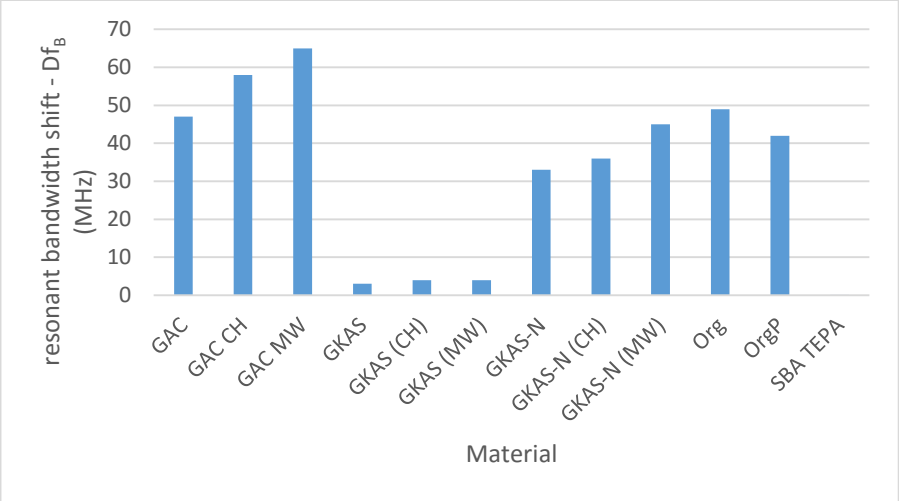

Figure A.1: Contribution to the resonant bandwidth (in MHz) for all 18 samples

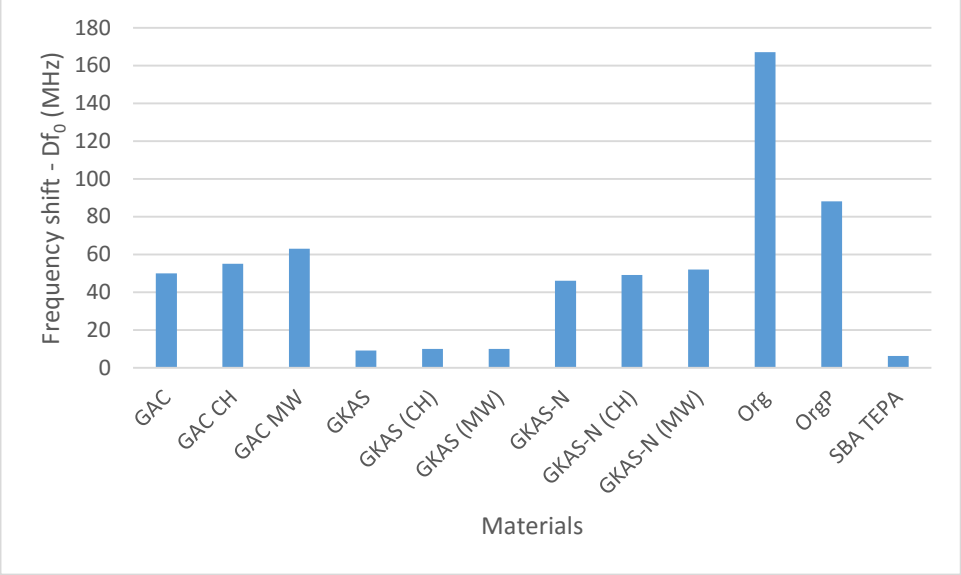

Figure A.2: Frequency shift (in MHz) for all of the samples

Table A.1: Average masses of the samples of each material

Material	Average Mass (mg)
SBA TEPA	64
GAC	119
GAC MW	125
GKAS MW	99
GKAS-N MW	109
GAC CH	115
GKAS CH	102
GKAS-N CH	105
Org	149
OrgP	149

Notes:

(i) 3 samples of each material prepared, standard error ± 2 mg

(ii) Volume of sample approximately constant, 200 µl.